

ÉCOLE DOCTORALE DES SCIENCES DE LA VIE ET DE LA SANTÉ

Institut de Génétique et de Biologie Moléculaire et Cellulaire

CNRS UMR 7104 – Inserm U 1258

THÈSE

présentée par :

Monica DAM

Soutenue le : **10 novembre 2022**

Pour obtenir le grade de :

Docteur de l'université de Strasbourg

Discipline/ Spécialité : Aspects moléculaires et cellulaires de la biologie

The role of DNA helicase PARI in the NoCut abscission checkpoint in human cells

THÈSE dirigée par :

M MENDOZA Manuel, PhD

Directeur de recherche (DR2), INSERM
IGBMC, Université de Strasbourg

RAPPORTEURS :

M ECHARD Arnaud, PhD

Professor
École Polytechnique, Paris
Directeur de recherche (DR1), CNRS
Institut Pasteur, Paris

M MARTIN-SERRANO Juan, PhD

Professor of Viral Cell Biology,
King's College, London

AUTRES MEMBRES DU JURY :

Mme SUMARA Izabela, PhD

Directrice de recherche (DR1), CNRS
IGBMC, Université de Strasbourg

Table of Contents

Table of Contents	1
Résumé.....	5
Introduction	5
Erreurs de ségrégation des chromosomes et instabilité génomique	5
Le checkpoint d'abscission inhibe l'abscission en présence de ponts chromatiniens	6
Le rôle de Srs2/PARI dans le point de contrôle NoCut/abscission.....	7
Résultats	9
L'ADN hélicase Srs2 est nécessaire pour l'inhibition de l'abscission et la résolution des ponts ...	9
PARI promeut la stabilisation des corps intermédiaires par une voie dépendante d'Aurora B....	10
PARI est strictement localisé à la chromatine pendant la phase S	12
PARI promeut la résolution du pont avant la mitose.....	12
Discussion	14
Summary	16
Introduction	16
Chromosome segregation errors and genomic instability.....	16
The abscission checkpoint inhibits abscission in the presence of chromatin bridges	17
The role of Srs2/PARI in the NoCut/abscission checkpoint.....	18
Results	19
Srs2 DNA helicase is required for abscission inhibition and bridge resolution	19
PARI promotes midbody stabilization through an Aurora B-dependent pathway	20
PARI is strictly localized to the chromatin during S-phase	21
PARI promotes bridge resolution before mitosis	22
Discussion	23
List of Figures & Tables	25
List of Abbreviations	27
1. Introduction.....	28
1.1 Overview of the eukaryotic cell cycle	30
1.1.1 The phases of the cell cycle	30
1.1.2 Cell cycle regulation.....	33
1.1.3 Cell cycle checkpoints	36
1.1.3.1 DNA damage repair and checkpoint	37
1.1.3.2 Spindle assembly checkpoint	39

1.2 Cytokinesis	41
1.2.1 Cytokinesis in vertebrate cells	41
1.2.1.1 Cleavage plane determination and actomyosin ring contraction.....	42
1.2.1.2 Central spindle assembly and midbody formation.....	44
1.2.1.3 ESCRT and membrane trafficking.....	46
1.2.1.4 Midbody disassembly and abscission of the intercellular bridge.....	47
1.2.2 Cytokinesis in budding yeast	50
1.3 Anaphase bridges	53
1.3.1 Anaphase bridge formation.....	53
1.3.1.1 Incomplete replication and unresolved recombination	54
1.3.1.2 Catenated anaphase bridges	56
1.3.1.3 The decatenation checkpoint	58
1.3.2 Chromatin bridge resolution.....	59
1.4 The NoCut/abscission checkpoint	62
1.4.1 The NoCut checkpoint in budding yeast.....	62
1.4.1.1 NoCut prevents completion of cytokinesis in cells with spindle midzone defects and chromatin bridges.....	62
1.4.1.2 The current model of how NoCut monitors the chromosome segregation	63
1.4.2 The abscission checkpoint in human cells.....	64
1.4.2.1 The mechanism of abscission checkpoint in human cells.....	66
1.4.3 Consequences of a deficient NoCut/abscission checkpoint	70
1.5 DNA helicase PARI.....	72
1.5.1 Yeast homolog Srs2	72
1.5.1.1 Srs2 in replication.....	74
1.5.1.2 Srs2 in recombinational repair.....	75
1.5.1.3 Srs2 in the DNA damage checkpoint	75
1.5.2 Human homolog PARI	76
1.5.2.1. PARI in tumorigenesis.....	77
2. Results.....	79
2.1. Aims of the study	79
2.2 Role of Srs2 in NoCut	80
2.2.1 The Srs2 DNA helicase is required for abscission inhibition in the presence of DNA replication stress.....	80
2.2.2 The Srs2 DNA helicase is required for abscission inhibition in the presence of catenated chromatin bridges	83
2.2.3 Srs2 prevents chromosome segregation with unreplicated DNA	84
2.2.4 The interaction of Srs2 with PCNA is important for a NoCut-dependent abscission delay	87

2.2.5 Retention of Srs2 on dicentric chromatin bridges inhibits abscission	90
2.3 Role of PARI in the abscission checkpoint	91
2.3.1 An assay to measure midbody stability in HeLa cells with chromatin bridges.....	93
2.3.2 The DNA helicase PARI, but not FBH1, promotes midbody stabilization in cells with topoisomerase II defects.....	94
2.3.3 PARI promotes actin stabilization at the abscission site.....	104
2.3.4 PARI regulates midbody stability through an Aurora B-dependent pathway	105
2.3.5 PARI does not stabilize midbodies in cells with NPC defects.....	107
2.3.6 PARI localization is restricted to the nucleus during S-phase	108
2.3.7 PARI does not promote anaphase DNA synthesis	112
2.3.8 The abscission machinery remains unperturbed in absence of PARI	114
2.3.9 Chromatin bridges persist hours after midbody disassembly	118
2.3.10 PARI promotes bridge resolution before mitosis	122
2.3.11 Cells with chromatin bridges do not accumulate DNA damage immediately after cytokinesis	128
2.4 Author's contribution.....	131
3. Summary: Budding yeast complete DNA synthesis after chromosome segregation begins.....	132
3.1 Contributions.....	133
4. Discussion & Perspectives.....	135
Srs2 prevents unreplicated DNA during anaphase.....	135
Chromatin bridge resolution and abscission in budding yeast	137
Srs2 requires the interaction with PCNA to inhibit abscission	139
Midbody stability and abscission	141
PARI regulates the abscission checkpoint through other signaling pathways.....	144
The physiological relevance of PARI and the abscission checkpoint.....	146
5. Conclusions	150
6. Methods	151
6.1 Yeast strains and culture	151
6.2 Human cell lines and culture conditions	153
6.2.1 Cell seeding	153
6.2.2 Plasmid and siRNA transfection	153
6.2.3 Colony survival assay	154
6.3 Quantitative PCR and analysis	155
6.4 Western blotting and immunoprecipitation	156

6.5 Microscopy techniques	158
6.5.1 Immunofluorescence microscopy and image analysis	158
6.5.2 CellProfiler Image Analysis.....	158
6.5.3 Time-lapse fluorescence spinning disk confocal microscopy	159
6.5.4 Correlative light electron microscopy.....	160
6.5.5 EdU incorporation.....	160
6.6 Flow cytometry	161
6.7 Statistical methods	162
<i>Acknowledgements</i>	163
<i>Supplementary Figures</i>	165
<i>References</i>	169

Résumé

Introduction

Erreurs de ségrégation des chromosomes et instabilité génomique

La mitose et la cytokinèse sont des processus étroitement régulés qui nécessitent la fixation correcte des chromosomes répliqués aux microtubules du fuseau, leur alignement à l'équateur de la cellule, et enfin leur séparation et leur ségrégation précise en deux cellules filles. La cytokinèse est la dernière étape du cycle cellulaire qui commence après la ségrégation des chromosomes par l'ingression du sillon de division, entraînée par l'anneau d'actomyosine au niveau du plan équatorial. Dans les cellules des vertébrés, l'avancée de la membrane forme un canal intercellulaire entre les cellules filles et resserre les microtubules non kinétochoriens antiparallèles du fuseau en un faisceau dense en électrons appelé corps central. Le corps de Flemming est formé au centre du corps central où les microtubules antiparallèles se chevauchent. Le corps central sert de plateforme pour le recrutement de nombreuses protéines impliquées dans l'abscission, notamment le complexe ESCRT-III qui a pour mission d'effectuer la résolution finale de la membrane plasmique de la cellule en division en deux membranes différentes (un processus appelé abscission) et de séparer physiquement les deux cellules filles. D'un point de vue mécanique, les protéines ESCRT-III forment des filaments hélicoïdaux qui courbent la membrane plasmique et s'éloignent du corps central, entraînant la scission de la membrane à côté du corps de Flemming, au niveau du site dit d'abscission. Cependant, avant que l'abscission ne se produise, la zone d'abscission doit être débarrassée des filaments d'actine et des microtubules qui stabilisent le canal intercellulaire (Mierzwa and Gerlich 2014; Addi, Bai and Echard 2018).

L'abscission doit être temporellement coordonnée avec la ségrégation des chromosomes, et les défauts de cette coordination sont liés à l'aneuploïdie et aux aberrations chromatiniennes structurelles dues à la chromatine piégée dans le canal intercellulaire. Les ponts de chromatine, caractérisés par des brins de chromatine étirés entre deux cellules sœurs, peuvent être causés par une réplication incomplète de l'ADN, des intermédiaires de recombinaison non résolus et des défauts dans la fonction de la condensine et de la topoisomérase II. L'incapacité à résoudre les ponts

chromatiniens avant l'abscission peut conduire à la rupture de la chromatine par la machinerie d'abscission ou à l'échec de la cytokinèse, ce qui entraîne la tétraploïdisation (Steigemann et al. 2009). La rupture du pont chromatiniens peut également induire des dommages à l'ADN, la formation de micronoyaux et des réarrangements chromosomiques aberrants (chromothripsis) qui sont fréquemment observés dans les cancers (Umbreit et al. 2020). Ainsi, une bonne coordination entre la ségrégation des chromosomes et la cytokinèse est essentielle pour maintenir la stabilité génomique.

Le checkpoint d'abscission inhibe l'abscission en présence de ponts chromatiniens

Ces dernières années, de nombreuses études ont montré que les ponts chromatiniens non résolus et persistants pendant la cytokinèse retardent l'abscission en raison de l'activation de l'activité d'Aurora B au niveau du corps central. Cette réponse cellulaire, connue sous le nom de point de contrôle de l'abscission dans les cellules humaines, ou de point de contrôle "NoCut" dans la levure bourgeonnante, stabilise le canal intercellulaire qui relie les cellules filles au stade de l'abscission, retarde l'achèvement de la cytokinèse jusqu'à ce que la zone médiane ait été débarrassée de sa chromatine, et empêche la tétraploïdisation et/ou les dommages à l'ADN (Petsalaki and Zachos 2021b).

La kinase Aurora B est un composant central du point de contrôle de l'abscission. Aurora B est essentielle à la fois pour une ségrégation chromosomique correcte et pour la cytokinèse. Faisant partie du complexe passager chromosomique (CPC) avec INCENP, borealin et survivin, le CPC est recruté aux centromères au début de la mitose où il surveille la fixation des chromosomes aux microtubules du fuseau et module le point de contrôle de l'assemblage du fuseau (SAC) pour corriger les erreurs de fixation. Une diminution de l'activité de CDK1 à la transition métaphase-anaphase, permet au CPC de se relocaliser aux microtubules du fuseau central et du corps central. À cet endroit, Aurora B joue des rôles à la fois positifs et négatifs pendant la cytokinèse. D'une part, Aurora B promeut l'assemblage et la fonction de l'anneau contractile (Carmena et al. 2012). D'autre part, en présence de chromatine, Aurora B peut agir comme un inhibiteur de l'abscission (Norden et al. 2006; Steigemann et al. 2009). Ce rôle inhibiteur d'Aurora B implique sa phosphorylation de la sous-unité

CHMP4C de l'ESCRT-III (Carlton et al. 2012; Capalbo et al. 2012). La CHMP4C phosphorylée inhibe une autre sous-unité de l'ESCRT-III, l'ATPase VPS4, pour empêcher son activité sur les filaments de l'ESCRT-III afin de compléter l'abscission. Bien que les mécanismes précis ne soient pas clairs, des expériences génétiques et biochimiques suggèrent que CHMP4C et une protéine supplémentaire appelée ANCHR forment un complexe ternaire avec VPS4 au niveau du corps central, empêchant VPS4 d'atteindre le site d'abscission (Thoresen et al. 2014).

Le rôle de Srs2/PARI dans le point de contrôle NoCut/abscission

La manière dont les ponts chromosomiques sont détectés et leur présence relayée à Aurora B reste inconnue. Des études sur la levure bourgeonnante ont permis de comprendre ce processus et de découvrir le point de contrôle de l'abscission (Norden et al. 2006). Les cellules de levure présentant des ponts chromatiniens retardent l'abscission d'une manière dépendante d'Aurora B (Mendoza et al. 2009). Cependant, tous les types de ponts chromatiniens n'inhibent pas l'abscission. Les ponts causés par l'inhibition de la réplication, de la condensation ou de la décaténation de l'ADN inhibent l'abscission, alors que ceux causés par la fusion de chromosomes par ailleurs normaux ne le font pas (Amaral et al. 2016). En outre, des travaux récents de notre laboratoire, auxquels j'ai contribué pendant mon doctorat, ont démontré que les ponts de chromatine causés par une réplication incomplète de l'ADN sont courants pendant la mitose dans les cellules de levure qui se divisent normalement (Ivanova et al. 2020). Ces résultats ont soulevé la possibilité que les ponts dont la réplication, la condensation et la décaténation de l'ADN sont défectueuses puissent contenir des molécules qui soutiennent, directement ou indirectement, l'activité d'Aurora B au niveau du corps central pour assurer l'inhibition de l'abscission.

Des résultats non publiés de notre laboratoire ont identifié une telle molécule candidate chez la levure bourgeonnante. Srs2 est une ADN hélicase de levure qui s'associe à l'antigène nucléaire des cellules proliférantes (PCNA), un clamp ADN qui agit comme un facteur de processivité pour l'ADN polymérase et qui est essentiel pour la réplication (Choe and Moldovan 2017). Srs2 n'est pas essentielle à la viabilité mais en son absence, les cellules ne peuvent pas inhiber l'abscission en réponse à des ponts chromosomiques non répliqués, décondensés ou caténés. L'inhibition de

l'abscission ne nécessite pas l'activité ADN hélicase de Srs2 mais dépend d'un domaine SIM qui médiatise son interaction avec PCNA. Nous supposons que Srs2 est un composant du checkpoint NoCut, nécessaire à l'inhibition de l'abscission et que ce mécanisme est conservé dans les cellules animales. L'objectif de ma recherche doctorale est de caractériser les hélicases d'ADN Srs2 et PARI et de déterminer leur rôle dans le point de contrôle NoCut/abscission.

Semblable à Srs2, PARI est recruté à la fourche de réplication par PCNA SUMOylée, où il fonctionne pour inhiber la recombinaison homologue (HR) non synchronisée en désassemblant les filaments RAD51 des fourches de réplication et en déplaçant Pol δ pour empêcher la synthèse de réparation de l'ADN, limitant ainsi le risque de croisements (Burkovics et al. 2016). La surexpression de PARI notamment dans le cancer du pancréas, des ovaires et de la prostate est corrélée à la progression tumorale en raison d'aberrations chromosomiques élevées. En revanche, la déplétion de PARI hyper-sensibilise les cellules aux agents endommageant l'ADN, augmentant le stress de réplication de l'ADN et l'accumulation de dommages à l'ADN et affectant par conséquent la survie cellulaire (O'Connor et al. 2013). Bien que ces défauts aient été attribués au rôle de PARI dans la réplication de l'ADN, nos résultats chez son homologue de la levure ont soulevé la possibilité que PARI puisse également préserver la stabilité du génome par son rôle dans le point de contrôle de l'abscission.

Résultats

L'ADN hélicase Srs2 est nécessaire pour l'inhibition de l'abscission et la résolution des ponts

Chez la levure bourgeonnante, tous les ponts ne sont pas détectés de la même manière par NoCut. Les ponts d'ADN concaténé générés par l'inactivation de la topoisomérase II ou les ponts induits par le stress de réplication de l'ADN retardent la constriction complète de la membrane plasmique au niveau du cou du bourgeon. Les ponts dicentriques formés par la fusion des chromosomes IV et XII qui peuvent persister dans la zone médiane pendant la cytokinèse ne déclenchent pas de retard d'abscission. Ceci suggère qu'il existe un signal basé sur la chromatine qui peut permettre la détection des ponts par NoCut. Nous avons supprimé diverses hélicases d'ADN et dans cette étude, je me concentrerai sur l'hélicase d'ADN Srs2.

Pour étudier le rôle de Srs2 pendant l'abscission, j'ai suivi l'invagination et la résolution de la membrane plasmique au niveau du cou du bourgeon par microscopie confocale en direct, en utilisant le rapporteur fluorescent GFP-CAAX (GFP inducible par le β -estradiol fusionné au motif CAAX de Ras2 ciblant la membrane). Le stress de réplication de l'ADN induit par l'hydroxyurée (HU) provoque un retard de résolution de la membrane plasmique, comme cela a été précédemment observé (Amaral et al. 2016). La délétion de SRS2 libère les cellules de ce retard d'abscission. L'inactivation de Top2 inhibe fortement la fraction de cellules capables d'abscission dans les 60 min après l'ingression de la membrane. De manière cohérente, l'absence de Srs2 permet la résolution de la membrane et la progression de l'abscission. Au total, cela suggère que Srs2 promeut l'inhibition de l'abscission en présence d'un stress de réplication de l'ADN et d'une inactivation de Top2. De plus, nous montrons que l'association de Srs2 à la chromatine par son interaction avec PCNA est importante pour sa fonction de signal putatif basé sur la chromatine pour NoCut.

L'exposition au stress de réplication de l'ADN perturbe la ségrégation des chromosomes et provoque la persistance des ponts chromatiniens. Dans les cellules humaines, l'inhibition du point de contrôle de l'abscission par la déplétion de CHMP4C entraîne une résolution prématurée des ponts chromatiniens. Cependant, l'inactivation de NoCut par la délétion de SRS2 chez la levure n'a pas provoqué de

résolution prématurée des ponts. Au contraire, l'absence de Srs2 a entraîné la persistance de ponts chromatiniens plus longs, ce qui suggère que Srs2 est nécessaire à la résolution des ponts chromatiniens.

PARI promeut la stabilisation des corps intermédiaires par une voie dépendante d'Aurora B

Les résultats ci-dessus suggèrent que Srs2 agit comme un signal basé sur la chromatine nécessaire pour déclencher le point de contrôle NoCut en présence de ponts chromatiniens. Les ponts de chromatine sont considérés comme un marqueur d'instabilité génomique dans les tumeurs humaines et jouent un rôle critique dans la tumorigenèse. La présence de chromatine piégée dans le plan de division peut être brisée par la machinerie d'abscission, conduisant à l'aneuploïdie et à la chromothripsie dans les cycles suivants. Le canal intercellulaire reliant les cellules filles peut également devenir instable, provoquant une régression de la membrane et une tétraploïdisation.

J'ai cherché à savoir si l'homologue de Srs2, PARI, est nécessaire pour l'inhibition de l'abscission dans les cellules humaines avec des ponts chromatiniens caténaux en utilisant la microscopie confocale à disque rotatif en temps réel. PARI a été appauvri dans les cellules de carcinome cervical HeLa Kyoto en utilisant un siRNA et synchronisé en G1/S. L'inhibiteur de topoisomérase II α (TOP2) ICRF-193 a été ajouté en phase G2/M pour induire des ponts d'ADN concaténés pendant la cytokinèse. Conformément à l'étude précédente, ICRF-193 induit des ponts chromatiniens (Bhowmick et al. 2019) observés avec un marqueur d'enveloppe nucléaire LAP2 β dans 80 % des cellules en cytokinèse, qui sont identifiés par la structure dense en microtubules appelée corps central entre deux cellules filles en division. La durée de vie du corps central, c'est-à-dire le temps entre la formation du corps central et son désassemblage, a été utilisée pour évaluer la progression de la cytokinèse tardive dans les cellules témoins et les cellules dépourvues de PARI. L'ajout de l'ICRF-193 a significativement retardé le désassemblage du corps central dans les cellules témoins de 131 min à 202 min. La déplétion de PARI n'a pas perturbé le désassemblage du corps central dans les cellules normales en division. En revanche, le retard de l'abscission causé par l'inactivation de TOP2 était significativement réduit dans les

cellules dépourvues de PARI. Les cellules dépourvues de PARI ne parviennent pas à stabiliser le corps central en présence de ponts chromatinien, ce qui suggère que le pont n'est pas détecté par le point de contrôle de l'abscission. Dans les mêmes conditions, j'ai observé un autre marqueur bien caractérisé du retard du point de contrôle de l'abscission, en présence de ponts chromatinien, on a observé que les filaments d'actine s'accumulent sous forme de plaques à chaque extrémité du pont intercellulaire (PIC) pour le stabiliser. La chromatine caténée au niveau du plan de division a induit une forte accumulation d'actine filamenteuse au niveau du PIC qui n'a été dissoute que dans 25% des cellules en division, mais la déplétion de PARI a soulagé le retard de 65% des cellules avec un pont chromatinien. Au total, PARI promeut la stabilisation du corps central et de l'actine au niveau de l'ICB, et peut agir comme un signal putatif associé à la chromatine pour le point de contrôle de l'abscission, ce qui est cohérent avec les observations chez la levure bourgeonnante.

Pour établir que PARI est effectivement un composant du point de contrôle de l'abscission, la kinase Aurora B a été inhibée dans les cellules au stade du corps central. Comme prévu, le retard du désassemblage du corps intermédiaire par le traitement à l'ICRF-193 a été complètement aboli par l'inhibition d'Aurora B. La durée de vie du corps intermédiaire a été accélérée par le traitement à l'ICRF-193. La durée de vie du corps central a été accélérée de 100 min et n'est pas significativement différente en l'absence de PARI. Puisque la déplétion de PARI et l'inhibition d'Aurora B n'ont pas atténué davantage la durée du corps central déjà raccourcie, cela suggère qu'Aurora B et PARI agissent dans la même voie pour réguler le désassemblage du corps central.

PARI est strictement localisé à la chromatine pendant la phase S

Les résultats obtenus jusqu'à présent ont montré que l'ADN hélicase PARI agit comme un signal chromatinien potentiel pour le point de contrôle de l'abscission. Ensuite, j'ai évalué la localisation de PARI en utilisant la microscopie à imagerie en direct dans des cellules HeLa exprimant de manière stable eGFP-PARI. Des foyers eGFP-PARI ont été observés dans le noyau, ce qui est cohérent avec son recrutement aux fourches de réplication pendant la phase S (Burkovics et al. 2016). Le signal est devenu homogène dans tout le noyau avant de se disperser dans le cytoplasme lors de la rupture de l'enveloppe nucléaire en mitose. eGFP-PARI n'a plus été observé jusqu'à l'entrée en phase S suivante. La présence de l'ICRF-193 pendant la cytokinèse n'a pas recruté PARI à la chromatine ni au corps central. Cela montre que PARI n'est pas présent lorsque le point de contrôle de l'abscission est actif et suggère que PARI peut agir indirectement par le biais d'autres voies de signalisation telles que les voies médiées par ATR/CHK1 ou ATM/CHK2 qui ont été montrées comme régulant le point de contrôle de l'abscission (Mackay and Ullman 2015; Petsalaki and Zachos 2021a). Pour étudier cette hypothèse, les niveaux de ATR, CHK1, ATM et CHK2 pendant la cytokinèse peuvent être évalués par microscopie et western blot en utilisant des anticorps spécifiques. Il est également possible que quelques molécules de PARI suffisent à déclencher le point de contrôle, mais qu'elles ne soient pas observées en raison de la sensibilité de détection limitée du microscope.

PARI promeut la résolution du pont avant la mitose

La fonction physiologique du point de contrôle de l'abscission a été démontrée pour protéger les ponts chromatiniens de l'acquisition de dommages à l'ADN, et les cellules de la tétraploïdisation (Steigemann et al. 2009; Carlton et al. 2012; Petsalaki and Zachos 2021a). L'absence de PARI dans les cellules en division avec un pont chromatinien montre systématiquement un point de contrôle d'abscission non réactif. Par conséquent, une question clé est de savoir ce qui arrive aux ponts dans les cellules déficientes en PARI où le point de contrôle de l'abscission ne répond pas correctement pour retarder le désassemblage du corps central et stabiliser l'actine au niveau du BIC. Dans ce but, j'ai réalisé une imagerie en direct pendant plus de 60 heures de cellules HeLa exprimant un autre marqueur de l'enveloppe nucléaire, l'eGFP-BAF, pour visualiser les ponts chromatiniens, et colorées avec un colorant

tubuline pour évaluer la durée de vie du corps central. Les ponts de chromatine ne se résorbent pas immédiatement après le désassemblage du corps central, mais persistent pendant des heures après, comme cela a été observé précédemment par Steigemann et al. (2009) et Carlton et al. (2012). Compromettre la stabilité du corps central en appauvrissant PARI n'a pas non plus affecté le temps de résolution du pont immédiatement. Cette observation a été validée par l'inhibition d'Aurora B pendant la cytokinèse, qui accélère le désassemblage du corps central, et même ainsi, les ponts chromatiniens ont persisté pendant plus de 18 heures après l'inactivation d'Aurora B.

En utilisant l'eGFP-BAF, des ponts chromatiniens " spontanés " ont également été observés dans 27 % des cellules témoins non traitées et dans 25 % des cellules dépourvues de PARI. L'exposition à l'ICRF-193 pendant la phase G2/M a induit des ponts chromatiniens dans toutes les cellules en division. Cela a conduit à la binucléation de 50% des cellules avec des ponts induits par l'ICRF-193 indépendamment du PARI. Les ponts spontanés observés dans les cellules déficientes en PARI ont été résolus dans 70% des événements avant la mitose, en moyenne à 1300 min après la formation du corps central. Comparée à la durée de vie moyenne du corps central dans les cellules témoins non traitées, la durée de vie des ponts est 100 fois plus longue. De façon remarquablement similaire à la perte de Srs2 chez la levure bourgeonnante, la déplétion de PARI retarde la résolution des ponts chromatiniens spontanés et induits par l'ICRF-193. En particulier, les ponts spontanés ont été résolus pendant la mitose plutôt que pendant l'interphase. Dans l'ensemble, cela suggère que PARI promeut un retard dans le désassemblage du corps central et de l'actine en présence de chromatine et la résolution des ponts chromatiniens avant la mitose.

Discussion

Le point de contrôle NoCut médié par Aurora B a été découvert pour la première fois chez la levure pour retarder l'abscission en réponse aux défauts de la zone médiane du fuseau et aux erreurs de ségrégation des chromosomes pendant la cytokinèse. En outre, NoCut retarde l'abscission en présence de ponts chromatiniens induits par l'inactivation de la topoisomérase II, la condensation et le stress de réplication de l'ADN (Mendoza et al. 2009; Amaral et al. 2016). Ces dernières années, de grands progrès ont été réalisés dans l'identification des composants clés du checkpoint d'abscission humain depuis sa découverte chez la levure bourgeonnante. Cependant, il reste encore beaucoup à comprendre sur la fonction physiologique du checkpoint, et le mécanisme derrière la détection des ponts chromatiniens. Dans cette thèse de doctorat, j'ai caractérisé le rôle de l'ADN hélicase Srs2 chez la levure bourgeonnante et de son homologue humain PARI dans le point de contrôle NoCut/abscission.

Nos résultats suggèrent que Srs2 et PARI promeuvent l'inhibition de la cytokinèse dans les cellules présentant des ponts chromatiniens persistants. En utilisant la microscopie d'imagerie en direct et HeLa exprimant de manière stable eGFP-PARI, je montre que eGFP-PARI est localisé dans le noyau initialement sous forme de foyers et devient homogène avant l'entrée en mitose. Ceci est cohérent avec les études précédentes de localisation de Srs2 et PARI, montrant que Srs2/PARI est recruté à PCNA pendant la réplication et aux sites de recombinaison homologue (Burgess et al. 2009; Burkovics et al. 2016; Mochizuki et al. 2017). De façon intéressante, PARI peut être recruté à la chromatine en G2 lors de dommages à l'ADN par irradiation (Mochizuki et al. 2017). Cependant, le signal se disperse rapidement dans le cytoplasme à l'entrée en mitose et n'est pas observé pendant la cytokinèse, même en présence de l'inhibiteur de topoisomérase ICRF-193. Une question clé qui se pose est de savoir comment Srs2/PARI peut réguler le point de contrôle de l'abscission s'il n'est pas observé pendant la cytokinèse. Une hypothèse plausible est que l'ADN hélicase entretient un signal par le biais des médiateurs de la réponse aux dommages de l'ADN, les voies de signalisation ATR/Chk1 ou ATM/Chk2, qui régulent Aurora B pour retarder le désassemblage du corps central. Un effet indirect du signal Srs2/PARI sur le point de contrôle de l'abscission peut expliquer pourquoi, en son absence, l'abscission ou la durée de vie du corps central n'est pas accélérée, ce qui est

couramment observé lors de la déplétion d'autres composants tels que ATR/Chk1, ATM/Chk2 et CHMP4C.

Des preuves antérieures suggèrent que le retard d'abscission médié par NoCut lors de la formation du pont chromatinien prévient les dommages à l'ADN dans la G1 suivante de la levure bourgeonnante (Amaral et al. 2016). Dans les cellules humaines, il a été démontré que le point de contrôle de l'abscission protège contre la résolution prématurée des ponts chromatiniens et les dommages à l'ADN (Carlton et al. 2012; Sadler et al. 2018; Petsalaki and Zachos 2021a). Une observation surprenante qui contredit ces études, est que les cellules de levure bourgeonnante et HeLa déficientes en Srs2/PARI ont des ponts chromatiniens plus durables. Malgré le retard dans la résolution des ponts par rapport aux cellules déficientes en Srs2, les cellules *srs2Δ* résolvent toujours leurs ponts avant l'abscission. Dans les cellules HeLa, la durée de vie du corps central ne semble pas affecter le moment de la résolution du pont, car le désassemblage du corps central se produit en moyenne 20 heures avant la résolution du pont. Le cycle cellulaire n'est pas arrêté pour résoudre les ponts chromatiniens dans les cellules HeLa. Ces ponts persistent en interphase, alors que les ponts de chromatine dans les cellules dépourvues de PARI se résolvent pendant la mitose. Au total, cela suggère que Srs2/PARI promeut la résolution des ponts chromatiniens. Pour évaluer si la résolution des ponts dépend de l'expression de PARI pendant S et G2, nous pouvons exprimer le marqueur d'enveloppe nucléaire BAF dans la lignée cellulaire HeLa exprimant de manière stable eGFP-PARI. Des recherches supplémentaires sont nécessaires pour savoir si le retard de résolution du pont en l'absence de PARI est physiologiquement important et si la stabilisation du corps central dépendante de PARI est découplée de l'abscission de la membrane plasmique.

En conclusion, l'ADN hélicase Srs2 a plusieurs homologues fonctionnels humains, mais PARI est impliqué comme étant le plus direct. Dans ce projet, j'ai découvert que Srs2/PARI est un composant du point de contrôle NoCut/abscission, cependant, il a une double fonction surprenante en favorisant la résolution des ponts chromatiniens.

Summary

Introduction

Chromosome segregation errors and genomic instability

Mitosis and cytokinesis are tightly regulated processes that require the proper attachment of the replicated chromosomes to spindle microtubules, their alignment at the cell equator, and finally their separation and accurate segregation into two daughter cells. Cytokinesis is the last step of the cell cycle that begins after chromosome segregation by ingression of the cleavage furrow, driven by the actomyosin ring at the equatorial plane. In vertebrate cells, the ingression of the membrane forms an intercellular canal between the daughter cells and further constricts the antiparallel non-kinetochore spindle microtubules into an electron-dense bundle called the midbody. The Flemming body is formed in the middle of the midbody where antiparallel microtubules overlap. The midbody serves as a platform for the recruitment of many proteins involved in cytokinesis, notably the ESCRT-III complex which is tasked to do the final resolution of the plasma membrane of the dividing cell into two different membranes (a process called abscission) and physically separate the two daughter cells. Mechanistically, ESCRT-III proteins form helical filaments that curve the plasma membrane and extend away from the midbody, leading to membrane scission next to the Flemming body, at the so-called abscission site. However, before abscission occurs, the abscission zone has to be cleared out of actin filaments and microtubules which stabilizes the intercellular canal (Mierzwa and Gerlich 2014; Addi, Bai and Echard 2018).

Abscission must be temporally coordinated with chromosome segregation, and defects in this coordination are linked to aneuploidy and structural chromatin aberrations due to trapped chromatin in the intercellular canal. Chromatin bridges, characterized by chromatin strands stretched out between two sister cells, can be caused by incomplete DNA replication, unresolved recombination intermediates, and defects in condensin and topoisomerase II function. Failure to resolve chromatin bridges before abscission takes place can lead to chromatin breakage by the abscission machinery or to cytokinesis failure, the latter resulting in tetraploidization (Steigemann et al. 2009). Breakage of the chromatin bridge can also induce DNA

damage, micronuclei formation, and aberrant chromosomal rearrangements (chromothripsis) that are commonly observed in cancers (Umbreit et al. 2020). Thus, proper coordination between chromosome segregation and cytokinesis is essential to maintain genomic stability.

The abscission checkpoint inhibits abscission in the presence of chromatin bridges

In recent years, numerous studies have shown that unresolved and persistent chromatin bridges during cytokinesis delay abscission due to activation of Aurora B activity at the midbody. This cellular response, known as the abscission checkpoint in human cells, or the “NoCut” checkpoint in budding yeast, stabilizes the intercellular canal that bridges daughter cells at the abscission stage, delays the completion of cytokinesis until the midzone has been cleared of chromatin, and prevents tetraploidization and/or DNA damage (Petsalaki and Zachos 2021b).

The Aurora B kinase is a central component of the abscission checkpoint. Aurora B is essential for both proper chromosome segregation and for cytokinesis. As part of the chromosomal passenger complex (CPC) together with INCENP, borealin, and survivin, the CPC is recruited to the centromeres in early mitosis where it monitors the attachment of chromosomes to spindle microtubules and modulates the spindle assembly checkpoint (SAC) to correct attachment errors. A decrease in CDK1 activity at the metaphase-anaphase transition, allows the CPC to relocate to the central spindle and midbody microtubules. At this location, Aurora B plays both positive and negative roles during cytokinesis. On one hand, Aurora B promotes the assembly and function of the contractile ring (Carmena et al. 2012). On the other hand, in the presence of chromatin Aurora B can act as an inhibitor of abscission (Norden et al. 2006; Steigemann et al. 2009). This inhibitory role of Aurora B involves its phosphorylation of the ESCRT-III subunit CHMP4C (Carlton et al. 2012; Capalbo et al. 2012). Phosphorylated CHMP4C inhibits another ESCRT-III subunit, the ATPase VPS4, to prevent its activity on ESCRT-III filaments to complete abscission. Although the precise mechanisms are unclear, genetic and biochemical experiments suggest that CHMP4C and an additional protein called ANCHR form a ternary complex with VPS4 at the midbody, preventing VPS4 from reaching the abscission site (Thoresen et al. 2014).

The role of Srs2/PARI in the NoCut/abscission checkpoint

How chromosome bridges are sensed and their presence relayed to Aurora B remains unknown. Insights into this process came from studies in budding yeast, in which the abscission checkpoint was discovered (Norden et al. 2006). Yeast cells displaying chromatin bridges delay abscission in an Aurora-B-dependent manner (Mendoza et al. 2009). However, not all types of chromatin bridges inhibit abscission. Bridges caused by inhibition of DNA replication, condensation, or decatenation inhibit abscission, whereas those caused by fusion of otherwise normal chromosomes do not (Amaral et al. 2016). In addition, recent work from our lab, to which I contributed during my Ph.D., demonstrated that chromatin bridges caused by incomplete DNA replication are common during mitosis in normally dividing yeast cells (Ivanova et al. 2020). These findings raised the possibility that bridges with defective DNA replication, condensation, and decatenation may contain molecules that sustain, directly or indirectly, for the inhibitory signal that inhibits abscission.

Unpublished results from our lab identified such a candidate molecule in budding yeast. Srs2 is a yeast DNA helicase that associates with Proliferating Cell Nuclear Antigen (PCNA), a DNA clamp that acts as a processivity factor for DNA polymerase and is essential for replication (Choe and Moldovan 2017). Srs2 is not essential for viability but in its absence, cells cannot inhibit abscission in response to unreplicated, or catenated chromosome bridges. Inhibition of abscission does not require the DNA helicase activity of Srs2 but depends on a SIM domain that mediates its interaction with PCNA. We hypothesize that Srs2 is a component of the NoCut checkpoint, necessary for abscission inhibition and that this mechanism is conserved in animal cells. The goal of my Ph.D. research was to characterize Srs2 and its human homologue, the PARI DNA helicase, and determine their role in the NoCut/abscission checkpoint.

Similar to Srs2, PARI is recruited to the replication fork by SUMOylated PCNA, where it functions to inhibit untimed homologous recombination (HR) by disassembling RAD51 filaments from replication forks and displacing Pol δ to prevent DNA repair synthesis, limiting the risk of crossovers (Burkovics et al. 2016). Overexpression of PARI particularly in pancreatic, ovarian, and prostate cancer correlates with tumor

progression due to elevated chromosomal aberrations. In contrast, depletion of PARI hyper-sensitizes cells to DNA-damaging agents, enhancing DNA replication stress and DNA damage accumulation and consequently affecting cellular survival (O'Connor et al. 2013). Although these defects have been attributed to the role of PARI in DNA replication, our results in its yeast homolog raised the possibility that PARI may also preserve genome stability through its role in the abscission checkpoint.

Results

Srs2 DNA helicase is required for abscission inhibition and bridge resolution

In budding yeast, not all bridges are detected equally by NoCut. Catenated bridges generated by topoisomerase II inactivation or bridges induced by DNA replication stress delay the complete constriction of the plasma membrane at the bud neck. Dicentric bridges formed by fusion of chromosome IV and XII which can persist at the midzone during cytokinesis do not trigger abscission delay. This suggests that there is a chromatin-based signal that can allow bridge detection by NoCut. We tested various DNA helicases and in this study, I will focus on the Srs2 DNA helicase.

To investigate the role of Srs2 during abscission I monitored the ingression and resolution of the plasma membrane at the bud neck by live-imaging confocal microscopy, using the fluorescent reporter GFP-CAAX (β -estradiol-inducible GFP fused to the membrane-targeting CAAX motif of Ras2). DNA replication stress induced by hydroxyurea (HU) causes a delayed resolution of the plasma membrane as previously observed (Amaral et al. 2016). Deletion of SRS2 relieves cells of the abscission delay. The inactivation of Top2 strongly inhibits the fraction of cells that are able to abscise within 60 min after membrane ingression. Consistently, the lack of Srs2 allows membrane resolution and abscission progression to occur. In all, suggesting that Srs2 promotes the inhibition of abscission in the presence of DNA replication stress and Top2 inactivation. Furthermore, we show that the association of Srs2 at the chromatin through its interaction with PCNA is important for its function as a putative chromatin-based signal for NoCut.

The exposure to DNA replication stress disrupts chromosome segregation and causes persisting chromatin bridges. In human cells, the inhibition of the abscission

checkpoint by CHMP4C depletion causes premature chromatin bridge resolution. However, the inactivation of NoCut by deleting SRS2 in yeast did not cause premature bridge resolution. Instead, the absence of Srs2 led to longer persisting chromatin bridges, suggesting that Srs2 is required for the resolution of chromatin bridges.

PARI promotes midbody stabilization through an Aurora B-dependent pathway

The above results suggest that Srs2 acts as a chromatin-based signal required to trigger the NoCut checkpoint in the presence of chromatin bridges. Chromatin bridges are considered a marker of genomic instability in human tumors and play a critical role in tumorigenesis. The presence of trapped chromatin in the cleavage plane can be broken by the abscission machinery, leading to aneuploidy and chromothripsis in the next cycles. The intercellular canal connecting the daughter cells can also become unstable, causing membrane regression and tetraploidization.

I investigated whether the Srs2 homolog, PARI is required for abscission inhibition in human cells with catenated chromatin bridges using live-imaging spinning disk confocal microscopy. PARI was depleted in HeLa Kyoto cervical carcinoma cells using siRNA and synchronized in G1/S. The topoisomerase II α (TOP2) inhibitor ICRF-193 was added G2/M phase to induce catenated chromatin bridges during cytokinesis. Consistent with the previous study, ICRF-193 induces chromatin bridges (Bhowmick et al. 2019) observed with a nuclear envelope marker LAP2 β in 80% of cells in cytokinesis, which are identified by the microtubule-dense structure called the midbody between two dividing daughter cells. The midbody lifetime, the time between midbody formation and midbody disassembly, was used to assess late cytokinesis progression in control and PARI-depleted cells. The addition of ICRF-193 significantly delayed midbody disassembly in control cells from 131 min to 202 min. PARI-depletion did not disrupt midbody disassembly in normal dividing cells. In contrast, delayed abscission caused by TOP2 inactivation was significantly reduced in cells lacking PARI. Cells lacking PARI fail to stabilize the midbody in the presence of chromatin bridges, suggesting that the bridge is not detected by the abscission checkpoint. Under the same conditions, I observed another well-characterized marker of the abscission checkpoint delay, in the presence of chromatin bridges actin filaments have been observed to accumulate as patches at each end of the intercellular bridge (ICB) to

stabilize it. Catenated chromatin at the cleavage plane induced a strong accumulation of filamentous actin at the ICB which was only dissolved in 25% of dividing cells, but the depletion of PARI relieved the delay of 65% of cells with a chromatin bridge. In all, PARI promotes stabilization of the midbody and actin at the ICB, and may act as a putative chromatin-associated signal for the abscission checkpoint, consistent with observations in budding yeast.

To establish that PARI is indeed a component of the abscission checkpoint, the Aurora B kinase was inhibited in midbody-stage cells. As expected, the midbody disassembly delay by ICRF-193 treatment was completely abolished by Aurora B inhibition. The midbody lifetime was accelerated by 100 min and is not significantly different in the absence of PARI. Since depletion of PARI and inhibition of Aurora B did not further attenuate the already shortened midbody duration, it suggests that Aurora B and PARI act in the same pathway to regulate midbody disassembly.

PARI is strictly localized to the chromatin during S-phase

The results so far have shown indications of the DNA helicase PARI acting as a potential chromatin signal for the abscission checkpoint. Next, I assessed the localization of PARI using live-imaging microscopy in HeLa cells stably expressing eGFP-PARI. eGFP-PARI foci were observed in the nucleus, consistent with its recruitment to replication forks during S phase (Burkovics et al. 2016). The signal became homogenous throughout the nucleus before the signal disperses into the cytoplasm upon nuclear envelope breakdown required for mitotic entry. eGFP-PARI was not observed again until the next S phase entry. The presence of ICRF-193 during cytokinesis did not recruit PARI to the chromatin nor to the midbody. This shows that PARI is not present when the abscission checkpoint is active and suggests that PARI may act indirectly through other signaling pathways such as ATR/CHK1 or ATM/CHK2-mediated pathways which have been shown to regulate the abscission checkpoint (Mackay and Ullman 2015; Petsalaki and Zachos 2021a). To investigate this hypothesis, levels of ATR, CHK1, ATM, and CHK2 during cytokinesis can be assessed by microscopy and western blot using specific antibodies. It is also possible that a few molecules of PARI is enough to trigger the checkpoint, but are observed due to the limited detected sensitivity of the microscope.

PARI promotes bridge resolution before mitosis

The physiological function of the abscission checkpoint has been shown to protect chromatin bridges from acquiring DNA damage, and cells from tetraploidization (Steigemann et al. 2009; Carlton et al. 2012; Petsalaki and Zachos 2021a). The absence of PARI in dividing cells with a chromatin bridge consistently shows a non-responsive abscission checkpoint. Therefore, a key question is what happens to bridges in PARI-deficient cells where the abscission checkpoint does not respond properly to delay midbody disassembly and stabilize actin at the ICB. To this aim, I performed 60+ hours live-imaging of HeLa cells expressing another nuclear envelope marker eGFP-BAF to visualize chromatin bridges, and stained with a tubulin dye to assess the midbody lifetime. Chromatin bridges do not resolve immediately upon midbody disassembly but persist for hours afterward as previously observed in Steigemann et al. (2009) and Carlton et al. (2012). Compromising the stability of the midbody by depleting PARI did not affect the resolution time of the bridge immediately either. This observation was validated by inhibiting Aurora B during cytokinesis, which accelerates midbody disassembly, and even so, chromatin bridges persisted for more than 18 hours after Aurora B inactivation.

Using eGFP-BAF, 'spontaneous' chromatin bridges were also observed in 27% of untreated control cells and 25% of PARI-depleted cells. The exposure to ICRF-193 during G2/M was observed to induce chromatin bridges in all dividing cells. This led to the binucleation of 50% of cells with ICRF-193 induced bridges independently of PARI. The spontaneous bridges observed in PARI-proficient cells were resolved in 70% of events before mitosis on average at 1300 min after midbody formation. Compared to the average midbody lifetime in untreated control cells, bridge lifetime is 100 times longer. Remarkably similar to the loss of Srs2 in budding yeast, depletion of PARI delays the resolution of both spontaneous and ICRF-193 induced chromatin bridges. In particular, spontaneous bridges were resolved during mitosis rather than during interphase. In all, this suggests that PARI promotes a delay in midbody and actin disassembly in the presence of chromatin and the resolution of chromatin bridges before mitosis.

Discussion

The Aurora B-mediated NoCut checkpoint was first discovered in yeast to delay abscission in response to spindle-midzone defects and chromosome segregation errors during cytokinesis. In addition, NoCut delays abscission in the presence of chromatin bridges induced by inactivation of topoisomerase II, condensin, and DNA replication stress (Mendoza et al. 2009; Amaral et al. 2016). In recent years a great advancement has been made in identifying key components of the human abscission checkpoint since its discovery in the budding yeast. However, much still remains to be understood about the physiological function of the checkpoint, and the mechanism behind chromatin bridge detection. In this Ph.D. thesis, I characterized the role of DNA helicase Srs2 in budding yeast and the human homolog PARI in the NoCut/abscission checkpoint.

Our results suggest that Srs2 and PARI promote inhibition of cytokinesis in cells with persistent chromatin bridges. Using live-imaging microscopy and HeLa stably expressing eGFP-PARI I show that eGFP-PARI is localized in the nucleus initially as foci and becomes homogenous before mitotic entry. This is consistent with previous localization studies of Srs2 and PARI, showing that Srs2/PARI is recruited to PCNA during replication and to sites of homologous recombination (Burgess et al. 2009; Burkovics et al. 2016; Mochizuki et al. 2017). Interestingly, PARI can be recruited to the chromatin in G2 upon DNA damage by irradiation (Mochizuki et al. 2017). However, the signal quickly disperses into the cytoplasm upon mitotic entry and is not observed during cytokinesis even in the presence of the topoisomerase inhibitor ICRF-193. One key question that arises is how Srs2/PARI can regulate the abscission checkpoint if it is not observed during cytokinesis. A plausible hypothesis is that the DNA helicase sustains a signal through the DNA damage response mediators ATR/Chk1 or ATM/Chk2 signaling pathways which are shown to regulate Aurora B to delay midbody disassembly. An indirect effect of the Srs2/PARI signal on the abscission checkpoint can explain why in its absence abscission or midbody lifetime is not accelerated, which is commonly observed when depleting other components such as ATR/Chk1, ATM/Chk2, and CHMP4C.

Previous evidence suggests that abscission delay mediated by NoCut upon chromatin bridge formation prevents DNA damage in the following G1 of budding yeast (Amaral et al. 2016). In human cells, the abscission checkpoint has been shown to protect against premature resolution of chromatin bridges and DNA damage (Carlton et al. 2012; Sadler et al. 2018; Petsalaki and Zachos 2021a). A surprising observation that contradicts these studies, is that budding yeast and HeLa cells deficient in Srs2/PARI have longer-lasting chromatin bridges. Despite the delay in bridge resolution compared to Srs2-proficient cells, *srs2Δ* cells still resolve their bridges before abscission. In HeLa cells, the midbody lifetime does not appear to affect the time of bridge resolution as midbody disassembly occurs on average 20 hours earlier than bridge resolution. The cell cycle is not arrested to resolve chromatin bridges in HeLa cells. These bridges persist into interphase, whereas chromatin bridges in PARI-depleted cells resolve during mitosis. In all, this suggests that Srs2/PARI promotes the resolution of chromatin bridges. To assess if the bridge resolution is dependent on PARI expression during S and G2 we can express the nuclear envelope marker BAF in the HeLa stably expressing eGFP-PARI cell line. Further investigation is required to know if the bridge resolution delay in absence of PARI is physiologically important and if the PARI-dependent stabilization of the midbody is uncoupled from the abscission of the plasma membrane.

In conclusion, DNA helicase Srs2 has several human functional homologs, but PARI is implicated to be the most direct one. In this project, I found that Srs2/PARI is a component of the NoCut/abscission checkpoint, however, has a surprising dual-function in promoting chromatin bridge resolution.

List of Figures & Tables

Figure 1. Mitotic cell cycle progression in vertebrates	29
Figure 2. Mitotic spindle formation in <i>S. cerevisiae</i>	31
Figure 3. Cell cycle regulation by cyclins and CDKs	33
Figure 4. Cytokinesis in vertebrates	42
Figure 5. Cleavage furrow ingression mediated by Aurora B and Citron Kinase	44
Figure 6. ESCRT complexes drives abscission of the intercellular canal.....	48
Figure 7. Cytokinesis in <i>S. cerevisiae</i>	51
Figure 8. Topoisomerase II decatenates intertwined DNA	56
Figure 9. Triggers of the abscission checkpoint and the possible outcomes	65
Figure 10. Overview of Srs2's role in inhibiting homologous recombination repair ...	73
Figure 11. Srs2 and PARI protein domains	77
Figure 12. Srs2 delays abscission in HU-treated budding yeast	81
Figure 13. Srs2 delays abscission after topoisomerase II inactivation	84
Figure 14. Srs2 promotes chromatin bridge resolution.....	85
Figure 15. Srs2 reduces the frequency of RPA foci during chromosome segregation	86
Figure 16. The role of Srs2 in NoCut depends on its association with PCNA	89
Figure 17. Inhibition of topoisomerase II using ICRF-193 induces catenated chromatin bridges	92
Figure 18. Correlative light electron microscopy shows catenated chromatin bridges pass through the midbody during cytokinesis.....	95
Figure 19. Another human homolog of Srs2, FBH1 is dispensable for midbody stability in the presence of catenated bridges	96
Figure 20. Absence of PARI slightly delays cells in S phase and exit from mitosis ..	98
Figure 21. PARI promotes a delay in midbody disassembly in the presence of catenated chromatin bridges	99
Figure 22. Validation of siPARI-1 resistant PARI stably expressed in HeLa	102
Figure 23. Expression of siPARI-1-resistant eGFP-PARI rescues the delay caused by TOP2 inactivation.....	104
Figure 24. PARI promotes actin-patch accumulation at the intracellular bridge in cells with chromatin bridges.....	105
Figure 25. PARI is part of the Aurora B-dependent abscission checkpoint.....	106

Figure 26. PARI is dispensable for delaying midbody disassembly upon nuclear pore assembly defects	107
Figure 27. eGFP-PARI has a nuclear localization during interphase	109
Figure 28. PCNA is localized to the nucleus of cells in interphase.....	111
Figure 29. DNA synthesis is absent on catenated chromatin bridges	113
Figure 30. PARI is not required for the localization of Aurora B, pCHMP4C and VPS4 to the midbody.	116
Figure 31. Overexpression of nuclear membrane marker LAP2 β stabilizes the midbody in the presence of catenated chromatin bridges	118
Figure 32. The time of chromatin bridge resolution is independent from midbody disassembly	120
Figure 33. Chromatin bridge resolution is independent of midbody stability	122
Figure 34. PARI promotes eGFP-BAF bridge resolution before the next mitosis....	126
Figure 35. The number of 53BP1 foci remains unperturbed in PARI-depleted cells treated with ICRF-193.....	129
Figure 36. Loss of PARI improves cell survival after first cell division with a catenated chromatin bridge	131
Supplementary Figure 1. Gating strategy of eGFP-PARI	166
Supplementary Figure 2. CellProfiler pipeline to quantify the number of 53BP1 foci per nucleus	168
Table 1. <i>Saccharomyces Cerevisiae</i> strains used.....	151
Table 2. Human cell lines used.....	153
Table 3. siRNA sequences for gene knockdown	154
Table 4. Primer sequences for qPCR.....	156
Table 5. Antibodies used for western blot and immunofluorescence	157

List of Abbreviations

APH	Aphidicolin
ANCHR	Abscission/NoCut Checkpoint Regulator
BAF	Barrier-to-Autointegration Factor
Boi1 & 2	Bem1(One) Interacting Protein 1 & 2
CEP55	Centrosomal Protein of 55kDa
CLEM	Correlative Light Electron Microscopy
CHMP	Charged Multivesicular body Protein
CIN	Chromosomal instability
CPC	Chromosome Passenger Complex
EdU	5-Ethynyl-2'-deoxyuridine
ELG1	Enhanced Level of Genomic instability 1
ESCRT	Endosomal Sorting Complexes Required for Transport
FACS	Fluorescence-Activated Cell Sorting
FBH1	F-Box Helicase 1
HeLa K	Human cervical carcinoma from Henrietta Lacks, K stands for Kyoto
HU	Hydroxyurea
HR	Homologous Recombination
ICB	Intercellular Bridge
IF	Immunofluorescence
LAP2 β	LaminA Associated Polypeptide 2 β
NEBD	Nuclear Envelope Breakdown
NERDI	Nuclear Envelope Rupture During Interphase
NHEJ	Non-Homologous End Joining
NUP	Nucleoporin
NPC	Nuclear Pore Complex
mES cells	mouse Embryonic Stem cells
MKLP1	Mitotic Kinesin-Like Protein 1
MTOC	Microtubule Organizing Center
PARI	PCNA Interacting Recombination Inhibitor
PCNA	Proliferating Cell Nuclear Antigen
PIP	PCNA-Interacting Protein
PtdIns(3)P	Phosphatidylinositol-3-phosphate
RPA	Replication Protein A
RT	Room Temperature
RT-qPCR	Reverse Transcription quantitative Polymerase Chain Reaction
SIM	SUMO-interacting motif
SiR	Silicon Rhodamine
SUMO	Small Ubiquitin-like Modifier
SRS2	Suppressor of Rad Six 2
TSG101	Tumor-Susceptibility Gene 101
VPS4	Vacuolar Protein Sorting-associated protein 4
WB	Western blot
WT	Wild-type
YPDA	Yeast Peptone Dextrose Adenine

1. Introduction

The NoCut pathway (in the budding yeast *Saccharomyces cerevisiae*) or the abscission checkpoint (in animal cells) is a recently discovered signaling mechanism proposed to protect cells against the deleterious consequences of chromatin bridges during cytokinesis. In this study, I addressed whether the DNA helicase PARI, known to inhibit homologous recombination and DNA damage repair during S phase, also acts as a component of the abscission checkpoint in both yeast and human cells. In this introduction, I will summarize our current knowledge on chromatin bridge formation and resolution mechanisms, and on how the abscission checkpoint delays cytokinesis in the presence of a chromatin bridge. Therefore, I will first summarize the cell cycle, in particular cytokinesis and the checkpoints which govern cell cycle progression. In addition, I will also review various cell cycle processes in *S. cerevisiae*, as it laid the foundation to the current project, and some questions were explored using budding yeast as a model organism.

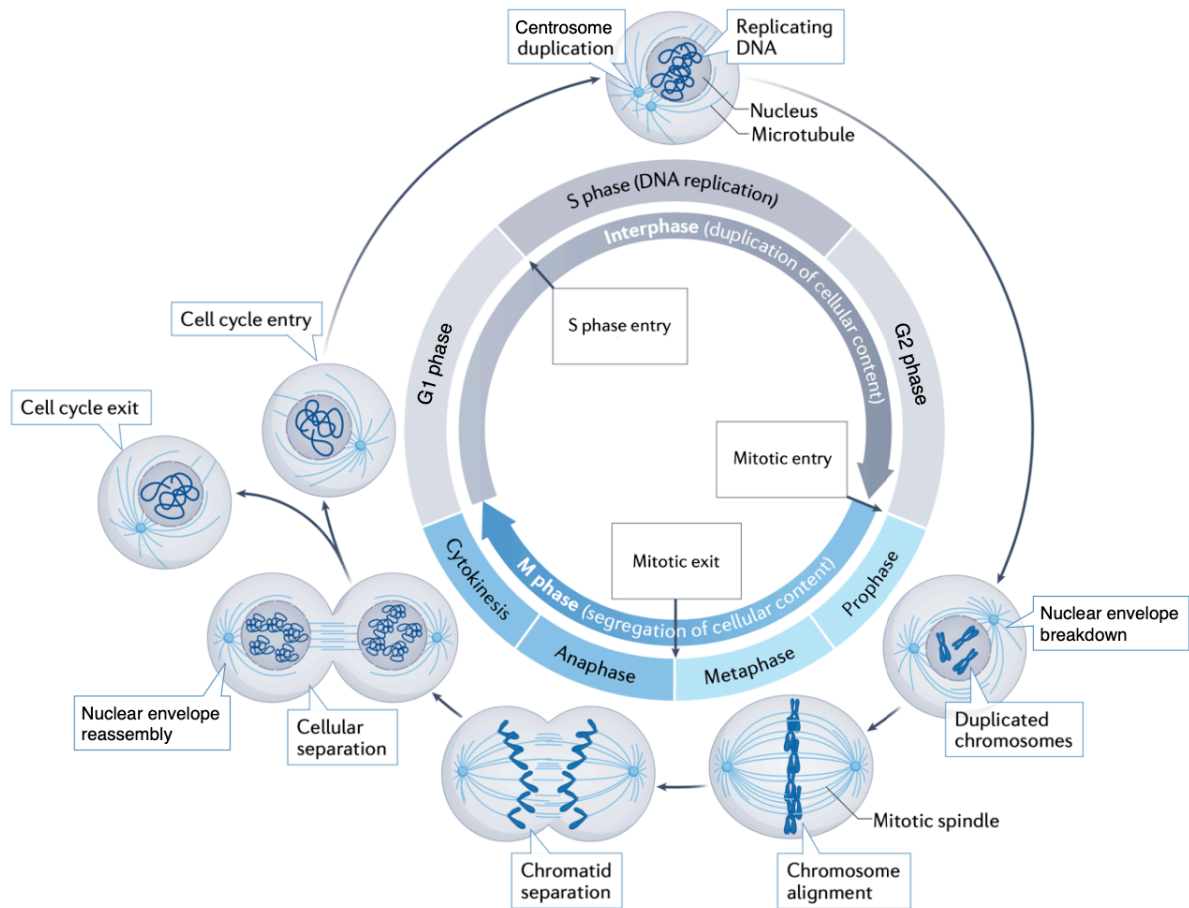


Figure 1. Mitotic cell cycle progression in vertebrates

A schematic drawing of a cell cycle in vertebrates with an open mitosis is shown. The mitotic cell cycle in vertebrates consist of two main phases; interphase in which the genome and cellular content of the cell is duplicated and is separated in M phase into two daughter cells. Interphase can be further divided into G1 (gap/growth 1) phase, S phase and G2 (gap/growth 2) phase. During G1, cells grow, repair possible DNA damage from the previous cycle and prepare for a new cell cycle entry. When the conditions are favorable cells pass the S phase entry and start replicating DNA and centrosome for M phase. G2 is another phase where cells prepare and ensure that genetic errors are not accumulating or propagating into M phase. M phase is divided into mitosis and cytokinesis, during mitosis the duplicated DNA condenses into chromosomes in prophase. Mitotic entry induces nuclear envelope breakdown which allows microtubules from the centromeres to access the chromosomes to align them at the equatorial plane during metaphase. Cells can only progress into anaphase when all chromosomes are properly attached to the mitotic spindle. Cells exit mitosis with the separation of the sister chromatids in anaphase. Following chromosome segregation, the nuclear envelope reassembles, and the cells are separated into two daughter cells in cytokinesis. Cells can either enter a new cell cycle or exit the cell cycle into G0 phase also known as quiescence. Figure reproduced with modifications from (Matthews, Bertoli and de Bruin, 2022) with permission under the license number 5379510528674.

1.1 Overview of the eukaryotic cell cycle

1.1.1 The phases of the cell cycle

The cell cycle is a series of events which are tightly regulated temporally and spatially to ensure complete duplication of the genome and accurate division of a cell into two daughter cells. There are two types of cell cycles in eukaryotic cells, the meiotic and the mitotic cell cycle. Meiosis and mitosis share many phases of the cell cycle, however, meiosis is a two-step process which produces four genetically different haploid gamete cells from one parental diploid cell. In contrast, the mitotic cell cycle generates two daughter cells that are genetically identical to their mother (haploid or diploid) (Figure 1). In this study I will focus on the mitotic cell cycle which is divided into two main phases; interphase where the cellular content is duplicated, and mitotic phase where the duplicated content is segregated into the daughter cells. Interphase is further divided into G1 (gap or growth phase 1), S (synthesis phase) and G2 (gap or growth phase 2). After G2, cells enter the M (mitotic) phase which consist of mitosis and cytokinesis. During mitosis, the chromatin is packed into chromosomes (prophase) which are aligned at the center of the cell (metaphase) and separated towards opposite poles (anaphase). Finally in cytokinesis, the cell separates into two identical nascent daughter cells.

It should be noted that the budding yeast *S. cerevisiae* undergoes a characteristic asymmetrical division producing a bud that is approximately one-third smaller than the mother cell (Figure 2). Another striking feature of the budding yeast is that it has a closed mitosis, the nuclear envelope does not disassemble upon mitotic entry. A G2 phase in the budding yeast is not well defined, as entry into mitosis can sometimes begin before replication is completed. The following section will first explore the general cell cycle with an open mitosis.

The duration of the cell cycle depends on the organism and cell type. For budding yeast in rich nutrients, the cell cycle lasts around 90 min, while the human cell cycle is on average 24 hours (Morgan 2007). Cells spend most of their time in G1 in preparation for a new cycle; the high rates of protein and RNA synthesis during G1 allow cells to grow in size and mass. In the early G1 phase, cells can also exit the replicative cell cycle and transition into a non-proliferative state called quiescence, or

G0. Once committed to initiate a new cycle, G1 is followed by S phase where the DNA content and microtubule organizing center (MTOC) are duplicated. MTOC, also known as the spindle pole body (SPB) in yeast and centrosome in human, is where microtubules emerge to form the mitotic spindle required for the separation of sister chromatids later in mitosis. After S phase cells enter the G2 phase, which is another period of cell growth and protein synthesis to prepare for mitosis. However, the budding yeast is an exception where there is no defined G2 phase between S phase and M phase (Morgan 2007).

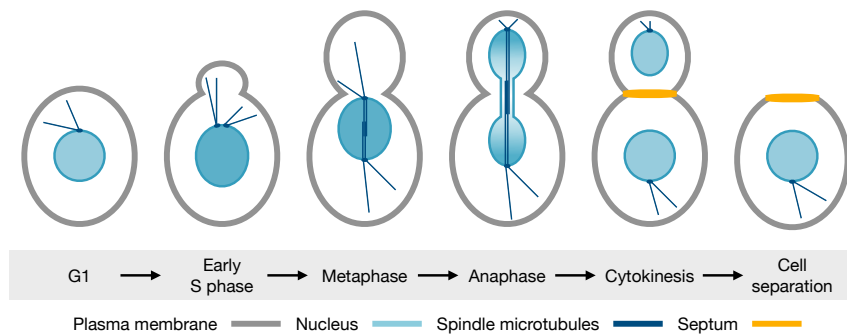


Figure 2. Mitotic spindle formation in *S. cerevisiae*

S. cerevisiae yeast divides asymmetrically with a closed mitosis which is defined by an intact nuclear envelope. In order to segregate the chromosomes, microtubules are nucleated from the spindle pole bodies (SBPs) into the cytoplasm and across the nucleus. Overlapping nuclear microtubules form the mitotic spindle. Cytoplasmic microtubules connect the nucleus to the cell cortex and aids in the positioning of the nucleus close to the bud neck during mitosis. The nucleus forms a dumbbell shape as the chromosomes segregate along the mother-bud-axis.

During DNA replication in S phase, the newly synthesized sister chromatids are held together by cohesins. Cohesin is a protein complex that takes the shape of a ring-like structure and links the sister chromatids at the centromeres and along the chromatid arms (Peters, Tedeschi, and Schmitz 2008). Entry into mitosis triggers the movement of the centrosomes to opposite poles and a dramatic reorganization of the chromatid structure. In a process called “condensation” chromatids are compacted up to 10,000-fold into the classic “X” chromosome shape by a complex called condensin (Morgan 2007). During replication of the double-helical DNA, supercoils arise ahead of the replication fork due to overwinding. Supercoils create torsion ahead of the replication fork, which can impede the DNA replication progress if left unchanged. Additionally, a second topological issue known as precatenanes can form behind the replication fork due to a compensatory underwinding which intertwines the newly replicated daughter

strands (Morgan 2007; Vos et al. 2011). Precatenanes can generate catenated DNA if the two adjacent replication forks collide. The formation of catenated DNA leads to extensive intertwining along the two duplicated DNA strands. A class of enzymes called DNA topoisomerase is responsible for resolving topological challenges during replication. Topoisomerase type I process supercoils by introducing a single-stranded break which allows the other strand to pass through the gap before it ligates the broken strand back together. Topoisomerase type II decatenates entangled double-stranded DNA behind replication forks and catenated DNA by introducing a double-strand break and passing the other double-stranded DNA through.

Topoisomerase II has also been implicated in aiding the organization of the DNA structure and the resolution of sister chromatids during mitosis (Hirano and Mitchison 1993; Toyoda and Yanagida 2006). In open mitosis, the nuclear membrane is disassembled allowing spindle microtubules to emerge from each of the centrosomes to capture the sister chromatid pairs at a protein structure assembled on the centromeres called the kinetochore. The kinetochores provide a platform for spindle microtubules to bind chromosomes and align them at the equator of the cell. The cohesion between the condensed sister chromatids is essential for the accurate bipolar orientation of each sister pair by the mitotic spindle during prophase. In the subsequent stage (anaphase), the sister-chromatid cohesion is cleaved, allowing the sister chromatids to move towards opposite poles of the cell. Following sister-chromatid segregation, the nuclear envelope reforms, and cytokinesis proceeds to complete the separation of two nascent daughter cells. Cytokinesis in yeast and vertebrate cells will be reviewed in detail in the next chapter.

In a closed mitosis, the SPBs are embedded in the nuclear envelope where they nucleate both cytoplasmic and nuclear microtubules (Figure 2). The separation of SPBs during S phase allows the formation of bipolar mitotic spindle across the nucleus (Winey and O'Toole 2001). The cytoplasmic microtubules facilitate the migration of the nucleus to the bud neck (Forsburg and Nurse 1991). Additionally, the cytoplasmic microtubules drive the correct spindle orientation together with dynein and align the mitotic spindle parallel to the mother-bud-axis (Segal and Bloom 2001). As in open mitosis, duplicated chromosomes are attached to microtubules by the kinetochores. However, budding yeast do not exhibit a clear metaphase chromosome alignment

during mitosis as in open mitosis systems (Carminati and Stearns 1997; Straight et al. 1997; Boettcher and Barral 2013). Despite not having the chromosomes aligned at a plane, budding yeast show a conserved movement of sister chromatids towards opposite poles. During anaphase the spindle elongates, pulling the sister chromatids apart and giving the nucleus a dumbbell shape.

1.1.2 Cell cycle regulation

The order and timing of the cell cycle are tightly regulated by a network of proteins called cyclins, and cyclin-dependent kinases (CDKs). The phosphorylating activity of CDKs changes throughout the cell cycle and depends on the direct interaction with cyclins. Different types of cyclins are expressed at different cell cycle stages, directing CDK phosphorylation and activation of cell cycle specific substrates. The binding of cyclin alone does not fully activate CDK, which requires additional phosphorylation by Cdk-activating kinases (CAKs). In contrast to cyclins, CAKs are abundant throughout the cell cycle and are not regulated in a cell cycle-dependent manner (Lolli and Johnson 2005). CDKs are also expressed at a constant level throughout the cell cycle. Whereas, cyclin protein levels “oscillate” during the cell cycle owing to cell cycle-dependent synthesis and degradation, the latter is dependent on cell cycle-regulated ubiquitylation (Arellano and Moreno 1997).

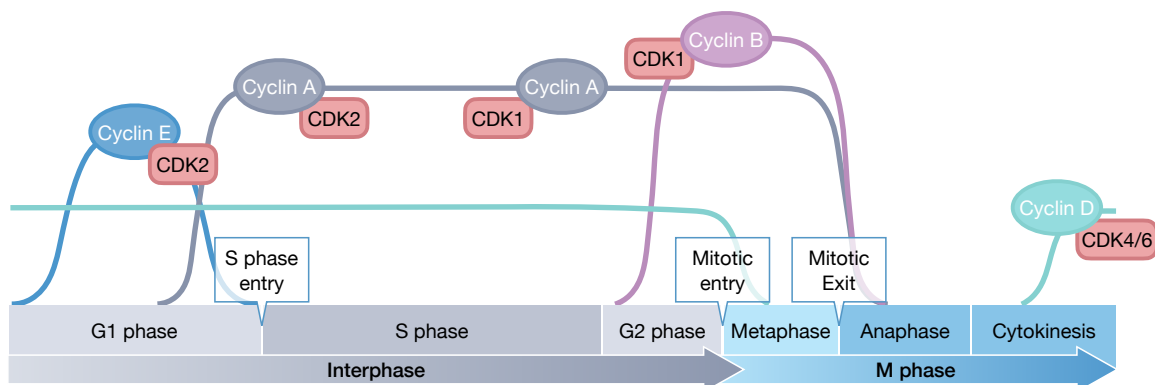


Figure 3. Cell cycle regulation by cyclins and CDKs

The cell cycle progression is tightly controlled by cyclins and CDKs to ensure that each phase only starts when the preceding one has been completed. S phase entry is prompted by the rapid increase of cyclin E-CDK2 which allows S phase specific genes to be expressed. One of those genes is cyclin A which together with CDK2 drive early S phase. Towards the end of S phase, M phase cyclins are expressed by the coupling of cyclin A to CDK1. The activation of CDK1 leads to a wide phosphorylation event of substrates which prepare cells for mitotic entry. The increased levels of cyclin B-CDK1 allows sister chromatid separation in anaphase and exit from mitosis into cytokinesis. During cytokinesis, cyclin D-CDK4/6 steadily increases and

promotes cell cycle re-entry in G1. Figure reproduced with modifications from (Matthews, Bertoli and de Bruin, 2022) with permission under the license number 5379510528674.

The budding yeast has one CDK (CDK1), whereas humans have four CDKs (CDK1-2, 4 and 6) (Morgan 2007). The successive expression of cyclins and the formation of distinct cyclin-CDK complexes contributes to a complex regulatory network which defines each cell cycle stage. During G1 phase the activity of Cyclin E (Cln1 and 2 in yeast) and its partner CDK2 quickly rises and drops in early S (Figure 3). CDK2 in a complex with cyclin E phosphorylates the retinoblastoma protein (pRB, Whi5 in yeast) which promotes its degradation. The degradation of pRB allows the transcription factor E2F to be released from its inhibitory state to activate and induce a set of genes essential for DNA replication. One of the genes expressed codes for cyclin E, which further amplifies CDK2 activity in a positive feedback loop. The high cyclin E-CDK2 activity drives the expression of cyclin A (Clb5,6 in yeast) which is required for initiating S phase and cell cycle entry. During S phase cyclin A associates with CDK2, replacing cyclin E to promote DNA replication and completion. In later stages of S phase, cyclin A binds to CDK1 which is thought to control the timing of mitotic entry by stabilizing and activating the complex of cyclin B (Clb1-4 in yeast) and CDK1 (De Boer et al. 2008). Once the cyclin B-CDK1 activity has reached a certain threshold, it triggers the mitotic entry by the phosphorylation of more than a thousand substrates of CDK1 (Morgan 2007).

Upon mitotic entry, CDK1 activates a set of mitotic kinases such as PLK1 (polo-like kinase 1), Citron K, the Aurora A and B kinases which further phosphorylate their substrates, in all, preparing the cell for mitosis (D'Avino 2017; Joukov and De Nicolo 2018). Aurora A plays an important role in early stages of mitosis in centrosome maturation and separation to form the mitotic spindle (Nigg 2001). Aurora B (Ipl1 in yeast) on the other hand interacts with the scaffolding protein inner centromere protein (INCENP), survivin and borealin to form the chromosomal passenger complex (CPC). In contrast to Aurora A which remains at the centrosomes and spindle poles, the CPC is recruited to the centromeres in early mitosis, where it has been shown to regulate chromosome structure, monitor the kinetochore-microtubule attachments and the spindle assembly checkpoint (Carmena et al. 2012). PLK1 plays a role in many

different processes during mitosis and are proposed to cooperatively regulate key processes with Aurora A and Aurora B (Joukov and De Nicolo 2018).

In parallel with the widespread phosphorylation of CDK1 substrates such as the mitotic kinases, the high cyclin B-CDK1 activity promotes the disassembly of the nuclear envelope. The dissolution of the nuclear envelope allows opposing microtubules to access the kinetochore of the sister-chromatid pairs and assemble the mitotic spindle. The mitotic spindle aligns the sister-chromatids at the center of the cell. To be able to transition from metaphase to anaphase the sister chromatids need to be able to separate towards opposite poles. However, after DNA replication the sister chromatids are linked along the arms and at the centromere by cohesin. To separate the sister chromatids at the metaphase-anaphase transition cohesin is rapidly cleaved by a protease called separase. When cells are not at the metaphase-anaphase transition, separase is prevented from cleaving cohesin by the association with the protein securin. The securin-separase complex is additionally maintained upon phosphorylation by the cyclin B-CDK1 complex.

The anaphase-promoting complex/cyclosome (APC/C) is an E3 ubiquitin-protein ligase that plays a vital role in the separation of the sister chromatids. The APC/C targets many substrates for ubiquitylation, but the two crucial targets are securin and S/M cyclins. Following metaphase, CDK1 phosphorylates APC/C subunits which enhances binding of the coactivator protein Cdc20 (or Cdh1) to APC/C (Gavet and Pines 2010; Fujimitsu, Grimaldi, and Yamano 2016). The activated APC/CCdc20 degrades securin, which releases separase to cleave cohesin that holds the sister chromatids together (de Gramont and Cohen-Fix 2005). At the same time APC/CCdc20 also degrades cyclin B, which reduces CDK1 activity thus promoting its' own inactivation. The rapid destruction of cyclin B allows a widespread dephosphorylation which triggers a series of events to separate the sister chromatids, and dividing the cell into two daughter cells that are reset to G1 (Matthews, Bertoli, and de Bruin 2022).

Lastly, Cyclin D-CDK4/6 (Cln3 in yeast) remains active throughout almost the whole cell cycle, except at mitotic exit when cyclin D is degraded by APC/CCdc20 (Alao 2007). Favorable conditions allow cyclin D-CDK4/6 to act as a primer to direct a new

cell cycle re-entry by preventing exit to G0 (Narasimha et al. 2014; Zerjatke et al. 2017).

1.1.3 Cell cycle checkpoints

Dividing cells rely on control mechanisms called “checkpoints” throughout the cell cycle which delays the progression until an earlier process has been completed. A delay mediated by a checkpoint is relieved by mutation or inhibition (Hartwell and Weinert 1989). However, the abolishment of a checkpoint can cause cell death, and the accumulation of genetic errors. The role of a cell cycle checkpoint is to monitor the integrity and fidelity of the major events of the cell cycle. There are several checkpoints in the cell cycle, the major ones are established at cell cycle phase transitions such as the G1/S checkpoint, to ensure that each phase occurs at the right time. Another type of checkpoint monitors a process detects the accumulation or propagation of genetic errors. All checkpoints arrest the cell cycle to prevent its progression until the conditions are met and recruit the appropriate repair machinery in the presence of damage.

A major checkpoint acts at the G1/S phase transition, which is when the cell commits to a new cycle but only after the environmental cues and internal signals which regulate cell size and growth rate are satisfied. Cells which are below the minimal size threshold and exhibit DNA damage do not achieve the requirements for start and can either be repaired for the DNA or are prevented from entering S-phase by exiting the cell cycle into a quiescent state. S phase has three main checkpoints: the replication checkpoint, intra-S checkpoint, and S/M checkpoint, which are triggered upon DNA damage during replication (Bartek, Lukas, and Lukas 2004). Interestingly, emerging evidence implicates that chromosomes can enter mitosis with unreplicated regions and unresolved DNA structures, suggesting that no checkpoint couples completion of DNA replication to the onset of mitosis (Moreno et al. 2016). Once committed, the expression of S-phase and M-phase cyclins drive the cell cycle progression through the next G2/M checkpoint. The G2/M checkpoint ensures that the DNA has been duplicated and that there is no accumulation of DNA damage. The entry into mitosis leads to reorganization of the chromatin into condensed chromosomes and the formation of the mitotic spindle. Activation of APC/CCdc20 drives progression into

anaphase which separates the sister chromatids. The third major checkpoint at the metaphase-anaphase transition arrests the cell cycle if the spindle microtubules are not properly attached to the kinetochores and thereby prevents defects in chromosome segregation.

Additionally, to the checkpoints at cell cycle phase transitions, there are many more checkpoints throughout the cell cycle that acts to monitor cell cycle events and protect the integrity of the genome. The NoCut/abscission checkpoint is one of these checkpoints which is proposed to inhibit cytokinesis if abscission is obstructed by chromatin and under-replicated DNA. The mechanism of the NoCut/abscission checkpoint is still actively being researched on and will be introduced in greater detail its own chapter. Here, I will summarize a few other well-established checkpoints.

1.1.3.1 DNA damage repair and checkpoint

Cells are constantly exposed to exogenous chemical agents or environmental factors that damage DNA. Endogenous metabolic processes including hydrolysis and alkylation are also common factors that can generate DNA damage. However, reactive oxygen species (ROS) released from metabolic processes is the most frequent source of endogenous DNA damage (De Bont and van Larebeke 2004). The main types of DNA lesions that arise are altered or missing nucleobases, single-strand breaks (SSBs), and double-strand breaks (DSBs). A SSB refers to a single nucleotide loss that occurs on one of the strands of the DNA double helix, and is usually accompanied by damaged 5'- and 3'- ends at the site of breakage (Caldecott 2022). DNA damages, in particular, SSBs and DSBs that are not repaired before replication result in fork collapse which leads to double-strand breaks in the DNA and loss of genetic material. While stalled replication forks caused by damaged nucleobases can be resolved they are unstable and at risk of collapse as well (Zeman and Cimprich 2014). Therefore, DNA damage must be detected early on and repaired to prevent genomic instability.

Sites of DNA damage recruit damage sensors which trigger a signal transduction pathway known as the DNA damage response pathway. The DNA damage response pathway consists of a network of sensors, transducers, and effectors. The damage signal is transmitted to various effector proteins, some of which lead to a damage-

induced transcription of genes involved in DNA repair, further enhancing the recruitment of DNA repair proteins to the site of damage. Others inhibit the cell cycle regulatory system leading to a cell cycle arrest until the damage has been repaired, this branch of the DNA damage response is also called the DNA damage checkpoint (Zhou and Elledge 2000). Most DNA lesions are rapidly repaired by damage-specific repair pathways. However, some damages can be extensive, for example when cells display DSBs and an accumulation of SSBs, or when the sister chromatid is not present to provide a template for error-free homologous recombination. These difficult-to-repair cases require the recruitment of one of the ataxia telangiectasia and Rad3-related (ATR) or ataxia telangiectasia mutated (ATM) kinases to orchestrate the DNA damage response pathway.

DSBs are recognized by the DNA damage sensor complex MRN (MRE11, RAD50, and NBS1) which triggers the ATM kinase to transduce a rapid signaling response. ATM phosphorylates mediators of DNA damage such as the p53 binding protein 53BP1, histone H2Ax, and breast cancer type 1 susceptibility protein (BRCA1) to amplify the response. One of the targets of ATM includes checkpoint kinase 2 (Chk2) which in turn phosphorylates the effector protein p53 to mediate cell cycle arrest and DSBs repair (Sulli, Di Micco, and d'Adda di Fagagna 2012). The repair of DSBs depends on the cell cycle stage. During G1, DSBs are repaired through the non-homologous end joining (NHEJ) pathway which does not require a homologous template. In NHEJ the DSB ends are stabilized by the Ku heterodimer consisting of Ku70 and Ku80, and the DNA-dependent protein kinase, catalytic subunit (DNA-PKcs) (Walker, Corpina, and Goldberg 2001). First, the broken ends are processed by nucleases to remove mismatched and damaged nucleotides. The processed ends are thereafter ligated back together by a specialized DNA ligase IV. The end processing makes NHEJ an error-prone pathway but is available throughout the cell cycle. However, in S and G2 the other sister chromatid is present and can be used for the error-free homologous recombination (HR) repair pathway which requires DNA end resectioning for its initiation.

During the other cell cycle phases, the Ku70/80 heterodimer is responsible for inhibiting resectioning of the DSB ends. Several proteins are involved in the DNA end resectioning (5'-3' strand degradation), most notably the MRN complex, BRCA1, and

the RecQ DNA helicase Bloom's syndrome (BLM, Sgs1 in yeast). DNA resection of the ends exposes single-stranded DNA, which is coated by the nucleoprotein replication protein A (RPA). RPA is the major ssDNA-binding protein and is required for normal replication progression and repair processes. RPA coats ssDNA of stalled replication forks and DNA resections to protect strands from degradation by nucleases. The accumulation of RPA on ssDNA activates the ATR kinase to phosphorylate checkpoint kinase Chk1. Chk1 mediates cell cycle arrest by the phosphorylation of phosphatase Cdc25 which prevents the downstream formation of cyclin B-CDK1 (Sanchez et al. 1997). Chk1 activation promotes the recruitment of the DNA repair protein RAD51 to DNA resections to replace the RPA-coating. RAD51 is assembled into a helical filament on ssDNA by the BRCA1-PALB2-BRCA2 complex (Prakash et al. 2015). The RAD51-ssDNA filament initiates homology search and strand invasion. Further steps in HR repair of DSBs are described in section 1.4.1.2. Activation of Chk1 at stalled replication forks triggers the S phase checkpoints and recruits appropriate repair proteins to aid either fork reversal or fork restart. The mechanisms of fork restart will be described in detail in section 1.4.1.1. In all, the recruitment of the checkpoint proteins Chk1 and Chk2 to the site of damage by ATR or ATM signaling pathway reinforces the link between checkpoint response and DNA damage.

1.1.3.2 Spindle assembly checkpoint

During mitosis, chromosomes are aligned at the center of the cell in a bipolar manner to prepare for chromosome segregation into new daughter cells. The process is initiated with kinetochore microtubules emerging from the opposite centrosomes/SPBs to attach to each sister kinetochore (amphitelic attachment). Premature segregation of the sister chromatids during mitosis is prevented by another major checkpoint called the spindle assembly checkpoint (SAC) which senses if only one of the sister kinetochores is attached to a spindle microtubule (monotelic attachment). The SAC, therefore, prevents segregation defects and aneuploidy by detecting chromosomes that do not have the proper bipolar attachment to the spindle microtubules during mitosis. In addition to monotelic attachments which normally occur during the process of chromosome bi-orientation, SAC is important for detecting incorrect attachments such as the attachment of polar microtubules to one sister kinetochore (syntelic

attachment). The lack of spindle microtubule attachment to the kinetochores triggers the SAC to inhibit APC/C activity by preventing Cdc20 co-activation until all chromosomes are bi-orientated and aligned at the equatorial plane. Specifically, a mitotic checkpoint complex (MCC) consisting of MAD2, BUBR1/Mad3, and BUB3, as well as Cdc20, binds to APC/C and inhibits it from degrading securin and cyclin B (Sudakin, Chan, and Yen 2001). The SAC machinery contains several other proteins, notably MAD1, the Aurora B kinase, and PLK1, which are required to amplify the signal (Kallio et al. 2002; Ditchfield et al. 2003). MCC and SAC proteins are concentrated at the kinetochores during prometaphase and maintain the checkpoint until every bipolar attachment of the sister kinetochores has been established (Musacchio and Salmon 2007). Once the kinetochore is occupied by a spindle microtubule, the SAC components are removed. The lack of SAC signaling leads to the disassembly of the MCC from APC/C allowing Cdc20 to activate APC/C for progression into anaphase (Matthews, Bertoli, and de Bruin 2022).

In addition to monitoring the interaction between microtubules and kinetochores, the SAC senses low tension across the sister kinetochores. When the sister kinetochores are properly bi-oriented, high tension is formed by the stretching of the centromeric chromatin. It is therefore proposed that sustained tension at the kinetochores is fundamental to identifying incorrect attachments and for the inactivation of SAC. The lack of tension, for example, when both sister kinetochores are attached by a single spindle pole, leads to an Aurora B-mediated destabilization of the microtubule-kinetochore attachment to correct for the mistake (Cimini and Degrossi 2005).

1.2 Cytokinesis

The term "cytokinesis" was coined in 1887 by the American zoologist Charles Otis Whitman (Whitman 1887), and combines the words "cyto" meaning cell, and "kinesis" meaning motion, to describe a cellular process in which the cytoplasm of the parental cell divides and become two daughter cells. Cytokinesis immediately follows mitosis and starts from anaphase and ends with a complete separation of the two daughter cells in a process called abscission. Mitosis and cytokinesis are two highly conserved cellular processes that must be tightly regulated spatially and temporarily to allow for faithful segregation of the genetic material.

1.2.1 Cytokinesis in vertebrate cells

Cytokinesis consists of two main processes; cleavage furrow ingression and abscission. Directly after anaphase, the cleavage furrow is ingressed to separate the nuclei and cytoplasm into two daughter cells which are connected by an intercellular canal (ICB) (Figure 4). Cleavage furrow ingression is followed by abscission which is a second ingression step at the ICB to physically separate the daughter cells. During mitosis, the kinetochore microtubules arrange the chromosomes in a bi-polar orientation. In parallel to mitotic spindle formation during mitosis, microtubules emerge from opposite centrosomes to overlap with each other at the center of the cell. These anti-parallel microtubule bundles remain after anaphase to form the central spindle. The central spindle provides a vital platform to recruit essential proteins for cytokinesis progression. One of the key complexes is the centralspindlin complex consisting of the kinesin motor protein MKLP1 and the Rho GTPase-activating protein MgcRacGAP. Centralspindlin is localized to the antiparallel microtubule bundles where it orchestrates critical processes of cytokinesis such as cleavage furrow ingression, midbody formation, and finally abscission. Although it is not known by which mechanism the centralspindlin is recruited to the central spindles, the Aurora B kinase has been implicated in its localization (White and Glotzer 2012).

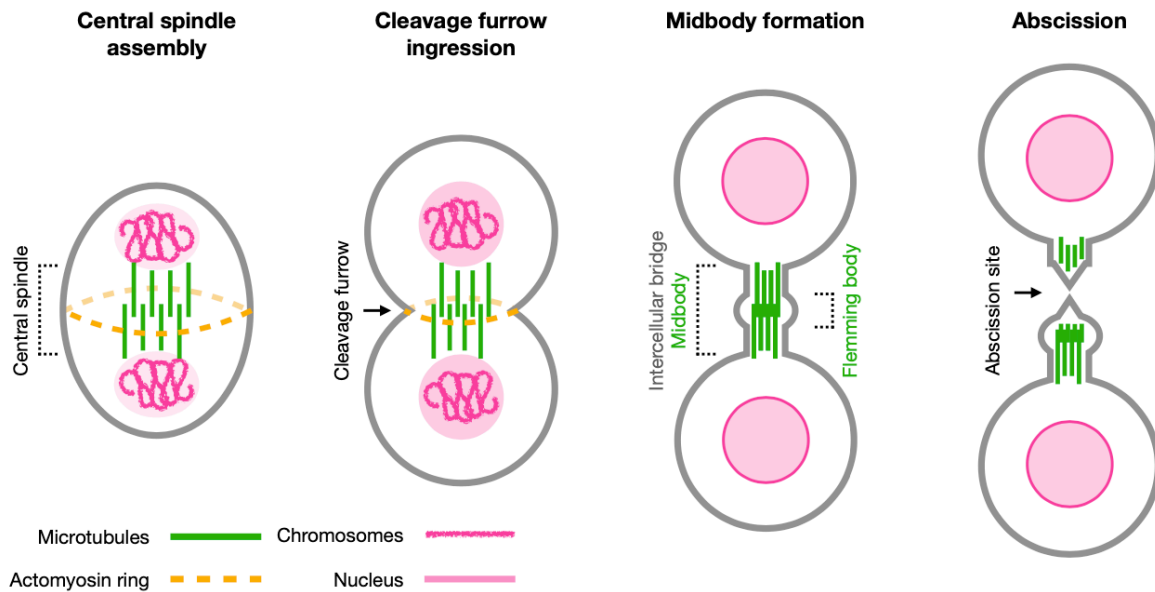


Figure 4. Cytokinesis in vertebrates

Cytokinesis immediately succeeds anaphase with the assembly of the central spindle. An actomyosin ring is formed around the equator of the cell (yellow dashed band). The drop in CDK1 activity at the metaphase-anaphase transition relocalize many kinases and proteins at the central spindle microtubules (green) to aid in its assembly and maturation. The actomyosin ring will contract leading to ingression of the cleavage furrow and the formation of a dense bundle of microtubules called the midbody. The midbody acts as a platform for many protein complexes involved midbody disassembly, F-actin clearance and abscission of the intercellular bridge to separate the two daughter cells.

1.2.1.1 Cleavage plane determination and actomyosin ring contraction

During anaphase, a ring structure consisting of actin filaments and myosin II called the actomyosin ring assembles around the equator of the dividing cell (Figure 5). The cleavage plane positioning is determined by two signals, one by the central spindle which distributes and concentrates the small GTPase RhoA at the equatorial cortex, and a second signal in which stable spindle asters inhibit RhoA activity close to the spindle pole (Foe and von Dassow 2008). The mechanism of how the spatial signal from the central spindle is transmitted to the equatorial cell cortex to establish the cleavage plane is not fully understood, although communication through MKLP1 and actin filaments has been suggested (Fededa and Gerlich 2012). RhoA is activated by guanine exchange factor ECT2 which is targeted to the central spindle via the interaction with MgcRacGAP (Burkard et al. 2009). The direct interaction between ECT2 and MgcRacGAP is mediated by PLK1 phosphorylation of MgcRacGAP. A drop in CDK1 activity during the metaphase-anaphase transition allows a fraction of the

central spindle associated ECT2 to translocate to the cleavage plane and establish local RhoA activity (Su, Takaki, and Petronczki 2011).

Once activated at the determined cleavage plane, RhoA promotes the assembly of the actomyosin ring by first stimulating nucleation of unbranched actin filaments, and second by activating the myosin light chain kinase ROCK, in addition to inhibiting the counteracting myosin phosphatase MYPT (Matsumura 2005). RhoA additionally recruits the scaffolding proteins formin and anillin to the equatorial cortex. Anillin can bind to actin, myosin, RhoA, and MgcRacGAP providing a link between the cortex and central spindle (Figure 5) (Fededa and Gerlich 2012).

Following its assembly, the actomyosin ring contracts and further constricts the cleavage furrow and initiates the start of the last phase of the cell cycle, cytokinesis. Despite its central function in initiating cytokinesis the mechanism by which forces are generated to contract the actomyosin ring is poorly understood (Cheffings, Burroughs, and Balasubramanian 2016). Nonetheless, the actomyosin ring facilitates the ingression of the cleavage furrow, transforming the spindle midzone into an intercellular bridge (ICB) which separates the nuclei into two daughter cells (Figure 4). The furrow ingression further constricts the central spindle microtubules at the midzone into a bundle termed the midbody. An electron-dense structure is formed in the middle of the midbody where the antiparallel microtubules meet, called the Flemming body. The Flemming body acts as an anchor for the ingressed cleavage furrow (Steigemann and Gerlich 2009). The complete assembly of the midbody serves as a platform for the dynamic remodeling of the cytoskeleton and plasma membrane at the cleavage plane, and the recruitment of endosomal sorting complexes required for transport (ESCRT) machineries involved in membrane traffic and the final scission of the midbody and ICB (Frémont and Echard 2018).

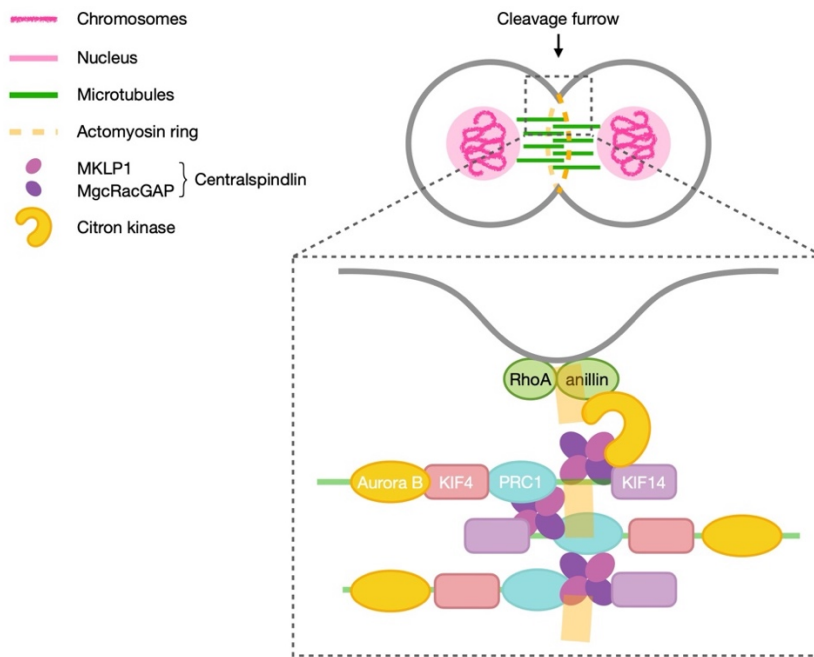


Figure 5. Cleavage furrow ingression mediated by Aurora B and Citron Kinase

Simplified illustration of the central spindle assembly. The central spindle functions as a platform during cytokinesis to recruit proteins which links the spindle microtubules to the cell cortex for cleavage furrow ingression and midbody assembly (see Figure 4). The presence RhoA and anillin at the cleavage plane establishes where the actomyosin ring will form and constrict the membrane. Aurora B (CPC complex) mediates spindle stability through kinesin motor protein KIF4, which interacts with the PRC1 kinase. Citron kinase interacts with PRC1, kinesin motor protein KIF14 and centralspindlin complex (tetrad of MKLP1 kinase and MgcRacGAP dimer pair) are associated with the spindle microtubules to assemble and maintain the central spindle. Citron kinase connects the spindle to the cortex by interacting with centralspindlin and anillin.

1.2.1.2 Central spindle assembly and midbody formation

The high CDK1-cyclin B activity during early mitosis prevents cytokinesis from taking place by inhibiting the initiation of central spindle assembly. However, the rapid decrease in CDK1 activity at the metaphase-anaphase transition leads to the dephosphorylation of multiple central spindle components involved in central spindle assembly. These include the CPC and the mitotic kinesin motor protein MKLP2 which are co-translocated from the centromeres where it was sequestered during metaphase to the microtubule plus ends of the central spindle (Hümmer and Mayer 2009). The centralspindlin complex is localized to the antiparallel microtubules by the phosphorylation of Aurora B to initiate the central spindle assembly (Mishima et al. 2004; Neef et al. 2006). PRC1, a microtubule-associated protein that was previously

held in its inactive monomeric state, is now able to form homodimers and facilitate the spatiotemporal organization of antiparallel microtubules into ordered bundles (Zhu et al. 2006).

The centralspindlin complex orchestrates the bundling of the microtubules and the ingression of the cleavage furrow through the interaction with the actin cytoskeleton. This provides a connection between the spindle microtubules with the cortex, which is further stabilized by Aurora B phosphorylation (Guse, Mishima, and Glotzer 2005; Basant et al. 2015). Additionally, Aurora B controls the length of the central spindle by recruiting the kinesin motor proteins KIF4A and KIF2A to the distal plus ends of microtubules which prevents further microtubule growth at the overlaps (Bieling, Telley, and Surrey 2010; Uehara et al. 2013). Phosphorylation of KIF4 by Aurora B promotes interaction with PRC1 which together slows down microtubule growth, and stabilizes the central spindle (Nunes Bastos et al. 2013).

The actomyosin ring continues to constrict the cleavage furrow until it has completely ingressed to a diameter of approximately 1-2 μm before the ring disassembles (Mierzwa and Gerlich 2014). Actomyosin ring disassembly depends on the inactivation of RhoA by the Protein Kinase C epsilon (PKC ϵ) and the adaptor protein 14-3-3 (Saurin et al. 2008). The two daughter cells remain connected through the intercellular canal (ICB) which contains the midbody formed from the central spindle (Figure 4). The formation of the midbody concentrates many components of the central spindle assembly into distinct regions of the midbody. The centralspindlin components MKLP1 and MgcRacGAP, and the RhoA activator ECT2 remain where the microtubules overlap and form a "midbody ring" structure in the middle of the Flemming body. PRC1 and KIF4 were observed on either side of the midbody ring, while MKLP2 and Aurora B flank the midbody arms next to the Flemming body (Hu, Coughlin, and Mitchison 2012). In contrast to Aurora B, the other major kinase during mitosis and cytokinesis, Citron K, is localized at the midbody ring. Citron K interacts with RhoA and anillin, further providing mechanistic stability of the ingressed cleavage furrow between the cortex and the microtubules in the Flemming body via MKLP1, PRC1, and kinesin motor protein KIF14 activity (Figure 5) (Gai et al. 2011; Watanabe et al. 2013; Bassi et al. 2013).

1.2.1.3 ESCRT and membrane trafficking

Proteins and complexes that are associated with midbody disassembly and abscission of the ICB are recruited to the midbody, such as the major membrane remodeling complexes ESCRT (endosomal sorting complexes required for transport). The ESCRT pathway consists of five core components: the ESCRT I-II-III subcomplexes, Bro1 domain protein ALIX and the AAA ATPase VPS4. Together, the ESCRT complexes and components participate in membrane remodeling by driving membrane sealing or scission throughout the cell. Membrane remodeling occurs in two directions relative to the cytoplasm, forming tubes or vesicles that are either inside-out containing cytoplasm or outside-in excluding cytoplasm. Membrane remodeling events by ESCRT machinery are initiated by site-specific adaptors that recruit ALIX, ESCRT-I, and ESCRT-II. The assembly of ALIX, ESCRT-I, and ESCRT-II at the bud neck allows the recruitment and nucleation of ESCRT-III. The formation of spiraling membrane-bound ESCRT-III filaments in cooperation with VPS4 promotes constriction of the membrane (Mierzwa et al. 2017). The ESCRT machinery has been implicated in various biological processes such as endosomal vesicle and multivesicular body formation, nuclear membrane resealing, viral budding, and abscission (Carlton and Martin-Serrano 2007; Henne, Stenmark, and Emr 2013; Olmos et al. 2015).

To complete cytokinesis, the two daughter cells are physically abscised at the ICB by the ESCRT machinery (Figure 6). Before abscission proceeds, cytoskeletal structures such as F-actin and microtubules in the ICB must be removed to allow the ESCRT machinery to constrict the plasma membrane (Mierzwa and Gerlich 2014). Membrane trafficking has a crucial role in this local remodeling. During cleavage furrow ingression, the local plasma membrane undergoes a major lipid remodeling to increase the cell surface, leaving the ICB enriched in specific class lipids, in particular the phosphoinositide $\text{PtdIns}(4,5)\text{P}_2$. Interestingly, despite the enrichment of $\text{PtdIns}(4,5)\text{P}_2$, this lipid is not required for furrow regression (Echard 2012). Rather $\text{PtdIns}(4,5)\text{P}_2$ plays an essential function after the ingression to promote ICB stability by stimulating F-actin accumulation (Emoto et al. 2005; Dambournet et al. 2011). However, F-actin needs to be removed from the ICB at later stages of cytokinesis to allow abscission. The endosome-associated GTPase Rab35 contributes to a targeted delivery of the $\text{PtdIns}(4,5)\text{P}_2$ 5-phosphatase Oculo-Cerebro-Renal syndrome of Lowe

(OCRL) to the ICB cortex where it hydrolyses $\text{PtdIns}(4,5)\text{P}_2$ and prevents F-actin accumulation. Additionally, Rab35 recruits and activates MICAL1 which depolymerizes F-actin through oxidization (Frémont et al. 2017). The removal of F-actin in the ICB is essential for ESCRT-III recruitment to the abscission site, and functions to constrict and complete abscission.

1.2.1.4 Midbody disassembly and abscission of the intercellular bridge

The decrease in CDK1 activity at the metaphase-anaphase transition, allows the Chromosome Passenger Complex (CPC) to relocalize to the central spindle microtubules and later remain on the midbody flanking the Flemming body. The CPC known as the "master controller" plays both positive and negative roles in coordinating each process during cytokinesis. Initially, the CPC promotes the stabilization of the central spindle, maturation of the contractile ring, and cleavage furrow ingression (Carmena et al. 2012). Subsequently, at the midbody, Aurora B plays an essential role in regulating abscission timing. In the presence of lagging chromosomes, chromatin bridges, and defective nuclear pore assembly Aurora B acts as an inhibitor of abscission, delaying complete cytokinesis as a crucial part of the abscission checkpoint (Steigemann et al. 2009; Mackay, Makise, and Ullman 2010; Janssen et al. 2011). This inhibitory role of Aurora B kinase involves the phosphorylation of ESCRT-III subunit CHMP4C, which prevents an ESCRT-III mediated constriction from abscising the ICB in an abscission checkpoint-dependent manner (Carlton et al. 2012; Capalbo et al. 2012).

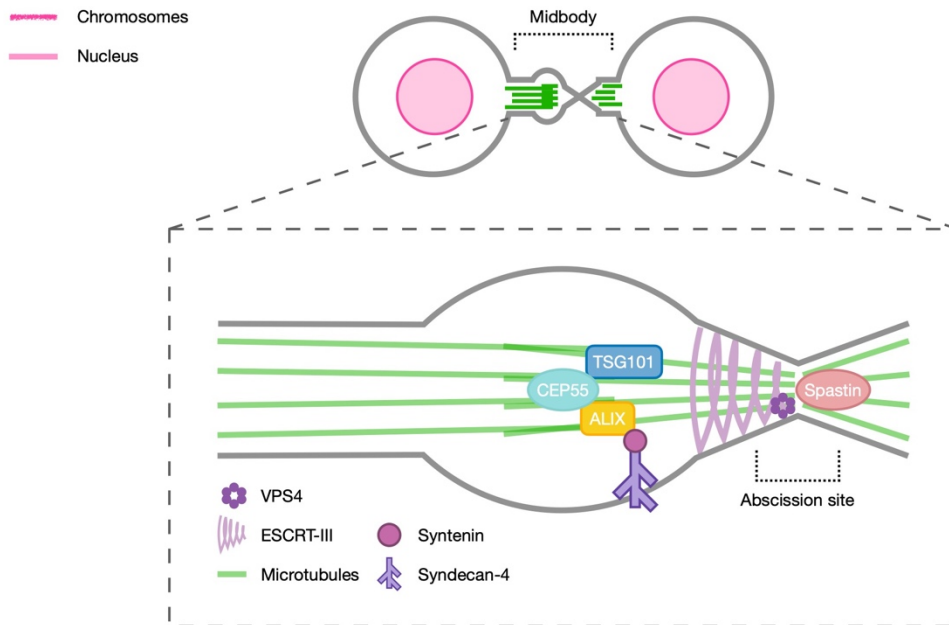


Figure 6. ESCRT complexes drives abscission of the intercellular canal

Simplified illustration of ESCRT components involved abscission of intercellular canal (ICB). After the formation of the midbody, CEP55 is localized to the center of the midbody where it recruits TSG101 (ESCRT-I component) and ALIX to the midbody. ALIX-interacting syntenin and downstream syndecan-4 couple the plasma membrane to ESCRT. TSG101 and ALIX can independently recruit ESCRT-III, which together with the ATPase VPS4 forms a spiral anchored to the membrane and constricts the ICB. In parallel, the microtubule-severing enzyme Spastin disassembles the midbody at the abscission site to allow plasma membrane constriction.

The recruitment of the ESCRT machinery to the ICB, and thereby abscission is inhibited by the Polo-like kinase 1 (PLK1) until the assembly of the midbody. PLK1 is a conserved protein kinase involved in regulating mitosis and cytokinesis. During metaphase PLK1 it is localized to centrosomes and kinetochores to ensure that a proper bipolar mitotic spindle is formed (Sumara et al. 2004). Later in anaphase PLK1 relocates to the central spindle and activates Rho-GTPase regulators to initiate cleavage furrow ingression and actomyosin contractility (Figure 6) (Petronczki et al. 2007). Active PLK1 phosphorylation during mitosis prevents the abscission factor CEP55 from its untimely localization to the spindle microtubules. However, as the cell progresses into the final stages of mitosis PLK1 is slowly degraded by APC/CCdc20, releasing CEP55 to eventually be recruited to the midbody by MKLP1 (Bastos and Barr 2010). At the midbody, CEP55 recruits the ESCRT-I subunit TSG101 and ALIX to initiate the assembly of the abscission machinery (Carlton and Martin-Serrano 2007; Carlton, Agomayor, and Martin-Serrano 2008). TSG101 establishes an ESCRT-I-

ESCRT-II-CHMP6 pathway that targets ESCRT-III subunits, notably CHMP4B and CHMP1B to the midbody (Agromayor et al. 2009; Elia et al. 2011). In parallel, ALIX can directly interact with CHMP4B to recruit ESCRT-III subunits to the midbody (Christ et al. 2016). Additionally, the recruitment of CHMP4C to the midbody is dependent on ALIX (McCullough et al. 2008; Christ et al. 2016). A recent proteomics of post-abscised midbodies identified new candidate regulators of abscission (Addi et al. 2020). Notably, the transmembrane protein syndecan-4 and associated protein syntenin couple the plasma membrane to ESCRT through the interaction with ALIX (Figure 6). Furthermore, the ALIX/syntenin/syndecan-4 axis is required for the proper localization and enrichment of CHMP4B at the midbody, and thus abscission (Addi et al. 2020). The telomere-associated, and nuclear membrane protein AKTIP is another recently discovered protein which plays a role in abscission by acting in parallel to TSG101 to recruit CHMP4B and another essential ESCRT-III component IST1 to the midbody (Merigliano et al. 2021).

During the final stages of abscission, the microtubule-severing protein Spastin is targeted to the late ICB by CHMP1B and IST1 to disassemble the midbody and facilitate ICB clearance for the ESCRT-III-mediated abscission machinery (Figure 6) (Yang et al. 2008; Connell et al. 2009; Renvoisé et al. 2010). Furthermore, IST1 plays an essential role in abscission as a component of the ESCRT-III machinery, interacting with notably CHMP1A/B and AAA+ ATPase VPS4 (Agromayor et al. 2009; Bajorek et al. 2009). The ICB is narrowed down on each side of the Flemming body forming two adjacent constriction sites, indicating that abscission will follow, although the mechanism determining which of the sides will be abscised is not known. The ESCRT-III machinery assembles into 17 nm filament helices extending away from the Flemming body to further constrict the ICB. As the ESCRT-III filament helix assembles, the AAA+ ATPase VPS4 induces dynamic growth and shrinkage of the filaments, facilitating constriction (Elia et al. 2011; Mierzwa et al. 2017).

Interestingly, the ESCRT-III subunit CHMP4C is not essential for the constriction of the ICB but as we shall see, plays a vital role in the Aurora B-mediated abscission checkpoint (Capalbo et al. 2012; Carlton et al. 2012). A recent study of Cep55 in Cep55-knockout mice showed that Cep55 and ESCRT-III are dispensable for cytokinesis of most mouse cells except primary neural progenitors (Tedeschi et al.

2020). This suggests that Cep55 and the ESCRTs might only be essential for abscission in a tissue-specific manner.

1.2.2 Cytokinesis in budding yeast

In contrast to vertebrates, the cleavage plane in budding yeast is already determined in G1 (e, Chew, and Balasubramanian 2009). This ensures that the right axis of cell polarization is achieved in coordination with the growth of a new bud. Septins are filament-forming proteins and are recruited to the presumptive bud site during early G1 where they assemble into a cortical ring (Figure 5) (Wloka and Bi 2012). The septin ring forms an hourglass-like structure in the early S phase and later splits into two separate rings flanking the actomyosin ring upon signaling by a kinase cascade known as the mitotic exit network (MEN) (Lippincott et al. 2001).

Cytokinesis in budding yeast is mechanically similar to vertebrates and is partially driven by the actomyosin ring contraction stimulated by Plk1 and the accumulation of Rho1 (RhoA in humans) at the bud neck. Interdependently, a new cell wall forms, termed the primary septum, between the mother and the daughter bud (Figure 7). The actomyosin ring contraction is considered to drive plasma membrane ingression, while the primary septum formation provides stability during constriction and separates the mother and daughter cells. In budding yeast, the actomyosin ring is assembled sequentially with the cell cycle progression starting at late G1 by the localization of Myo1 (myosin type II) to the septin ring (Fang et al. 2010). Only in late anaphase is F-actin recruited to the bud neck to assemble into a functional contractile ring Myo1 (Fang et al. 2010). During cytokinesis, the bud neck undergoes tremendous membrane remodeling which requires targeted delivery of vesicles. Through polarized actin cables towards the bud neck, secretory vesicles, and cargoes containing enzymes, notably Chs2 (chitin synthase 2) are delivered to promote cytokinesis (Bi and Park 2012). The primary septum is formed between the two layers of plasma membrane and is composed of chitin that is synthesized locally by Chs2. The faithful timing of primary septum formation at cytokinesis is regulated by Cdk1 phosphorylation. During mitosis, Chs2 is sequestered at the ER until the declining Cdk1 activity at metaphase-anaphase transition which releases it to the secretory pathway to be delivered to the bud neck (Chin et al. 2012).

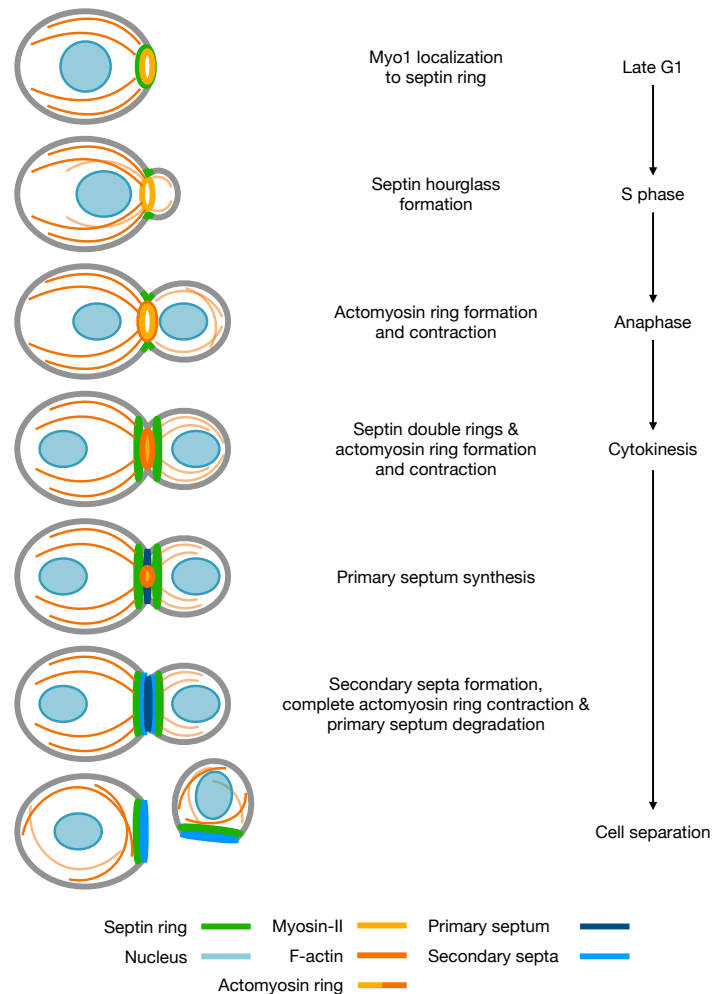


Figure 7. Cytokinesis in *S. cerevisiae*

S. cerevisiae divides asymmetrically, therefore the mother-bud-axis is determined in early G1 by the formation of a septin ring (green) which also marks the site of cytokinesis. The myosin type-II Myo1 (yellow) is recruited to the septin ring in late G1 and is joined by F-actin (orange) during S phase to form the actomyosin ring required for membrane ingression at the bud neck. The septin ring takes the shape of an hourglass which splits into two flanking rings surrounding the actomyosin ring. As the actomyosin contracts the primary septum (dark blue) is formed at the bud neck followed by the synthesis of the secondary septa (light blue). The primary septum is degraded which leads to the separation of the mother and daughter cell. Figure reproduced with modifications from (Wloka and Bi, 2012) with permission under the license number 5378351154316.

Following primary septum formation, two secondary septa are synthesized on each side of the primary septum (Figure 7). After its maturation, the primary septum is cleaved across the bud neck and parts of the secondary septa are degraded, leading to cell separation (Yeong 2005; Lesage and Bussey 2006). The remaining secondary septum on the mother defines the bud-scar and the birth-scar on the daughter cell.

The position of the scar determines a budding pattern and marks the site where the next budding will be established (Slaughter, Smith, and Li 2009).

In budding yeast, the ingression of the cleavage furrow and the abscission of the plasma membrane have to be coordinated with the formation of the primary septum and the secondary septa. The Inn1 protein was initially implied to link the actomyosin ring contraction to the ingression of the plasma membrane by interacting with the SH3 protein Hof1, a component of the actomyosin ring. Heat-inducible degradation of Inn1 did not prevent actomyosin ring contraction but caused failure to ingress the plasma membrane (Sanchez-Diaz et al. 2008). However, in a different study Inn1 was shown to not depend on the actomyosin ring contraction. Instead, Inn1 was shown to interact with Hof1 and another SH3 protein Cyk3 to promote primary septum formation by activating Chs2, which allows actomyosin ring contraction and membrane ingression (Nishihama et al. 2009).

The precise mechanism of abscission in yeast remains diffuse but is thought to depend on the formation of the secondary septa. Whose timing is regulated by Cyk3 which can temporarily inactivate Rho1 during membrane ingression to prevent premature formation of the secondary septa. Cyk3 most likely disassociates from Rho1 to promote secondary septa formation and abscission (Onishi et al. 2013). In parallel to Cyk3 function, the secondary septa formation is also inhibited by the small GTPase Cdc42. However, the inhibitory activity of Cdc42 drops in cytokinesis which is mediated by the upstream Cdc5/Polo kinase, allowing abscission to occur.

In both budding yeast and vertebrate cells, cytokinesis consists of cleavage furrow ingression followed by abscission to separate the daughter cell. Although the morphology of cells progressing through cytokinesis takes different shapes depending on the organism, the fundamental processes are highly conserved. From central spindle determination, actomyosin ring contraction, cleavage furrow ingression, and stabilization of the cleavage plane for abscission.

1.3 Anaphase bridges

1.3.1 Anaphase bridge formation

Chromatin bridges were first observed in maize after an X-ray treatment, where broken chromosome ends fused to each other, generating a dicentric chromosome. In the following anaphase, the dicentric chromosome is pulled towards opposite poles forming a chromatin bridge (McClintock 1941). Chromatin bridges arise from many different processes primarily failing to topologically separate entangled DNA stands, decondensed or catenated chromatin from each other. Another source of bridge formation is defects associated with an aberrant mitotic progression such as defective SAC or the segregation of acentric or dicentric chromosomes.

Chromatin bridges are defined as a strand of chromatin that is stretched out between two dividing daughter nuclei. In contrast to ultrafine bridges (UFB), which lack histones and cannot be resolved with conventional DNA binding dyes (Chan, North, and Hickson 2007), chromatin bridges can be easily observed through microscopy with dyes such as DAPI and Hoechst or using antibodies against histone 2B. Chromatin bridges and UFBs are collectively called anaphase bridges. Protein perturbations, and topoisomerase II inhibitors such as ICRF-193 induce the formation of both types of bridges, suggesting that chromatin bridges and UFBs can originate from the same type of DNA substrate and region but differ in how and when they are resolved (Germann et al. 2014). It also argues that UFBs can derive from chromatin bridges by "dechromatization", according to the time of resolution. However, a chromatin bridge has rarely been observed to have turned into a UFB or vice versa, indicating the fate of a potential DNA structure is determined before anaphase onset (Germann et al. 2014). UFBs but not chromatin bridges are formed by exposure to DNA replication inhibitors such as hydroxyurea (HU) and aphidicolin (APH) in human cells, suggesting that UFBs additionally have a distinct origin from chromatin bridges which is caused by replication stress (Chan et al. 2009). Several studies have tried to elucidate the different origins of anaphase bridges, which I will summarize in this section.

1.3.1.1 Incomplete replication and unresolved recombination

S phase is tightly regulated to ensure that the genome is faithfully replicated. However, certain regions of the genome due to their important structural function are more difficult to replicate and are thereby more susceptible to remain unreplicated or contain unresolved recombination intermediates into mitosis, particularly after conditions of replication stress (e.g., exposure to APH). Common fragile sites (CFS), are chromosomal regions that are prone to gaps and breaks upon replication stress. In unperturbed conditions, these sites often display incomplete replication, or late-replication intermediates (LRI) (Chan et al. 2009). The telomere is another specialized structure at the end of the chromosome that consists of repeated DNA sequences that are prone to form a secondary DNA structure called G-quadruplexes. The presence of telomere-binding proteins and G-quadruplexes disrupts progressive DNA replication causing the telomeres to exhibit LRI due to frequent replication fork stalling (Barefield and Karlseder 2012).

Stalled replication forks due to DNA lesions during S phase can be repaired by homologous recombination (HR), in particular through the template switch (TS) pathway. Recombination intermediates occur as double Holliday junctions are formed between the sister strands during HR repair. Failure to resolve Holliday junctions before anaphase provides another source of interlinked sister chromatids and anaphase bridge formation during chromosome segregation. However, compared to LRIs that originate from CFS and telomeres, it is not known whether anaphase bridges that stem from unresolved recombination intermediates originate from a distinct chromatin region. LRIs are structurally similar to recombination intermediates which form a hemicatenane structure. A hemicatenane consists of two double-strand helices that are joined through the catenation of one strand from each the of helices. Due to the structure similarity both recombination intermediates and LRIs can be unwound by the same Bloom's complex despite different origins (Mankouri, Huttner, and Hickson 2013).

The Bloom's complex (also abbreviated as BTR) consists of the DNA helicase BLM, topoisomerase type IA TOPOIII α and the oligonucleotide binding proteins RMI1 and RMI2. The RecQ DNA helicase BLM (Bloom syndrome protein) is an essential DNA

helicase for HR repair, as well as a common marker of UFBs. BLM is recruited to persisting DNA linkages originating from incomplete replication and unresolved recombination intermediates as part of the BTR complex. The processing of UFBs by BTRR reveals ssDNA that is coated with RPA and eventually broken during mitosis (Chan, Fugger, and West 2018). This suggests that bridges originating from issues during replication have the potential to become pathological in anaphase.

The BTR complex was initially shown to suppress catenated and hemicatenated bridges that frequently linked centromeric DNA during replication (Chan, North, and Hickson 2007; Mankouri, Huttner, and Hickson 2013). Recently, it was suggested that the BTR complex senses increased RPA-ssDNA complexes during DNA replication stress and associates with the replication fork to restart replication (Shorrocks et al. 2021). Exactly how the temporal activities of the BTR complex are regulated is unclear. However, the loss of the BLM is correlated with elevated levels of anaphase bridges and lagging chromosomes suggesting inefficient resolution of HR intermediates (Chan North Hickson 2007) (Chan, North, and Hickson 2007). In yeast, the replication and repair factor Dpb11 (hTopBP1) is localized to chromatin bridges, while UFBs are additionally decorated with the DNA helicase Sgs1 and the type IA DNA topoisomerase Top3 (hBLM-hTOPIII α), and the ssDNA-binding complex RPA. The depletion of Dpb11 leads to an increase in chromatin bridges and shorter UFBs. Thus, it has been proposed to both suppress the formation of chromatin bridges by inhibiting HR initiation and promote the stability and resolution of UFBs (Germann et al. 2014). In all, showing that the failure to resolve recombination intermediates at difficult-to-replicate regions is strongly associated with the origin of anaphase bridges, which are marked by factors involved in recombination.

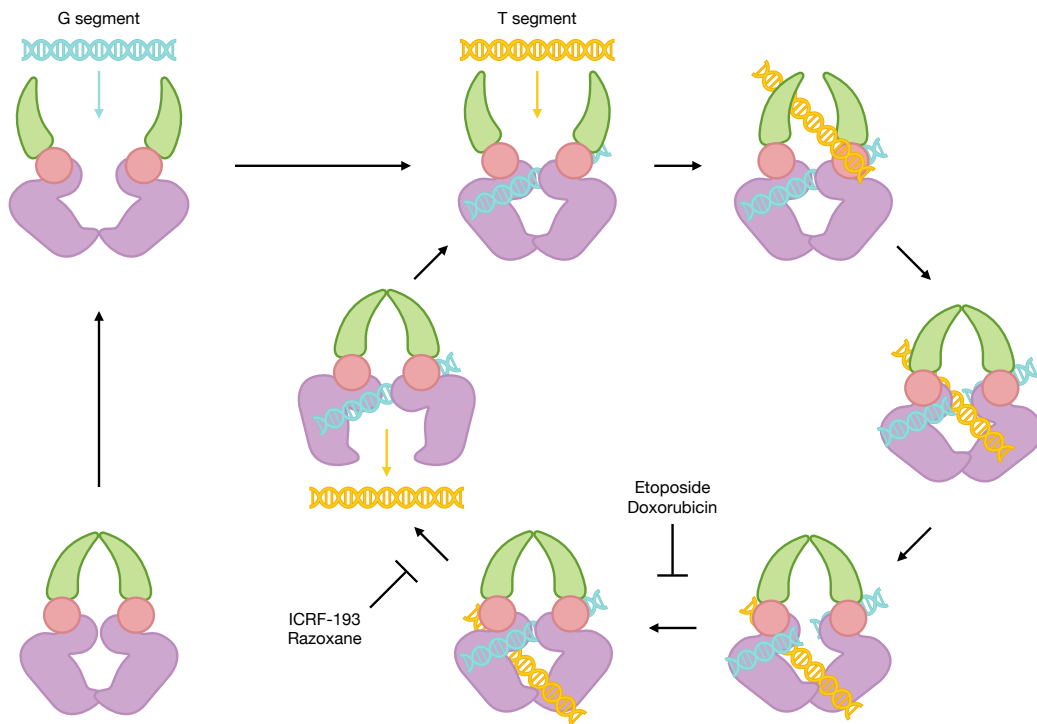


Figure 8. Topoisomerase II decatenates intertwined DNA

Topoisomerase II decatenates intertwined DNA by introducing a double-strand break in the first strand (G segment) while passing the second strand (T segment) through the break. After ligating the G segment, the T segment is released and a new decatenation process can occur with the same G segment. Catenated chromatin bridges are often induced by inhibitors. Inhibitors of topoisomerase II falls into two classes; poisons such as etoposide and doxorubicin which prevents the ligation step of the G segment, and catalytic inhibitors including ICRF-193 and razoxane which prevents the release of the T segment after ligation of the G segment.

1.3.1.2 Catenated anaphase bridges

Most topological issues such as supercoils and catenated DNA formed during replication are resolved before mitotic entry. Yet, the most common cause of anaphase bridges is catenated DNA. Interestingly, in addition to resolving catenations during replication, TOP2 is found accumulated at the centromeres after S phase which are protected from decatenation by cohesion until anaphase onset (Wang et al. 2010). Once cohesin is cleaved by separase at the onset of anaphase, the centromeric DNA is exposed for decatenation by TOP2 which allows the proper segregation of centromeres. TOP2 decatenates intertwined DNA by interacting with two DNA strands (Figure 8), in the first step TOP2 introduces a DSB in one of the DNA strands, termed gate (G) segment (Nitiss 2009). In the presence of ATP, TOP2 will form a closed clamp around the two DNA strands and pass the second DNA strand termed the T segment

through the cleaved G segment. After passing the T segment through, the G segment re-ligates, and the T segment is released through the carboxy terminus of the G segment. The second hydrolysis reopens the clamp and allows the release of the G segment, alternatively, a new cycle of decatenation can be initiated without the release of the G segment.

The formation of catenated bridges in mammalian cells is frequently accomplished with topoisomerase II inhibitors, which can be divided into two classes: poisons and catalytic inhibitors. A Topo II poison such as etoposide and doxorubicin functions by crosslinking Topo II in the stage with cleaved DNA (G segment, Figure 8). The covalently bound TOP2:DNA complex prevents the re-ligation of the cleaved strand, leading to double-stranded DNA breaks and elevated DNA damage response (Montecucco, Zanetta, and Biamonti 2015). Bisdioxopiperazines belongs to the class of catalytic inhibitors that lock TOP2 as a clamp around the DNA after the ligation of the cleaved DNA strand (Figure 8), preventing the complete release of the T segment (Jensen et al. 2000). The best-characterized bisdioxopiperazine is ICRF-193, which has been shown to induce both UFBs and chromatin bridge formation (Germann et al. 2014; Piskadlo, Tavares, and Oliveira 2017; Bhowmick et al. 2019). Bisdioxopiperazines such as ICRF-193 has been reported not to cause DNA damage (Downes et al. 1994; Jensen et al. 2000; Ye et al. 2010; Deiss et al. 2019), although it remains controversial as several publications have reported the contrary (Pastor et al. 2002; Park and Avraham 2006; Lossaint et al. 2011). However, the DNA damage observed is most likely caused by a different mechanism than a topoisomerase II poison and is poorly understood (Pastor et al. 2002). Notably, the extent of DNA damage is weaker compared to topoisomerase poisons (Jensen et al. 2000).

Inactivation of Top2 in yeast leads to failure to decatenate sister chromatids, which induces chromatin bridge formation during anaphase and compromised cell viability (Holm et al. 1985). Immunofluorescence microscopy of *Drosophila* S2 cells depleted of Top2 showed that cells were able to progress through mitosis without significant delay, however, exhibited aberrant chromosome morphology and chromosome segregation (Chang et al. 2003). Inhibition of TOP2 in mammalian cells causes chromatin bridges and UFBs which are coated with BLM and the PLK1-interacting checkpoint helicase (PICH). PICH is not implied in processing anaphase bridges but

is essential to recruit BTR to the bridge. PICH belongs to the SNF2 helicase-like family of ATPases which possess dsDNA translocase activity (Baumann et al. 2007), and has been shown to bind with high affinity to dsDNA that is under tension-induced stretching such as UFBs and catenated bridges (Biebricher et al. 2013). This sensing mechanism of bridge tension can explain how PICH recruits BTR to the UFBs. Loss of PICH causes increased chromatin bridge formation, micronucleation, and binucleation (Kaulich, Cubizolles, and Nigg 2012; Nielsen et al. 2015). UFBs were observed in almost all anaphases regardless of PICH depletion or in the expression of rescue construct. Ectopic expression of a PICH ATPase mutant did not rescue the high frequency of chromatin bridges but further elevated it, suggesting that the ATPase activity is important to suppress the formation of chromatin bridges but not UFBs (Kaulich, Cubizolles, and Nigg 2012). Therefore, the different frequencies of chromatin bridges and UFBs suggest that the structures are of different origins and causes.

1.3.1.3 The decatenation checkpoint

Insufficient decatenation of sister chromatids from G2 to mitosis can trigger an ATR-BRCA1-mediated decatenation checkpoint which will delay the onset of mitosis until the chromatids have been properly separated (Deming et al. 2001; Skoufias et al. 2004). The decatenation checkpoint responds to inhibition of topoisomerase II by the addition of ICRF-193. Arrested cells with ICRF-193 do not recruit the spindle assembly checkpoint (SAC) components MAD2 and BUB1 to the kinetochores and also do not exhibit histone H2Ax phosphorylation and is therefore distinct from the SAC, and the DNA damage checkpoint (Skoufias et al. 2004). The decatenation checkpoint relies on ATR and BRCA1 to arrest the cell cycle by inhibiting the nuclear localization of cyclin B/CDK1, required for progression into mitosis (Deming et al. 2001). Remarkably, TOP2 has been implicated to directly recruit the mediator of DNA damage checkpoint protein-1 (MDC1) to the chromatin, which is required for checkpoint response to catenation (Luo et al. 2009). A recent study developed an auxin-induced degron system to degrade TOP2 in human cells. TOP2 depleted from prometaphase to avoid triggering the decatenation checkpoint caused an increased fraction of dividing cells with anaphase bridges and severe chromatin entanglement, consistent with other model organisms (Nielsen et al. 2020). The decatenation checkpoint ensures that the sister chromatids are decatenated by TOP2 before

anaphase. However, it is not known if such level of decatenation is physiologically reached as these studies usually rely on exposure to ICRF-193.

Inhibition of topoisomerase II prevents efficient decatenation of intertwined DNA in S phase and mitosis, causing chromatin bridges and ultrafine bridges to form during anaphase. Lower concentrations of ICRF-193 can be used to not trigger the checkpoint (Germann et al. 2014; Bhowmick et al. 2019), suggesting that some level of decatenation is tolerable but most notably still allow bridge formation. In all, suggesting that there are common and physiological bridges, and these bridges are later detected by the NoCut checkpoint and processed before abscission.

1.3.2 Chromatin bridge resolution

The abscission checkpoint is thought to protect dividing cells with chromatin bridges against chromatin breakage and DNA damage, and/or tetraploidization. In Steigemann et al. (2009) it was reported that not all cells with chromatin bridges regress the furrow, it was observed that the majority of cells have bridges that persist long into the next interphase, but what happened to these bridges was not addressed and the study was limited in the length of bridge acquisition. The persistence of chromatin bridges and delay in abscission might allow time for the resolution of bridges in interphase rather than becoming binuclear, however, it is also possible that the factors needed for resolution of chromatin are not expressed until later in interphase. How the checkpoint-mediated abscission delay and resolution of bridges are coordinated remains under debate. Some studies have observed a strong correlation between chromatin bridge damage and breakage with failure of a timely resolution of bridges due to accelerated abscission and uncoordinated abscission checkpoint signaling. This suggests that constricting forces by the cleavage furrow and/or at the abscission site are the cause of damage and breakage of chromatin bridges (Janssen et al. 2011; Carlton et al. 2012; Petsalaki and Zachos 2016). Whereas other studies refute the possibility of chromatin bridge resolution during cytokinesis, it is inevitable that chromatin will be trapped in the cleavage plane before resolving during interphase (Maciejowski et al. 2015; Umbreit et al. 2020).

Nonetheless, profound consequences are associated with the breakage of chromatin bridges as it induces structural chromosome aberrations such as nuclear buds and micronuclei formation (Pampalona et al. 2010). Micronuclei contain fragmented DNA with abnormal replication and DNA damage and were shown to participate in the chromosome breakage-fusion-bridge (BFB) cycle promoting massive genomic rearrangement termed chromothripsis (Stephens et al. 2011; Maciejowski et al. 2015; Zhang et al. 2015). A BFB cycle is initiated with the breakage of a chromosome or chromatin bridge. In the successive anaphase a new bridge can be formed from an end-to-end fusion of the sister chromatids (McClintock 1939), incomplete recombination intermediates (West et al. 2015), or unresolved DNA catenation (Nielsen et al. 2015), generating a dicentric chromosome which can undergo a second cycle of bridge breakage in the following cytokinesis and the cycle continues. The BFB process generates genomic rearrangements, which are commonly accompanied by other chromosome alterations such as chromothripsis (Maciejowski et al. 2015; Umbreit et al. 2020).

The first mechanistic model on how chromatin bridges in human cells are resolved proposes the occurrence of NERDI, a transient rupture of the nuclear envelope during interphase which allows the entry of a cytoplasmic 3' exonuclease called TREX1 to gain access to the bridge and enzymatically resolve it (Maciejowski et al. 2015). Before bridge resolution 3-20 hours after anaphase, bridges were observed to be coated by TREX1, which processed the chromatin into ssDNA. The ssDNA bridge was subsequently protected by RPA, a process strongly correlated with bridge resolution and fragmentation by TREX1, but TREX1 may not be the only responsible factor as bridge resolution was not completely abrogated by TREX1 deficiency. The bridge remnants with fragmented bridge DNA were shown to be exposed to aberrant DNA repair, which may contribute to further chromosome alterations.

An endonuclease, LEM-3 (hANKLE1), has been alluded to resolve chromatin bridges in *C. elegans*. The LEM-3 nuclease was initially identified in a genetic screen for DNA repair genes in *C. elegans* and was found to process recombination intermediates and DNA structures caused by DNA replication stress (Dittrich et al. 2012; Hong et al. 2018). LEM-3 and its phosphorylated state were observed to be forming a ring structure around chromatin bridges independently of furrow ingression during

anaphase onset and is then accumulated at the cleavage plane in the presence of a chromatin bridge. Furthermore, loss of LEM-3 led to persisting bridges induced by replication stress or decondensation. Double mutants of *lem-3* and *slx-4*, another helicase involved in resolving Holliday junctions displayed compromised chromosome segregation and increased frequency of binucleation. Additionally, the localization of LEM-3 at the midbody is dependent on AIR-2 and proper central spindle formation, in all, implicating that LEM-3 has a role in resolving chromatin bridges before complete furrow ingression in *C. elegans*. ANKLE-1 has a conserved function in resolving a wide variety of DNA junctions (Song et al. 2020). However, it has yet to be observed and described as a potential nuclease able to process chromatin bridges in human cells.

Another recent paper by Umbreit et al. (2020) is the first study to propose chromatin bridge breakage by mechanical stress due to stretching of the actomyosin cytoskeleton after cleavage ingression. It is worth noting that the cell lines used in the study, RPE-1 and BJ foreskin fibroblasts, exhibit high mobility in comparison with HeLa and U2OS which rarely underwent bridge breakage before the next mitosis (Umbreit et al. 2020). Most important, the study expands our understanding of the consequences of how a single presence of a chromatin bridge during cytokinesis can generate a downstream cascade of complex mutational events through defective replication of micronuclei. Additionally, using the same cell line and dicentric bridge induction method as in Maciejowski et al. (2015), the bridge lifetime was not observed to be delayed in cells deficient in TREX1 and neither was there a significantly different bridge lifetime in cells with or without the occurrence of NERDI.

To this date, different models have been proposed and disputed, it remains unclear by which mechanism these bridges are resolved and when, if at all possible that there is a mechanism for an error-free resolution of bridges.

1.4 The NoCut/abscission checkpoint

Chromatin bridges and ultrafine bridges (collectively called anaphase bridges) can arise from incomplete replication and unresolved recombination intermediates during S phase. The failure to properly condense and decatenate intertwined sister chromosomes before anaphase onset also causes bridge formation. These bridges connect the two daughter nuclei during cytokinesis and interferes with normal abscission of the plasma membrane. The presence of DNA in the cleavage plane triggers a checkpoint delay known as the NoCut or the abscission checkpoint.

1.4.1 The NoCut checkpoint in budding yeast

1.4.1.1 NoCut prevents completion of cytokinesis in cells with spindle midzone defects and chromatin bridges

As the final phase of the cell cycle and the last possibility to maintain genomic stability before abscission, cytokinesis is a tightly monitored process by the Aurora B-mediated abscission checkpoint (NoCut). The lack of microtubule binding protein Ase1 (hPRC) causes spindle midzone defects which strongly impairs chromosome segregation and leads to improper formation of the primary septum. Spindle midzone defects also delayed complete plasma membrane resolution. In all, suggesting that the spindle midzone is required for plasma membrane resolution and thus abscission (Norden et al. 2006). The delay caused by spindle midzone defect was abolished upon the inactivation of the Ipl1 (Aurora B) kinase at the midzone. However, Ipl1 is not localized to the bud neck and requires the regulator of exocytosis Boi2, but not Boi1 as previously thought, to relay the signal and delay abscission (Norden et al. 2006; Masgrau et al. 2017). Boi1 and Boi2 are required for an efficient bud growth by promoting an exocyst-dependent vesicle fusion to the plasma membrane. Indeed, both Boi1-GFP and Boi2-GFP were observed by time-lapse microscopy to be translocated from the nucleus in G1 to the bud neck until spindle breakdown. By the time of cell separation, the Boi1-GFP and Boi2-GFP signals were gone. In cells inactivated of Ipl1, Boi1-GFP and Boi2-GFP are failed to translocate to the bud neck and remained in the nucleus the whole cell cycle (Norden et al. 2006). Implicating that Boi1/2 act downstream of Ipl1 and require Ipl1 for their localization to the bud neck. The deletion of BOI1 and BOI2 does not suppress the spindle midzone defects in

ase1Δ mutants but lead to a resolved plasma membrane (Norden et al. 2006). However, in a following study from Masgrau and Battola et al. (2017) it was shown that Boi2 alone but not Boi1 was sufficient to inhibit abscission. Furthermore, *ase1Δ* mutants show chromosome segregation defects which in absence of Boi1/2 accumulate double-strand breaks (DSBs). In all, suggesting that the Ipl1 kinase monitors chromosome segregation at the midzone and inhibits abscission from progressing until the cleavage plane is cleared of chromatin. This surveillance system termed the NoCut checkpoint relies on Ipl1 to translocate Boi2 to the bud neck to delay abscission and protect against chromosome breakage.

NoCut responds to spindle midzone defects which also associated with impaired chromosome segregation. Follow-up studies confirmed that chromatin bridges generated by inactivating topoisomerase II and condensin, and DNA replication stress are sufficient to delay plasma membrane contraction without perturbing the spindle midzone (Mendoza et al. 2009; Amaral et al. 2016). Deletion of BOI1 and BOI2, and inactivation of Ipl1 bypass the delayed phenotype, implicating that chromatin bridges can also trigger a NoCut-dependent abscission inhibition. However, not all chromatin bridges are detected equally, dicentric chromosomes generated by fusing the telomeres of chromosome 4 and 12, do not trigger an abscission checkpoint. This suggests that the molecular origin of chromatin bridges determines if the NoCut checkpoint can elicit a response to stall abscission.

1.4.1.2 The current model of how NoCut monitors the chromosome segregation

It is still not well understood how the Ipl1 kinase senses chromatin bridges in yeast. For a NoCut-dependent abscission delay, it is proposed that Ipl1 must be directly involved with the chromatin. Deletion of Ahc1, a scaffolding component of the histone acetyltransferase complex, ADA, can also rescue the arrested phenotype of cells with compromised chromosome segregation due to anaphase-spindle defects and DNA replication stress (Mendoza et al. 2009). Implying that the interaction with acetylated chromatin is important to trigger NoCut. Interestingly, tethering of Ipl1 to the chromatin alone using the TetR-TetO system was sufficient to trigger a NoCut abscission delay independently of spindle defects or chromatin bridges (Mendoza et al. 2009). This suggests that at the spindle midzone, Ipl1 detects chromatin, or interacts with

chromatin-associated proteins and delays cytokinesis through Boi2 until the abscission site has been cleared out of chromatin. However, a direct mechanism and chromatin-associating factors that can be detected by NoCut have yet to be proposed.

Recently, the E3 ubiquitin ligase APC/CCdh1 has been implicated as a downstream target of NoCut. APC/C associated with the co-activator Cdh1 degrades spindle-stabilizing proteins including Ase1, leading to the spindle breakdown (Woodruff, Drubin and Barnes 2010). Deletion of CDH1 causes a mild abscission delay in wild-type cells are dicentric cell without bridge formation. However, dicentric bridges which are usually not detected by NoCut, strongly inhibits abscission in *cdh1Δ* cells. The abscission delay can be rescued by inactivation of Ipl1 and deletion of AHC1. In all, spindle stabilization mediated by APC/CCdh1 is important for the detection of chromatin bridges by the NoCut checkpoint.

1.4.2 The abscission checkpoint in human cells

The Aurora B-mediated NoCut is an evolutionarily conserved abscission checkpoint. In response to depletion of topoisomerase, cohesin, condensin, and CENP-A in *C. elegans* the Aurora B homolog AIR-2 is hyper-activated at the spindle midzone (Bembenek et al. 2013). Acute inactivation of AIR-2 causes failure in cytokinesis by cleavage furrow regression in cells with chromosome segregation defects. Additionally, it was observed that condensin I is enriched at the midbody in the presence of chromatin in an AIR-2-dependent manner, its depletion interfered with the resolution of the bridge, suggesting that condensin I in *C. elegans* has a role in aiding chromatin bridge resolution (Bembenek et al. 2013).

Chromosome mis-segregation and the appearance of chromatin bridges during anaphase are significantly more common in human cancer cells, in particular neoplastic cells (Gisselsson et al. 2000). These phenotypes are strongly associated with chromosomal instability (CIN), one of the hallmarks of cancer and are believed to play a critical role in cancer progression and contribute to the karyotypic diversity in cancers (Nicholson and Cimini 2011). Highly conserved, the NoCut checkpoint or the abscission checkpoint in human cells has been shown to control abscission timing through Aurora B and protect cells with chromatin bridges and lagging chromosomes

against DNA damage, chromatin breakage, aneuploidy (Carlton et al. 2012; Petsalaki and Zachos 2016; Dandoulaki et al. 2018) or tetraploidization by regressing the cleavage furrow (Steigemann et al. 2009; Thoresen et al. 2014; Bai et al. 2020). However, it is important to note that not all cells with chromatin bridge regress the furrow, a large fraction of bridges persists and resolves in interphase long after the time of midbody disassembly (Carlton et al. 2012; Sadler et al. 2018).

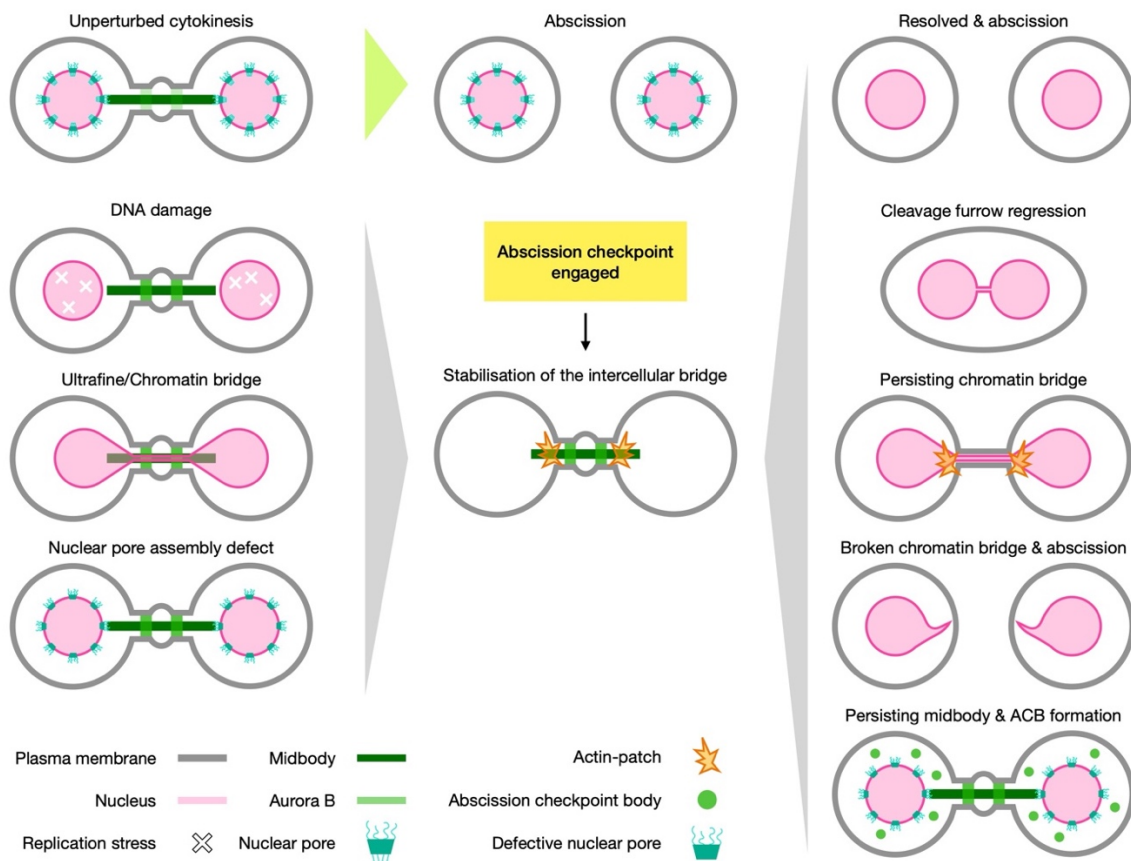


Figure 9. Triggers of the abscission checkpoint and the possible outcomes

Under unperturbed conditions cells complete chromosome segregation and undergo cytokinesis and abscise the intercellular bridge. The abscission checkpoint is known to be triggered by several factors; DNA damage by the activation of ATR/Chk1 pathway, ultrafine bridges, chromatin bridges, and defects in nuclear pore assembly. The presence of aberrant nuclear integrity or DNA damage signals delays cytokinesis progression and prevents completion of abscission. The delay is mediated by the Aurora B kinase (light green) at the midbody arms which stabilizes the intercellular bridge by promoting the recruitment of F-actin (orange), and preventing midbody disassembly (dark green) and ESCRT-III assembly at the abscission site. There are several possible outcomes that have been observed with each phenotype. The best possible outcome is resolution of the chromatin bridge or repair of the DNA damage before abscission. However, chromatin bridges are unlikely to be resolved, and can persist for hours after the delayed disassembly of the midbody. Chromatin bridges can be removed by nucleases or by mechanical forces which leads to bridge breakage. Alternatively, cells can undergo tetraploidization by regressing the cleavage furrow. This pathway prevents

the formation of aberrant chromatin and the accumulation of DNA damage but generates a binucleated cell. Cells with nuclear pore assembly defects arrests at the midbody-stage for many hours and exhibit abnormal localization of Aurora B in “abscission checkpoint bodies” in the cytoplasm.

1.4.2.1 The mechanism of abscission checkpoint in human cells

The mechanism of how the human abscission checkpoint detects the presence of chromatin at the cleavage plane is not well understood. Compared to yeast, the spindle is foremost formed spatially separated from the nucleus. In other words, the presence of a chromatin bridge has to be transmitted through the nuclear membrane to trigger the Aurora B-mediated abscission checkpoint. The checkpoint responds by sustaining the midbody and recruiting actin to the midbody, which stabilizes the ICB (Figure 9) (Steigemann et al. 2009; Dandoulaki et al. 2018; Bhowmick et al. 2019; Bai et al. 2020). The Aurora B kinase is localized to the midbody microtubules to regulate the abscission timing and maintain the checkpoint by phosphorylating various downstream proteins. One of these proteins is the ESCRT-III component CHMP4C. While it is dispensable for viral budding and endosomal sorting, CHMP4C plays a crucial role in coordinating the timing of midbody disassembly and the abscission checkpoint, on one hand, CHMP4C is involved in regulating normal abscission of the ICB, and on the other hand, it is part of the abscission checkpoint in preventing untimely resolution of chromatin bridges (Carlton et al. 2012). Although the precise mechanism is unclear, genetic and biochemical experiments suggest that upon phosphorylation, pCHMP4C together with the abscission/NoCut checkpoint regulator (ANCHR) protein form a ternary complex with VPS4 at the Flemming body. This action sequesters VPS4 at the Flemming body and prevents the VPS4-mediated spiral ESCRT-III filament formation towards the abscission zone and thereby abscission (Thoresen et al. 2014). Interestingly, both depletion of CHMP4C and ANCHR accelerates the midbody disassembly and while the overexpression delays midbody disassembly, suggesting that they are inhibitors of abscission. However, in the presence of a chromatin bridge, ANCHR-depleted cells regress the furrow with an increased frequency (Thoresen et al. 2014), while CHMP4C-depleted cells do not display an increased cytokinesis failure but are rather associated with advanced resolution of the bridge and DNA damage (Carlton et al. 2012; Sadler et al. 2018).

Indicating that the regulation of abscission by CHMP4C and ANCHR each relies on several branches.

ANCHR was initially discovered through a siRNA screen targeting PtdIns(3)P -binding proteins, its depletion leads to a strong fraction of multinucleated cells compared to the control similar to depletion of PtdIns(3)P (Sagona et al. 2010; Thoresen et al. 2014). It should be noted that PtdIns(3)P is also found enriched on endosomal membranes, and is involved in the regulation of vesicular trafficking in the endolysosomal system. Therefore, its depletion can have global signaling defects affecting other cell cycle-related processes other than cytokinesis. PtdIns(3)P was shown to be localized to the midbody where it recruits ANCHR to the midbody. Interestingly, the interaction with PtdIns(3)P at the midbody is not essential for the function of ANCHR as an abscission inhibitor.

The strong accumulation of actin in patches at both sides of the ICB is associated with the abscission checkpoint stabilizing the ICB in the presence of a chromatin bridge (Steigemann et al. 2009). However, it was only in recent years that more studies have started to decipher the mechanism. One recent study demonstrated how MsrB2, a reductase that promotes actin polymerization, is recruited to the midbody to control the actin levels specifically in response to chromatin being retained in the ICB (Bai et al. 2020). MsrB2 counteracts MICAL1 at the ICB where it was previously shown to depolymerize actin filaments by oxidation and promote ESCRT-III localization at the abscission site by clearing out F-actin (Frémont et al. 2017). Depletion of MsrB2 leads to accelerated abscission and decreased F-actin levels at the bridge, whereas depletion of MICAL1 showed the opposite, indicating that the interplay between reduction and oxidation of actin at the ICB is important for the timing of abscission, but also highlights the essential role of MsrB2 in stabilizing the ICB (Bai et al. 2020). Additionally, loss of MsrB2 lead to an increase of tetraploidization in a fraction of cells dividing with a chromatin bridge, due to an unstable ICB.

Interestingly, in the same study, it was shown that there is an increased accumulation of ANCHR at the midbody in the presence of chromatin bridges, which depends on MsrB2. The depletion of MsrB2 and ANCHR consistently exhibit similar phenotypes which might suggest that they are in the same pathway (Thoresen et al. 2014; Bai et

al. 2020). So far, ANCHR has been associated with both the inhibition of the midbody disassembly by preventing complete abscission together with CHMP4C and actin polymerization with MsrB2 at the ICB, suggesting parallel functions in stabilizing the ICB during an abscission checkpoint response to a chromatin bridge. How and in which contexts the Aurora B kinase fine-tunes all parallel mechanisms in regulating abscission and the outcome has still not been described.

In recent years, numerous studies have shown insight into the signaling pathways that act upstream of Aurora B to trigger a delay in abscission. One of the pathways that are involved in regulating the Aurora B activity is the Cdc-like kinases (Clks) 1, 2, and 4 (Petsalaki and Zachos 2016). Clk1, Clk2, and Clk4 localize to the midbody where they are required for the phosphorylation of Aurora B at S331, a residue important for the complete catalytic activity of Aurora B (Petsalaki et al. 2011). The complete phosphorylation of Aurora B is in turn required for the optimal phosphorylation and localization of the ESCRT-III component CHMP4C to the midbody in cells with chromatin bridges. Cells deficient in Clks prematurely disassembled the midbody and caused chromatin bridge breakage and DNA damage.

In yeast, NoCut prevents damage to chromatin bridges after DNA replication stress by HU (Amaral et al. 2016). In a proceeding study, it was observed that the presence of unreplicated DNA throughout anaphase was correlated with chromatin bridge formation and a prolonged resolution, suggesting a maintained NoCut checkpoint (Ivanova et al. 2020). Indeed, it has become increasingly more apparent that human cells frequently enter mitosis with under-replicated, or unresolved DNA (Mankouri, Huttner, and Hickson 2013). In contrast to yeast, the exposure of HU or APH in human cells does not induce chromatin bridges but aggravates the under-replicated state observed by an increased number of 53BP1 persisting into cytokinesis and G1 (Harrigan et al. 2011; Mackay and Ullman 2015). The presence of 53BP1 foci during cytokinesis is correlated with a delayed midbody disassembly, interestingly, the inhibition of Chk1 and ATR but not ATM shortened the delay. The increased level of replication stress was shown to trigger an Aurora B-dependent abscission delay mediated by a "postmitotic genome surveillance" ATR and Chk1-dependent signaling pathway, demonstrating a link between a DNA damage checkpoint pathway and the abscission checkpoint (Mackay and Ullman 2015). Although ATM was not found to

play a role in the abscission checkpoint, phosphorylated Chk2 at T68, a preferred substrate of ATM, was found to be localized to the midbody, suggesting that ATM or other kinases involved in the DNA damage are active and in proximity (Tsvetkov et al. 2003; Mackay and Ullman 2015).

Complementary to Mackay and Ullman (2015), another study showed by immunofluorescence that ATM, Chk2, and INCENP localize at the Flemming body, in contrast, the inhibition of ATM and Chk2 using specific kinase inhibitors was observed to accelerate midbody disassembly (Petsalaki and Zachos 2021a). The difference in observations compared to the previous study is not known, and could be due to cell line and/or drug concentration used. In addition, they showed that the essential Mre11-Rad50-Nbs1 (MRN) complex for DNA damage recognition and signaling, is exclusively localized to the Flemming body of unbroken chromatin bridges. Depletion of MRN proteins and inhibition of Chk2 was further correlated with a higher frequency of broken chromatin bridges and loss of ATM at the midbody. Proposing a model in which cells with chromatin bridges require the localization of MRN complex to the Flemming body, where it activates an ATM-Chk2-INCENP pathway to delay abscission and prevent bridge breakage.

Another interesting defect that triggers an Aurora B-dependent abscission delay but is not directly associated with chromatin is aberrant nuclear pore assembly (Figure 9). Disruption of Nup153, an essential nucleoporin for the formation of the NPC basket, leads to an extensive delay in the disassembly of the midbody. Although more modest than the depletion of Nup153, the absence of another basket nucleoporin, Nup50, was also sufficient to trigger the abscission checkpoint. This suggests that the abscission checkpoint not only contributes to protecting the genomic DNA from damage but furthermore ensures that NPCs are properly assembled, and that the nuclear envelope integrity is maintained in daughter cells.

In parallel with Aurora B, the Unc-like kinase 3 (ULK3), has also been shown to regulate the abscission timing, interact with and phosphorylate several components of the ESCRT-III complex, but notably, IST1 which is essential for abscission (Agromayor et al. 2009; Caballe et al. 2015). Depletion of ULK3 accelerates midbody disassembly at a similar timing to cells depleted of CHMP4C, and consistently, also resolved

chromatin bridges faster. Similar to overexpression of CHMP4C, overexpression of ULK1 leads to stabilized midbodies. Furthermore, the interconnection between ULK3 and CHMP4C functions in abscission was observed by the shortened delay in midbody disassembly in overexpressed cells by depleting the other protein. However, in contrast to CHMP4C, ULK3 is not involved in furrow regression. Interestingly, the phosphorylation of IST1 by ULK3 was dispensable for a prolonged midbody duration by high membrane tension but was required for incomplete NPC assembly and untimely bridge resolution. Indicating that the checkpoint can control in what context delayed abscission is required.

Over the past years there has been a big advancement towards broadening our understanding of how the abscission checkpoint is regulated in human cells. Factors that can trigger an abscission delay and their signaling pathways upstream of Aurora B have been identified. We also have better understanding of how the intercellular canal is stabilized by actin and the midbody in the presence of chromatin bridges or nuclear pore defects. However, the evidence of a physiological relevance of the abscission checkpoint has just in recent years started to be described (Sadler et al. 2018).

1.4.3 Consequences of a deficient NoCut/abscission checkpoint

Increased DNA damage is observed by time-lapse microscopy in cells that exhibit chromatin bridges or chromosome segregation defects when NoCut has been inactivated. Fluorescently-tagged DNA damage reporters of double-strand breaks such as Ddc1 and Mre11 were accumulated in the following G1 after the bridge resolution, linking the absence of NoCut to chromatin bridge damage (Norden et al. 2006; Mendoza et al. 2009; Amaral et al. 2016). Loss of Cyk3 a promoter of cytokinesis, which delays progression through cytokinesis and abscission, can prevent DNA damage caused by chromatin bridge formation and NoCut checkpoint inactivation (Amaral et al. 2016). Together, this suggested that NoCut is important to protect chromatin bridges and abnormal chromosome segregation against damage by cytokinesis.

Damage to chromatin bridges has also been observed in human cells when the abscission checkpoint is deficient to delay cytokinesis. Depletion of CHMP4C, an ESCRT-III component important for regulating abscission in an Aurora B-dependent manner, accelerates abscission and damages pre-existing chromatin bridges. The inhibition of Clk1, 2 and 4, and ATM-Chk2 signaling pathways which promotes an Aurora B-mediated delay in the presence chromatin in the cleavage plane, also leads to damage of the trapped chromatin bridge (Petsalaki and Zachos 2016; Petsalaki and Zachos 2021a). In contrast, direct inhibition of the Aurora B kinase by inhibitors including Hesperadin and ZM1 also leads to an accelerated abscission and increased tetraploidization with a continuous chromatin bridge between the daughter nuclei (Steigemann et al. 2009). The deletion of the actin reductase MsrB2, a downstream target of Aurora B destabilizes actin filaments in the intracellular canal leading to tetraploidization (Bai et al. 2020). In all, implicating that the Aurora B kinase on one hand protects against DNA damage by delaying abscission and on the other hand it is required to protect against tetraploidization by stabilizing the intracellular canal. It is not well understood how the dividing cell takes the decision to either abscise or regressing the plasma membrane. The contrasting observations between checkpoint perturbations could be due to different degrees of Aurora B inhibition. Further study into the fine-tunings of Aurora B activity is required.

In a study by Janssen et al. (2011), the authors propose that missegregating chromosomes are damaged by the ingressing plasma membrane during cytokinesis in non-transformed RPE-1 cells. Chromosome segregation defects were induced by inhibiting the mitotic spindle motor protein KIF11 with Monastrol (cells arrested in mitosis with monoastral spindles) or by using a specific inhibitor against mitotic kinase Mps1, which is required for the bipolar attachment of microtubules to the kinetochores. Damage to missegregating chromosomes treated with Monastrol was relieved by inhibiting cytokinesis through Aurora B inhibition (cells fail to progress into anaphase and become tetraploid). Implicating that cytokinesis induces DNA damage on lagging chromosomes. These results contradict what was previously shown in budding yeast, where inactivation of Ipl1 aggravates the DNA damage accumulated in cells dividing with chromatin bridges (Amaral et al. 2016). It is possible that the abscission checkpoint functions to protect the trapped chromatin against DNA damage in some cell types and not in others, but also whether or not the type of segregation error can

be detected by the checkpoint. Therefore, identifying the chromatin-based signal that triggers the abscission checkpoint will help us gain insight into the origin of the chromatin bridge and the consequence associated with a specific defect.

1.5 DNA helicase PARI

Not all chromatin bridges delay abscission, surprisingly, dicentric bridges are not detected by the NoCut checkpoint (Amaral et al. 2016). This suggests that NoCut senses a chromatin-associated factor specific to bridges that are induced by catenation, decondensation and replication stress. We performed a genetic screen and deleted various DNA helicases, including helicases known to be bound to ultrafine bridges. This study will focus on elucidating the function of DNA helicase Srs2 in budding yeast, and its human homolog, PARI. Srs2/PARI is involved in inhibiting homologous recombination during replication and DNA repair. However, its' role during cytokinesis has yet to be described.

1.5.1 Yeast homolog Srs2

The SRS2 gene was first identified in a screen for metabolic suppressors of rad6 mutants (Lawrence and Christensen 1979) and subsequently revealed to have strong homologies with Rep and UvrD helicases in *E. coli* participating in error-prone repair mechanism for UV-induced damage (Aboussekhra et al. 1989). RAD6 plays an essential role in cell survival, as strains carrying a rad6-1 mutation were more readily killed by various chemical mutagens and DNA-damaging agents such as UV light and ionizing radiation, and was later found to be encoding a ubiquitin-conjugating (E2) enzyme which mediates the ubiquitylation of H2A and H2B (Jentsch, McGrath, and Varshavsky 1987). Srs2 was demonstrated to have in vitro ATPase and 3'-5' DNA helicase activities. Endogenous levels of Srs2 were not detectable by WB, correlating with low abundant mRNA levels. Interestingly, the overexpression of a truncated Srs2 missing the terminal 127 residues, was at least five times higher than that of the full-length protein, suggesting that the terminal region of the protein inhibits expression or promotes degradation of the protein (Rong and Klein 1993). Additionally, the C-terminal contains a conserved RAD51 binding domain, and a SIM and PIP-box, suggesting an interaction with SUMO and PCNA.

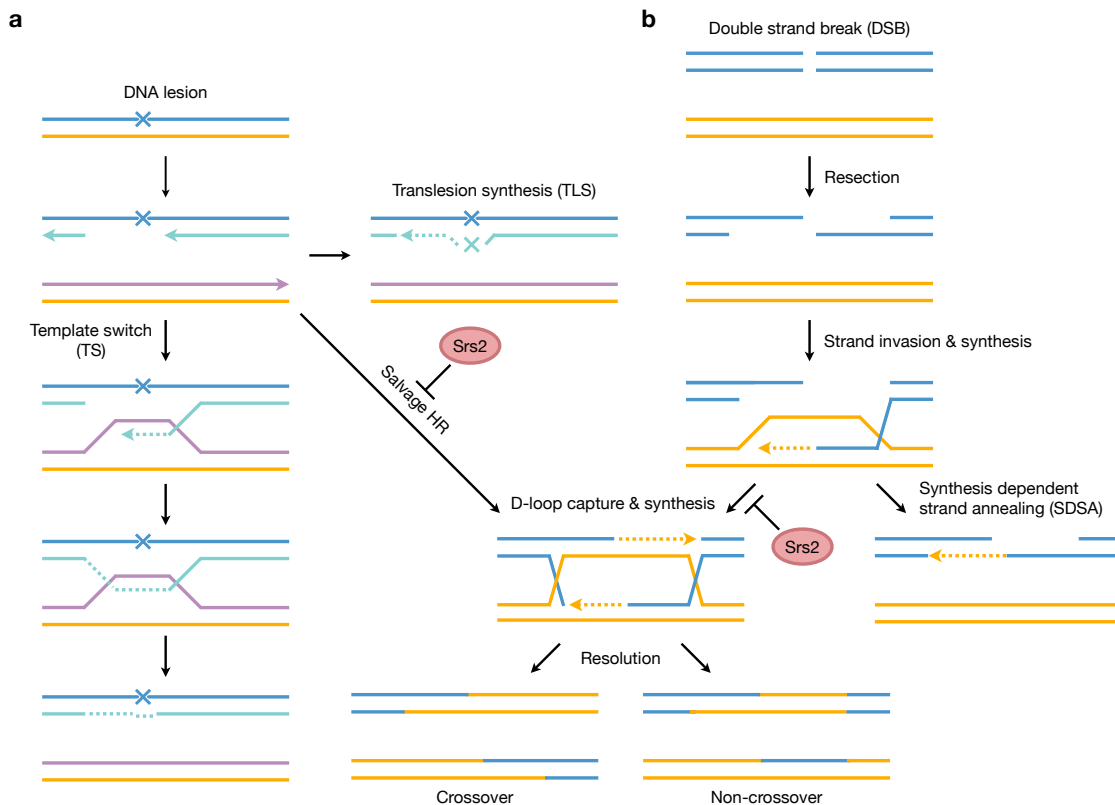


Figure 10. Overview of Srs2's role in inhibiting homologous recombination repair

Single stranded DNA (ssDNA) lesions during DNA replication and double-strand breaks (DSBs) can be repaired with homologous recombination (HR) which requires ssDNA to initiate.

(a) DNA lesions encountered during replication can be repaired by two pathways; Template switch (TS) or Translesion synthesis. During translesion synthesis the DNA polymerase simply overrides the lesion, introducing a mutation. Template switch invades and utilizes the other newly synthesized sister chromatid as a template for an error-free repair. An alternative repair mechanism is the salvage homologous recombination (HR) pathway. However, this pathway is not preferred as crossover can be generated. Consequently, DNA helicase Srs2 is recruited to SUMOylated-PCNA to inhibit salvage HR, and promote the use of the other two repair mechanism.

(b) During S and G2 phase, with an available sister chromatid DSBs can be repaired by HR. The broken ends are first resected to single-stranded overhangs before strand invasion of the sister template. A D-loop is formed with a single Holliday junction (sHJ) by strand invasion and the 3' invading strand is extended in a 5'-3' direction along the homologous DNA duplex. The DNA helicase Srs2 in yeast prevents the formation of double Holliday junctions (dHJ) which has a high risk of crossovers to promote synthesis dependent strand annealing (SDSA) pathway for an error-free repair of DSBs. Eventually the sHJ will slide in the same direction as the synthesis, displacing the extended strand. The extended strand has a new 3' overhang which will anneal to the complementary resection on the other side of the break. DNA synthesis will continue to extend and fill remaining single stranded DNA breaks, and produce a non-crossover product. Figure reproduced with modifications from (Patrick Sung et al. 2006; Bi 2015) with permission under the terms of the Creative Commons Attribution Licenses CC BY 4.0 and license number 5378361510787.

1.5.1.1 Srs2 in replication

Srs2 is required for maintaining genomic stability in various contexts by counteracting untimed HR, and thus prevents HR from interfering with normal replication progression and with other DNA repair mechanisms. Post-translational modifications such as SUMOylation and ubiquitinylation of the proliferating cell nuclear antigen (PCNA), a sliding DNA clamp that acts as a co-factor for DNA polymerases, are essential for coordinating DNA replication, DNA repair, and DNA damage tolerance (DDT) pathways (Moldovan, Pfander, and Jentsch 2007; Choe and Moldovan 2017). DNA is constantly damaged by both intrinsic and extrinsic factors, which causes replication fork uncoupling and stalling. Sustained fork stalling has the potential to collapse, leaving a single-stranded gap behind the replication fork. The DDT pathways ensure the completion of DNA replication by two mechanisms; translesion synthesis (TLS) involving specific DNA polymerases directly bypassing the lesion or template switching (TS) which uses with the newly synthesized sister-chromatid to repair the gap (Figure 10a) (Branzei and Szakal 2016). Alternatively, the ssDNA gap can be rescued by the salvage HR pathway, with the risk of aberrant recombination leading to crossovers and loss of heterozygosity (Branzei, Vanoli, and Foiani 2008).

During normal replication SUMOylation of PCNA recruits the Srs2 DNA helicase to the replication fork where it prevents untimed HR by disrupting Rad51 nucleoprotein filaments (Krejci et al. 2003; Veaute et al. 2003; Pfander et al. 2005). Ubiquitination of PCNA at K63 and K164 during the S phase is commonly associated with promoting the bypass of replication-stalling DNA lesions through DDT pathways, whereas SUMOylation of PCNA at K164 occurs even in absence of exogenous damage suggesting that Srs2 acts as surveillance of untimed HR (Papouli et al. 2005; Pfander et al. 2005). Moreover, upon the encounter of DNA lesions, Srs2 has been implicated in promoting DDT by inhibiting the HR-driven salvage pathway (Papouli et al. 2005). Despite the predicted ATP-dependent motor activity, Srs2 is not sufficient to displace Rad51 from the DNA. Rather, findings indicate that the interaction of Srs2 and RAD51 stimulates ATP hydrolysis within the RAD51 filament causing RAD51 to disassociate from the DNA (Antony et al. 2009). Interestingly, in the presence of a DNA lesion, ubiquitin and SUMO do not affect nor compete with each other, therefore suggesting

that the two modifications coordinate to facilitate the switch from DNA replication to DTT (Papouli et al. 2005).

1.5.1.2 Srs2 in recombinational repair

In addition to inhibiting unwanted recombination initiation during DNA replication and at stalled forks, Srs2 has also been shown to be involved in HR-mediated DSB repair. By limiting HR on D-loops in a Rad51-Rad52-dependent manner Srs2 thereby promotes the non-crossover synthesis-dependent strand annealing (SDSA) pathway (Figure 10b), and protects against genomic rearrangements and loss-of-heterogeneity (Miura et al. 2012; Miura, Shibata, and Kusano 2013). The role of Srs2 is strongly implicated in various cell cycle-dependent processes, and its activities can be modulated through phosphorylation by Cdk1, SUMOylation, and interaction with proteins such as SUMOylated-PCNA and Rad51. Interestingly, phosphorylation of Srs2 is required to dismantle D-loop structures to complete the SDSA pathway in DSB repair but is dispensable for the removal of toxic Rad51 filaments during D-loop extension (Saponaro et al. 2010). Another in vitro model suggests that Srs2 can disrupt D-loops and prevent long crossovers, by disassociating actively extending DNA polymerase δ (Liu et al. 2017).

1.5.1.3 Srs2 in the DNA damage checkpoint

In yeast, RPA has a strong affinity for ssDNA and acts as a sensor of DNA damage for the DNA damage checkpoint (DDC), the bound RPA-ssDNA filaments recruit the co-factor of Mec1 (ATM homolog), Ddc2 which subsequently targets Mec1 to the site of DNA lesion to activate Rad53 and/or Cdk1 to initiate a cascade of phosphorylation of substrates important in inducing cell cycle arrest, DNA repair, and other checkpoint responses. Srs2 is phosphorylated by Cdk1 in response to DNA damage induced during the S phase and was furthermore, shown to be dependent on a Mec1 and Rad53-mediated DNA damage checkpoint activation (Liberi et al. 2000). However, the role of Srs2 in checkpoint regulation has not been clear but provided a plausible connection between a checkpoint response to the roles of Srs2 in recombinational repair.

Timely termination of checkpoint signaling is important for cell cycle resumption and faithful proliferation. Interestingly, Srs2 has been implicated in terminating DDC after DSB, possibly by removing a checkpoint-signaling protein (Vaze et al. 2002). A recent study proposes a model for Srs2 in dampening the DNA damage checkpoint signaling by recycling RPA, which is independent of the previously described roles of Srs2 (Dhingra et al. 2021). Indeed, loss of Srs2 or its helicase activity leads to an accumulation of RPA and Mec1 on the chromatin, and cells consequently exhibited a hyperactive DCC.

1.5.2 Human homolog PARI

Several anti-recombinases have been identified in higher eukaryotes, suggesting a considerably higher complexity in HR regulation compared to yeast. Four functional homologs of Srs2 have been described in humans RECQL5, FBH1, RTEL1, and PARI (Hu et al. 2007; Barber et al. 2008; Fugger et al. 2009; Moldovan et al. 2012). Similar to Srs2 all the human homologs are capable of inhibiting HR during replication and preventing crossovers during DSB repair by limiting the D-loop extension, however, they each act with different affinities to substrates and at different times. The DNA helicase PARI has been indicated as the most direct homolog of Srs2 due to being the only HR suppressor that interacts with PCNA and is recruited to the replication fork during the S phase through SUMOylation of PCNA (Figure 11) (Moldovan et al. 2012; Burkovics et al. 2016). PARI is not an active helicase due to the absence of Walker A and B motifs and has a weak ATP hydrolysis activity. In a recent mechanistic study, PARI did not have an effect on Rad51-mediated D-loop formation, whereas RECQL5 and FBH1 showed disassembly. Instead, PARI was shown to be involved in inhibiting unrestrained D-loop extension by displacing DNA polymerase δ required for the extension, thus decreasing the risk of crossover (Burkovics et al. 2016). DNA fiber analyses of mES cells showed that loss of PARI does not affect normal replication dynamics but interestingly revealed that PARI reduces nascent-strand lengths, recapitulating the role of Srs2 and PARI in preventing D-loop extension in vitro (Mochizuki et al. 2017). The exact substrate of PARI remains unclear as depending on the assay system used findings do not agree with each other.

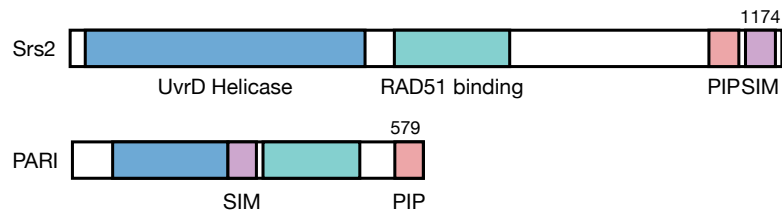


Figure 11. Srs2 and PARI protein domains

The DNA helicase PARI is the most direct human homolog of *S. cerevisiae* DNA helicase Srs2 due to structural similarities. Both proteins contain domains which interact with SUMOylated PCNA (purple). The N-terminus of Srs2 interacts with SUMOylated PCNA PARI, while PARI has a SUMO-interacting motif (SIM) and a PCNA-interacting protein-box (PIP-box). In addition, they share a conserved UvrD helicase domain and RAD51 binding domain. Srs2 consist of 1174 aa while PARI is 579 aa.

PARI is not essential for cell cycle progression in mice but cells lacking PARI exhibit hypersensitivity when exposed to DNA-damaging agents targeting replication rather than with etoposide, a TOP2 inhibitor, and gamma irradiation (Mochizuki et al. 2017). The absence of PARI leaves cells more susceptible to untimely HR and hyperrecombination which may interfere with faithful replication and DNA repair when exposed to replication stress. Interestingly, in Fanconi Anemia/BRCA deficient cells, loss of PARI improves cell survival (Moldovan et al. 2012). PARI is therefore important for maintaining genomic stability by suppressing HR and its dysregulation has implications for tumorigenesis.

1.5.2.1. PARI in tumorigenesis

PARI is lowly expressed in most normal tissues but can be found at higher levels in the testis in both humans and mice, coincidentally the testis contains highly proliferative cells (Piao et al. 2011; Mochizuki et al. 2017). Additionally, PARI mRNA was detected at higher levels in mouse spleen, embryonic stem cells, and primary embryonic fibroblasts. Dysregulated HR drives genomic instability and carcinogenesis, PARI has been observed to be overexpressed in several types of cancers such as myeloid leukemia, and pancreatic and gastric cancers (Piao et al. 2011; O'Connor et al. 2013; Zhang et al. 2018; Nicolae et al. 2019). These cancers rely on the overexpression of PARI for their survival, as depletion of PARI dramatically reduced their viability, and sensitized them to DNA-damaging agents such as HU and

MMC (Piao et al. 2011; O'Connor et al. 2013; Nicolae et al. 2019). Pancreatic cancer cells exhibit increased radial chromosomes and chromosome aberrations after exposure to DNA-damaging agents but were nevertheless able to progress through S phase and proliferate. In contrast, the absence of PARI sensitized pancreatic cancer cells to DNA-damaging agents which caused reduced cell viability (O'Connor et al. 2013). These results were consistent with similar findings in myeloid leukemia cells (Nicolae et al. 2019). PARI promotes the proliferation of myeloid leukemia, and gastric and pancreatic cells in xenograft tumor models and significantly reduces mouse survival (O'Connor et al. 2013; Zhang et al. 2018; Nicolae et al. 2019). In all, the overexpression of PARI suppresses the cell cycle arrest normally induced by DNA damage, possibly by limiting HR repair and thereby promoting replication through damaged DNA. PARI additionally contributed to the metastasis of gastric cancer *in vitro* and *in vivo* (Zhang et al. 2018).

2. Results

2.1. Aims of the study

Cytokinesis needs to be tightly coordinated with the completion of chromosome segregation to maintain genomic stability. The abscission checkpoint, also called NoCut, responds to the presence of chromatin bridges in the intercellular canal formed between the daughter cells during cytokinesis. By delaying completion of abscission, the checkpoint was proposed to allow time for the resolution of the chromatin bridges and thus prevent DNA damage. However, the mechanism which the checkpoint senses the chromatin bridge has yet to be established.

Main aim: The main aim of this study is to determine if the DNA helicase Srs2 acts as a potential signal of chromatin bridges, and investigate if it has a conserved role in the human abscission checkpoint, as chromatin bridges are frequently observed in human cancer cells.

Aim 1: Characterize the phenotype of *srs2Δ* in yeast and PARI-depleted human cells and confirm its role in the abscission checkpoint.

Aim 2: Assess the localization of PARI throughout the cell cycle and its association with the chromatin.

Aim 3: Investigate the mechanism by which PARI aid in the detection of chromatin bridges by the abscission checkpoint.

Aim 4: Investigate the consequences of failed a NoCut checkpoint response for chromatin bridges and cell proliferation.

2.2 Role of Srs2 in NoCut

2.2.1 The Srs2 DNA helicase is required for abscission inhibition in the presence of DNA replication stress

The NoCut checkpoint delays abscission in response to chromatin bridges induced by DNA replication stress, decatenation, and condensation defects in budding yeast (Amaral et al. 2016). Remarkably, not all bridges delay abscission: bridges induced by dicentric chromosomes do not trigger the NoCut checkpoint. This suggested that a chromatin-based signal allows bridge detection by NoCut. It was proposed that this signal is present in catenated, decondensed, and replication stress-dependent bridges, but not in dicentric chromosomes (Amaral et al. 2016). To gain insight into the molecular nature of this chromatin-based “NoCut signal”, we deleted various non-essential DNA helicases, some of which are known to be associated with ultrafine bridges (UFBs) in humans (Chan, Fugger, and West 2018). In this study, we are focusing on the DNA helicase Srs2, which is involved in DNA repair and DNA damage checkpoint recovery (Marini and Krejci 2010) but has no known roles in abscission.

To first characterize the role of Srs2 in abscission regulation, I monitored ingression and resolution of the plasma membrane at the abscission site by time-lapse confocal microscopy, using the fluorescent reporter GFP-CAAX (β -estradiol-inducible GFP fused to the membrane-targeting CAAX motif of Ras2). As previously described (Amaral et al. 2016) the morphology of membranes labeled with GFP-CAAX allows to visualize the progression of abscission (Figure 12c): immediately after anaphase onset, the actomyosin ring starts to constrict the bud neck, which leads to the ingression of the membrane at and eventually to its separation. The separation of the mother and daughter membrane marks abscission. To determine abscission kinetics, wild-type and *srs2* Δ cells were grown at 30°C to log phase and exposed to a 3-hour hydroxyurea (HU) pulse to perturb DNA replication (Figure 12a-b). HU stalls replication fork progression by decreasing the pool of dNTPs, increasing the risk of fork collapse and thus generating DNA damage (Singh and Xu 2016). Cells exposed to HU for 3 hours and then allowed to divide in fresh media were previously shown to display chromatin bridges and to delay abscission (Amaral et al. 2016). As previously shown (Amaral et al. 2016), I find that the median time from membrane ingression to abscission in wild-type cells is 16 min, and is significantly delayed to 24 min in cells

exposed to a 3-hour HU pulse (Figure 12d). In contrast, deletion of DNA helicase SRS2 led to advanced abscission of 18 min in presence of HU-induced chromatin bridges (Figure 12d). The absence of Srs2 does not advance abscission in the absence of HU (16 min). This suggests that Srs2 is important for the inhibition of abscission in the presence of DNA replication stress.

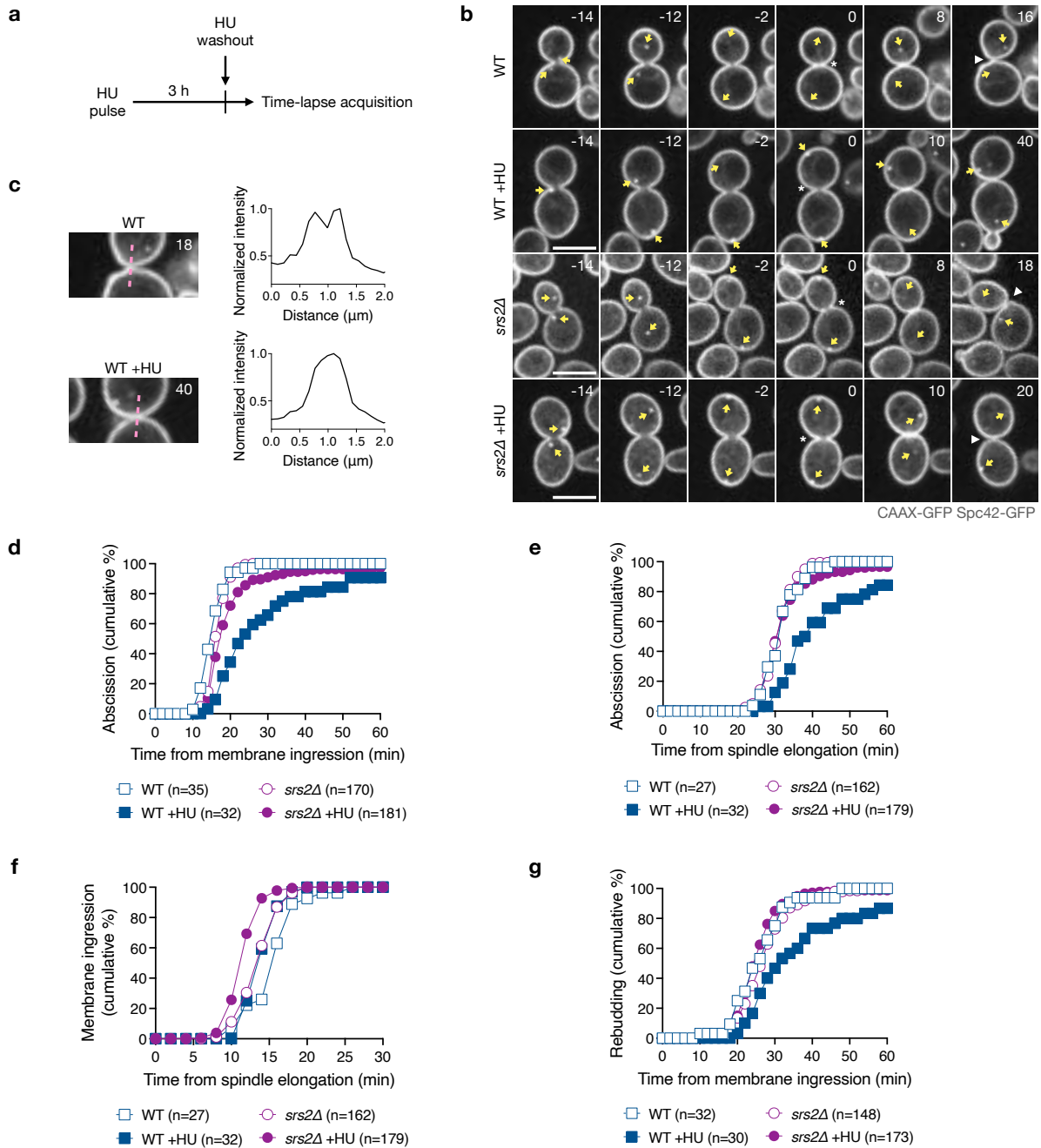


Figure 12. Srs2 delays abscission in HU-treated budding yeast

(a) Experimental workflow to induce DNA replication stress upon HU pulse at 30°C.

(b) Montage of membrane ingression and abscission in WT and *srs2Δ* cells with or without HU pulse. Cells express the plasma membrane marker CAAX-GFP and the spindle pole marker Spc42-GFP. Time is indicated in minutes; 0 min indicates the start of membrane

ingression. Yellow arrows mark the spindle poles. Asterisk specifies membrane ingression. White arrowhead marks complete constriction of the plasma membrane (abscission). Single Z-slices are shown, but 12 Z-slices spaced 0.3 μm , spanning the whole cell were used for image analysis. Scale bar 5 μm .

(c) Abscission is scored by measuring the distribution of GFP intensity values across the mother-daughter cell axis at the bud neck. Upper panel: membrane separation is marked by two distinct peaks in GFP intensity. Lower panel: cells that have yet to abscise show a single peak of intensity at the bud neck.

(d) Graph showing the fraction of cells that complete abscission from the time of membrane ingression. WT; n=number of cells from 1 experiment, *srs2 Δ* cells; n =number of cells pooled from N =3 independent experiments with similar results. WT vs. WT +HU, P <0.0001, Mann-Whitney test. WT +HU vs. *srs2 Δ* +HU, P <0.0001, Mann-Whitney test.

(e) Graph showing the fraction of cells that complete abscission from the time of spindle elongation. WT; n=number of cells from 1 experiment, *srs2 Δ* cells; n =number of cells pooled from N =3 independent experiments with similar results. WT +HU vs. *srs2 Δ* +HU, P <0.0001, Mann-Whitney test.

(f) Graph showing the fraction of cells that complete membrane ingression from the time of spindle elongation. WT; n=number of cells from 1 experiment, *srs2 Δ* cells; n =number of cells pooled from N =3 independent experiments with similar results. WT vs. WT +HU, P =0.035, Mann-Whitney test. WT +HU vs. *srs2 Δ* +HU, P <0.0001, Mann-Whitney test.

(g) Graph showing the fraction of re-budding events relative to the time of membrane ingression. WT; n=number of cells from 1 experiment, *srs2 Δ* cells; n =number of cells pooled from N =3 independent experiments with similar results. WT +HU vs. *srs2 Δ* +HU, P <0.0001, Mann-Whitney test.

Using the spindle pole marker Spc42-GFP, elongation of the spindle can be monitored as the two Spc42 foci in the short metaphase spindle quickly separate towards opposite poles during anaphase (Figure 12b). When measuring the time from onset of spindle elongation to abscission, *srs2 Δ* cells with or without the exposure to HU show the same dynamics as with non-treated wild-type cells (Figure 12e). However, when onset of spindle elongation is measured relative to membrane ingression it surprisingly reveals that *srs2 Δ* cells ingress the membrane slightly earlier by 2 minutes than non-treated wild-type cells (Figure 12f). Advanced membrane ingression is more pronounced after exposure to HU by 4 minutes earlier (from 16 to 12 min), suggesting that *srs2 Δ* cells progress faster after anaphase (spindle elongation) into abscission than wild-type cells.

Entry into a cell cycle, marked by a new budding event after cytokinesis (rebudding), was also delayed in HU-treated wild-type cells compared to non-treated and *srs2 Δ* cells (Figure 12g), implying that the delayed membrane resolution in HU-treated wild-

type cells affects entry into the next cell cycle. A similar observation was made in both condensin mutants, and topoisomerase II mutants, which had a delayed rebudding event. The mechanism remains unknown but may be due DNA damage in G1 (Amaral et al. 2016).

2.2.2 The Srs2 DNA helicase is required for abscission inhibition in the presence of catenated chromatin bridges

Next, I investigated if Srs2 is involved in abscission delay caused by catenated chromatin bridges by inactivating topoisomerase II using the temperature-sensitive allele *top4-2*. Cells were grown at 25°C and synchronized in G1 with α -factor for 2 hours (Figure 13a). G1 arrested cells were released into 37°C pre-heated media and placed in a 37°C pre-heated chamber for acquisition. Wild-type and *srs2* Δ cells expressing the GFP-CAAX plasma membrane marker undergo abscission at similar timing as at 30°C (Figure 12d). As observed in Amaral et al. (2016) inactivation of *top4-2* leads to a strong impairment in membrane resolution, with 92% of cells failing to complete abscission within 60 min (Figure 13b-d). This impairment is partially but significantly rescued in cells lacking Srs2 from 92% to 41% failing to abscise. Altogether, these data suggest that Srs2 is important to inhibit abscission in cells challenged with both HU-induced and catenated chromatin bridges.

Absence of the DNA helicases BLM and PICH has been shown to increase chromatin bridges in human cells exposed to DNA replication stress (by aphidicolin), possibly due to their vital role in resolving recombination intermediates during S phase (Chan, North, and Hickson 2007). In yeast, Sgs1 (hBLM), Top3 (hTOP3 α) and repair protein Dpb11 (hTopBP1) are associated with ultrafine bridges. Loss of Dpb11 leads to an accumulation of chromatin bridges which triggered a NoCut-dependent response (Germann et al. 2014). In contrast, loss of Srs2 minimizes the NoCut-mediated abscission delay. Next, I assayed the frequency of chromatin bridges in HU-exposed cells lacking Srs2.

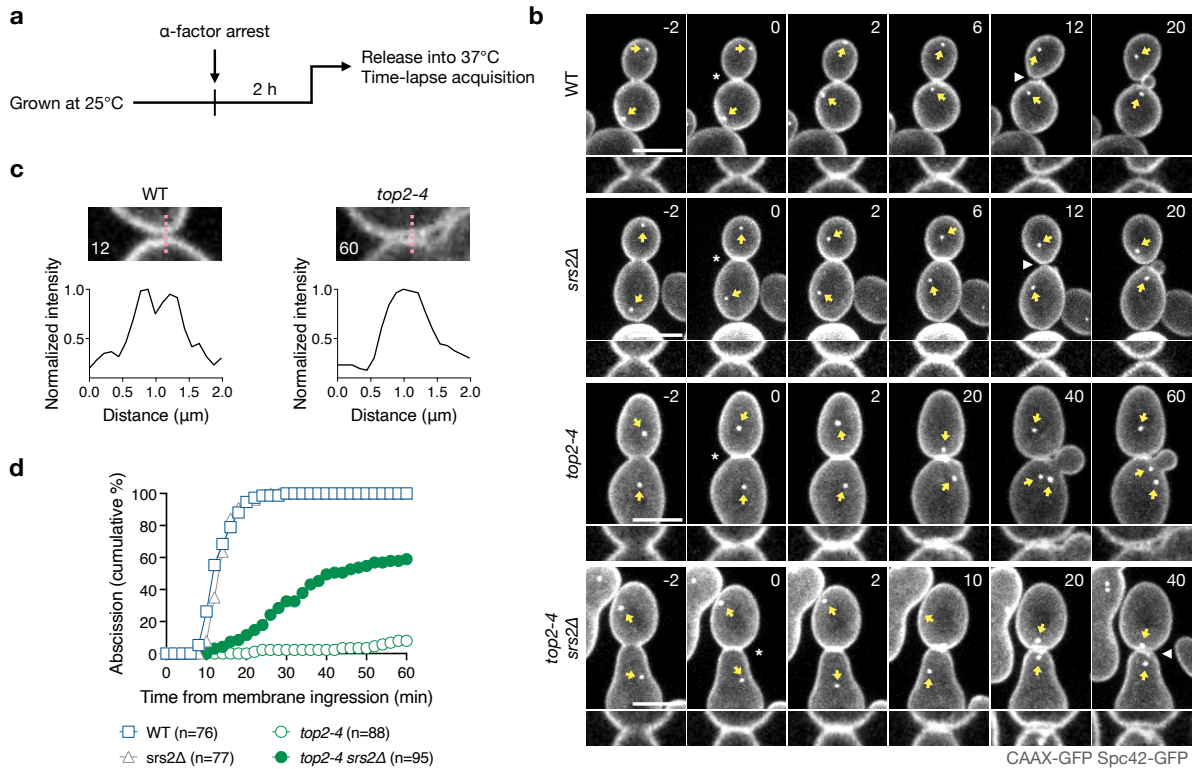


Figure 13. Srs2 delays abscission after topoisomerase II inactivation

(a) Experimental workflow for cell cycle synchronization with α -factor and *top2-4* inactivation by temperature shift.

(b) Membrane ingression and abscission in cells of the indicated genotypes. Cells are expressing plasma membrane marker CAAX-GFP and spindle pole marker Spc42-GFP. Time in minutes, 0 min indicates the start of membrane ingression. Yellow arrow marks the position of spindle poles. Asterisk specifies membrane ingression. White arrowhead marks complete separation of the plasma membrane. Z-projections are shown, 12 Z-slices spaced 0.3 μm spanning the whole cell were used for image analysis. Lower Zoom-in panel shows the dynamics of membrane ingression at the central Z-slice. Scale bar 5 μm .

(c) Abscission is scored by measuring the GFP intensity across the bud neck. Left panel: membrane separation is marked by a drop in intensity. Right panel: cells that have yet to abscise show a single peak of intensity at the bud neck.

(d) Graph showing the fraction of cells that complete abscission from the time of membrane ingression. n = cells pooled from $N = 3$ independent experiments with similar results. WT vs. *top2-4*, $P < 0.0001$, Mann-Whitney test. *top2-4* vs. *top2-4 srs2Δ*, $P < 0.0001$, Mann-Whitney test.

2.2.3 Srs2 prevents chromosome segregation with unreplicated DNA

Previous results from the lab, to which I contributed (Ivanova et al. 2020) showed that DNA synthesis during anaphase is associated with the appearance of single-stranded DNA marked by RPA foci. Moreover, we showed that freely-cycling cells undergoing anaphase with RPA foci were also delayed in completion of nuclear division, compared

to cells without RPA foci during anaphase. These results suggested that unreplicated DNA can cause a delay in chromosome segregation. In addition, Srs2 has been shown to be important for DNA damage checkpoint regulation in yeast through its ability to remove RPA along with Rad51 from the chromatin, thus inhibiting homologous recombination (Sasanuma et al. 2019; Dhingra et al. 2021). Therefore, deletion of *SRS2* leads to an increased RPA level on the chromatin and an overactivated DNA damage checkpoint signaling (Dhingra et al. 2021).

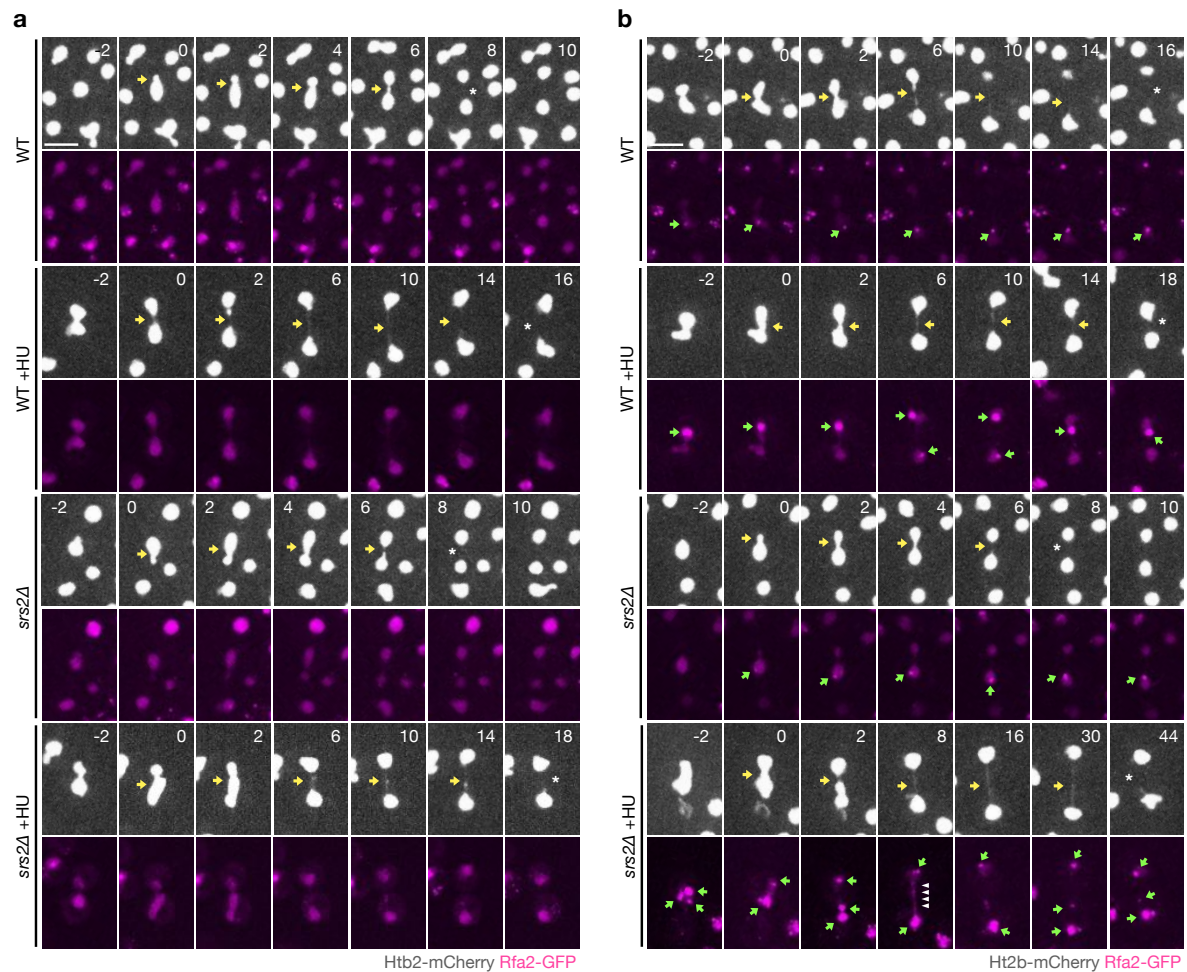


Figure 14. Srs2 promotes chromatin bridge resolution

(a) Chromosome segregation (Htb2-mCherry) and RPA foci formation (Rfa2-GFP) in WT and *srs2Δ* cells exposed to a pulse of HU as in Figure 1a, without the appearance of RPA foci during anaphase. Yellow arrow indicates chromatin bridge. Scale bar 5 μm.

(b) Chromosome segregation (Htb2-mCherry) and RPA foci formation (Rfa2-GFP) in WT and *srs2Δ* cells exposed to a pulse of HU, with the appearance of RPA foci during anaphase. Yellow arrow indicates chromatin bridge, green arrow points towards RPA foci, white arrowheads mark RPA bridges and asterisk notes bridge resolution. Scale bar 5 μm.

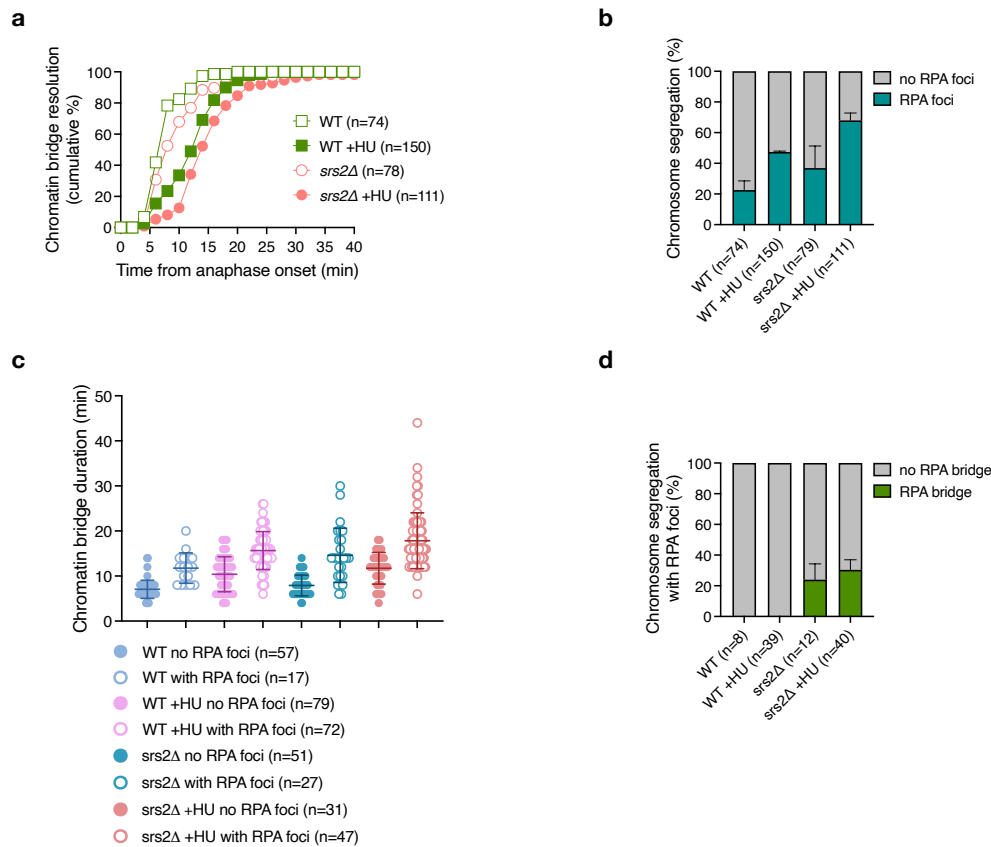


Figure 15. Srs2 reduces the frequency of RPA foci during chromosome segregation

(a) Quantification of cells shown in Figure 3. Graph showing the fraction of resolved bridges from the time of anaphase onset, defined by the rapid elongation of the nucleus. n =number of cells pooled from N =2 independent experiments with similar results. WT +HU vs. *srs2Δ* +HU, P =0.0002, Mann-Whitney test.

(b) Graph showing the fraction of chromosome segregations with RPA foci. Mean \pm SD.

(c) Quantification of the bridge lifetime (time from anaphase onset to bridge resolution) in cells with or without the appearance of RPA foci during anaphase (see Figure 3). Mean \pm SD.

(d) Graph showing the fraction of cells which segregated with RPA foci and had RPA-coated chromatin bridge. Mean \pm SD.

Yet, cells deleted of SRS2 have a normal abscission timing even in the presence of HU-induced chromatin bridges (Figure 12d) but start elongating the spindle earlier than wild-type relative to membrane ingression (Figure 12f). The time window of which chromosomes segregate before membrane ingression is thereby shortened in cells lacking Srs2, suggesting a loss of coordination between spindle elongation, membrane ingression and abscission. Therefore, I next assessed the stability of HU-induced chromatin bridges in *srs2Δ* cells and if there is a possible link between the increased levels of RPA in SRS2 deleted cells and the delay in nuclear resolution previously observed in cell with RPA foci during anaphase (Ivanova et al. 2020).

To this aim, I imaged cells expressing Ht2b-mCherry as a marker of the chromatin and Rfa2-GFP (subunit of RPA) were exposed to a HU pulse (Figure 14a-b) as in Figure 1a. The chromatin bridge duration was measured from the time of rapid elongation of the nucleus (anaphase onset) to the disappearance of a connecting chromatin bridge (Figure 14, Figure 15a). In unperturbed wild-type cells, the bridge resolves in 8.1 ± 3.1 min (\pm SD), but cells exposed to HU are delayed in resolving the bridge by 12.9 ± 4.8 min. Remarkably, HU-treated *srs2* Δ cells did not rescue the delayed HU-induced bridge resolution but rather significantly increased the time to resolve the chromatin bridge to 15.8 ± 6.1 min, even in the absence of HU. An increased fraction of cells undergoing anaphase with RPA foci were observed after exposure to an HU pulse, and this fraction was further elevated in absence of Srs2 (Figure 15b).

As previously shown in Ivanova et al. (2020), the presence of RPA is associated with a delayed bridge resolution in unperturbed wild-type cells (Figure 15c). The addition of HU delays bridge resolution even in anaphase cells without RPA foci, and further accentuates the delay in those that segregate with RPA foci. In dividing *srs2* Δ mutants, the delay in bridge resolution is even more aggravated in the presence of RPA foci. Interestingly, RPA-coated bridges never occurred in wild-type cells but were present in 20% of *srs2* Δ mutants which had RPA foci during anaphase (Figure 14b: bottom panel, Figure 15d). In summary, an increased fraction of cells lacking Srs2 undergo mitosis with under-replicated DNA, which also correlates with a prolonged bridge duration and is more elevated after replication stress. In addition, the loss of Srs2 also reduces the NoCut-mediated abscission delay. This is compatible with previous observations about NoCut inhibiting abscission to prevent chromatin bridge breakage.

2.2.4 The interaction of Srs2 with PCNA is important for a NoCut-dependent abscission delay

Srs2 is recruited by SUMOylated PCNA to the replication fork, where it inhibits HR. To test if its recruitment to chromatin is important for the role of Srs2 in delaying abscission, we first carried out the abscission assay with a cold-sensitive mutant of PCNA (*pol30-S115P*) and inactivated PCNA activity by switching from the permissive temperature to 14°C (Figure 16a). Inactivation of the *pol30-S115P* mutant has been shown to prevent the accumulation of *pol30-S115P* on the chromatin after MMS

treatment (Johnson et al. 2016), impairing DNA replication and possibly DNA repair (Ayyagari et al. 1995). Cells were grown at 30°C and exposed to HU for two hours before shifting the temperature to 14°C. Compared to the abscission dynamics at 30°C wild-type cells grown at 14°C take longer to abscise (median 22 min at 14C vs. 16 min at 30°C). While PCNA is essential for replication, inactivation of *pol30-S115P* does not significantly affect abscission (Figure 16a). The exposure to an HU pulse delays abscission (by 35 min) as similarly seen at 30°C and the delay can be rescued by the reduced activity of PCNA, suggesting that the presence of PCNA, and thereby Srs2 on the chromatin is important for NoCut.

Srs2 interacts with SUMOylated PCNA through its' C-terminal SIM and PIP-box, to further investigate which interaction is essential for its potential role as a bridge sensor we first deleted the SIM of Srs2. In a *top4-2* mutant, we induced catenated chromatin bridges by a temperature switch to 37°C in which all mutants fail to properly abscise within 60 min (Figure 16b). Interestingly, the deletion of SIM alone was not sufficient to rescue the abscission failure of *top4-2* mutants. Srs2 has a higher affinity to SUMOylated PCNA but can still interact with PCNA without the SIM (Pfander et al. 2005). We next deleted the PIP-box in the *srs2ΔSIM* mutant, disrupting the protein's interaction with SUMOylation and PCNA. The lack of both SIM and PIP-box partially but significantly ($p < 0.0001$) rescued the fraction of cells able to abscise by 28%. In summary, the recruitment of Srs2 to the chromatin and interaction with PCNA is important for Srs2 in promoting a NoCut-mediated abscission delay in the presence of catenated bridges. The deletion of both SIM and PIP-box on Srs2 prevents the interaction with SUMOylated-PCNA, which is important for its role in inhibiting abscission in the presence of catenated chromatin bridges.

(d) Graph showing abscission in dicentric strains deleted of PCNA-unloader Elg1. Dicentric cells; n = number of cells from N = 2 independent experiments, Dicentric *elg1Δ* cells; n = number of cells pooled from N = 3 independent experiments with similar results. Dicentric, with bridge vs. Dicentric, *elg1Δ* with bridge, P < 0.0001, Mann-Whitney test. Data shown panel **a**, **b** and **c** was collected by Nicola Brownlow, I generated the plots.

2.2.5 Retention of Srs2 on dicentric chromatin bridges inhibits abscission

Not all types of bridges are detected by NoCut, dicentric chromatin bridges do not inhibit abscission (Amaral et al. 2016). Dicentric strains were generated by first introducing a strong GAL1,10 promoter in front of the centromeric region of chromosome IV (CEN4), and the ends of chromosome IV and chromosome XII were fused together in the presence of galactose (Figure 16c). The addition of galactose to the growing media activates the gene expression of the GAL1 promoter, and its expression inactivates centromere 4 by an unknown mechanism, giving rise to a long monocentric chromosome that becomes dicentric upon a switch to glucose-containing media. Upon the re-activation of CEN4, as the cells progress into anaphase the two sister kinetochores bi-orient independently of each other, leading to dicentric chromatin bridges in 50% of anaphases (Figure 16c).

Interestingly, dicentric chromatin bridges do not trigger a NoCut response, indeed, cells with dicentric bridges have similar abscission kinetics to the wild-type regardless of the presence of bridges (Amaral et al. 2016). Therefore, we next investigated whether the retention of Srs2 onto the chromatin could render the dicentric chromatin bridges detectable by the NoCut checkpoint. Srs2 is recruited to the chromatin by SUMOylated PCNA, which is loaded onto the DNA by replication factor C. Once the replication fork has terminated PCNA is unloaded from the chromatin by the Elg1 replication factor C-like complex. By depleting its unloader Elg1, PCNA and Srs2 has been demonstrated to be retained on the chromatin (Parnas et al. 2010; Kubota et al. 2013). Subsequently, we deleted ELG1 in the conditionally dicentric mutants which expressed GFP-CAAX and Htb2-mCherry, and confirmed that abscission with a dicentric bridge is near the efficiency of wild-type (Figure 16d). Cells deleted of ELG1 with normal chromosome segregation also abscised with similar dynamics as wild-type, however in the presence of a dicentric bridge cells are delayed in abscission with 40% not being able to resolve the membrane within 60 min (vs. 95% Dicentric *elg1Δ*,

no bridge). This suggests that the presence of Srs2 on dicentric chromatin bridges is sufficient for an abscission delay when ELG1 is deleted.

Srs2 is important for inhibiting abscission while also being important for promoting segregation of chromosomes and (maybe) completion of DNA replication. The mechanisms are unclear, but it does raise the question of whether these functions are conserved in human cells.

2.3 Role of PARI in the abscission checkpoint

In the first part of the thesis, I showed that in the budding yeast DNA replication stress induced by HU pulse generates chromatin bridges with RPA foci. The presence of HU-induced chromatin bridges and catenated bridges by Top2 inactivation delay abscission, which was previously described to be mediated by the Aurora B-dependent NoCut checkpoint. We hypothesize that a chromatin-based signal is required for NoCut to trigger the abscission delay, and indeed, by deleting the DNA helicase Srs2 the abscission delay is abolished or reduced, indicating a defective checkpoint. In contrast, by presumably retaining Srs2 on dicentric bridges which normally do not trigger NoCut, abscission is now delayed specifically in the presence of chromatin bridges. We further established the importance of Srs2 associating with PCNA and its recruitment on the chromatin for delaying abscission in the presence of catenated bridges. Thus, our results support the possibility that Srs2 may act as a putative sensor of chromatin bridges for the NoCut checkpoint.

Chromatin bridges are commonly found in human cancer cells. Bridges are considered a marker of genomic instability and precursors of cell transformation as they can be damaged during either cytokinesis or the next interphase (Janssen et al. 2011; Finardi, Massari, and Visintin 2020) leading to chromothripsis, aneuploidy, and tetraploidy. The second part of the project will focus on the role of the human homolog of Srs2, in the response of HeLa cervical carcinoma cells to chromatin bridges.

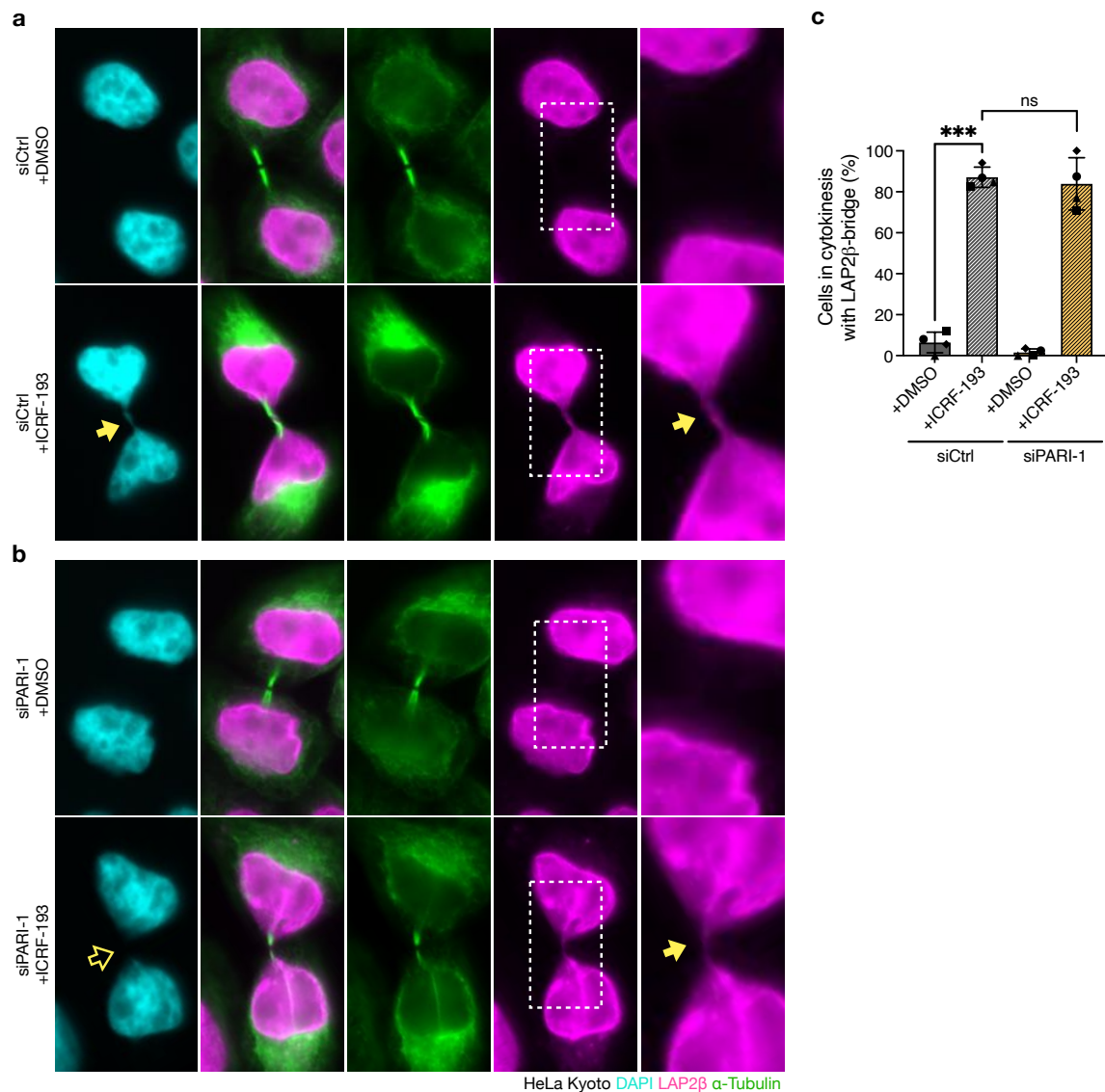


Figure 17. Inhibition of topoisomerase II using ICRF-193 induces catenated chromatin bridges

(a) Representative images of asynchronous siCtrl cells exposed to ICRF-193 for 16 hours. Cells stained with DAPI (cyan), and for LAP2β (magenta) and α-Tubulin (green). Yellow arrow point at bridge, outlined yellow arrow indicates a weakly stained DAPI bridge.

(b) Representative images of asynchronous cells transfected with siPARI-1 and exposed to ICRF-193 for 16 hours. Cells stained with DAPI (cyan), and for LAP2β (magenta) and α-Tubulin (green). Yellow arrow point at bridge, outlined yellow arrow indicates a weakly stained DAPI bridge.

(c) Quantification of the fraction of cells in cytokinesis with chromatin bridge, marked by LAP2β. Student's paired t test (mean ±SD, *P <0.05, **P <0.01; ***P <0.001; ****P <0.0001, n ≥1496 in total of N =4).

2.3.1 An assay to measure midbody stability in HeLa cells with chromatin bridges

To assay chromatin bridges, I used a catalytic inhibitor of topoisomerase II called ICRF-193 known to cause both catenated chromatin bridges and UFBs (Germann et al. 2014). Additionally, UFBs can be specifically generated at lower concentrations (Bhowmick et al. 2019). Asynchronous cells were incubated with 250 nM ICRF-193 for 16 hours, at this concentration the cell cycle is the least perturbed. The overall efficiency of the drug at generating chromatin bridges with the concentration of 250 nM was scored in cells undergoing cytokinesis (Figure 17). Cells in cytokinesis have a midbody connecting the daughter cells, thus, to identify cells at this stage by immunofluorescence (IF) an antibody against α -Tubulin was used. To score cytokinetic cells with a chromatin bridge DAPI can be used but it does not stain chromatin bridges very well, depending on the thickness of the bridge (Figure 17a). Therefore, I co-stained for the nuclear membrane protein LAP2 β as a marker of chromatin bridges. A small fraction (8%) of untreated cells displays LAP2 β -bridges in cytokinesis; I refer to these bridges as “spontaneous”. The fraction of cytokinetic cells with bridges was significantly increased with inhibition of TOP2 by ICRF-193 (8% and 88%, Figure 17a, c); I refer to these bridges as “catenated”.

The results in Figure 17 demonstrate that chromatin bridges induced by ICRF-193 persist during midbody formation. Next, I investigated the detailed structure of the midbody in the presence of a chromatin bridge using correlative fluorescence microscopy and electron microscopy (CLEM). The time human cells spend in cytokinesis is normally less than 10% of their whole cell cycle, so to assess the abscission dynamics of as many dividing cells with a chromatin bridge as possible, cells were synchronized with the double thymidine method. Cells are exposed to excess thymidine for 16 hours which inhibits the deoxynucleotide synthesis and arrest cells throughout S phase (Ma and Poon 2011). The arrest is followed by 8-hours release into normal cell culture media, and another 16-hours arrest with thymidine to induce a more synchronized block at the G1/S boundary (time 0, Figure 20b). Following the release from double thymidine block, cells reached G2/mitosis after about 7.5 hours, and cytokinesis after approximately 12 hours (left panel, Figure 20b). Various concentrations of ICRF-193 were tested at different time points from the release. Ultimately, the lowest tested concentration (250 nM) and late G2/early mitosis

(7.5 hours after release) were chosen to induce bridges, to minimize perturbing S-phase as much as possible (Figure 18a). Using CLEM with HeLa cells stably expressing H2B-mCherry and GFP- α -Tubulin, continuous chromatin can be observed going through the ICB and the microtubule-dense midbody and Flemming body in control cells (Figure 18b). Increased protrusions of the membrane are also observed around the midbody, possibly promoting stabilization of the intercellular canal with a chromatin bridge by increasing anchorage to the surface. However, other functions cannot be discarded. The microtubules of the midbody remained straight and ordered along the ICB even in the presence of a chromatin bridge. In summary, this will be the standard treatment to trigger catenated bridges.

2.3.2 The DNA helicase PARI, but not FBH1, promotes midbody stabilization in cells with topoisomerase II defects

Having established conditions to trigger chromatin bridge formation with high efficiency, I then assessed whether putative Srs2 human homologs are involved in the abscission checkpoint. Srs2 has four functional homologs RECQL5, FBH1, RTEL and PARI, in this project I will be focusing on its most direct homolog, PARI. The midbody stability is used to assess late cytokinesis progression into abscission. The time from midbody assembly (defined as the time when central spindle microtubules constrict into a bundle), to midbody disassembly (when the midbody severance by the ESCRT-III machinery and Spastin is complete), has been shown to be increased in the presence of chromatin bridges (Bhowmick et al. 2019). This interval will be referred to as the midbody lifetime. To assess midbody lifetime, I used time-lapse spinning disk confocal microscopy of synchronous HeLa cells stably expressing H2B-mCherry and GFP- α -tubulin. Cells were exposed to a low dose of ICRF-193 as previously described to generate bridges (Figure 18a). Anaphase can be clearly observed with MTOC and spindle microtubules pulling the chromosomes towards each future daughter cell (Figure 8a). In average, untreated control cells (treated with DMSO) disassemble the midbody 110 min after midbody formation. Interestingly, the addition of ICRF-193 delayed the midbody lifetime to 130 min. Thus, TOP2 inhibition caused a stabilization of the midbody, consistent with Bhowmick et al. (2019).

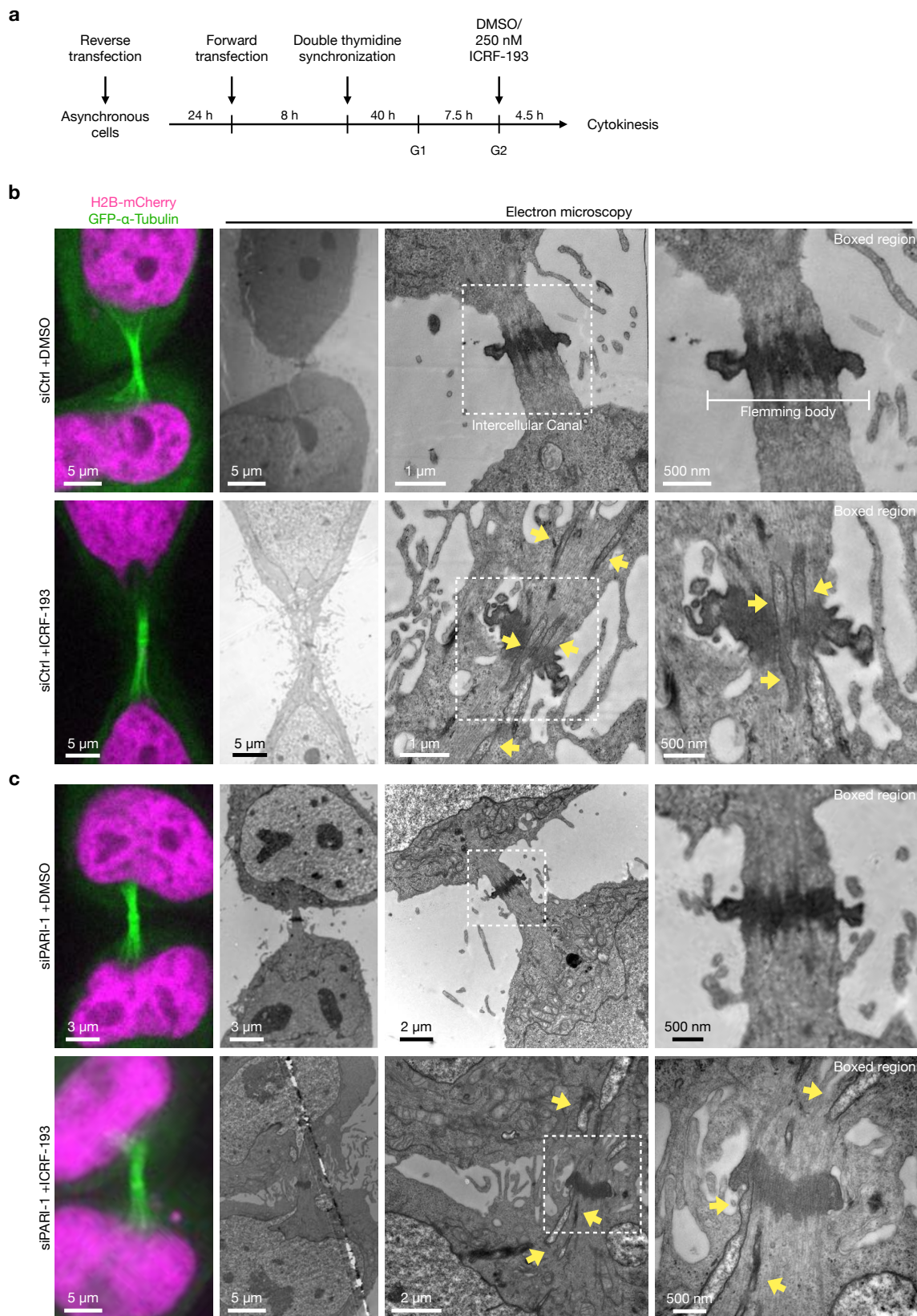


Figure 18. Correlative light electron microscopy shows catenated chromatin bridges pass through the midbody during cytokinesis

(a) Experimental workflow to synchronize siRNA transfected cells and inducing catenated chromatin bridges during cytokinesis by the addition of ICRF-193 at G2.

(b) Side by side comparison of electron microscopy images and fluorescent max projection images of HeLa cells stably expressing H2B-mCherry and GFP- α -Tubulin transfected with siCtrl. Yellow arrows pointing towards chromatin, boxed region zooming in on the Flemming body.

(c) Side by side comparison of electron microscopy images and fluorescent max projection images of HeLa cells stably expressing H2B-mCherry and GFP- α -Tubulin transfected with siPARI-1. Yellow arrows pointing towards chromatin, boxed region zooming in on the Flemming body.

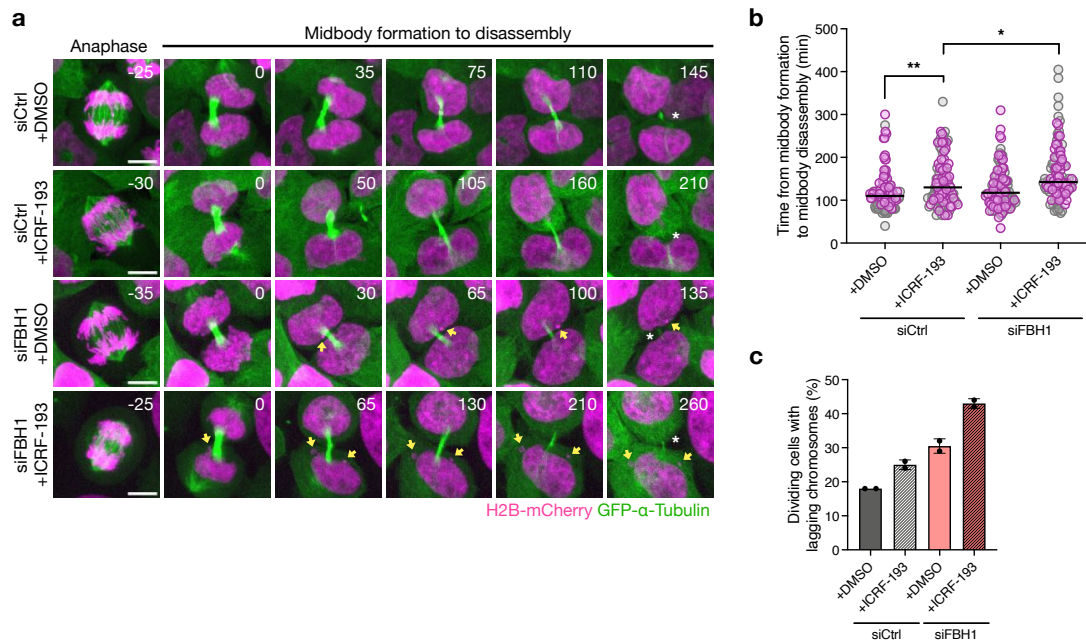


Figure 19. Another human homolog of Srs2, FBH1 is dispensable for midbody stability in the presence of catenated bridges

(a) Montage of representative FBH1-depleted HeLa cells progressing from anaphase to midbody formation and disassembly (GFP- α -Tubulin) with or without the presence of a catenated chromatin bridge (H2B-mCherry) induced by ICRF-193. Asterisk specifies midbody disassembly, yellow arrows point towards the presence of lagging chromosomes. Scale bar 5 μ m.

(b) Quantification of the midbody lifetime (time from midbody formation to disassembly). Mann-Whitney t (median, *P <0.05, **P <0.01; ***P <0.001; ****P <0.0001, n =100, N =2).

(c) Fraction of cells from b that had lagging chromosomes during cytokinesis. Mean \pm SD, N =2.

I next used siRNA to deplete the Srs2 human homolog FBH1, to assess if the DNA helicase has a role in cytokinesis. Instead, I observed a significant extended delay by 12.5 min compared to control cells treated with ICRF-193 suggesting that FBH1 is not required for the increased midbody lifetime. In addition, I observed an increased frequency of lagging chromosomes in FBH1-depleted cells (Figure 19a, c). I speculate that the increased delay in disassembling the midbody in FBH1-depleted cells is due to the increased frequency of lagging chromosomes, although this has yet to be described in the literature. In contrast, the presence of lagging chromosomes was observed to be damaged by cytokinesis (Janssen et al. 2011). In summary, FBH1 is not involved in stabilizing the midbody in the presence of catenated chromatin bridges.

Similarly, siRNA was used to deplete the most direct putative Srs2 homologue, PARI, and, I optimized a transfection protocol to efficiently knockdown PARI (Figure 20a). Unfortunately, neither commercially bought antibodies nor in-house generated polyclonal antibodies against PARI detected a specific band at the predicted size of 65 kDa in HeLa cells extracts. Consequently, RT-qPCR was used to determine PARI knockdown efficiency. With the optimized siRNA transfection protocol, siPARI-1 and siPARI-2 reduced PARI mRNA levels by 80% relative to HeLa cells transfected with the control siRNA. Next, cells were synchronized in G1 with double thymidine, released, and collected at various time points to determine the DNA content of control and PARI-depleted cells using flow cytometry (Figure 20b-c). Cells treated with PARI-specific siRNAs are slightly delayed in S compared to control cells (34% vs. 16%) at 7.5 hours after G1 release, although most cells at this timepoint are in G2/M. Most of the control cells segregated the chromosomes 12 hours after the G1 release (17%), while most PARI-depleted cells are still in G2/M (65%, Figure 20c). These results suggest that PARI downregulation leads to a slight delay (<2 hours) in S phase progression and in chromosome segregation. However, 14 hours after release of the cell cycle block, most (siCtrl 83% vs. siPARI-1 81%) siRNA-treated cells are in G1 phase. The observed cell cycle delay assayed by flow cytometry is consistent with a previous study (O'Connor et al. 2013).

Unlike depletion of FBH1, depletion of PARI did not increase the fraction of cells with chromatin bridges (1%, Figure 17b-c). Similarly, there is no significant difference in the frequency of chromatin bridge formation between control and PARI-depleted cells

treated with ICRF-193 (84%, Figure 17a-c). Together, these data indicate that depletion of PARI does not lead to the formation of chromatin bridges or accentuates the frequency of catenated chromatin bridges. Additionally, depletion of PARI does not seem to perturb the structure of the ICB during cytokinesis as seen by EM, as the morphologies are similar to cells with PARI (Figure 18c). There are similar protrusions of the plasma membrane around the ICB with a chromatin bridge, and the microtubules remain perpendicular to the ICB and in a dense bundle.

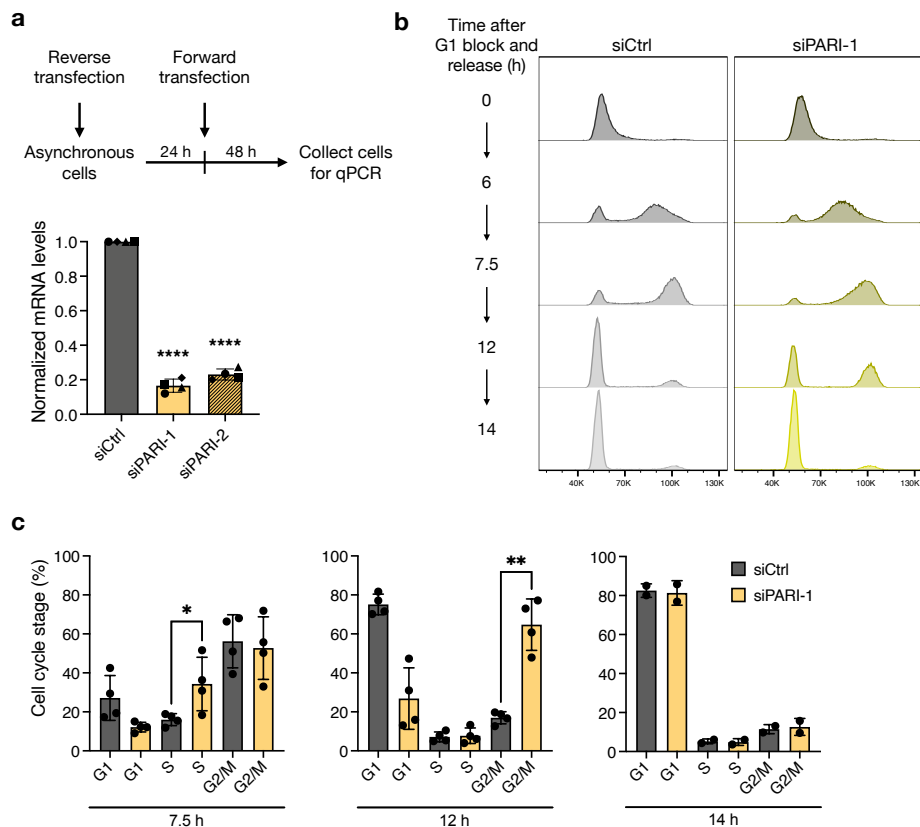


Figure 20. Absence of PARI slightly delays cells in S phase and exit from mitosis

(a) RT-qPCR measuring the mRNA levels of PARI in HeLa cells after transfecting twice with 25 nM siCtrl, siPARI-1 and siPARI-2. Relative mRNA levels have been normalized to siCtrl. One sample t and Wilcoxon test (mean \pm SD, *P < 0.05, **P < 0.01; ***P < 0.001; ****P < 0.0001, N = 4). (b) Cell cycle profile of siCtrl and siPARI-1 depleted cells. Transfected cells were synchronized in G1 with double thymidine and released. Cells were fixed with 70% EtOH at indicated times and stained with propidium iodide for 40 min to measure the DNA content by flow cytometry, 30.000 cells were measured.

(c) Quantification of the fraction of cells in G1, S and G2/M by given time point after G1 release. Student's paired t test (mean \pm SD, *P < 0.05, **P < 0.01; ***P < 0.001; ****P < 0.0001, N = 2-4).

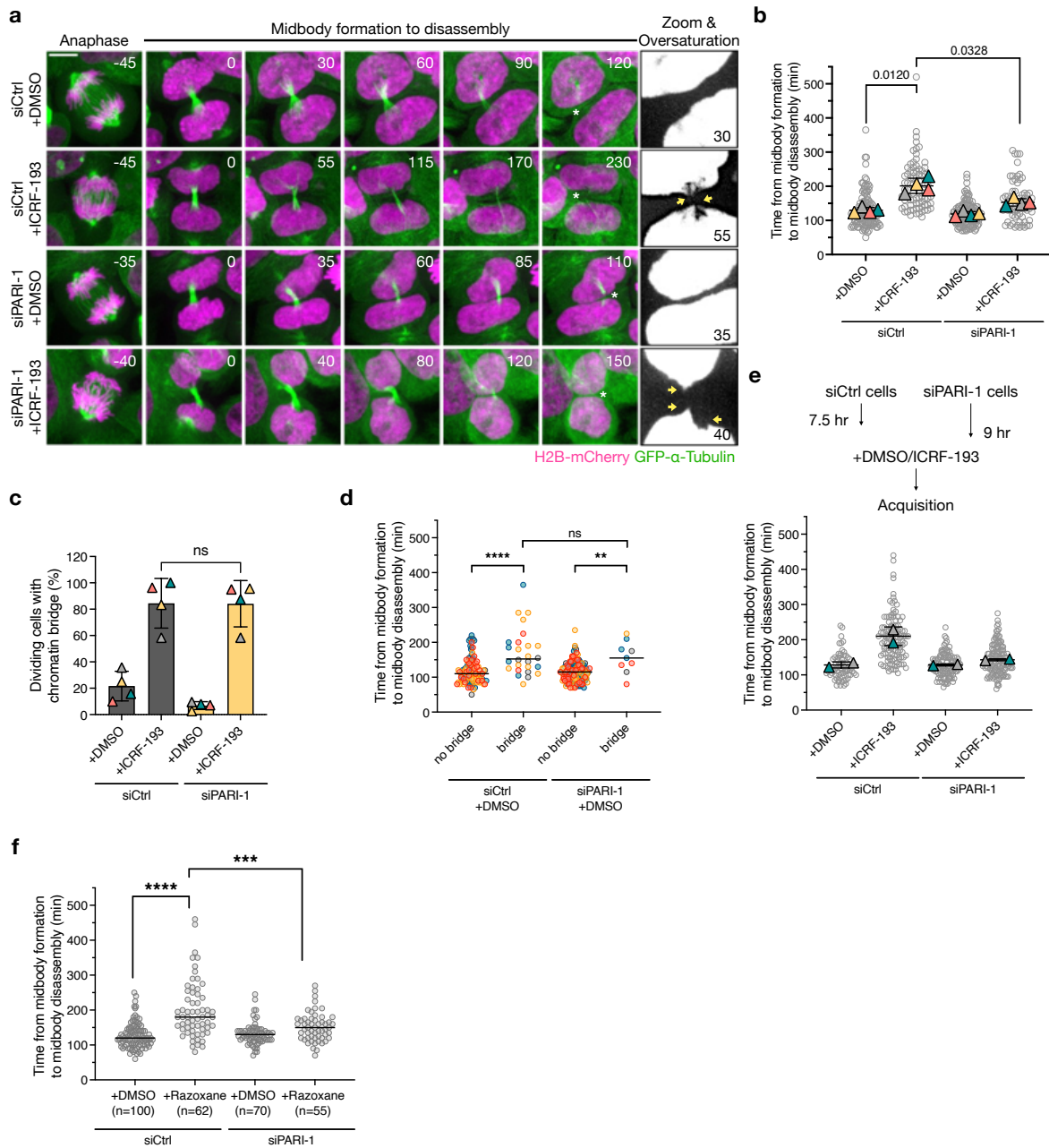


Figure 21. PARI promotes a delay in midbody disassembly in the presence of catenated chromatin bridges

(a) Montage of representative HeLa cells progressing from anaphase to midbody formation and disassembly (GFP- α -Tubulin) with or without the presence of a catenated chromatin bridge (H2B-mCherry) induced by ICRF-193. Cells were synchronized and treated as illustrated in Figure 8. Asterisk specifies midbody disassembly, yellow arrows pointing towards the presence of a chromatin bridge. Scale bar 5 μ m.

(b) SuperPlot showing the quantification of the midbody lifetime (time from midbody formation to disassembly). Each cell is represented as a grey dot, the mean of each independent experiment is represented as a triangle. Student's paired t test (mean \pm SD, *P <0.05, **P <0.01; ***P <0.001; ****P <0.0001, N =4).

- (c) Graph showing the fraction of cells with a chromatin bridge (H2B-mCherry). Each cell is represented as a dot, colors indicate each independent experiment. Student's paired t test (mean \pm SD, *P <0.05, **P <0.01; ***P <0.001; ****P <0.0001, n \geq 71, N =4).
- (d) The midbody lifetime of cells with spontaneous chromatin bridges. Median, n \geq 9.
- (e) Experimental workflow, ICRF-193 was added 1.5 hours later to PARI-depleted cells. SuperPlot showing the quantification of the midbody duration (time from midbody formation to disassembly) when ICRF-193 is added 1.5 hours later to PARI depleted cells. Mean \pm SD, n \geq 70, N =2.
- (f) SuperPlot showing the quantification of the midbody lifetime (time from midbody formation to disassembly) of cells treated with razoxane.

Next, I assessed the midbody stability of PARI-depleted HeLa cells expressing H2B-mCherry and GFP- α -Tubulin using the spinning disk microscope (Figure 21a). In untreated control cells, the midbody lifetime is on average 131 ± 8.1 min, whereas in the presence of ICRF-193 the midbody disassembly is significantly delayed to 202 ± 22 min (Figure 21b). Intriguingly, in absence of PARI, the delayed midbody disassembly is partially but significantly rescued to 154 ± 11 min. These results are reminiscent of the delay in completing abscission observed in budding yeast in response to catenated chromatin bridges, which is shortened in cells deficient in Srs2. Similar results were observed in cells treated with a different TOP2 catalytic inhibitor Razoxane, to validate that inhibition of topoisomerase II indeed delays midbody disassembly (Figure 21f). Together, these results suggest that the human homolog of Srs2, delays midbody disassembly specifically in the presence of chromatin bridges induced by topoisomerase II inactivation.

To address whether the role of PARI in regulating midbody lifetime is specific to PARI and not due to a possible off-target effects of the siRNA used, a siPARI-1 resistant version of PARI was designed. The putative seed region of siPARI-1 was identified, and three silent mutations were introduced that did not perturb the expression of the wild-type protein sequence but made the mRNA sequence non-detectable for degradation by siPARI-1 (Figure 22a). Finally, an eGFP-tag was added to the N-terminus of PARI for localization assays. Three HeLa Kyoto cell lines stably expressing eGFP, eGFP-PARI wild-type (eGFP-PARI^{WT}), and siPARI-1-resistant eGFP-PARI (eGFP-PARI^R) were generated (see Methods 6.2.2). Expression of these proteins was driven by the CMV promoter. The size and expression level of the GFP fusion proteins were assessed by western blotting of total cell extracts, and after immunoprecipitation

using an anti-GFP antibody (Figure 22b). GFP is detected in both the total extract (Input) and the IP at 25 kDa, whereas PARI fusions are not detected in the total extract (Input), suggesting their expression is low or perhaps because the PARI protein is intrinsically unstable. PARI fusions of the expected size are detected in the IP for both wild-type PARI and PARI-resistant, indicating that they are expressed at similar levels). In addition, eGFP-PARI^R resistance to siPARI-1 but not siPARI-2 was validated by qPCR (Figure 22c) and immunofluorescence (Figure 22d-e). Cells stably expressing PARI-fusions were fixed at late S phase, 6 hours after double thymidine block and release (Figure 20b). Consistent with previous PARI localization studies, eGFP-PARI is localized in the nucleus and foci can be observed throughout the nucleus suggesting its recruitment to replication forks or sites of repair (Burkovics et al. 2016; Mochizuki et al. 2017).

If a checkpoint-mediated delay is indeed lost in the absence of PARI, the reintroduction of the protein should restore the checkpoint response. Next, to see if the midbody disassembly delay caused by catenated bridges is restored in PARI-depleted cells by the expression of eGFP-PARI^R, HeLa Kyoto cells expressing eGFP or eGFP-PARI^R were depleted of the endogenous PARI using siPARI-1 and treated with ICRF-193 as in Figure 18a. The midbody and microtubules were visualized using SiR-Tubulin dye, and the midbody lifetime was measured from its assembly to the disassembly (Figure 23a). In cells expressing eGFP, addition of siPARI-1 significantly reduced the midbody lifetime, as previously observed in control HeLa cells (Figure 23, compare “eGFP” with ICRF-193-treated cells in Figure 21a). In contrast, siPARI-1 did not reduce midbody lifetime in cells expressing eGFP-PARI^R (Figure 23). Altogether, the results establish that stabilization of the midbody in cells with chromatin bridges is specifically mediated by PARI.

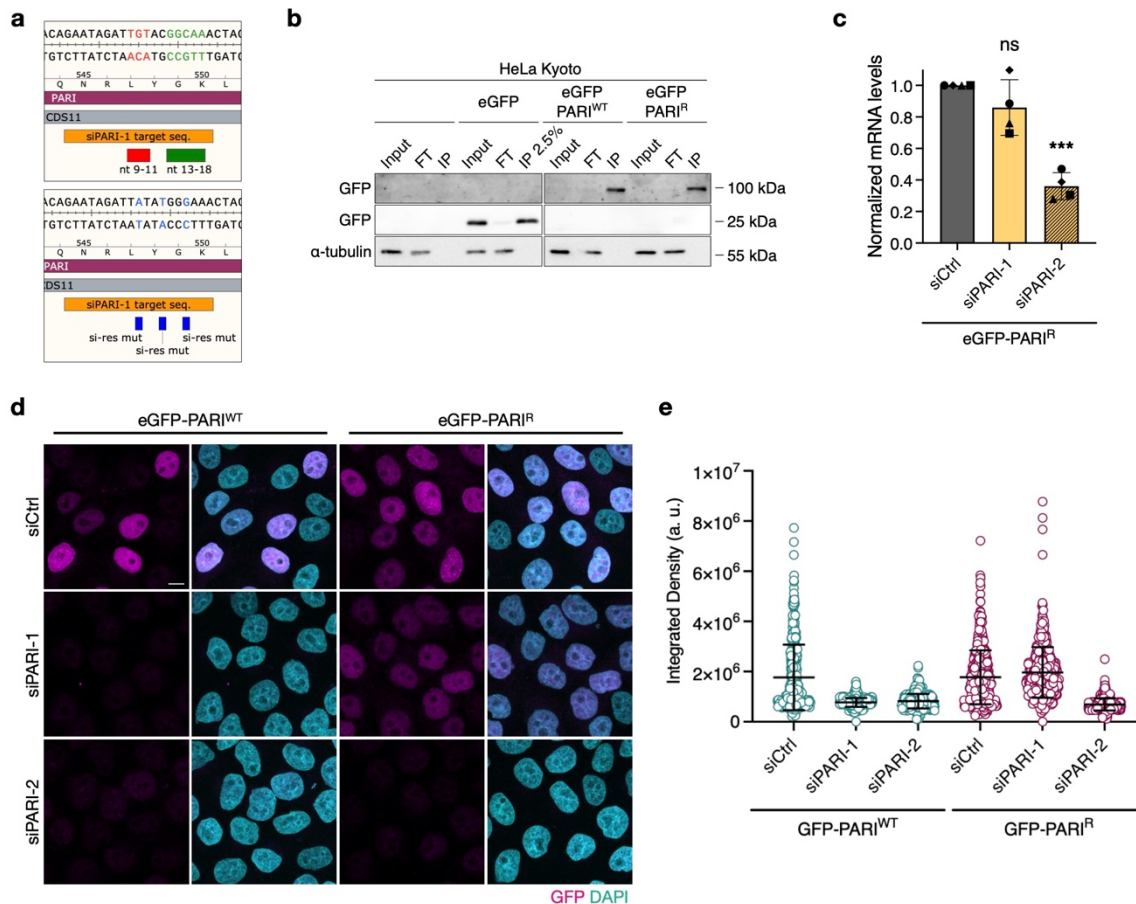


Figure 22. Validation of siPARI-1 resistant PARI stably expressed in HeLa

(a) Upper panel: WT siPARI-1 target sequence, features highlighting seed sequences. Lower panel: siPARI-1 resistant PARI sequence, features show where three silent point mutations were introduced by cloning.

(b) Western blot of HeLa cells stably expressing GFP, eGFP-PARI^{WT}, eGFP-PARI^R collected for IP with GFP-Trap magnetic agarose beads. Membrane probed with a GFP antibody and α -Tubulin as a loading control. (c) RT-qPCR measuring the mRNA levels of PARI in HeLa cells stably expressing siPARI-1 resistant eGFP-PARI^R after transfecting with siCtrl, siPARI-1 or siPARI-2. Relative mRNA levels have been normalized to siCtrl. One sample t and Wilcoxon test (mean \pm SD, *P <0.05, **P <0.01; ***P <0.001; ****P <0.0001, N =4).

(d) Representative fluorescent images of S phase synchronized HeLa cells stably expressing eGFP-PARI^{WT} and eGFP-PARI^R transfected with siCtrl, siPARI-1 and siPARI-2. Scale bar 5 μ m. Image analysis was performed by Bertrand Vernay of the Microscope facility at IGBMC.

(f) Quantification of nuclear GFP levels (integrated density). Mean \pm SD, n \geq 192.

In the assays presented so far, TOP2 is inactivated 7.5 hours after the release from G1. However, cells depleted of PARI are approximately 2 hours delayed compared to control cells (Figure 20b-c). Therefore, to ensure that the degree of late S phase/G2 perturbation is the same in control and PARI-KD cells, the midbody lifetime assay was repeated as in Figure 20a-b, except that ICRF-193 was added 1.5 hours later to PARI-

depleted cells to compensate for its cell cycle delay (Figure 20e). The midbody duration was measured and showed similar midbody disassembly dynamics as previously, the midbody of dividing control cells disassemble in 128 ± 8.7 min but is delayed to 210 ± 26 min with ICRF-193. Knockdown of PARI reduced the delay to 143 ± 2.8 min. Hence, adjusting the addition of ICRF-193 to PARI-depleted cells to approximately the same cell cycle stage as control cells do not change the rescue of the midbody delay in presence of a chromatin bridge.

Using H2B-mCherry to observe the appearance of chromatin bridges, spontaneous chromatin bridges were observed in 22% of untreated control cells and 7% in PARI-depleted cells, the percentage was increased to 85% when cells were treated with ICRF-193. The fraction of cells with a chromatin bridge is not significantly different in absence of PARI. Similar to asynchronous cells, PARI does not modulate the occurrence of chromatin bridges (Figure 17b). Subsequently, I asked if spontaneous chromatin bridges in the untreated conditions delayed midbody disassembly, previous study by Steigemann et al. (2009), showed that the midbody duration was not affected by the presence of spontaneous bridges. However, in my hands dividing control cells with a spontaneous bridge does significantly delay midbody disassembly (Figure 21d). In contrast to catenated bridges, spontaneous bridges in PARI-depleted cells significantly delay midbody disassembly. A caveat is that number of cells with a spontaneous bridge is much smaller (9 cells with spontaneous bridges in siPARI-1 and 26 cells in siCtrl) than those without (>104 cells without bridges) and does not hold the same weight when calculating the significance, more cells are needed to make a proper conclusion in regard to spontaneous bridges. Indeed, longer time-lapses and therefore more cells imaged confirm that PARI depletion shortens the delay in midbody disassembly in cells with spontaneous bridges (Figure 34b). Furthermore, the use of a nuclear envelope marker eGFP-BAF allowed improved bridge visualization compared to the previous time-lapse acquisition using H2B-mCherry (Figure 21d). In these experiments, spontaneous bridges were more easily identified in cells with proficient TOP2 (27% of dividing siCtrl cells vs. 25% in siPARI-1). The presence of spontaneous bridges in control cells delays midbody disassembly and similar to catenated bridges PARI depletion shortens the midbody lifetime of cells with spontaneous bridges (Figure 34b).

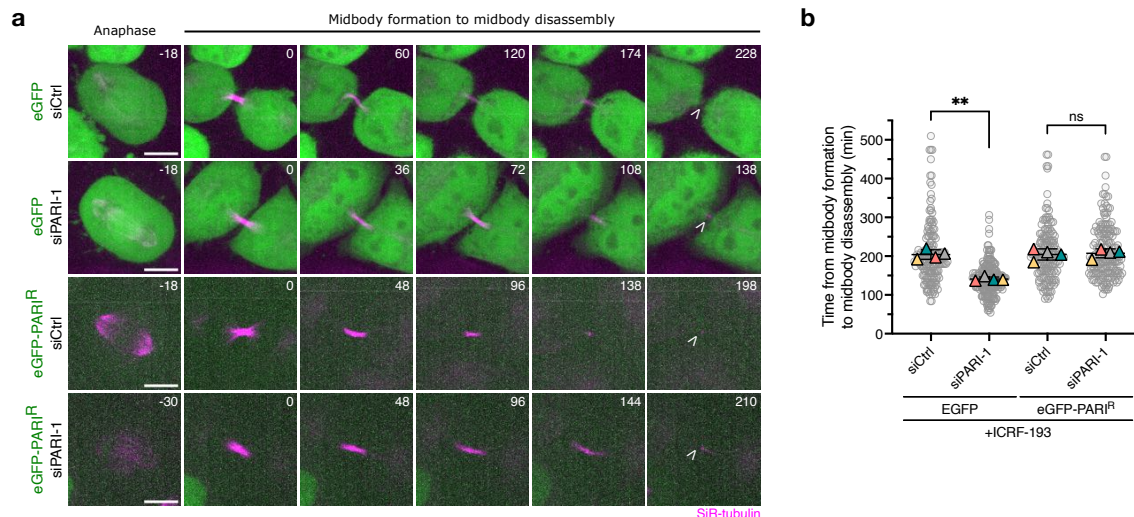


Figure 23. Expression of siPARI-1-resistant eGFP-PARI rescues the delay caused by TOP2 inactivation

(a) Montage of representative HeLa cells treated with ICRF-193 progressing from anaphase to midbody formation (SiR-Tubulin) and its disassembly. Cells have been synchronized and treated as illustrated in Figure 8. Open arrowhead specifies midbody disassembly. Scale bar 5 μ m.

(b) SuperPlot showing the quantification of the midbody lifetime (time from midbody formation to disassembly). Student's paired t test (mean \pm SD, *P <0.05, **P <0.01; ***P <0.001; ****P <0.0001, n \geq 165, N =4).

2.3.3 PARI promotes actin stabilization at the abscission site

In addition to midbody stabilization, F-actin has been shown to promote abscission checkpoint-mediated delay by accumulating at the ICB as actin-patches and stabilizing the canal in the presence of chromatin bridges (Steigemann et al. 2009; Dandoulaki et al. 2018; Bai et al. 2020). Next, I investigated if the accumulation of F-actin is dependent on PARI. Using HeLa stably expressing H2B-mCherry and GFP-actin, I assessed if catenated bridges caused accumulation of actin-patches near the ICB (Figure 24a). Indeed, upon ICRF-193 treatment in control cells strong accumulation of actin was observed near the chromatin bridge which persisted for at least 200 min from the time of membrane ingression, and within 700 min after membrane ingression only 25% of PARI-proficient cells with catenated bridges disassembled the actin-patches (Figure 24b). Interestingly, PARI-depleted cells disassembled the actin-patches faster than control cells with 60% of cells lacking actin-patches at 700 min after membrane ingression. Thus, PARI is required for the

stabilization of both midbodies and actin patches, structures that regulate normal abscission timing.

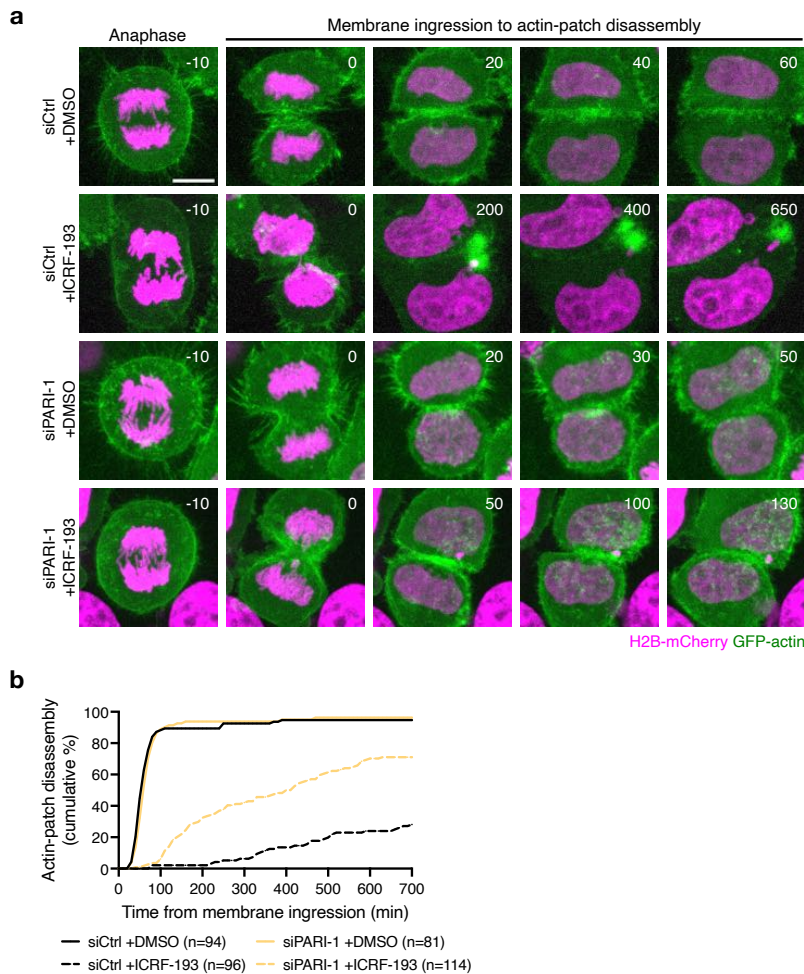


Figure 24. PARI promotes actin-patch accumulation at the intracellular bridge in cells with chromatin bridges

(a) Montage of representative HeLa cells progressing from anaphase to membrane ingression and actin-patch disassembly (GFP-actin) with or without the presence of a catenated chromatin bridge (H2B-mCherry) induced by ICRF-193.

(b) Quantification of the actin-patch duration (time from membrane ingression to actin-patch disassembly). n =cells pooled from N =3 independent experiments with similar results. siCtrl +DMSO vs. siCtrl +ICRF-193, $P < 0.0001$, Mann-Whitney test. siCtrl +ICRF-193 vs. siPARI-1 +ICRF-193, $P < 0.0001$, Mann-Whitney test.

2.3.4 PARI regulates midbody stability through an Aurora B-dependent pathway

To test whether catenated bridges induce a delay in midbody disassembly dependent on the Aurora B-mediated abscission checkpoint and to investigate if PARI is a component of the checkpoint, Aurora B was inhibited at the time of cytokinesis. HeLa cells stably expressing H2B-mCherry and GFP- α -Tubulin were synchronized with

double thymidine and treated with ICRF-193 according to the standard protocol. Based on previous acquisitions, midbody assembly occurred on average 120 min after acquisition start, at this point hesperadin was added in-between time intervals (Figure 25). Consistent with previous results control cells treated with only ICRF-193 had a midbody lifetime of 206 ± 67 min. Remarkably, the midbody lifetime was accelerated by 110 min to 94.4 ± 20 min and the absence of PARI does not significantly reduce the midbody lifetime (88.9 ± 21 min) as previously observed in the presence of catenated bridges. Depletion of PARI and inhibition of Aurora B did not further attenuate the already shortened midbody lifetime, suggesting that Aurora B and PARI act in the same pathway to regulate midbody disassembly.

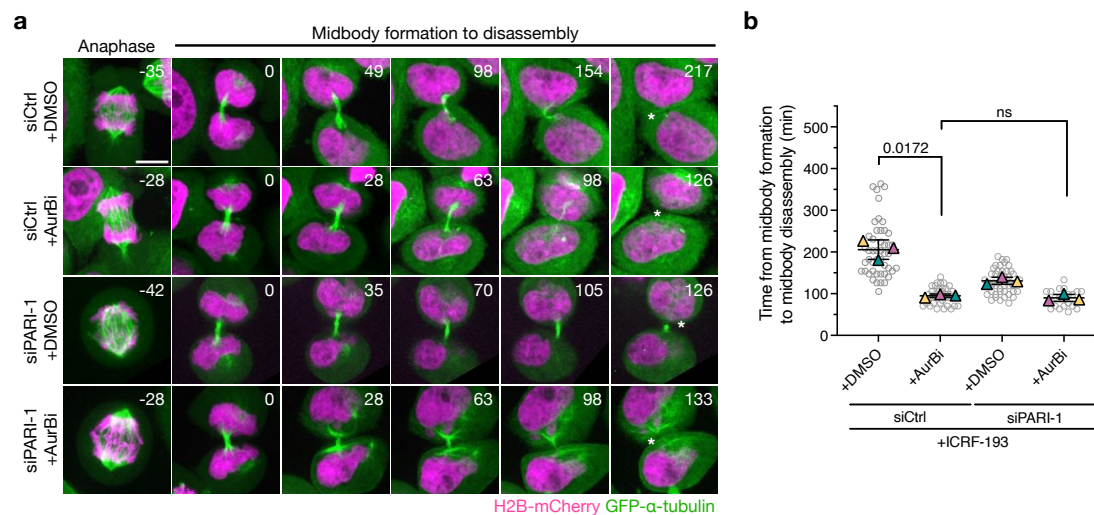


Figure 25. PARI is part of the Aurora B-dependent abscission checkpoint

(a) Montage of representative HeLa cells treated with ICRF-193 progressing from anaphase to midbody formation (GFP- α -Tubulin) and its disassembly. Cells have been synchronized and treated as illustrated in Figure 8, the Aurora B inhibitor hesperadin was added 120 min after the start of acquisition when most cells on average had formed the midbody. Asterisk specifies midbody disassembly. Scale bar 5 μ m.

(b) Quantification of the midbody lifetime (time from midbody formation to disassembly). Student's paired t test (mean \pm SD, *P <0.05, **P <0.01; ***P <0.001; ****P <0.0001, n \geq 20, N =3).

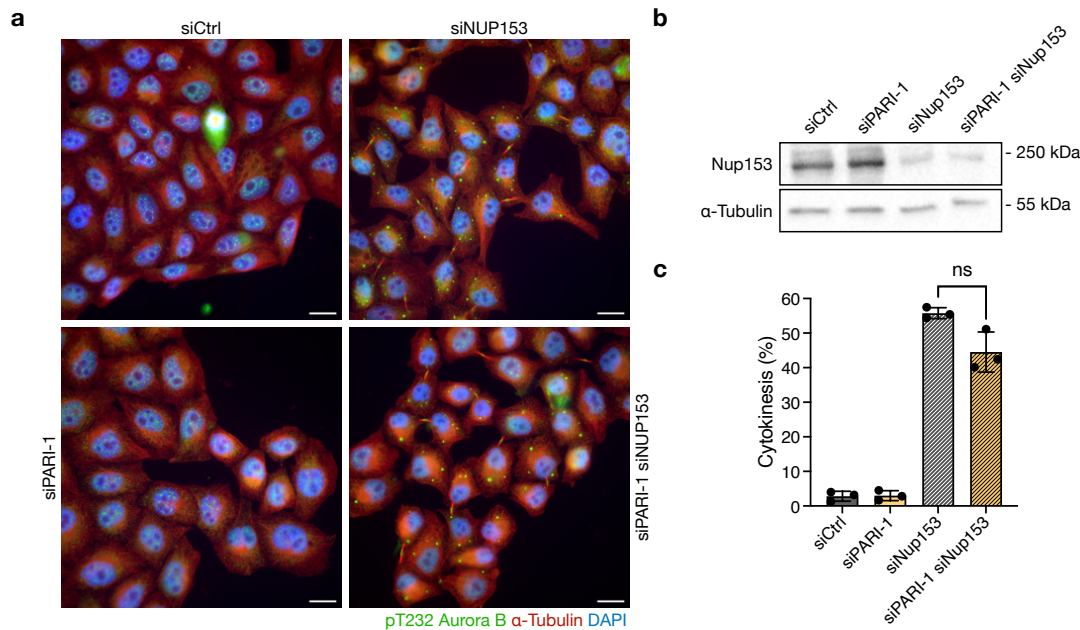


Figure 26. PARI is dispensable for delaying midbody disassembly upon nuclear pore assembly defects

(a) Representative fluorescent images of HeLa cells transfected with siCtrl, siNUP153, siPARI-1 and a combination of siPARI-1 + siNUP153. Cells were synchronized with thymidine for 24 hours, released for 16 hours and fixed.

(b) Western blot showing partial depletion of NUP153. Membrane probed with a NUP153 antibody and α -Tubulin as a loading control.

(c) Quantification of the fraction of cells arrested in cytokinesis. Student's paired t test (mean \pm SD, *P <0.05, **P <0.01; ***P <0.001; ****P <0.0001, n \geq 789, N =3).

2.3.5 PARI does not stabilize midbodies in cells with NPC defects

It has been shown that defects in nuclear pore assembly by depleting the essential nucleopore basket component NUP153 delay midbody disassembly without the occurrence of chromatin bridges (Mackay, Makise, and Ullman 2010). To test if PARI is involved in this response, NUP153 was partially co-depleted with PARI (see Methods 4.2.2). The NUP153 protein level of asynchronous HeLa cells was determined by WB and observed to be partially depleted after transfection, co-depletion with PARI did not alter the levels (Figure 25b). Cells were synchronized in G1/S with thymidine for 24 hours and released for 16 hours. The NUP153-depleted cells were distinctively arrested in cytokinesis with cytoplasmic "abscission checkpoint bodies" (ACB) which was suggested to indicate a responsive abscission checkpoint (Strohacker et al. 2021) (Figure 26a). Only 3% of control and PARI-depleted cells were in cytokinesis 16 hours after the G1 release (cell cycle analysis in Figure 6 showed

that most cells already divided after 14 hours), whereas the partial depletion of NUP153 arrested 56% of cells in cytokinesis. The fraction of midbody-stage cells appears slightly reduced in the absence of PARI (56% vs. 45%) but this difference was not statistically significant ($p = 0.0984$, student's t-test) (Figure 26c). Therefore, PARI is not required for midbody stabilization upon nuclear pore assembly defects, but rather it seems to be important specifically to stabilize the midbody in the presence of chromatin bridges.

2.3.6 PARI localization is restricted to the nucleus during S-phase

The results so far have shown indications of the DNA helicase PARI acting in the abscission checkpoint. My experiments in yeast suggest that retention of the yeast PARI homologue Srs2 in chromatin bridges is sufficient to delay abscission (Figure 12d, 13d). Therefore, I investigated whether PARI is localized to chromatin bridges in HeLa cells to promote midbody stability. In human embryonic kidney 293T cells, GFP-PARI has been observed by immunofluorescence to localize as nuclear foci during S phase as it is being recruited to the replication fork (Burkovics et al. 2016; Mochizuki et al. 2017). In addition, GFP-PARI is diffusely distributed in the nucleus during G2 but can rapidly accumulate within a few seconds at sites of DNA damage induced by laser irradiation. However, the localization of PARI in G1 and M phase has yet to be described. Using time-lapse microscopy, I imaged where PARI is localized throughout the cell cycle using HeLa Kyoto stably expressing eGFP-PARI (Figure 16a). At the beginning of the acquisition (timestamp 00:00) no eGFP signal is observed in the nucleus. However, at timestamp 5:20 eGFP foci are observed in the nucleus (marked with dotted line) most likely marking S phase. The signal becomes homogenous throughout the nucleus after 3 hours, marking G2. As the centrosomes segregate towards opposite poles and the mitotic spindle is formed which also marks nuclear envelope breakdown, the GFP signal disperses into the cytoplasm (Figure 27a-b). I was not able to detect any PARI localization to the chromatin nor to the midbody after mitotic entry in cells treated with either ICRF-193 or DMSO.

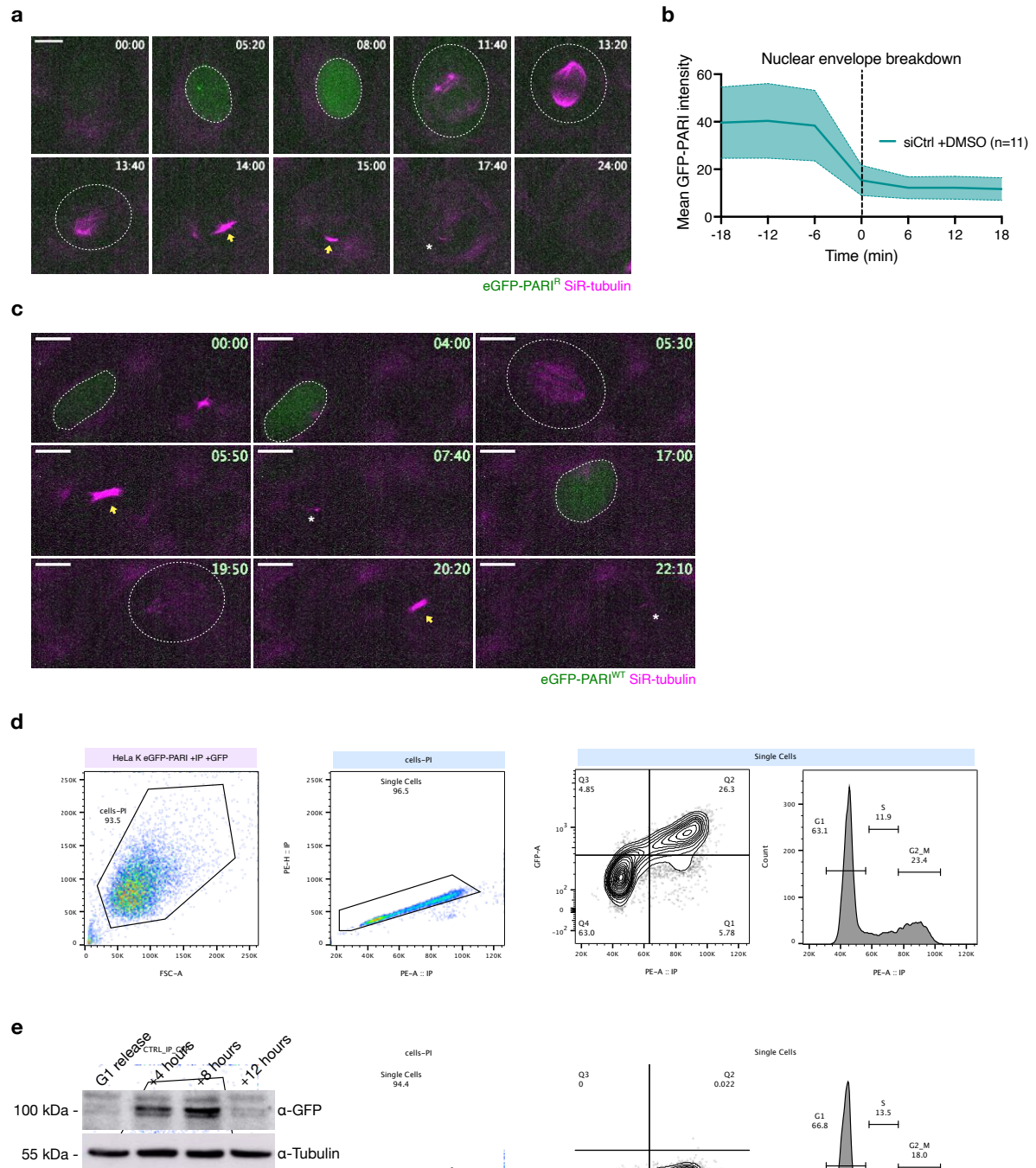


Figure 27. eGFP-PARI has a nuclear localization during interphase

(a) Montage of HeLa cells stably expressing eGFP-PARI^R treated with ICRF-193 progressing from pre-nuclear localization through mitosis and cytokinesis. Time is indicated in h:min, dotted lines roughly outline the nucleus, and the cytoplasm as seen by the GFP distribution, yellow arrow points at midbody, asterisk marks midbody disassembly. Scale bar 5 μm.

(b) Quantification of GFP-PARI levels as the nuclear envelope breaks down, marked by centrosomes moving to opposite poles. n = number of cells from N = 1 experiment.

(c) Montage of non-treated HeLa cells stably expressing eGFP-PARI^{WT} progressing from pre-nuclear localization through two cell cycles. Time is indicated in h:min, dotted lines roughly outline the nucleus, and the cytoplasm as seen by the GFP distribution, yellow arrow points at midbody, asterisk marks midbody disassembly. Scale bar 5 μm.

(d) Analysis of the eGFP-PARI intensity relative to the cell cycle stage. Gating strategy in Supplementary Figure 2.

(e) HeLa Kyoto cells stably expressing GFP-PARI were synchronized using double thymidine and released into fresh media. Lysates were collected at indicated hours after release and analyzed by western blot.

Upon a new cell cycle entry, PARI becomes nuclear again possibly during S-phase, but not immediately after midbody disassembly, suggesting that early G1-phase cells have lower amounts of PARI than S-phase cells (Figure 16c). The eGFP-PARI signal peaking at S phase and G2 was recapitulated by WB of double thymidine synchronized cells collected at various time-points after release (Figure 27e). Notably, despite the expression of eGFP-PARI, the signal difficult to detect in living cells. To analyze the eGFP-PARI signal relative to the cell cycle stage, asynchronous cells were fixed and stained with a GFP antibody coupled with Alexa-488, and the GFP signal intensity was determined in cells with different DNA content using flow cytometry (Figure 27d, Supplementary Figure 1). The cell cycle analysis showed that all G1 cells are GFP-negative; note that this population probably includes cells in cytokinesis as they have formed two new daughter nuclei if they are separated during the flow cytometry procedure. The eGFP-PARI signal increases with the cell cycle progression into G2/M, suggesting PARI-GFP levels increase during cell cycle progression. Finally, a subpopulation of G2/M cells show a lower GFP signal, suggesting that PARI levels drop at the end of the cell cycle. In summary, PARI is probably not associated with chromatin bridges in HeLa cells, at least within the detection limit of our microscopy setup.

The recruitment of PARI to chromatin is dependent on PCNA. Indeed, deletion of SIM and the PIP-box abrogates the formation of PARI foci during S-phase (Burkovics et al. 2016). Although I cannot detect PARI in chromatin bridges, I decided to test whether its partner PCNA (for which there are available specific antibodies) can be detected at this location. To verify whether PCNA is retained on chromatin bridges, HeLa K cells were synchronized with double thymidine and released from G1 and fixed at cytokinesis, 12 hours after the release. PCNA was visualized with an antibody under methanol fixation. However, under this fixation condition, anti-tubulin antibodies did not stain microtubule structures. Therefore, to identify cells in cytokinesis I stained for the localization of monophosphorylated CHMP4C, an ESCRT-III component.

pCHMP4C localizes at the midbody ring, and cells without the pCHMP4C ring were assumed to be in interphase (Figure 28a). Similar to PARI, PCNA was only observed in the nucleus of cells in interphase (Figure 28b), no PCNA was observed in nuclei with a chromatin bridge, or in bridges themselves. Notably, the fraction of PCNA-positive interphase cells is higher in PARI-depleted cells after ICRF-193 treatment than the other conditions, therefore it is possible that these cells are delayed in G2 rather than being in the next S-phase. In any case, conclude that PARI and PCNA are localized to the nucleus during S-phase and G2, but that neither of these proteins is detectable from mitotic entry until the next S-phase. Neither PARI nor PCNA is actively localized to the chromatin or midbody after mitosis, even in the presence of a catenated chromatin bridge. These results suggest that PARI might act in S or G2 phases to indirectly prolong midbody stability during cytokinesis.

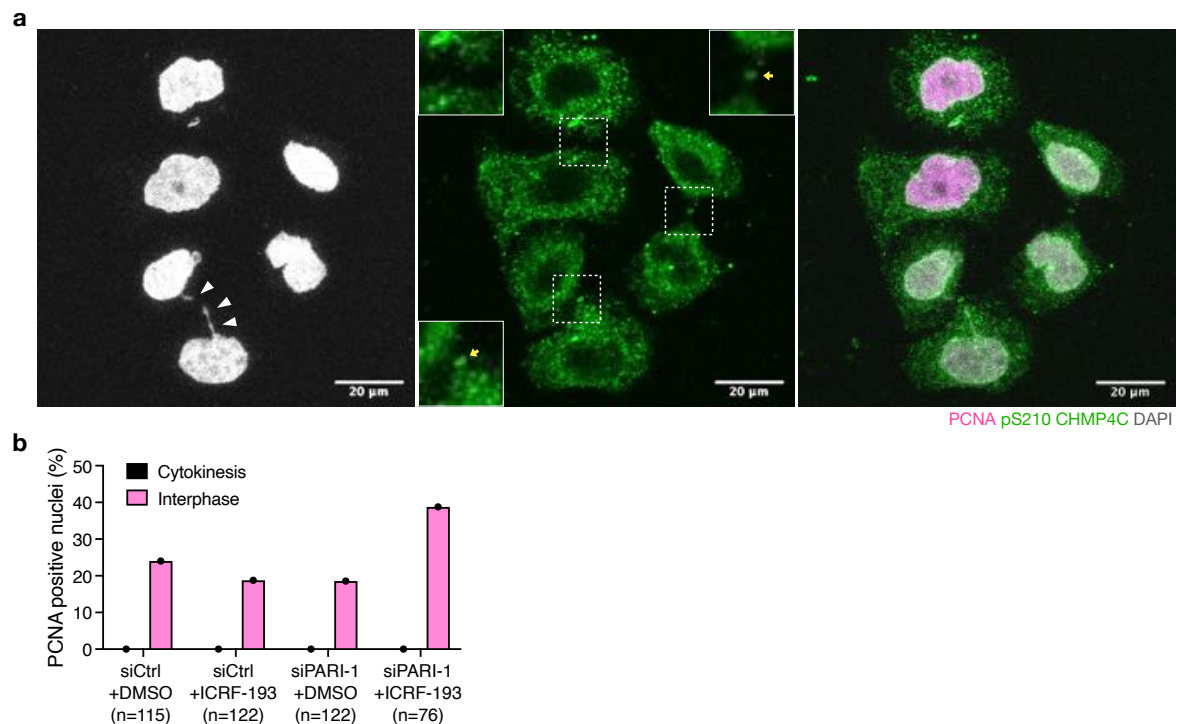


Figure 28. PCNA is localized to the nucleus of cells in interphase

(a) A representative fluorescent image of ICRF-193 treated HeLa cells stained for PCNA (magenta), pS210 CHMP4C (green) as a marker of cytokinesis and DAPI (grey). White arrowhead marks a chromatin bridge, yellow arrows points towards the localization of pS210 CHMP4C at the midbody (see Figure 17c).

(b) Quantification of PCNA positive nuclei in interphase or cytokinesis. n =number of cells from N =1 experiment.

2.3.7 PARI does not promote anaphase DNA synthesis

The knockdown of PARI leads to hypersensitivity to DNA-damaging agents due to an increased HR and therefore increased toxic DNA repair synthesis (Moldovan et al. 2012; Burkovics et al. 2016). To test if PARI and the additional catenation stress by ICRF-193 causes DNA synthesis on catenated chromatin bridges, an EdU incorporation assay was performed to detect active DNA repair synthesis. Cells were synchronized with double thymidine, released from G1 as in Figure 18a. At different times of the cell cycle, cells were treated with the nucleotide analogue EdU for 40 minutes to allow its incorporation into replicating DNA. As a positive control, EdU was added during S phase; in parallel, EdU was added to cells in cytokinesis to detect DNA synthesis in the late cell cycle (Figure 29, experimental setup). Cells were then fixed during cytokinesis and EdU was coupled to an Alexa-647 fluorophore through Click-iT reaction for detection by microscopy (see Methods 4.5.3).

Cells exposed to EdU pulse during S-phase showed intense foci of active DNA synthesis throughout the nucleus, which was absent or very faint along the chromatin bridge in cells treated with ICRF-193 (Figure 29a). The low detection of EdU on the chromatin bridges could be due to limited detection sensitivity for small amounts of DNA, similarly to how DAPI and H2B-mCherry do not work well as a marker of chromatin bridges with our current microscopy setup. Alternatively, low levels of EdU in chromatin bridges could indicate that they contain regions of unreplicated DNA. However, a recent paper by Umbreit et al. (2020) chromatin bridges were shown to be poorly replicated. Cells exposed to EdU during cytokinesis showed no EdU incorporation, and there was no distinct difference observed between control cells and cells treated with ICRF-193 (Figure 29b). Interestingly, depletion of PARI did not promote EdU incorporation under the conditions examined. In all, these results do not support mitotic DNA synthesis on ICRF-193-induced chromatin bridges. Moreover, depletion of PARI did not appear to increase DNA synthesis during cytokinesis to detectable levels. Absence of PARI has been observed to increase DNA synthesis in vitro (Moldovan et al. 2012; Mochizuki et al. 2017).

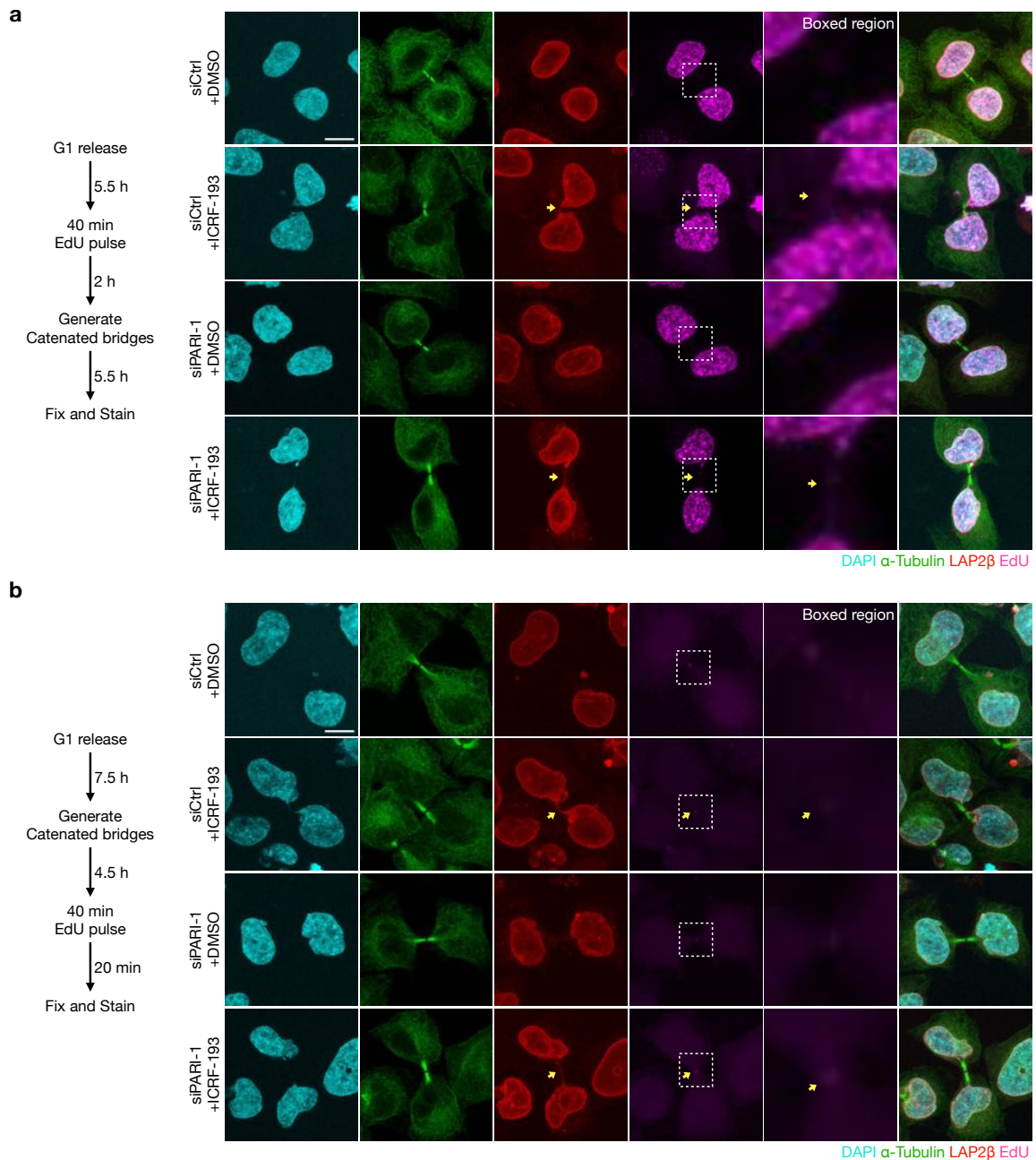


Figure 29. DNA synthesis is absent on catenated chromatin bridges

(a) Experimental workflow of control experiment. Representative fluorescent image showing EdU incorporation (magenta) during S phase persisting into cytokinesis. Co-stained with DAPI (cyan) and against α -Tubulin (green) and LAP2 β (red). Yellow arrow points towards a LAP2 β -bridge, boxed region highlights the ICB.

(b) Experimental workflow of test experiment. Representative fluorescent image of a cell in cytokinesis exposed to EdU pulse (magenta). Co-stained with DAPI (cyan) and against α -Tubulin (green) and LAP2 β (red). Yellow arrow points towards LAP2 β -bridge, boxed region highlights the ICB.

In all, these data leave an open question of whether PARI can directly act as a sensor of chromatin bridges to the abscission checkpoint by associating with the chromatin or if it is promoting abscission delay through the checkpoint by a different pathway, such as the DNA damage checkpoint. We cannot completely exclude the possibility of PARI and PCNA being localized to the chromatin bridge, due to limited detection.

2.3.8 The abscission machinery remains unperturbed in absence of PARI

Aurora B inhibits abscission by phosphorylating the ESCRT-III component CHMP4C on Ser210, among other residues (Capalbo et al. 2016). In the presence of chromatin bridges, phosphorylation of CHMP4C leads to retention of another ESCRT-III component, the ATPase VPS4, at the midbody. This prevents the migration of VPS4 to the site of abscission next to the Flemming body, where VPS4 is required for the complete constriction of the intercellular canal (Thoresen et al. 2014). Therefore, in the presence of a chromatin bridge, VPS4 is accumulated at the midbody with activated Aurora B and CHMP4C (Carlton et al. 2012; Thoresen et al. 2014). Consistent with these observations, a recent study showed that an abscission checkpoint-mediated delay induced by ICRF-193 lead to the accumulation of pCHMP4C and VPS4 at the midbody (Bhowmick et al. 2019).

Next, I asked if the reduced midbody lifetime in PARI-depleted cells with catenated bridges (Figure 21b) were due to altered localizations of phosphorylated Aurora B, CHMP4C, and VPS4 to the midbody (Figure 30). HeLa cells stably expressing H2B-mCherry and GFP- α -Tubulin were treated as Figure 18a and fixed 12 hours after release. Cells were then stained with antibodies specific for pT232 Aurora B. The presence of bridges was assessed with H2B-mCherry, and the midbody with GFP- α -Tubulin. The intensity of active Aurora B was measured by tracing around the Flemming body. There was a slight but not significant increase of pT232 Aurora B in the presence of a chromatin bridge, but no clear difference in absence of PARI (Figure 30a-b). Therefore, Aurora B activity and localization is not dependent on PARI.

In normally dividing cells, monophosphorylated CHMP4C is localized as a ring in the Flemming body. To measure the intensity of pCHMP4C, a line was drawn across the ring and midbody, and the highest intensity value was plotted (Figure 30c-d). There

was no significant difference in intensity observed between conditions, and the localization pattern of pS210 CHMP4C remained the same. Therefore, neither exposure to ICRF-193, nor depletion of PARI affects the accumulation or the localization of phosphorylated CHMP4C at the midbody, which is in contradiction to previous study by Bhowmick et al. (2019) which showed that ICRF-193 induced abscission checkpoint delay led to accumulation of pCHMP4C and VPS4 at the midbody.

Lastly, I monitored the localization of VPS4 using an antibody, which recognizes both orthologs VPS4A and VPS4B. The microtubules in the Flemming body cannot be stained by antibodies and are detected as a gap in the middle of the midbody. Notably, VPS4 did not localize to the Flemming body nor as rings flanking the Flemming body as previously reported (Thoresen et al. 2014; Mierzwa et al. 2017; Bhowmick et al. 2019). Rather, VPS4 was observed along the midbody arms and peaking in intensity at the sides of the Flemming body (Figure 30e). Possible reasons for discrepancies are the different cell lines used such as osteosarcoma U2OS and fibrosarcoma HT1080 and using a stable expression versus antibodies to visualize VPS4. The fixation and permeabilization protocol also affect the accessibility for antibodies. Three localization patterns were observed relative to the tubulin staining; no peaks of VPS4, one peak of VPS4, and two peaks of VPS4 on the sides of the Flemming body. Late midbodies, close to complete abscission show two peaks with one of the peaks shaped in a cone pointing towards the site of abscission (Figure 30g). I speculate that the localization of VPS4 temporarily and spatially starts as no peak, then as one peak and, finally as two peaks before abscission. The one peak pattern was more frequent in control cells with a catenated chromatin bridge and diminished upon the depletion of PARI (Figure 30f). This suggests that midbodies are stabilized in a specific stage with VPS4 as “one peak”.

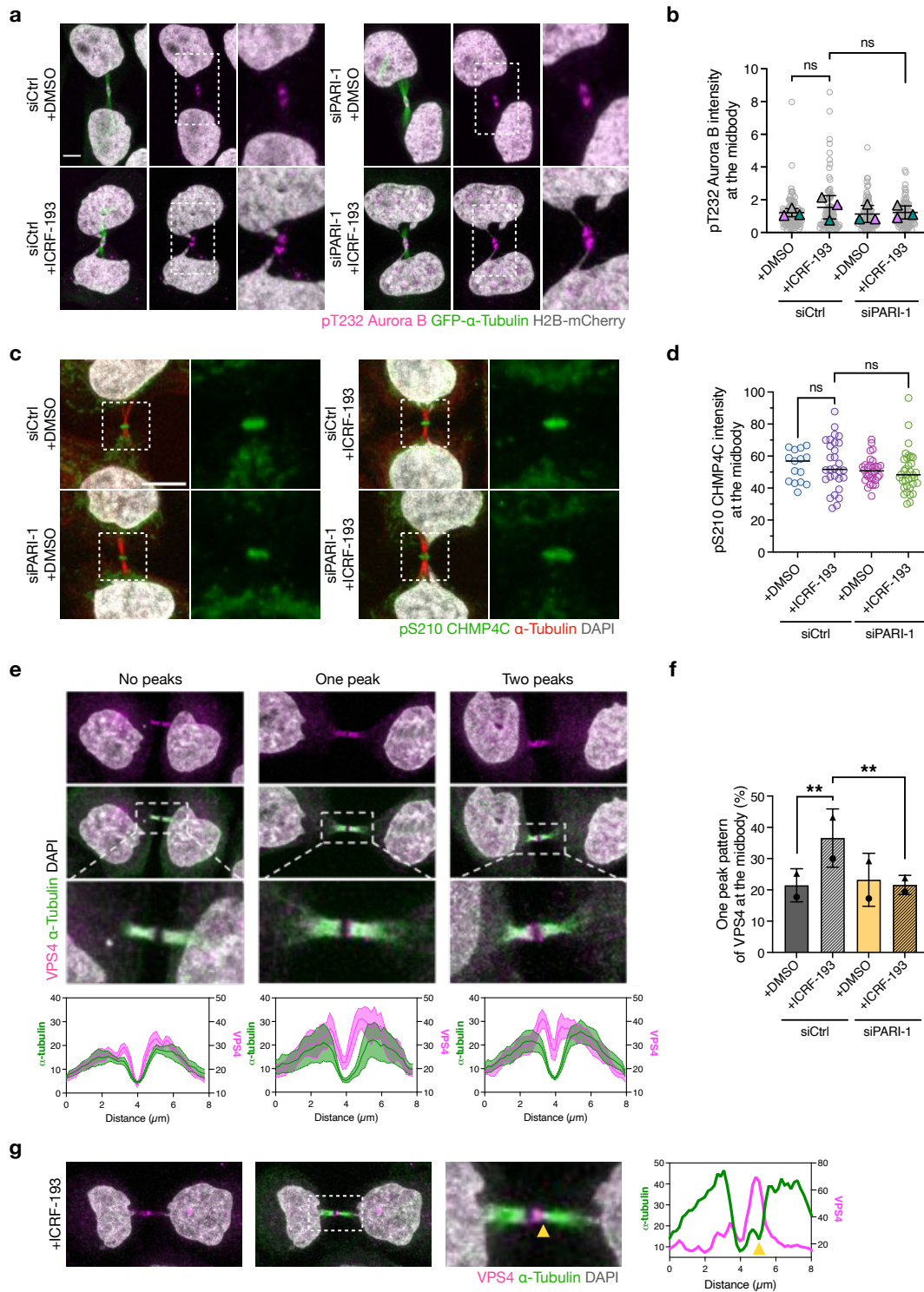


Figure 30. PARI is not required for the localization of Aurora B, pCHMP4C and VPS4 to the midbody.

(a) Representative fluorescent images of HeLa stably expressing H2B-mCherry (grey) and GFP- α -Tubulin (green), and stained for pT232 Aurora B (magenta), transfected with siCtrl and treated with DMSO or ICRF-193.

(b) Quantification of pT232 Aurora B intensity at the midbody using GFP- α -Tubulin (green) as a marker. Each measured intensity has been normalized to the median of the respective

condition and experiment. Student's paired t test (mean \pm SD, *P <0.05, **P <0.01; ***P <0.001; ****P <0.0001, n \geq 88, N =3).

(c) Representative fluorescent images of DMSO or ICRF-193 treated HeLa cells, stained for pS210 CHMP4C (green), α -Tubulin (red) and DAPI (grey). Boxed regions zoom in on the localization of pS210 CHMP4C at the midbody.

(d) Quantification of pS210 CHMP4C intensity at the midbody by drawing a line across the midbody and plotting the highest intensity value. Mann-Whitney test (median, *P <0.05, **P <0.01; ***P <0.001; ****P <0.0001, n \geq 15, N =1).

(e) Representative fluorescent images of DMSO treated HeLa cells, stained for VPS4 (magenta), α -Tubulin (green) and DAPI (grey). Boxed regions highlighting three localization patterns of VPS4 at the midbody. Lower graphs show the intensity profile of VPS4 and α -Tubulin across the midbody.

(f) Graph showing the fraction of cells with the one peak pattern of VPS4 at the midbody. Fisher's exact test (mean \pm SD, *P <0.05, **P <0.01; ***P <0.001; ****P <0.0001, n \geq 147, N =2).

(g) Left: Representative fluorescent image of ICRF-193 treated HeLa cells undergoing midbody constriction, stained for VPS4 (magenta), α -Tubulin (green) and DAPI (grey). The abscission site is indicated by the narrowing of the midbody and is marked by a yellow arrowhead. Boxed region zooms in on the midbody. Right: Graph shows the intensity profile of VPS4 and α -Tubulin across a midbody which is being constricted at the abscission site, marked by yellow arrowhead.

In summary, I assessed if PARI has a role on the localization of the abscission regulators Aurora B, pCHMP4C, and VPS4 during cytokinesis. However, I did not observe a correlation between the abscission delay and the phosphorylation levels of Aurora B and CHMP4C at the midbody. Furthermore, depletion of PARI does not affect the phosphorylation or localization of Aurora B and CHMP4C. Therefore, the role of PARI in the abscission checkpoint probably is independent of Aurora B localization and activity, and of the regulation of pCHMP4C and VPS4 to the midbody and to the site of abscission.

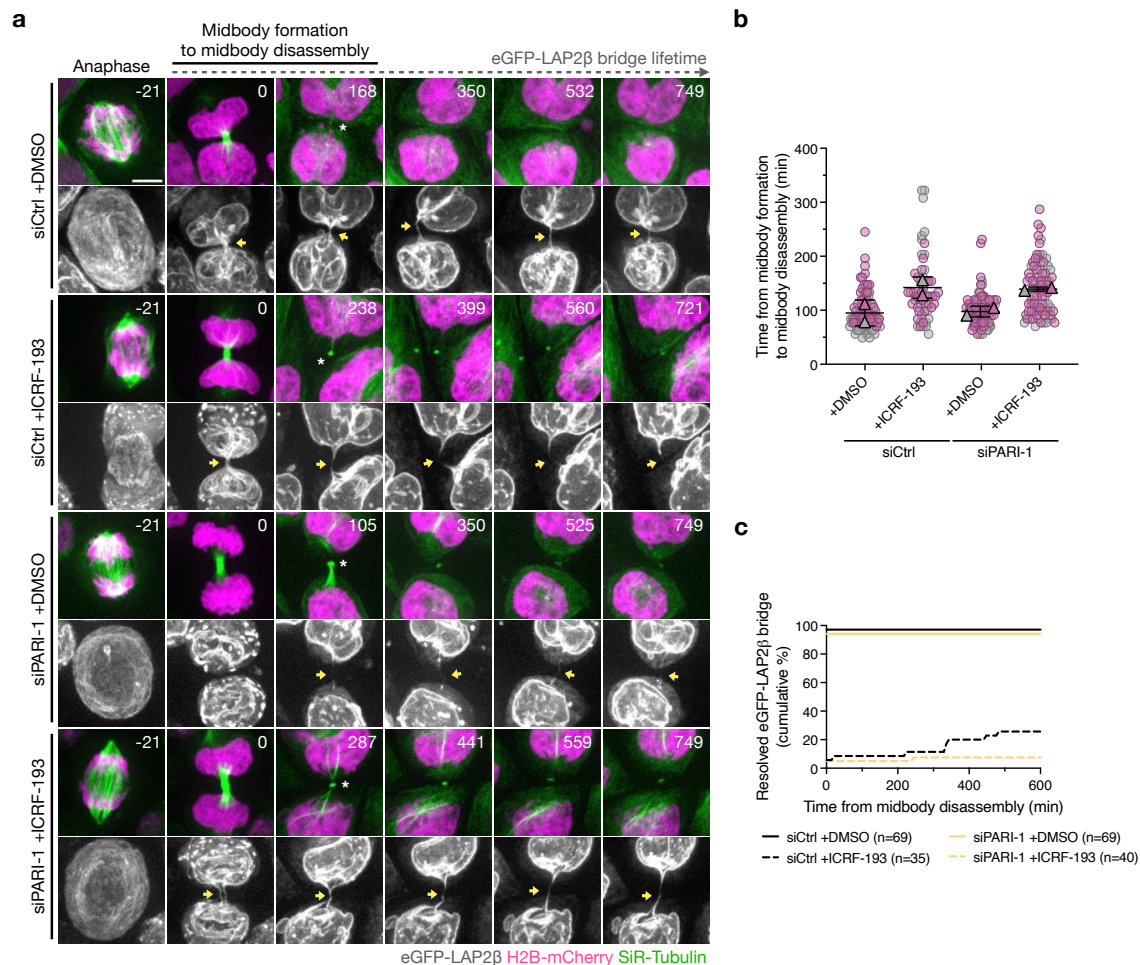


Figure 31. Overexpression of nuclear membrane marker LAP2β stabilizes the midbody in the presence of catenated chromatin bridges

(a) Montage of representative HeLa stably expressing H2B-mCherry and LAP2β-GFP cells progressing from anaphase to midbody formation (SiR-Tubulin) and its disassembly with or without the presence of a catenated chromatin bridge induced by ICRF-193. Time in minutes, asterisk marks midbody disassembly, yellow arrow points towards LAP2β-GFP-bridge. Scale bar 5 μm.

(b) Quantification of the midbody lifetime (time from midbody formation to disassembly). Mean ±SD, n ≥55, N =2.

(c) Quantification of the LAP2β-bridge lifetime from midbody formation to 1. resolution (resolved, green) or 2. until the end of the acquisition (unresolved, yellow). Midbody lifetime scored from panel b is interpolated (grey) in the graph. Median, N =2. siCtrl +ICRF-193 vs. siPARI-1 +ICRF-193, P =0.9390 Mann-Whitney test.

2.3.9 Chromatin bridges persist hours after midbody disassembly

As shown in the previous sections, PARI is required for stabilization of the midbody and actin patches in response to catenated bridges. The abscission checkpoint has been proposed to protect chromatin bridges from acquiring damage. In budding yeast, the deletion of NoCut components in the presence of chromatin bridges causes an

increase of double-strand breaks after abscission (Norden et al. 2006; Amaral et al. 2016). Similar observation has been made in human cells, depletion of CHMP4C a component of ESCRT-III and a target for Aurora B regulation of abscission timing, accelerated midbody lifetime causing premature chromatin bridge breakage and an increase of γ H2Ax (Carlton et al. 2012). Inhibition of upstream ATM and Chk2 of Aurora B also accelerated midbody lifetime which led to chromatin bridge damage (Petsalaki and Zachos 2021a). Therefore, I next asked if bridges show differences in morphology and/or stability in cells with a compromised abscission checkpoint. To this aim, chromatin bridges were visualized in synchronized HeLa cells stably expressing the nuclear envelope marker eGFP-LAP2 β , and the chromatin reporter H2B-mCherry. The tubulin probe SiR-Tubulin was used to measure the midbody lifetime. Untreated eGFP-LAP2 β H2B-mCherry cells disassemble the midbody on average at 95 ± 24 min (Figure 31a-b), which is 36 min faster than in HeLa cells expressing H2B-mCherry and GFP- α -Tubulin (Figure 21b). Despite the acceleration in midbody disassembly, the addition of ICRF-193 prolonged the midbody lifetime by 48 min to 143 ± 20 min. Therefore, topoisomerase II inhibition delays midbody disassembly in both cell lines to a similar extent (by 154% vs. 150% in eGFP-BAF, respectively). Notably, >70% of catenated eGFP-LAP2 β bridges persisted for more than 600 minutes after midbody disassembly (Figure 31c). eGFP-LAP2 β bridges in PARI-depleted cells appear to be more stable than in control but is not significant different. This indicates that although the lifetime of the midbody is extended in the presence of bridges, its disassembly not correlated with the time of bridge resolution. The few spontaneous chromatin bridges (3% of dividing siCtrl vs. 6% in siPARI-1) in DMSO treated cells showed similar longevity. Similar phenotype was observed in spontaneous bridges labeled with mRFP-LAP β in Steigemann et al. (2009). Moreover, I observed that unlike in previous abscission assays, PARI depletion did not shorten midbody lifetime in cells treated with ICRF-193 (compare with Figure 21a-b). The midbody lifetime of PARI-depleted cells remained at 140 ± 4 min, in average only 3 min shorter than the control cells treated with ICRF-193). Therefore, in these cells, PARI depletion does not shorten midbody lifetime. This difference with previous results is not due to the use of SiR-tubulin to label microtubules, because PARI depletion shortened midbody lifetime also in eGFP cells treated with SiR-Tubulin at the same concentration (Figure 23). Efficient mRNA depletion of PARI in HeLa cells expressing eGFP-LAP2 β was measured to 89% by RT-qPCR compared to 87% in HeLa cells (data not shown). An alternative

explanation for these results is that increased expression of eGFP-LAP2 β functionally alters the properties of the chromatin bridge and/or of PARI-dependent signaling. Interestingly, a previous study showed that over-expression of LAP2 β prevents nuclear membrane ruptures in nuclear Lamin-deficient cells (Chen et al. 2021).

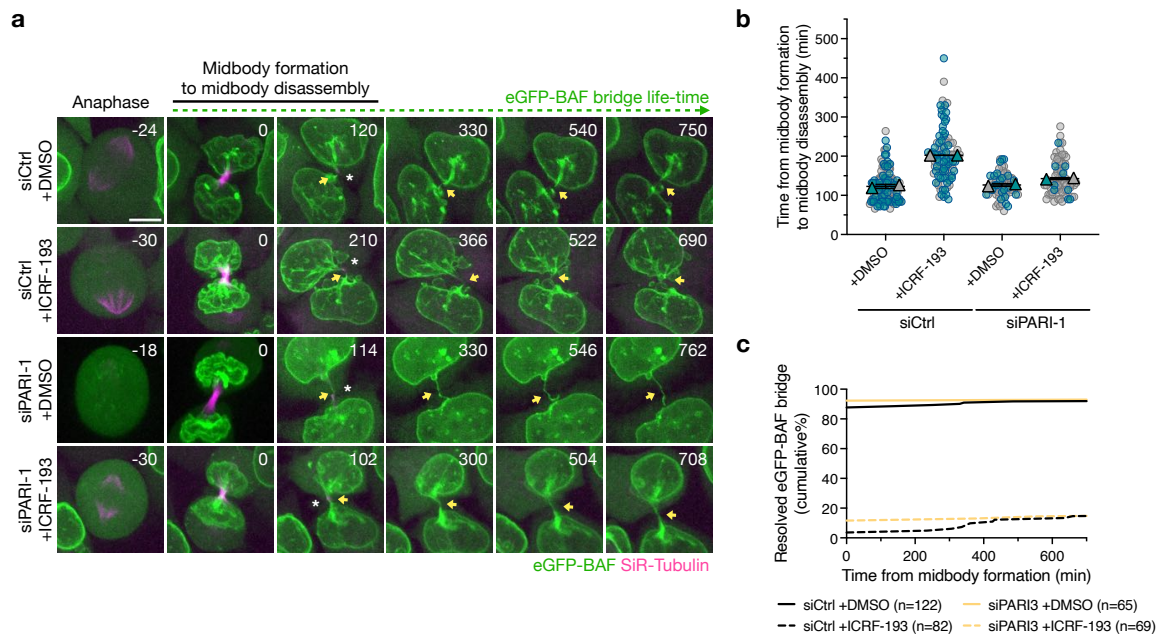


Figure 32. The time of chromatin bridge resolution is independent from midbody disassembly

(a) Montage of representative HeLa stably expressing eGFP-BAF cells progressing from anaphase to midbody formation (SiR-Tubulin) and its disassembly with or without the presence of a catenated chromatin bridge induced by ICRF-193. Time in minutes, asterisk marks midbody disassembly, yellow arrow points towards eGFP-BAF-bridge. Scale bar 5 μ m. (b) Quantification of the midbody lifetime (time from midbody formation to disassembly). Mean \pm SD, n \geq 65, N =2. (c) Graph showing the fraction of cells that resolved the eGFP-BAF-bridge relative to midbody formation. N =2.

To further assess the lifetimes of chromatin bridges and to verify the potential stabilization of the ICB when over-expressing a nuclear membrane marker, I repeated the above experiments using a different HeLa cell line stably expressing the nuclear envelope protein eGFP-BAF, another well-established and reliable marker of chromatin bridges. BAF plays an essential role in bridging chromosomes together during anaphase to promote formation of a single nucleus in daughter cells (Samwer et al. 2017). Cells were imaged for more than 60 hours, and to prevent ICRF-193 from potentially further disrupting the cell cycle progression the drug was washed away in-between time-points after 16 hours of incubation. In contrast to cells expressing eGFP-

LAP2 β , the midbody lifetime for eGFP-BAF cells is 123 ± 5 min (Figure 32a-b) and closer to what was previously observed HeLa cells expressing H2B-mCherry and GFP- α -Tubulin (Figure 21b). In the presence of catenated bridges, the midbody disassembly was delayed to 203 min similar to before. In addition, the midbody lifetime in cells with eGFP-BAF catenated bridges was shortened to 143 ± 2 min after PARI knockdown. Therefore, increased midbody stability in the previous experiment (Figure 31) is probably specific to the eGFP-LAP2 β cell line. Remarkably, eGFP-BAF bridges persisted for >700 min after midbody disassembly in both siPARI-1 and siCtrl cells. Therefore, PARI does not regulate the stability of GFP-BAF bridges, at least within 600 minutes after midbody formation.

The above results demonstrate that the shorter midbody lifetime in PARI-depleted cells does not lead to advanced resolution of catenated chromatin bridges. I next asked whether inactivation of the abscission checkpoint by means other than PARI knockdown has an effect on chromatin bridge stability. To test whether the time of chromatin bridge resolution is independent of when the midbody disassembles, I inactivated Aurora B during cytokinesis in cells with chromatin bridges. HeLa K cells were arrested in the cell cycle with a double thymidine block as in Figure 18a, released from the late G1 block, and treated with DMSO or ICRF-193 7.5 hours after the release. Thirteen hours after the G1/early S release cells were subjected to a 1-hour hesperadin pulse to inactivate Aurora B. The fraction of cells in cytokinesis, scored by the appearance of the midbody, drastically dropped after the inactivation of Aurora B (Figure 33a-b). In contrast, cells not exposed to the inhibitor gradually abscised, at 18 hours after the release, majority of cells had undergone abscission. Remarkably, the fraction of cells with a chromatin bridge, visualized with LAP2 β , remained consistent throughout the 12 hours after the initial timepoint (12 hours after G1 release) in both untreated and Aurora B inhibited cells (Figure 33c). The fraction of binucleated cells also increased as a consequence of Aurora B inhibition. These results are consistent with Steigemann et al. (2009) which showed that binucleation occurs more frequent in cells with spontaneous bridges if the abscission checkpoint has been compromised by inhibiting Aurora B with hesperadin and ZM1. Taken together, these data indicate that premature midbody disassembly caused by either PARI knockdown or Aurora B inhibition does not drive chromatin bridge resolution.

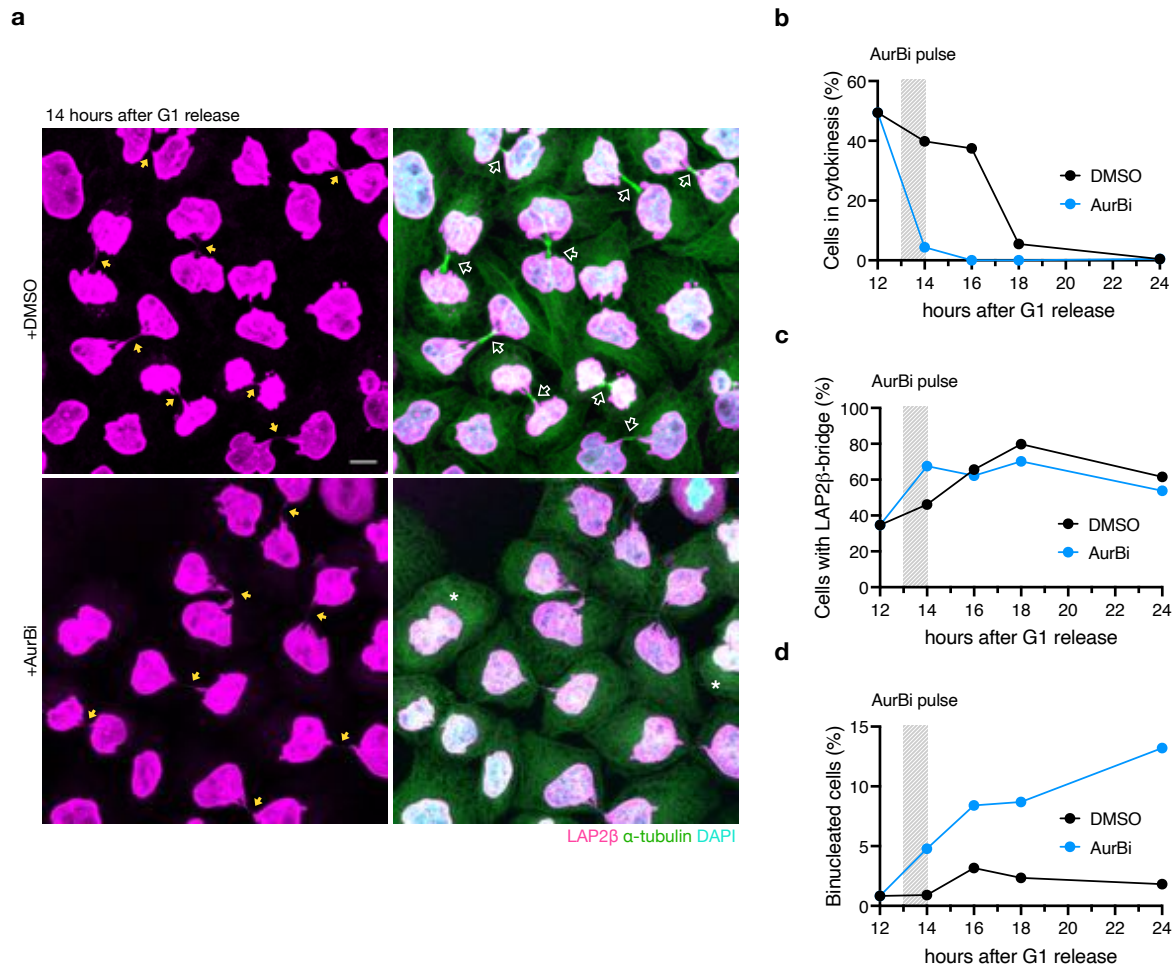


Figure 33. Chromatin bridge resolution is independent of midbody stability

(a) A representative fluorescent image of ICRF-193 treated HeLa cells 4 hours after a 1-hour pulse of DMSO or Aurora B inhibitor hesperadin. Cells have been synchronized with double thymidine and treated with ICRF-193 7.5 hours after the release from G1. Yellow arrow points towards a chromatin bridge, open white arrow indicates a midbody marking a cell in cytokinesis and an asterisk specifies a binucleated cell. Scale bar 10 μm .

(b) Quantification of the fraction of ICRF-193 treated cells that are in cytokinesis with midbodies at a given time point after G1 release. $n \geq 307$, $N = 1$.

(c) Quantification of the fraction of ICRF-193 treated cells that are in cytokinesis with a LAP2 β -bridge at a given time point after G1 release. $n \geq 307$, $N = 1$.

(d) Quantification of the fraction of ICRF-193 treated interphase cells with more than one nucleus. $n \geq 307$, $N = 1$.

2.3.10 PARI promotes bridge resolution before mitosis

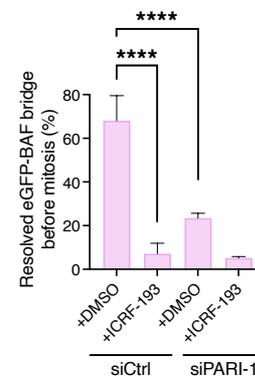
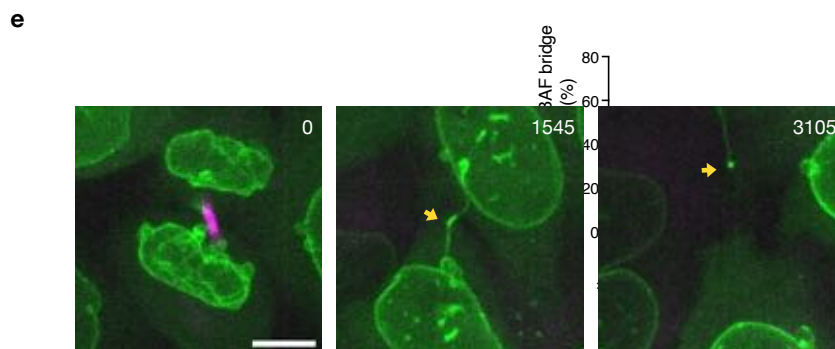
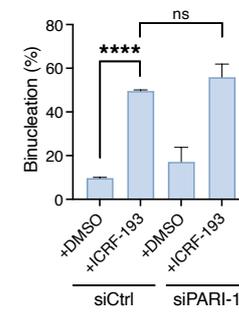
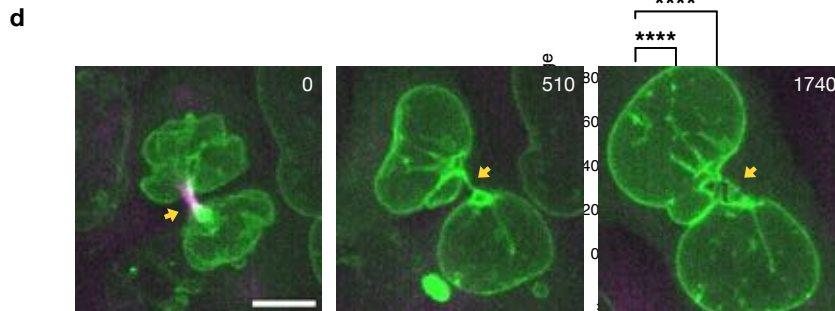
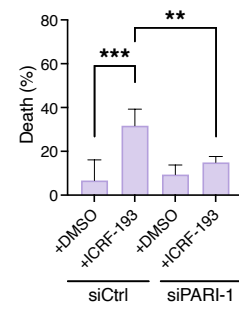
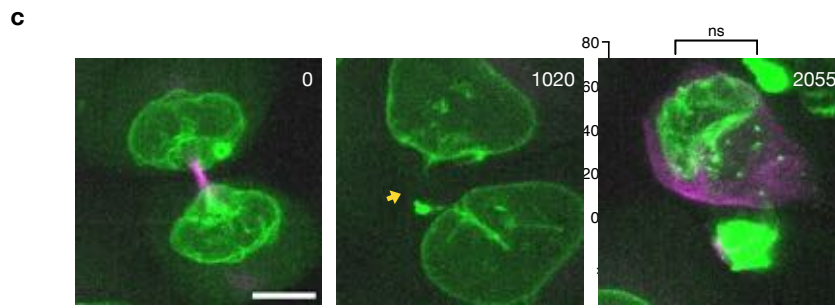
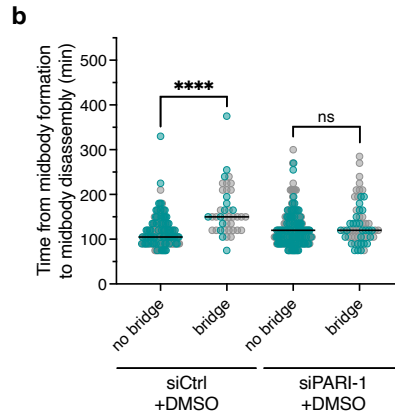
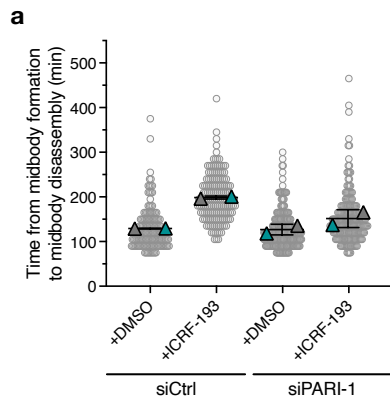
The previous results show that midbody disassembly and catenated bridge resolution are uncoupled from each other, and that both spontaneous and catenated chromatin bridges appeared to persist for at least 600 min after midbody formation when visualized by time-lapse microscopy (Figure 31, 32) and IF (Figure 33). However,

these experiments do not reveal exactly when after midbody disassembly bridges resolve, or whether PARI knockdown has any impact in the viability of cells with chromatin bridges. To this aim, HeLa cells stably expressing eGFP-BAF and stained with SiR-Tubulin were imaged for 72 hours to be able to observe the 2nd mitosis after bridge formation.

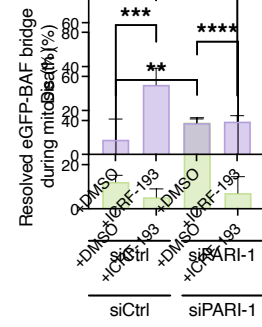
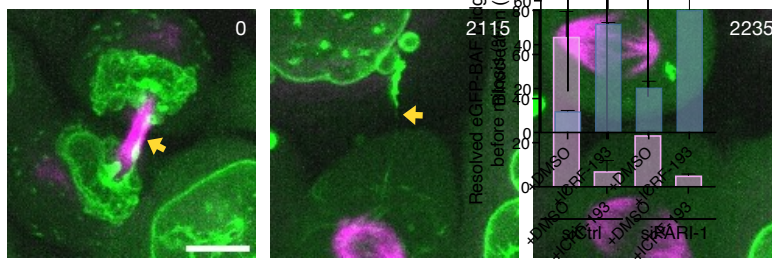
In cells with eGFP-BAF bridges, I assigned the fate of dividing cells among six possible phenotypes; (i) death of both daughter cells, (ii) binucleation, (iii) resolved bridge before mitosis, (iv) resolved during mitosis, (v) unresolved before mitosis (bridge persisting until the end of the acquisition without entering mitosis) and (vi) unresolved after mitosis (bridge persisting after mitosis until the end of acquisition). Spontaneous bridges in untreated conditions arose in 27% of dividing control cells and 25% PARI cells. Exposure to ICRF-193 induced chromatin bridges in all dividing cells at the beginning of the acquisition. Notably, PARI-proficient cells treated with ICRF-193 are slightly more prone to cell death in interphase than PARI-depleted cells (Figure 34c). ICRF-193 treated cells become binucleated at a higher frequency (approx. 50%) than untreated cells (less than 10%), suggesting a failure in retaining ICB stability. Notably, the frequency of binucleation in cells with catenated bridges was not altered by PARI knockdown (Figure 34d). Thus, PARI does not prevent binucleation of cells with persistent chromatin bridges. A significant fraction (70%) of TOP2- and PARI-proficient cells with spontaneous bridges resolved their chromatin bridge before the 2nd mitosis (Figure 34e). In contrast, 40% of cells with spontaneous bridges in PARI-depleted cells persisted until the next mitotic entry (Figure 34f). This suggests that in absence of PARI, spontaneous chromatin bridges are more stable and resolve possibly during nuclear envelope breakdown (NEBD) marking mitotic entry rather than during interphase. Interestingly, ICRF-193-induced catenated bridges take on average 638 min longer to resolve than spontaneous chromatin bridges which resolve 1300 min after midbody formation, however, the absence of PARI further delays the resolution of both spontaneous by 458 min and catenated bridges by 280 min (Figure 34g). A small fraction of control cells (3.3% in DMSO and 4.5% in ICRF-193) had bridges that failed to resolve and persisted throughout the whole acquisition without entering the next mitosis (Figure 34h), the fraction was slightly but significantly increased in PARI-depleted cells (to 10.9% in DMSO and 11.6% in ICRF-193). An

even smaller fraction of catenated bridges persisted throughout mitosis after the 2nd mitosis (Figure 34i), this fraction is not significantly increased in PARI-depleted cells.

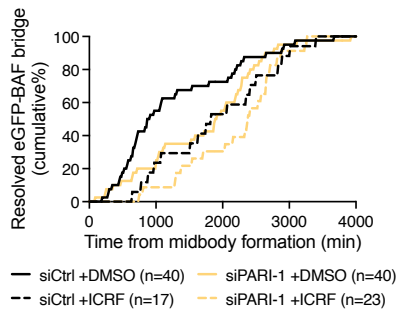
In summary, depletion of PARI shortens the midbody disassembly delay of both spontaneous and catenated chromatin bridges. Spontaneous bridges in untreated control cells resolves much later than the midbody (1300 min resp. 130 min after midbody formation), but depletion of PARI does not shorten the bridge lifetime like the midbody lifetime. In contrast, spontaneous and catenated bridges persist for longer. Therefore, PARI promotes the resolution of spontaneous bridges and catenated bridges, as the absence of PARI contributes to the resolution of bridges during mitosis. Furthermore, dividing cells with catenated chromatin bridges regress the cleavage furrow more often than cells with spontaneous chromatin bridges. It is possible that it is more difficult to stabilize the ICB in the presence of catenated bridges.



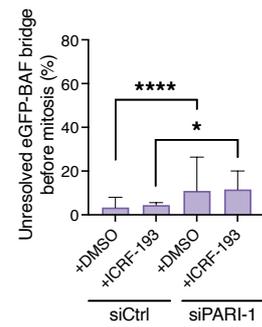
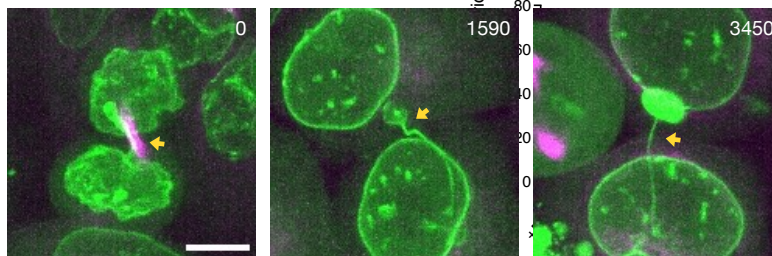
f



g



h



i

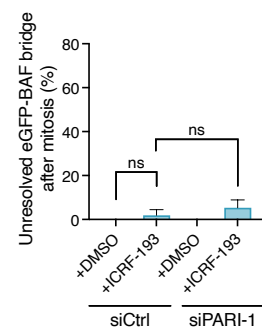
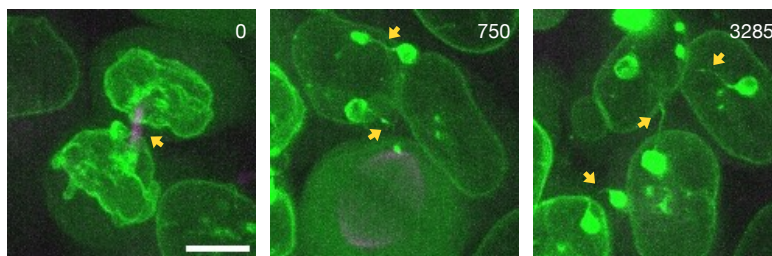


Figure 34. PARI promotes eGFP-BAF bridge resolution before the next mitosis

(a) SuperPlot showing the quantification of the midbody lifetime (time from midbody formation to disassembly) in HeLa cells stably expressing eGFP-BAF and stained with SiR-Tublin. Each cell is represented as a grey dot, the mean of each independent experiment is represented as a triangle. Mean \pm SD, $n \geq 148$, $N = 2$).

(b) SuperPlot showing the quantification of the midbody lifetime (time from midbody formation to disassembly) of DMSO-treated cells with spontaneous bridges. Each cell is represented as a dot, colors indicate each independent experiment. Mann-Whitney test (median, *P <0.05, **P <0.01; ***P <0.001; ****P <0.0001, $n \geq 41$, $N = 2$).

(c) Left: Montage of representative HeLa cells stably expressing eGFP-BAF dividing with a bridge leading to the death of two daughter cells. Right: Quantification of the fraction of deaths among dividing cells with eGFP-BAF bridge. Fisher's exact test (Mean \pm SD, *P <0.05, **P <0.01; ***P <0.001; ****P <0.0001, $n \geq 51$, $N = 2$)

(d) Left: Montage of representative HeLa cells stably expressing eGFP-BAF dividing with a bridge leading to binucleation. Right: Quantification of the fraction of binucleation among dividing cells with eGFP-BAF bridge. Fisher's exact test (Mean \pm SD, *P <0.05, **P <0.01; ***P <0.001; ****P <0.0001, $n \geq 51$, $N = 2$)

(e) Left: Montage of representative HeLa cells stably expressing eGFP-BAF dividing with a bridge which resolves before mitosis. Right: Quantification of the fraction of resolved eGFP-BAF bridges among dividing cells with bridge. Fisher's exact test (Mean \pm SD, *P <0.05, **P <0.01; ***P <0.001; ****P <0.0001, $n \geq 51$, $N = 2$)

(d) Left: Montage of representative HeLa cells stably expressing eGFP-BAF dividing with a bridge which resolves during mitosis. Right: Quantification of the fraction of resolved eGFP-BAF bridges among dividing cells with bridge. Fisher's exact test (Mean \pm SD, *P <0.05, **P <0.01; ***P <0.001; ****P <0.0001, $n \geq 51$, $N = 2$)

(f) Graph showing the fraction of eGFP-BAF bridges that are resolved from the time of midbody formation. n =number of cells from $N = 2$ independent experiments with similar results. siCtrl +DMSO vs. siCtrl +ICRF-193, $P = 0.0088$, Mann-Whitney test. siCtrl +DMSO vs. siPARI-1 +DMSO, $P = 0.0242$, Mann-Whitney test. siPARI-1 +DMSO vs. siPARI-1 +ICRF-193, $P = 0.0205$, Mann-Whitney test.

(g) Left: Montage of representative HeLa cells stably expressing eGFP-BAF dividing with a bridge which is not resolved at the end of the acquisition. Right: Quantification of the fraction of unresolved eGFP-BAF bridges among dividing cells with bridge. Fisher's exact test (Mean \pm SD, *P <0.05, **P <0.01; ***P <0.001; ****P <0.0001, $n \geq 51$, $N = 2$).

(h) Left: Montage of representative HeLa cells stably expressing eGFP-BAF dividing with a bridge which persisted through the next mitosis but is not resolved at the end of the acquisition. Right: Quantification of the fraction of unresolved eGFP-BAF bridges among dividing cells with bridge. Fisher's exact test (Mean \pm SD, *P <0.05, **P <0.01; ***P <0.001; ****P <0.0001, $n \geq 51$, $N = 2$).

2.3.11 Cells with chromatin bridges do not accumulate DNA damage immediately after cytokinesis

Several studies have linked DNA damage as a consequence of a dysregulated abscission checkpoint, and specifically after inactivation of Aurora B in yeast (Amaral et al. 2016), other checkpoint components such as Boi2 (Norden et al. 2006), CHMP4C (Carlton et al. 2012) and Chk2 (Petsalaki and Zachos 2021a). Therefore, I asked if there is an increased accumulation of DNA damage when the bridge-induced delay in midbody disassembly is abolished by the depletion of PARI. Hence, I investigated the accumulation of DNA damage in cells with a chromatin bridge by using the presence 53BP1 foci as a marker for DNA damage. 53BP1 is a key mediator of DNA damage response and can be detected for microscopy by using a specific antibody. Transfected cells with siCtrl or siPARI-1 were fixed at various times from 12 hours after double thymidine release and ICRF-193 treatment. Using the software CellProfiler, I created a pipeline to segment the nucleus based on the DAPI signal and detect nuclear 53BP1 foci (Supplementary Figure 2a). The nuclei were then manually categorized into single nucleus or a nucleus with chromatin bridge based on the LAP2 β staining (Figure 35a-c). Interestingly, the number of 53BP1 foci is maintained at equal levels throughout cytokinesis and into the next cell cycle in each condition, suggesting that cells depleted of PARI are not sensitive to damage by ICRF-193. In particular, cells with a chromatin bridge do not appear to accumulate more DNA damage than control cells. When comparing between control and PARI-depleted cells relative to the hour fixed after G1 release, there is no apparent difference (Figure 35d-e). Altogether, there are no distinct changes in the number of foci with time. Nuclei with a chromatin bridge do not accumulate more damage than unperturbed or interphase nuclei, and PARI-depleted cells are not sensitive against damage by catenation.

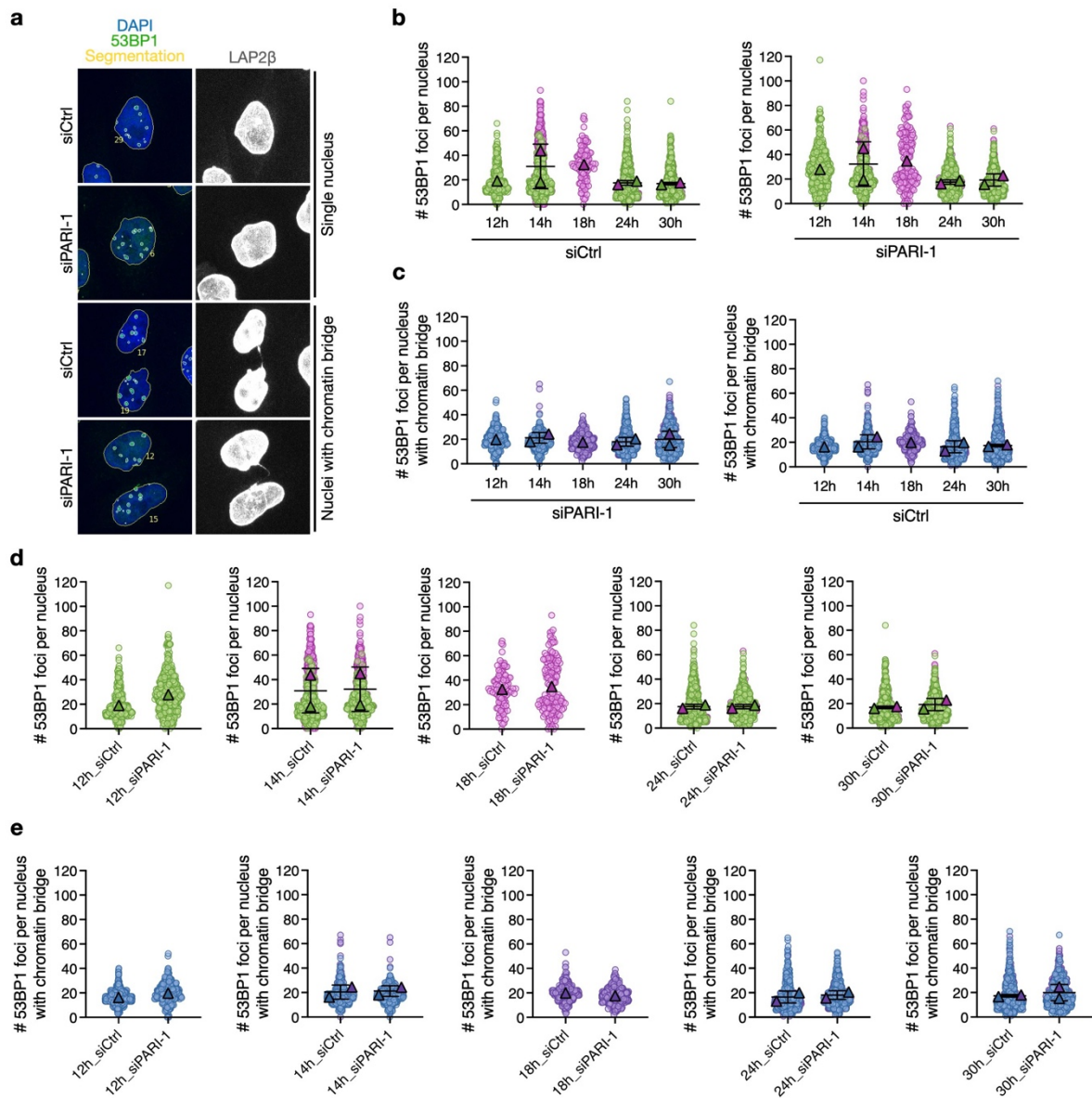


Figure 35. The number of 53BP1 foci remains unperturbed in PARI-depleted cells treated with ICRF-193

(a) Representative images of HeLa cells stained for 53BP1 (green), LAP2 β (grey) and DAPI (blue), 30 hours after G1 release. The nucleus and 53BP1 foci have been segmented using CellProfiler pipeline (see Supplementary Figure 1). Upper panel: single nucleus, lower panel: nuclei with chromatin bridge.

(b) Quantification of the number of 53BP1 foci in a single nucleus. Cells were collected at indicated time points after G1 release. Mean \pm SD, $n \geq 102$, $N = 1-2$.

(c) Quantification of the number of 53BP1 foci in nucleus with chromatin bridge. Cells were collected at indicated time points after G1 release. Mean \pm SD, $n \geq 304$, $N = 1-2$.

(d) Same nuclei as scored in Figure 21b, but graphed according to the fixed time point.

(e) Same nuclei as scored in Figure 21c, but graphed according to the fixed time point.

As previously shown, chromatin bridges persist for many hours before they resolve. Catenated bridges in control cells resolve on average 32 hours after bridge formation,

catenated bridges in PARI-depleted cells persist for additional 5 more hours. The last timepoint fixed after thymidine release for IF (Figure 33) is at least 10 hours earlier than the end of a bridge lifetime as observed by time-lapse microscopy. It is possible that no major differences were observed due to the underestimation of the bridge lifetime. To study the downstream effects of dividing once with a catenated chromatin bridge, I assessed the viability of cells in a cell survival assay (Figure 36). Cells were transfected with siCtrl or siPARI-1 and synchronized with double thymidine. However, before the second arrest cells were trypsinized, and 500 cells were seeded into a new well with thymidine (triplicates were prepared for each condition, Figure 36a). Remaining cells were used to check the knockdown efficiency of siPARI-1. DMSO or ICRF-193 was added 8 hours after the second release and removed after incubating for 16 hours. Cells were fixed 11 days after the first cytokinesis with ICRF-193, and immediately stained with crystal violet (see Methods 4.2.3 for details). The colony survival was measured by OD after dissolving the crystal violet in acetic acid. OD₆₀₀ measurement was preferred to assay overall growth; the number of surviving colonies and colony size. Undergoing one cell division in the presence of a catenated bridge led to a survival rate of only 20% cells compared to DMSO. Intriguingly, in contrast to previous studies showing DNA damage sensitivity in PARI-depleted cells and reduced cell viability, the absence of PARI improves cellular survival in cells dividing with catenated chromatin bridges to 80% compared to DMSO (Figure 36a-b). Depletion of FBH1 did not have the same rescue effect as PARI with the survival rate remaining at 20% similar to control cells (Figure 36c), suggesting that PARI specifically improves viability in cells dividing with catenated chromatin bridges.

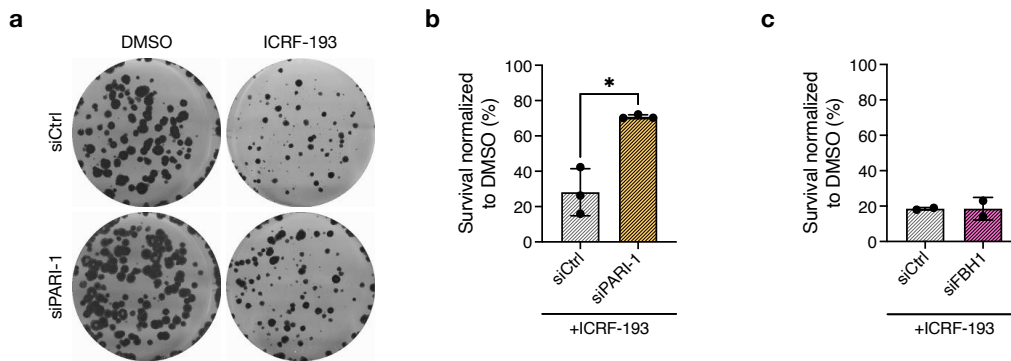


Figure 36. Loss of PARI improves cell survival after first cell division with a catenated chromatin bridge

(a) Representative image of the cellular survival of HeLa cells following PARI depletion, G1 synchronization with double thymidine and DMSO or ICRF-193 treatment in the first cycle of cytokinesis.

(b) Cell survival was measured by the optical density at 595 nm and normalized to DMSO. Student's paired t test (mean \pm SD, *P <0.05, **P <0.01; ***P <0.001; ****P <0.0001, N =3).

(c) The cell survival assay was repeated in cells depleted of FBH1. Mean \pm SD, N =2.

2.4 Author's contribution

I designed and performed all the experiments in yeast and human cells presented in the Ph.D. thesis unless otherwise stated. Nicola Brownlow started the investigation on the role of Srs2 in NoCut while in the lab of Manuel Mendoza and collected preliminary data on the role of PARI in human cells. The final stages of this work were done in close collaboration with Audrey Furst, who provided technical support in cell culture, generation of cell lines, fluorescent microscopy and biochemical experiments. Léna Christ performed abscission assay and cell survival assay to investigate if another Srs2 homolog FBH1 has similar functions as PARI. Coralie Spiegelhalter further prepared samples after light microscopy and performed electron microscopy.

3. Summary: Budding yeast complete DNA synthesis after chromosome segregation begins

Tsvetomira Ivanova*1, Michael Maier*1, Alsu Missarova*1, Céline Ziegler-Birling, Monica Dam, Mèrce Gomar-Alba, Lucas B. Carey & Manuel Mendoza.

<https://doi.org/10.1038/s41467-020-16100-3>

The entire genome must be completely replicated before cell division to ensure that the genetic material is faithfully transmitted into each daughter cell. Replication and chromosome segregation must therefore be temporally regulated in a strict manner to maintain genomic stability. Interestingly, in 20%-40% of *Saccharomyces cerevisiae* cells, DNA synthesis continues after chromosome segregation. Indeed, by perturbing the DNA synthesis machinery during late mitosis, cells display chromatin bridges with a delayed nuclear division. This suggests that DNA synthesis in late mitosis is important to promote timely nuclear division. Cells arrested in metaphase do not undergo DNA synthesis which can be explained by the high cyclin-CDK activity inhibiting its completion. Whereas cells with early mitotic exit defects display an increased fraction of chromatin bridges which are resolved by the DNA synthesis machinery. DNA synthesis is therefore required for the resolution of chromosome bridges emerging from an uncoordinated mitotic exit. In summary, the drop in cyclin-CDK levels after chromosome segregation allows the completion of DNA synthesis and faithful transmission of genetic material.

3.1 Contributions

During my first year of Ph.D. from February 2019 until March 2020, I took part in the revisions for the paper of Ivanova, Maier and Missarova et al. published in Nature Communication 2020. Together with Celine Ziegler-Birling we generated the strains for the following figures: Figure 2a-c and 5c, and Supplementary Figures 8: Cdc15-as1 mutants lacking BIR components Rad51 and Pol32, and 5. Additionally, I carried out imaging experiments and quantified and analyzed them for the following figures: Figure 2a-c, and Supplementary Figures 2, 5, and 6.

One of the key points and experiments of the paper is Figure 1 showing the incorporation of EdU in G1 cells but not in metaphase arrested cells, suggesting that cells continue DNA synthesis after chromosome segregation. To complement the IF results, we wanted to perform flow cytometry to measure the EdU incorporation at a given cell cycle stage using the same experimental setup as Figure 1a. I collected samples as described in Figure 1a and additional cells released into S phase were also collected as a positive control for EdU incorporation. EdU Click-iT reaction and SYTOX green staining were carried out for flow cytometry as described in the paper. However, the signal was not strong enough to be detected by the laser of BD LSRII and background EdU incorporation in the mitochondria disrupted the measurement by flow cytometry.

One reviewer asked if the increase of EdU observed in G1 cells (Figure 1) was really due to EdU being incorporated into the DNA or if it was due to an increase of EdU uptake during mitotic exit and suggested to inactivate one of the polymerases involved in DNA synthesis during late mitosis (Figure 2). However, EdU incorporation did not work well at restrictive temperature for the ts polymerase mutants used, instead we sought out to deplete the polymerases using auxin-inducible degrons. The degrons for Pol2, Pol3 and Psf2 were designed by Lucas B. Carey and generated by Celine Ziegler-Birling and I, but only Pol3 was successfully showing a lethal phenotype and was chosen for further experiments. However, auxin-induced degradation of Pol3 in metaphase-arrested cells inhibited anaphase onset (Supplementary Figure 5), thus preventing us from demonstrating that EdU incorporation observed in G1 depends on DNA synthesis by Pol3. On the other hand, this results also suggested that mitotic

DNA synthesis promotes nuclear division, as demonstrated by other experiments in the same paper.

4. Discussion & Perspectives

Abscission marks the final stage of cytokinesis when the daughter cells are physically separated from each other. Each individual process of cytokinesis from chromosome segregation to cleavage furrow ingression and abscission are tightly coordinated and regulated. The last stage of cytokinesis is monitored by the NoCut/abscission checkpoint which temporarily delays abscission in response to chromosome segregation defects such as anaphase bridges, and nucleopore assembly defects (Mackay, Makise, and Ullman 2010; Amaral et al. 2016; Bhowmick et al. 2019). Previous work from the lab suggests that a chromatin-based molecule could be important to trigger a checkpoint response. In this Ph.D. work I focused on characterizing the role of DNA helicase Srs2 and its human homolog PARI. Studies on Srs2/PARI so far have been dedicated to its role as an inhibitor of homologous recombination during S phase and G2, and in this work I have established a role for Srs2 and PARI in the NoCut/abscission checkpoint.

Srs2 prevents unreplicated DNA during anaphase

Several chromatin-based proteins have been observed to be associated with ultrafine bridges (UFBs), including Rif1, RPA and the helicases PICH and Sgs1/BLM (Germann et al. 2014; Hengeveld et al. 2015). These helicases in particular are thought to be required for the resolution of UFBs. The role of DNA helicase Srs2 is implicated in inhibiting homologous recombination (HR) from interfering with normal replication progression during S and preventing extensive DNA synthesis during HR repair which increases the risk of crossovers. Srs2 also has an independent role from HR, in inhibiting DNA damage checkpoint signaling by removing RPA (Dhingra et al. 2021).

The presence of RPA reflects single-stranded DNA (ssDNA) and DNA synthesis. RPA foci can be observed in untreated freely cycling cells with during anaphase and are associated with having a delay in chromatin bridge resolution (Ivanova et al. 2020). This suggests that the presence of unreplicated DNA disturbs faithful chromosome segregation. Interestingly, as previously reported deletion of SRS2 causes an increase of RPA associated to the chromatin (Dhingra et al. 2021). Here, using confocal spinning disk microscopy I observed that in 20% unperturbed wild-type anaphases have persisting RPA foci, and it is aggravated to 50% upon DNA replication stress

(Figure 15b). Exposure to an HU-pulse disrupts DNA replication which can explain the increase of unreplicated DNA during anaphase (Figure 15b). One origin of UFB formation during anaphase is associated with unreplicated regions from S phase (Chan et al. 2009). A subset of these UFBs is bound by RPA and its recruitment to the UFB is regulated by UFB-associated proteins including Rif1 and BLM (Hengeveld et al. 2015; Liu et al. 2014). The RPA-coated bridges observed in *srs2Δ* cells could therefore potentially reflect the presence of UFBs (Figure 15d). Anaphases in wild-type cells despite exposure HU do not exhibit RPA-coated bridges (Figure 15d), suggesting that the formation of UFBs are prevented before anaphase. In all, this suggests that Srs2 prevents against the accumulation of unreplicated DNA which increases the risk of UFBs formation. Another interpretation could be that the RPA-coated bridges observed in *srs2Δ* mutants are not UFBs, but a causation of an overall increased RPA level due to a lack of RPA removal from the chromatin.

Persisting RPA during anaphase is correlated with a prolonged bridge lifetime (Figure 15c), consistent with previous observations in the lab (Ivanova et al. 2020). DNA replication stress elevates both the number of cells dividing with RPA and their bridge lifetime and by deleting *srs2Δ* both of these phenotypes are aggregated. This suggests that *srs2Δ* is important to suppress/maintain RPA levels. The assay presented here does not address the amount of RPA, which should be complemented with WB or by counting the number of foci and measuring the size of the RPA foci which are considerably bigger after HU (Figure 14).

An accelerated midbody disassembly has been correlated with earlier resolution of the chromatin bridge in human cells (Carlton et al. 2012; Petsalaki and Zachos 2016, Petsalaki and Zachos 2021a), but has yet to be implicated in budding yeast. However, contradictory to observations in human cells, chromatin bridges in *srs2Δ* persist for longer than of those in wild-type cells (Figure 15c) despite that deletion of SRS2 minimizes the abscission delay in cells with bridges (Figure 12d-e, 13d). I speculate that these two phenotypes of *srs2Δ* mutants are independent from each other. In absence of Srs2 the delayed bridge resolution is because of the excess of RPA on the chromatin during anaphase, which notably also prolongs bridge resolution in unperturbed conditions of wild-type cells (Figure 15c). The helicase activity of Srs2 is required for the removal of RPA from the chromatin. To test that the delayed bridge

resolution in *srs2Δ* cells is not a consequence of an unresponsive checkpoint, we can use the helicase-dead allele *srs2-K41A* which causes accumulation of RPA but if the presence of Srs2 on the chromatin is sufficient to trigger a checkpoint it should be delaying abscission. The opposite can also be tested by using the *srs2ΔSIMΔPIP* mutant, which should be repressing RPA accumulation and the abscission delay. The addition of HU increases the fraction of wild-type cells which has RPA foci during anaphase, therefore the condition should allow for bridge formation which can be detected by NoCut without causing increased ssDNA-RPA formation.

Chromatin bridge resolution and abscission in budding yeast

The NoCut checkpoint is suggested to protect against chromatin bridge breakage and DNA damage by delaying abscission (Norden et al. 2006). However, the above observation suggests that at least in yeast, abscission and chromatin bridge resolution are not correlated since *Srs2* mutants have the same abscission dynamics as untreated wild-type cells despite dividing with a chromatin bridge (Figure 12d, 13d). In absence of *Srs2*, chromatin bridges persist for longer compared to wild-type, but are they resolved before abscission or are they broken by abscission?

In budding yeast chromatin bridges in untreated cells resolve well before myosin ring contraction, whereas HU-induced, decondensed and decatenated bridges disappeared only after the myosin ring has contracted, but before abscission was complete (Amaral et al. 2016; Ivanova et al. 2020). The duration of myosin ring contraction remained the same despite the presence of catenated and decondensed bridges. This suggests the myosin ring contraction is independent of the NoCut checkpoint which ensures that abscission (resolution of the plasma membrane) does not occur before complete bridge resolution. Inactivating NoCut checkpoint components such as Aurora B and Boi2 causes DNA damage in the following G1 which is why it was proposed that bridges are damaged/cut by a deficient NoCut.

Deletion of *SRS2* abolishes the abscission delay normally caused chromatin bridges (Figure 11d-e, 12d) yet prolongs the appearance of HU-induced bridges (Figure 15a). We can use the elongation of spindle and anaphase onset as a common starting point to compare the time of bridge resolution and abscission. Spindle elongation is in

concert with anaphase onset observed as the elongation of the nucleus marked by Htb2 (Figure 14). Abscission occurs on average within 30 min from spindle elongation for untreated wild-type cells and *srs2Δ* cells. In the presence of HU-induced chromatin bridges wild-type cells are delayed to 37 min, whereas abscission in *srs2Δ* cells with HU remains the same as *srs2Δ* cells without HU. Chromatin bridges induced by DNA replication stress resolve 13 min after anaphase onset and the absence of Srs2 significantly prolongs bridge duration by 3 min (Figure 15a). Despite having longer-lived chromatin bridges and an abolished abscission delay, *srs2Δ* bridges are resolved 14 min before abscission.

However, the limitation is that we can only draw parallels since two different strains were used, one to look at chromosome segregation (nuclear resolution) and another to assess the abscission. While the average bridge resolution is 16 min, and abscission is 30 min, there are bridges that persist for longer than 30 min. To validate that bridge resolution always occurs before abscission even in *srs2Δ* cells and to answer questions regarding the coordination between these two processes, we need to use a strain which expresses the plasma membrane marker CAAX-GFP and Htb2-mCherry in a *srs2Δ* background.

Inactivation of topoisomerase II (*top2-4*) strongly inhibits abscission for at least 60 min from membrane ingression in 92% of dividing cells (Figure 13), which consistent with a previous study from the lab (Amaral et al. 2016). In the same study it was also observed that chromatin bridges in *top2-4* inactivated cells resolve on average 23 min after anaphase onset. Anaphase onset occurs earlier than membrane ingression and if we extrapolate, the bridge resolution from membrane ingression is shorter than 23 min. Therefore, from the time of bridge resolution there is a minimum of 37 min before abscission occurs (if at all). This suggests that there might be another mechanism which prevents abscission in the presence of grossly catenated bridges. It would, therefore, be interesting to investigate the coordination between catenated chromatin bridge resolution and abscission in a *srs2Δ* background, since bridge resolution is extended in absence of Srs2.

Srs2 requires the interaction with PCNA to inhibit abscission

Abscission is delayed upon HU-pulse and topoisomerase II inactivation. Cells lacking the DNA helicase Srs2 are unable to enforce this delay (Figure 12d, 13d). Interestingly, we found that Srs2 requires the interaction with PCNA to delay abscission indicating that Srs2 may function as a chromatin-based signal for chromatin bridges.

During S phase Srs2 is recruited to replication forks by SUMOylated PCNA to prevent homologous recombination (HR) (Pfander et al. 2005). Additionally, Srs2 have two important domains which binds to SUMOylation (SIM) and PCNA (PIP). To test if the interaction with PCNA is required for delaying abscission we used a strain which expresses a partially functional PCNA (Figure 16a). This was sufficient to rescue HU-induced abscission delay, possibly due to indirectly reducing Srs2 recruitment and activity. The presence of PCNA does not promote the delay as deletion of Srs2 alone is adequate to rescue the delay and complete membrane constriction (Figure 12d). This suggests that Srs2 is dependent on the activity of PCNA for its role in promoting abscission delay in the presence of HU-induced bridges. SUMOylation of PCNA is heavily implicated in the specific recruitment of Srs2, however, it does not exclude that Srs2 can bind to other chromatin-based proteins that are SUMOylated.

Another approach to assess the interaction between Srs2 and PCNA is to disrupt the recruitment of Srs2 by expressing the mutant PCNA *pol30-K164R*. *Pol30-K164R* is a mutant allele that prevents the lysine 164 residue to be SUMOylated and ubiquitinated. This will preserve a fully functional Srs2 but affect the recruitment of Srs2 by PCNA. Ubiquitination of K167 however also plays a role in promoting the translesion pathway (Figure 10) and is an important residue in controlling which of the DDT pathways will be used to repair the DNA lesion (Arbel et al. 2020). The switch to SUMOylation at K167 will prevent the salvage pathway. A second approach to investigate if Srs2 depend on PCNA is to prevent Srs2 recruitment to the chromatin by overexpressing the PCNA unloader Elg1 (Arbel et al. 2020). Similar to *pol30-K164R* other SUMO-independent activities of PCNA will be reduced, which has to be considered when interpreting the results due to the shared regulatory site with ubiquitin-binding repair proteins.

To validate that the interaction with PCNA is essential for the role of Srs2 in delaying abscission, the SUMO-interacting motif (SIM) and PCNA-interacting protein box (PIP-box) of Srs2 were deleted. Interestingly, the deletion of SIM alone was not sufficient to null the delay caused by Top2 inhibition (Figure 16b). While Srs2 has a higher affinity for SUMOylated PCNA it can still interact with PCNA through the PIP-box *in vitro* (Pfander et al. 2005). Indeed, when both PIP-box and SIM are deleted, abscission is partially restored (Figure 16b). This may suggest that the role of Srs2 in promoting abscission delay is independent of its SUMO-interacting motif. It has been observed by microscopy that *srs2ΔSIM* mutants or the expression of a non-SUMOylated form of PCNA (*pol30-KK127,164RR*) prevent the formation of S phase Srs2 foci (Burgess et al. 2009). This implies that the recruitment of Srs2 to the site of replication requires PCNA SUMOylation. However, despite defective SUMO-interaction, Burgess et al. (2009) observed that the localization of Srs2 to sites of recombination (by the co-localization with Rad52) remained unaffected. Therefore, the role of Srs2 in regulating HR during repair is independent of SUMOylated PCNA, but SUMOylated PCNA is required to inhibit untimed HR during replication (Burgess et al. 2009). An increased fraction of cells deficient of Srs2 exhibit RPA foci (marker of single-stranded DNA) during cytokinesis after replication stress, suggesting that DNA repair synthesis is compromised (Figure 14). This is consistent with the work of Burgess et al. (2009) which also shows that these foci are additionally co-localized with the Swi/Snf-like protein and HR component Rad54. Therefore, it is possible that it is the accumulation of Srs2 at recombination sites is what triggers NoCut, since SIM deletion itself did not rescue the delayed phenotype.

To test if the presence of Srs2 on the chromatin bridge is sufficient to trigger the NoCut checkpoint we took advantage of the conditionally dicentric chromosome assay developed by Amaral et al. (2016) In budding yeast, dividing cells with dicentric bridges do not inhibit abscission, suggesting that the NoCut checkpoint does not detect dicentric bridges (Amaral et al. 2016). In contrast, *elg1Δ* mutants with dicentric chromosomes in the cleavage plane are delayed in completing abscission compared to *elg1Δ* mutants without a bridge. The deletion of ELG1 leads to accumulation of PCNA and Srs2 on the chromatin (Parnas et al. 2010). However, the excessive PCNA on chromatin and ubiquitin-binding proteins can potentially also affect the checkpoint. To rule out the possibility that PCNA and ubiquitin-binding proteins are responsible for

the abscission delay observed, it would be necessary to additionally delete SRS2 in a dicentric *elg1Δ* background. However, initial strain constructions by crossing dicentric *elg1Δ* mutant with a *srs2Δ* mutant were not successful with unviable haploids or viable but lacking the correct genotype. It is possible that the deletion of ELG1 and SRS2 are synthetically lethal. To confirm this, we are currently constructing a strain to degrade Elg1 using an auxin-inducible system. Alternative to deleting ELG1 which may affect the general dynamics of PCNA, TetO/TetR system can also be employed to artificially recruit Srs2 to the dicentric chromatin. Srs2 can be fused to the Tet repressor (TetR) which binds to Tet operator (TetO) arrays introduced on the dicentric chromosome.

Srs2 promotes an abscission delay upon in the presence of chromatin bridges. However, to determine if the delay is mediated by NoCut, additional genetic interaction of Srs2 with NoCut components has to be established. To this aim, strains in a *srs2Δ* background have been constructed to inactivate Aurora B (*Ipl1-321*) during cytokinesis after DNA replication stress as in the assay described in Figure 12a. To inactivate *Ipl1-321* during cytokinesis, HU-arrested cells should be released into 37°C media. The inactivation of *Ipl1-321* at 37°C in cells with HU-induced chromatin bridges rescues abscission delayed cells (Amaral et al). If Srs2 is indeed part of the NoCut checkpoint the dynamics of cells able to abscise with a chromatin bridge should be the same as cells deficient of Ipl1.

Midbody stability and abscission

In budding yeast, the constriction of plasma membrane and abscission can be directly visualized by GFP-CAAX. In human cells abscission of the plasma membrane is most commonly observed using phase contrast microscopy. Before abscission occurs, the intercellular bridge must be cleared out of actin and microtubules. The midbody is disassembled as ESCRT-III helices constrict and Spastin is localized to the abscission site. The time of abscission in human cells was first assessed using phase contrast time-lapse microscopy (Kouranti et al. 2006). Indeed, abscission of the plasma membrane is correlated with the separation of the cytoplasm as determined by the expression of photoactivatable GFP (PAGFP), which is activated in one of the daughter cells (Steigemann et al. 2009). If the cytoplasm of the daughter cells is still connected, the PAGFP signal will diffuse into the non-photoactivated daughter cell.

Abscission has occurred when there is no longer a change in the diffusion rate. The midbody lifetime using mRFP- α -Tubulin was determined in parallel to the photoactivation and abscission. The time of midbody disassembly was strongly correlated with the time of abscission (Steigemann et al. 2009; Guizetti et al. 2011). To this date, midbody stability is a common marker to assay abscission. However, it is not abscission, as this process refers to the complete resolution of the plasma membrane. Moreover, in the study of Steigemann et al. (2009), the presence of chromatin bridges does prolong the PAGFP diffusion, suggesting that abscission is delayed, but the midbody disassembly still occurred in the presence of a spontaneous bridge at the same time as normally segregating cells. Our results suggests that the midbody is stabilized in the presence of a chromatin bridge (Figure 34b), but only for a short time relatively to the chromatin bridge lifetime (Figure 34g). In all, this suggests that the time of midbody disassembly is not correlated with abscission in the presence of a chromatin bridge. Therefore, the midbody lifetime should not be used to determine when abscission occurs, and only to describe the stability of the midbody.

In this study I show that inhibition of topoisomerase II causes a stabilization of the midbody, by using both GFP- α -Tubulin and SiR-Tubulin dye (Figure 21a-b, e-f, 32a-b). This is consistent with the study by Bhowmick et al. (2019) where ICRF-193 was used to induce ultrafine bridges. In contrast to Steigemann et al. (2009), I found that spontaneous bridges delay midbody disassembly (Figure 34b). There is a lot of variation in midbody lifetime even in absence of chromatin bridges (75 to 200+ min, median =105, Figure 34b), therefore a large number of cells (at least 50) is required to give an accurate measurement of the midbody stability.

Depletion of PARI partially rescues the delay by reducing the time from midbody assembly to disassembly, without introducing more chromatin bridges (Figure 21). The role of PARI in midbody stabilization corresponds well to the observed role of Srs2 in inhibition of abscission after topoisomerase II inactivation (Figure 13). Previous publications from our lab showed that spindle stabilization is required for Aurora B activity and NoCut checkpoint response in the presence of a bridge (Norden et al. 2006; Amaral et al. 2016). The spindle microtubules in budding yeast are comparable to the midbody of human cells. In budding yeast, Ipl1 (Aurora B) in part drives spindle disassembly by facilitating microtubules depolymerization by phosphorylating and

deactivating microtubule-stabilizing Bim1 (Zimniak et al. 2009). Ipl1 also phosphorylates and activates the microtubule-associated She1, which together with the inactivation of Bim1 promotes the disassembly of the spindle at the mitotic exit (Woodruff, Drubin, and Barnes 2010). The regulator of exocytosis Boi2, but not Boi1 plays a role in destabilizing the spindle by promoting proper She1 localization at the spindle (Pigula, Drubin, and Barnes 2014). This suggests that Ipl1 monitors both spindle integrity, and faithful chromosome segregation, and that these processes might be coordinated.

In *top2-4* mutants, the spindle disassembles after the myosin ring has contracted (Amaral et al. 2016), similar to how TOP2 inhibition stabilizes the midbody. Next, I would like to confirm if the spindle disassembles prematurely in a *top2-4 srs2Δ* mutants expressing tubulin marker Tub1-GFP and Myo1-GFP. These results could possibly add another link between spindle stability and NoCut-mediated abscission in the presence of chromatin bridges.

The midbody disassembly depends on the activity of the microtubule-severing ATPase Spastin, which is recruited to the midbody by CHMP1B and IST1, two ESCRT-III components (Yang et al. 2008; Connell et al. 2009; Renvoisé et al. 2010). CHMP4B (ESCRT-III component) is recruited to the midbody by ESCRT-I/II-CHMP6 axis and the ESCRT-associated protein ALIX. ESCRT-I and ALIX are in turn dependent on the midbody protein CEP55 (Agromayor and Martin-Serrano 2013). Only after PLK1 is degraded by APC/CCdh20 can CEP55 interact with centralspindlin component MKLP1 and localize to the midbody. ALIX on one hand also regulates CHMP4C in the abscission checkpoint (Christ et al. 2016). CHMP1 is recruited to the midbody by the CHMP4/6-CHMP2/3-CHMP1/5 axis, which finally allows the localization of Spastin (Yang et al. 2008). In its current model, it is possible that CHMP1B is recruited by the ESCRT-I/II-CHMP4B-CHMP1B axis to allow Spastin to sever the midbody while the ALIX-CHMP4C and ALIX-CHMP4B axes promote abscission. The delay in midbody disassembly after topoisomerase II inhibition could perhaps reflect a partial ESCRT-III activity which is “inefficient” at disassembling the midbody. Assaying CHMP1B or IST1 localization and distribution could potentially answer the question if PARI inhibits midbody disassembly in the presence of a chromatin bridge.

PARI regulates the abscission checkpoint through other signaling pathways

UFBs are coated with various helicases such as BLM, PICH and Rif1 (Bhowmick et al. 2019). UFBs induced by low concentration of ICRF-193 delay midbody disassembly. Additionally, Rif1 localizes to the spindle microtubules and midbody, and its depletion leads to a prolonged midbody lifetime (Bhowmick et al. 2019). It was initially thought that Rif1 acted as a bridge sensor for the abscission checkpoint. However, the localization of Rif1 to the midbody was independent of UFBs. Instead, it was proposed that Rif1 at the midbody recruits PP1 to dephosphorylate CHMP4C which explains the delayed midbody disassembly in Rif1 deficient cells. It is an attractive idea to hypothesize that the DNA helicases Srs2 and PARI are also localized to the chromatin (or the midbody) to signal for bridges and promote abscission checkpoint delay. On the contrary, it was observed that PARI is strictly expressed and localized to the nucleus during S and G2 even under an ICRF-193 condition (Figure 27). The localization of Srs2 was not investigated in this study and currently, there is only one paper studying the localization of Srs2 in budding yeast and its localization is described to be limited to S phase when replication and recombination events are active (Burgess et al. 2009). This all implies that Srs2/PARI must be acting indirectly on the abscission checkpoint. However, we cannot exclude technical limitations in detecting small amounts of PARI.

The protein expression level of endogenous PARI in HeLa cells and other cell types is very low and cannot be detected by WB without overexpressing it (Piao et al. 2011; Moldovan et al. 2012; O'Connor et al. 2013). This observation is similar to how endogenous levels of Srs2 failed to be detectable by WB unless it is being overexpressed (Rong and Klein 1993). However, even at an overexpressed state Srs2 is expressed at much lower levels in comparison to the overexpression of other proteins using the same overexpressing systems (Heude, Chanet and Fabre 1995). The terminal region of Srs2 is proposed to inhibit the expression or promote degradation of the protein which can explain the low levels of endogenous Srs2 and PARI (Rong and Klein 1993). An intrinsic degradation signal suggest that Srs2 is regulated to be present in limiting amounts at a specific cell cycle stage, which can explain the low abundancy across cell types.

The currently used HeLa Kyoto cell line which stably expresses eGFP-PARI^{WT} has the strongest expression out of the few positive clones generated yet requires additional signal enhancement (GFP-Alexa488) to be clearly detected. Boosted eGFP-PARI signal for immunofluorescent microscopy confirms live-acquisitions that midbody-staged cells with or without chromatin bridges are devoid of PARI localization (preliminary data not shown). The eGFP-PARI signal returns in the next S phase and was observed to be homogeneously distributed between daughter cells that were still connected by a chromatin bridge. As we will later discuss, this might be important for the resolution of chromatin bridges. In all, these data strongly suggest that Srs2/PARI indirectly promotes an abscission checkpoint-mediated delay through midbody stabilization in the presence of chromatin bridges.

In human cells it has been proposed that ATR-Chk1 and ATM-Chk2 signaling pathways are not limited to the DNA damage checkpoint but are additionally engaged to maintain the spindle assembly checkpoint and the abscission checkpoint. ATM and Chk2 were observed at the Flemming body, where it is shown to regulate the abscission timing. The inhibition of either ATM and Chk2 accelerates midbody disassembly and causes premature chromatin bridge breakage marked by γ H2Ax (Petsalaki and Zachos 2021a). ATR and Chk1, when inhibited also show an accelerated midbody disassembly phenotype (Mackay and Ullman 2015) and have been observed to be localized to the centromeres where the formation of R-loops recruits Aurora B and activates a mitosis specific ATR-pathway to promote faithful chromosome segregation (Kabeche et al. 2018). Additionally, Chk1 exhibit distinct localization pattern along chromosome arms during prometaphase and co-localizes with Aurora B at kinetochores (Peddibhotla et al. 2009). During central spindle formation Chk1 translocalizes along the spindle microtubules and remains on the midbody arms. Abrogated Chk1 during mitosis leads to increased binucleation. It is proposed that upstream ATR-Chk1 and ATM-Chk2 signaling can trigger an Aurora B-mediated abscission checkpoint delay.

One explanation of how PARI and Srs2 can promote a delay in midbody disassembly/abscission is through sustained signaling pathways from S phase into cytokinesis. In contrast to depleting CHMP4C or inhibiting ATR-Chk1 and ATM-Chk2

which accelerates abscission and leads to chromatin bridge breakage (Carlton et al. 2012; Petsalaki and Zachos 2021a). This indirect but distinctive effect by PARI on the abscission checkpoint can explain why unlike the depletion or inactivation of other checkpoint components PARI depletion does not accelerate midbody disassembly on its own. Depletion of PARI also does not relieve the midbody-arrested phenotype of cells with defective NPC, suggesting that a PARI signal might be important to distinguish chromatin-based defects from defects in nuclear pore assembly (Figure 21, 26).

To test if PARI promotes abscission delay through triggering ATR-Chk1 or ATM-Chk2 signaling pathway, we can assay the level of activated or phosphorylated kinases through western blot. I have collected some preliminary data on phosphorylated kinases using DNA damage antibody sampler kit from Cell Signaling (#9947), including antibodies against; pATR (Ser418), pATM (Ser1981), pBRCA1 (Ser1524), p-Chk2 (Thr68), p-Chk1 (Ser345), γ H2Ax (Ser139) and p-p53 (Ser15). However, some did not reveal any bands and other were not reproducible in the detection, more careful consideration of antibodies has to be taken into account. Alternatively, we can assess the localization and distribution of the proteins using microscopy.

The physiological relevance of PARI and the abscission checkpoint

PARI-depleted cells are delayed in S phase progression and thus entry into M phase (Figure 20b-c), this is consistent with previous report showing that PARI-depleted cells are delayed in S phase due to reduced replication fork progression (O'Connor et al. 2013; Nicolae et al. 2019). Overexpression of Srs2 and srs2 helicase-dead mutants exhibit perturbations in S phase progression in budding yeast (León Ortiz et al. 2011). In this study, we show that cells lacking Srs2 and PARI do not respond to chromatin bridges during cytokinesis, and yet maintain similar timing in cytokinesis as unperturbed cells. Despite the delay in S phase, with or without chromatin bridges srs2 mutants and PARI-depleted cells undergo cytokinesis in a timely manner. In other words, srs2 mutants and PARI-depleted cells might be compensating for the delay in S phase by shortening cytokinesis independently of persisting chromatin bridges. This suggests that Srs2 and PARI are important for maintaining cell cycle progression, and to accordingly promote cytokinesis delay.

The depletion of PARI has been correlated with worsen cell viability and heighten sensitivity to DNA damage in pancreatic and leukemia cells (Piao et al. 2011; O'Connor et al. 2013; Nicolae et al. 2019). Indeed, the absence of PARI compromises the tumor growth in xenograft mouse models (O'Connor et al. 2013; Nicolae et al. 2019). Implicating that PARI has an important physiological function in cancers. A contrasting study by Moldovan et al. (2012), showed that the depletion of PARI improves genomic stability of particularly HR-deficient BRCA2-mutated, and FANCD1-mutated cell lines after induction of DNA damage. This is in agreement with our colony survival assay results showing that depletion of PARI (but not FBH1) improves the survival of HeLa cells dividing with an ICRF-193 induced chromatin bridge (Figure 36). It was therefore proposed that in HR-deficient cells loss of PARI increases HR which promotes DNA repair and protects against the accumulation of DNA damage. However, the same study showed that PARI-depletion in HeLa cell exposed to the DNA-damaging agent MMC have decreased cellular survival. There are two main differences between the experiment in Moldovan et al. (2012) and in this project ICRF-193 was used to induce chromatin bridges during cytokinesis of synchronized cells. Double thymidine did not affect PARI-deficient cells any differently than control cells, PARI-depleted cells in DMSO had 2% more surviving cells than control cells ($P=0.3356$, One sample t and Wilcoxon test, $N=3$, data not shown), implicating that PARI depletion does not affect overall cell survival in unperturbed synchronized condition. Furthermore, we found that PARI-deficient cells are not sensitive to DNA damage by ICRF-193 (Figure 35). In all, suggesting that PARI might be sensitizing HeLa cells to chromatin bridges induced by topoisomerase inhibition. The lack of PARI protects the cells against genomic instability and cell death perhaps due to upregulated HR.

Interestingly, nuclei with a chromatin bridge did not have more DSBs marked by 53BP1 than a properly formed nuclei after ICRF-193 exposure (Figure 35b-c), which implies at least at these timepoints after midbody formation (approximately 12 hours after thymidine release) the presence of chromatin bridges do not generate DNA damage. Additionally, PARI-depleted cells were not observed to be more prone to DNA damage (Figure 35) despite previous reports that PARI-deficient cells are hypersensitive to DNA-damaging agents such as MMC, Camptothecin and hydroxyurea.

This suggests that ICRF-193 does not generate additional DSBs in PARI-deficient cells, and that the shortened midbody lifetime in PARI-depleted cells is independent of DNA damage signals. Because the experiment in Figure 35 only looked at cells exposed to ICRF-193, it is not possible to say whether ICRF-193 causes more DNA damage than unperturbed cells. However, differences in the amount of DNA damage are not the reason why PARI deficient cells are not triggering a delay in midbody disassembly. It is possible though that PARI regulates the signaling pathways, a closer look on the ATM/ATR and downstream targets might aid to answer how PARI regulates the midbody stability and abscission checkpoint. Chromatin bridges persist for longer than what cells in Figure 35 were last fixed at, thus, to assay DNA damage after bridge resolution in control cells and cells lacking PARI, we have to collect at later timepoints.

Additionally, inactivation of yeast NoCut components causes DNA damage in the following cycle. To determine if Srs2 is an inhibitor of the NoCut checkpoint which protects against bridge breakage we could monitor the formation of MRE11 foci after cytokinesis. MRE11 is a component of the MRN complex which together with Rad50 and Nbs1 marks double-strand DNA breaks for NHEJ or HR repair. The increased DNA damage after perturbing the NoCut checkpoint can be rescued by additionally deleting the cytokinesis gene *Cyk3* which delays the formation of the septum (Onishi et al. 2013; Amaral et al. 2016). *lpl-321* inactivated cells and *ahc1Δ* mutants exhibit elevated DNA damage in the following G1 after an HU-pulse than cells with functional NoCut. However, when delaying cytokinesis by deleting *CYK3* the fraction of cells with DNA damage diminishes to the same level as cells with proficient NoCut. If Srs2 functions as a component of NoCut in protecting against DNA damage, the absence of Srs2 should cause more DNA damage after an HU-pulse and the *srs2Δ cyk3Δ* double-mutant DNA damage by should be prevented.

PARI has strongly been implicated in having a biological function in certain types of cancers. However, the physiological relevance of the abscission checkpoint is not well understood. It has been proposed that this checkpoint protects dividing cells with chromatin bridges against tetraploidization, premature resolution of chromatin bridges and DNA damage (Norden et al. 2006; Steigemann et al. 2009; Carlton et al. 2012).

Supporting this interpretation, the inactivation of the abscission checkpoint causes chromatin increased multinucleation (Steigemann et al. 2009) and bridge breakage (Dandoulaki et al. 2018; Petsalaki and Zachos 2021a) which is correlated with the DNA damage observed in the following G1 (Carlton et al. 2012; Amaral et al. 2016). Most chromatin bridges in human cells persist for hours after the midbody has disassembled. However, it is still not clear how they are resolved and what breaks/damages the chromatin bridge in absence of the abscission checkpoint. A direct causation has yet to be described.

A recent study by Sadler et al. (2018) showed a significant biological importance of the abscission checkpoint. Aurora B regulates abscission by phosphorylating the ESCRT-III component CHMP4C which prevents ESCRT-III/VPS4 activity from constrict the plasma membrane in the presence of a chromatin bridge (Thoresen et al. 2014). A polymorphism (variant allele) in the human CHMP4C where A232 is substituted by T232 has been observed to increase the susceptibility to cancer, in particular to prostate cancer and ovarian cancer. Cells expressing the CHMP4C^{T232} risk allele were shown to be deficient in abscission checkpoint. In the presence of chromosomes segregation errors these cells exhibited a premature resolution of chromatin bridges and increased levels of DNA damage. In all, suggesting that cells which have a dysregulated abscission checkpoint are genetically predisposed to tumorigenesis. In this regard, the next coming years are most likely going to focus on elucidating the contribution of the abscission checkpoint to human health and to identify the signaling pathway which triggers the checkpoint in the presence of anaphase bridges.

5. Conclusions

Conclusion 1: DNA helicase Srs2 have two roles in cytokinesis 1) to promote an abscission delay in the presence of HU-induced and catenated chromatin bridges, and 2) to promote the resolution of chromatin bridges.

Conclusion 2: The human homolog of Srs2, DNA helicase PARI, is a component of the abscission checkpoint by promoting midbody stabilization and actin patch formation in the presence of catenated chromatin bridges.

Conclusion 3: PARI is localized to the nucleus during S-phase but disperses into the cytoplasm (or is degraded) upon mitotic entry when the nuclear envelope breaks down and re-enters the nucleus in the next S-phase.

Conclusion 4: PARI is not detected at chromatin bridges or the midbody in the presence of bridges during cytokinesis to exert its action, suggesting that it does not act directly in abscission inhibition.

Conclusion 5: PARI promotes the resolution of chromatin bridges before next mitosis.

Conclusion 6: PARI enhances proliferation defects of HeLa cells after exposure to ICRF-193

6. Methods

6.1 Yeast strains and culture

All *Saccharomyces cerevisiae* strains are derived from S288c (Table 1). Gene deletions and insertions were generated by standard PCR methods (Janke et al. 2004) or through crossing. Cells were grown in YPDA media (yeast extract, peptone, 2% glucose, and adenine) at the permissive temperature of 30°C, and temperature-sensitive strains were grown at 25°C and shifted to 37°C to inactivate the protein. Dicentric strains were grown in YPDA supplemented with 2% galactose instead of glucose.

For all synchronizations, cells were grown overnight in YPDA at the permissive temperature, diluted to OD₆₀₀ =0.1, and grown for 3 hours to reach the log phase. To induce expression and localization of CAAX-GFP to the plasma membrane, 90 nM β -estradiol was added to the media for 3 hours. To generate replication stress 200 mM HU was added to the media for 3 hours. To arrest cells in G1, cells synchronized with 20 μ m/ml α -factor for 2 hours. To release from the G1 block or HU-treatment cells were washed twice in freshly prepared and pre-heated minimal synthetic (Yeast nitrogen base, 2% glucose, essential amino acids) media and immediately plated on concanavalin A-coated Lab-Tek chambers for microscopy.

Table 1. *Saccharomyces Cerevisiae* strains used

YMM ID	Background	Genotype
1335	S388C	ADEGV:URA3 Gal1:GFP-CAAX:HIS3 SPC42-GFP:HphMX leu2 lys2-801 ade2-101 trp1 Δ 63
3399	S388C	SRS2::NAT ADEGV:URA3 Gal1:GFP-CAAX:HIS3 SPC42-GFP:HphMX leu2 lys2-801 ade2-101 trp1 Δ 63
2378	S388C	top2-4 ADEGV:URA3 Gal1:GFP-CAAX:HIS3 SPC42-GFP:HphMX leu2 lys2-801 ade2-101

3401	S388C	SRS2::NAT top2-4 ADEGV:URA3 Gal1:GFP-CAAX:HIS3 SPC42-GFP:HphMX leu2 lys2-801 ade2-101
3949	BY4741	RFA2-GFP:HIS Htb2-mCherry:HphMX
6161	BY4741	SRS2::NAT RFA2-GFP:HIS Htb2-mCherry:HphMX
4581	S288C	POL30-S115P ADEGV:URA3 pGal1:GFP-CAAX:HIS3 SPC42-GFP:HphMX leu2 lys2-801 ade2-101 trp1Δ63
3298	S288C	SRS2ΔSIM::NAT top2-4 ADEGV:URA3 pGal1:GFP-CAAX:HIS3 SPC42-GFP:HphMX leu2 lys2-801 ade2-101
3960	S288C	SRS2ΔSIMΔPIP::NAT top2-4 ADEGV:URA3 pGal1:GFP-CAAX:HIS3 SPC42-GFP:HphMX leu2 lys2-801 ade2-101
2833	Mostly S228C mixed with W303	ChrXII(1059):nat:ChrIV(19.5) pGal:CEN4:KanMX4 Htb2-mCherry:URA pGal1:GFP-CAAX:TRP1 ura3-52 his3Δ200 leu2 lys2-801 ade2-101 trp1Δ63
4578	Mostly S228C mixed with W303	ELG1::HYG ChrXII(1059):nat:ChrIV(19.5) pGal:CEN4:KanMX4 Htb2-mCherry:URA pGal1:GFP-CAAX:TRP1 ura3-52 his3Δ200 leu2 lys2-801 ade2-101 trp1Δ63

6.2 Human cell lines and culture conditions

All cell lines were cultured at 37°C in a 5% CO₂ humidified incubator. Standard media, DMEM GlutaMAX (4.5 g/L glucose) supplemented with 10% fetal calf serum, 1% penicillin, and streptomycin was used to culture all cell lines. The HeLa Kyoto cell line was obtained from the in-house cell culture facility.

The following HeLa stable cell lines were kindly shared by Dr. Daniel Gerlich and were grown in standard media with additional selective antibiotics.

Table 2. Human cell lines used

Fluorescent marker	Antibiotics
H2B-mCherry and Actin-eGFP	0.5 µg/mL puromycin + 0.5 mg/mL G418
H2B-mCherry and eGFP- α -Tubulin	0.5 µg/mL puromycin + 0.5 mg/mL G418
H2B-mRFP and GFP-LAP2 β	0.5 µg/mL puromycin + 0.5 mg/mL G418
eGFP-BAF	6 µg/mL blasticidin

6.2.1 Cell seeding

Cells were trypsinized with 2.5% Trypsin-EDTA and resuspended in media. The concentration was calculated using a Bürker chamber. For IF experiments 20.000 cells were seeded on a 13 mm glass coverslip in a 24-well plate. For time-lapse microscopy, 12.500 cells were seeded in a 4-chamber 35 mm glass-bottom dish. For RT-qPCR, WB, and flow cytometry 200.000-300.000 cells were seeded in a 6-well plate.

6.2.2 Plasmid and siRNA transfection

A FLAG-PARI Gateway Destination plasmid was kindly gifted by Dr. Peter Burkovics, and the sequence of PARI was further cloned into pcDNA3.1(+) plasmid by the molecular biology facility at IGBMC. All plasmid cloning and primer design were performed by the molecular biology facility. An eGFP fluorophore was introduced at the N-terminal of PARI. For the siPARI-1 resistant version of eGFP-PARI three silent mutations were introduced at the seed region of the siPARI-1 target site (Figure 22a).

To generate stable cell lines, HeLa Kyoto cells were transfected with linearized pcDNA3.1(+) derived plasmids using X-tremeGENE 9 DNA Transfection Reagent

(ROCHE) according to the manufacturer's protocol. Transfected cells were selected for 2-3 weeks in standard media supplemented with G418 (0.8 mg/mL). Transgene-positive cells were isolated by FACS (FACS ARIA, BD Biosciences) or by manually isolating single colonies. Expression was validated by PCR, IF, and WB.

All siRNAs used are of the siGENOME product line from Dharmacon and were purchased from Horizon (Table 1). To knockdown PARI, resuspended cells were (reverse) transfected using 25 nM siRNA and Lipofectamine RNAiMAX (Invitrogen) according to the manufacturer's protocol, the siRNA-lipid complexes were removed after 7 hours, and a second (forward) transfection was performed 24 hours after the first one. FBH1 was depleted once with 25 nM siRNA pool using the forward transfection method and RNAiMAX. For co-depletion of PARI and NUP153 depletion, 10 nM siNUP153 was used together with 25 nM siCtrl or siPARI-1 24 hours after reverse transfection with siCtrl and siPARI-1, and the amount of Lipofectamine RNAiMAX was adjusted accordingly.

Table 3. siRNA sequences for gene knockdown

siRNA	Sequence 5'-3'
siCtrl pool	UAAGGCUAUGA AGAGAUAC, AUGUAUUGGCCU-GUAUUAG, AUGAACGUGAAUUGCUCAA, UGGUUUACAUGUCGA-CUAA
siPARI-1	GAATAGATTGTACGGCAA
siPARI-2	CCAAGGACAAGTTGATTC
siFBH1 pool	GGAAAUAGCUUAUGUGGGA GAGCCAAGCUUGUGUGUAA UCACGUGCCUAUUUGGUGU GCACUUCAGAGUUGAGUCA
siNUP153	GAGGAGAGCUCUAAUUA

6.2.3 Colony survival assay

Here we asked how well cells survival after one cell division with a chromatin bridge induced by ICRF-193. To this aim, 30.000 cells were seeded per well in 24-well plate and transfected accordingly. To have a homogenous population, transfected cells were synchronized with double thymidine according to Figure 18a. However, before the second thymidine block the cells were trypsinized and 500 cells were seeded into

three wells (triplicate) of a 6-well plate. Cells are distributed at this stage to eliminate the possibility of counting errors after incubating dividing cells with ICRF-193 and to account for cells that die during the first division with a catenated chromatin bridge.

DMSO or 250 nM ICRF-193 was added 8 hours after the second thymidine release and incubated for 16 hours. Cells were then washed away of ICRF-193 and left to grow for 10 days. The culture medium was changed in between. After 10 days, cells are washed with 1x PBS and fixed with 4% PFA, 1x PBS for 30 min at RT. PFA is washed out of the wells with 1x PBS and immediately stained with 0.1% crystal violet for 30 min at RT with gentle agitation. Excess crystal violet and non-adherent cells are then rinsed off underneath running tap water and stained cells are left to dry upside down.

To quantify the survival after one division with ICRF-193 we are measuring the OD₅₉₀. 2 ml of 20% acetic acid is added to each well to solubilize the crystal violet (of stained cells). The OD₅₉₀ was measured for each of the triplicate wells, and the average of those three is normalized to the average OD₅₉₀ of DMSO-treated siCtrl.

6.3 Quantitative PCR and analysis

RNA was extracted using RNAeasy kit (Qiagen), and 2.5 ug RNA was incubated with ezDNase for 10 min at 37°C before performing reverse transcription using superscript IV VILO Master Mix according to the manufacturer's protocol. Alternatively, DNase I was used, and reverse transcription was performed with random hexamer and oligo(dT) primers, SuperScript IV, and RNaseOUT Recombinant RNase Inhibitor according to the manufacturer's protocol. SYBR Green-based qPCR and analysis were carried out on the LightCycler480.

All primer pairs were validated with PCR and serial dilution to determine the primer efficiency, only those that are close to 100% amplification efficiency were used for analysis (Table 2). The Ct value was obtained from the LighCycler480 software and used to measure the relative expression (RE) of each sample, which was calculated using the following equation

Table 4. Primer sequences for qPCR

Target gene	Forward/Reverse	Sequence 5'-3'
ACTIN B	Forward	AGGCACCAGGGCGTGAT
ACTIN B	Reverse	GCCCACATAGGAATCCTTCTGAC
PARI	Forward	GCATCAAAGCCTTTGTGTG
PARI	Reverse	CCTGTCTGACTGGTTGAT
FBH1	Forward	CACGCTGAAATGAGACGGTT
FBH1	Reverse	CTTTGACTTCCCTGACCCC

$$RE = 2^{-\Delta Ct}$$

where $\Delta Ct = Ct(\text{target gene}) - Ct(\text{reference gene})$

The RE of the test sample is then normalized to the RE of the control.

6.4 Western blotting and immunoprecipitation

To validate transgene-positive colonies 1x Laemmli buffer with 0.1 mM DTT was directly added to the dish, cells were scraped off and mechanically lysed through pipetting and immediately boiled to be resolved on 8% polyacrylamide gels. Whole cell extracts were prepared using RIPA buffer (50 mM Tris HCl pH 7.5, 150 mM NaCl, 1% Triton X-100, 0.5% Sodium Deoxycholate, 0.1% SDS, 1 mM PMSF, 1x Protease Inhibitor Cocktail Complete). Cells were lysed on ice by vigorous pipetting every 5 min for 30 min. Samples were then centrifuged at 14,000 rpm for 20 min at 4°C and the supernatant was transferred to a new tube. The protein concentration was measured by Bradford assay in 1 mL cuvettes. 15µg - 25µg of protein was boiled for 15 min at 96°C in 1x Laemmli buffer with 0.1 mM DTT and subjected to SDS-page to be resolved on 8 or 10% polyacrylamide gels or 4-12% Bis-Tris gradient gels, and transferred to a 0.22 µm nitrocellulose membrane using wet transfer. Membranes were blocked in 5% non-fat milk, TBS 0.1% Tween-20 for 1 hr at RT, and incubated with antibodies (Table 5). Membranes were developed using SuperSignal West Pico or Femto with Cytiva Amersham ImageQuant 800.

For immunoprecipitation of GFP, whole cell extracts were prepared in lysis buffer (50 mM Tris HCl pH 7.5, 150 mM NaCl, 1% Triton X-100, 1 mM EDTA, 1 mM EGTA, 2 mM Na₄O₇P₂, 1 mM NaVO₄, 1 mM NaF), and GFP-fusion proteins were

immunoprecipitated using GFP-Trap A magnetic beads (Chromotek). The magnetic beads were blocked in 3% BSA at 4°C for 2 hours with constant rotation and equilibrated by washing the beads in dilution buffer (lysis buffer without Triton X-100) three times. The equilibrated beads were then incubated with 1000 ug whole cell extracts overnight at 4°C under constant rotation and washed three times with 0.5x lysis buffer for 10 min under constant rotation before eluting at 96°C in 1x Laemmli buffer with 1 mM DTT.

Table 5. Antibodies used for western blot and immunofluorescence

Primary antibodies				
Raised in	Against	Reference	Dilution	Figure
Chicken	GFP	ab13970	1:3,000 (IF, PFA) 1:10,000 (WB)	22b, 22d, 27d-e
Mouse	α -Tubulin	T9026	1:1000 (IF, PFA & MeOH)	26a, 30c, 30e, 30g
Mouse	LAP2 β	611000	1:500 (IF, PFA)	17, 29, 33a, 35a
Mouse	Nup153	ab24700	1:1,000 (WB)	26b
Mouse	PCNA	sc-56	1:200 (IF, MeOH)	28a
Rabbit	53BP1	NB100-304	1:500 (IF, PFA)	35a
Rabbit	α -Tubulin	ab52866	1:1000 (IF, PFA) 1:5,000 (WB)	17, 22b, 26b, 27e, 29, 33a
Rabbit	pS210 CHMP4C	Paolo D'Avino	1:200 (IF, MeOH)	28a, 30c
Rabbit	pT323 Aurora B	039600-401-677	1:500 (IF, PFA)	26a, 30a
Rabbit	VPS4	AB-20.0003	1:200 (IF, PFA)	30e, 30g
Secondary antibodies				
Goat	Anti-chicken IgY Alexa Fluor 488	A-11039	1:500	22d, 27d
Goat	Anti-mouse IgG Alexa Fluor Plus 488	A32723	1:500	26a, 30c, 30e, 30g
Goat	Anti-mouse IgG Alexa Fluor 568	A-11031	1:500	17, 26a, 28a, 29, 33a, 35a
Goat	Anti-rabbit IgG Alexa Fluor 488	A32731	1:500	17, 26a, 28a, 29, 33a, 35a
Goat	Anti-rabbit IgG Alexa Fluor 647	A32733	1:500	30a, 30c, 30e, 30g
Goat	Anti-chicken IgY Alexa Fluor 488	A-11039	1:500	22d, 27d
Goat	Anti-chicken IgY HRP	ab6877	1:10,000	22b, 27e
Goat	Anti-mouse IgG HRP	170-6516	1:10,000	26b
Goat	Anti-rabbit IgG HRP	31460	1:10,000	22b, 26b, 27e

6.5 Microscopy techniques

6.5.1 Immunofluorescence microscopy and image analysis

20.000 cells were seeded on 13 mm sterile glass coverslips in 24-well culture plates and fixed with 4% PFA for 15 min at RT. PFA was washed out three times with 1x PBS and cells were permeabilized in 0.2% Triton X-100 in 1x PBS, for 10 min at RT, followed by a 1-hour block with 3% BSA in 1x PBS at RT with gentle agitation. For methanol fixation, cells were fixed in ice-cold 100% methanol for 5 min at -20°C, following three washes with 1x PBS and a 1-hour block with 3% BSA in 1x PBS at RT with gentle agitation. HeLa Kyoto eGFP-PARI cells were pre-extracted with 0.1% Triton X-100 in 1x PBS for 30 s before adding 4% PFA on top for 10 minutes on ice. A second fixation is performed with new 4% PFA at RT for 10 min, followed by permeabilization and blocking as described. After blocking, cells are incubated with primary antibodies (Table 5) for 1 hour at RT or overnight at 4°C, followed by three washes with 1x PBS. Cells are then subjected to secondary antibodies (Table 5) and DAPI for 1 hour at RT, followed by three washes with 1x PBS. Excess 1x PBS was carefully tapped off from the coverslips and mounted on a glass slide with Vectashield mounting medium (Vecta Laboratories) or ProLong Gold (Invitrogen).

For fluorescent acquisition in Figure 17 and 26, the HCX PL APO 63x/1.40 OIL PH3 C3 objective was used on an upright motorized Leica DM 4000 B equipped with CoolSNAP HQ2 camera. For confocal images in Figure 22, 28, 29, 30, 33 and 36, HC PL APO CS2 63x/1.40 OIL objective was used on an Inverted Leica DMI6000 confocal microscope, and Z-stacks were acquired with 0.5 μm step size.

Images were analyzed using Fiji. For intensity measurements in Figure 30 and 22, the sum projection of Z-stack images was used. Max projection is used for illustration purposes in all figures, and object segmentations in Figure 22 and 36. Graphpad Prism was used to generate all graphs.

6.5.2 CellProfiler Image Analysis

For the experiment in Figure 36 using 53BP1 as a marker for DNA damage. Three channels were acquired by confocal microscopy; DAPI for nucleus, LAP2 β -Alexa568

for chromatin bridges and 53BP1-Alexa488 for DNA damage. A pipeline was generated using CellProfiler software to count 53BP1 foci per nucleus. The pipeline is able to automatically process all images in an input folder. The nucleus is identified based the DAPI channel, and is assigned as an object with a unique number. The contrast between the background and 53BP1 signal was increased to improve the segmentation of each individual focus using the “Enhance Or Suppress Features” module. The outlines of the foci were then overlapped with the nucleus to categorize the foci that belonged to a specific nucleus (Supplementary Figure 2e). CellProfiler then measures the number of foci for each individual nucleus and the information is saved in an Excel file for further analysis. The file holds information including the image number, experiment condition, and the nucleus number with how many foci it contains. To assess if cells with chromatin bridges had more 53BP1 foci we manually went through each nucleus and assigned it to “nucleus” or “nucleus with chromatin bridge”. Errors in nuclear segmentation and mitotic cells were removed from the analysis.

6.5.3 Time-lapse fluorescence spinning disk confocal microscopy

For abscission assays, HeLa cells were seeded 3 days in advance on a 4-chamber 35 mm glass bottom dish (Cellvis) and placed in a preheated chamber at 37°C and 5% CO₂ for time-lapse microscopy. For cell lines that do not stably express fluorescently tagged Tubulin, cells were incubated with 15 nM SiR-Tubulin (Spirochrome) and 1 µM Verapamil for 9 hours in media before acquisition.

All time-lapse acquisitions were set up using MetaMorph software. Images were acquired using 63x water objective (HC PL APO 63x/1,20 W CORR CS2) with Leica water immersion micro dispenser connected to a Bartek extended micropump on an inverted Leica DMI8 microscope equipped with Yokogawa CSU W1 spinning disk and Evolve 512 camera or an inverted Nikon eclipse equipped with Yokogawa CSU X1 spinning disk and photometric prime 95B camera. Z-stack (15 µm range, 0.3 µm step size) images were acquired every 5-7 min for 14 hours.

For chromatin bridge lifetime assays with HeLa Kyoto stably expressing eGFP-BAF, Z-stack (15 µm range, 1 µm step size) images were acquired every 15 min for 72 hours. ICRF-193 was removed after 16 hours by washing the well three times with

pre-heated media supplemented with SiR-Tublin and Verapamil in-between intervals. New media was added on top every 24 hours. For time-lapse microscopy of Aurora B inhibition with hesperadin, media with a final concentration of 100 nM hesperadin was added on top of the cells in between intervals.

6.5.4 Correlative light electron microscopy

For CLEM, adherent HeLa Kyoto stably expressing H2B-mCherry GFP- α -Tubulin cells were first cultured on laser micro-patterned Aclar[®] supports (Spiegelhalter et al. 2010, Lenormand et al. 2013), synchronized with double thymidine and released for 12 hours. Cells were then fixed with 1% glutaraldehyde and 4% formaldehyde in 0.1M phosphate buffer for 30 minutes. Cells in cytokinesis with or without a catenated chromatin bridge were selected, precisely located, and imaged by an inverted Nikon eclipse equipped with a photometric prime 95B camera. At the end of the experiment, cells were immediately fixed with 2.5% glutaraldehyde and 4% formaldehyde in 0.1 M phosphate buffer for 1 hour (or longer) at 4°C, rinsed in buffer, and followed by 1-hour postfixation in 1% osmium tetroxide [OsO₄] reduced by 0.4% potassium hexacyanoferrate (III) [K₃Fe(CN)₆] in H₂O at 4°C. Samples were rinsed in distilled water and stained with 1% tannic acid for 30 minutes on ice and after extensive rinses, with 2% uranyl acetate for 1 hour at room temperature, rinsed in water. Samples were dehydrated with increasing concentrations of ethanol (25%, 50%, 70%, 90%, and 3x100%), and embedded with a graded series of epoxy resin. Samples were finally polymerized at 60°C for 48 hours. Ultrathin serial sections (70nm) were picked up on 1% pioloform coated copper slot grids and observed with a Philips CM12 operated at 80kV equipped with an Orius 1000 CDD camera (Gatan, Pleasanton, USA).

6.5.5 EdU incorporation

HeLa Kyoto cells were synchronized with double thymidine and released from G1. As a positive control for EdU incorporation, cells were exposed to 10 μ M EdU for 40 min at 5.5 hours after the release. DMSO or 250 nM ICRF-193 was added to the cells 7.5 hours after the release to induce catenated chromatin bridges. To assess if EdU gets incorporated in the presence of a catenated chromatin bridge, cells were exposed to 10 μ M EdU for 40 min 12 hours after the release. All conditions were fixed 13 hours after the release from G1 arrest with 4% PFA, followed by a 0.2% Triton X-100

permeabilization for 10 min and 1-hour blocking with 3% BSA. The coverslips were washed three times with 1x PBS. EdU incorporation was detected using the Click-iT EdU Alexa Fluor 647 imaging kit (Invitrogen) and according to the manufacturer's protocol. Two modifications were made in the Click-iT reaction cocktail, Component E was replaced with homemade CuSO_4 and the Reaction buffer additive was replaced with 113 mM ascorbic acid (final concentration).

Remaining EdU was washed away thrice in 1x PBS and the coverslips were incubated with primary antibodies for 1 hour at RT, washed three times with 1x PBS, and incubated with secondary antibodies, Click-iT reaction cocktail and DAPI for 1 hour before being washed three times with 1X PBS.

6.6 Flow cytometry

Cells were grown and collected from two p6-wells and fixed with ice-cold 70% EtOH for at least 30 min on ice. To stain the DNA, cells were incubated with 50 $\mu\text{m}/\text{ml}$ propidium iodide (PI) and 100 $\mu\text{g}/\text{ml}$ RNase A in 1x PBS for 40 min. Before analyzing the cell cycle profile using flow cytometry (BD LSRII with BD FACSDiva software) samples were strained through a 40 μm filter. Single cells were separated from doubles during the run and the DNA content of 30.000 cells was analyzed.

To measure how the GFP-PARI expression changes with the cell cycle, resuspended asynchronous HeLa cells stably expressing GFP-PARI were fixed with ice-cold 4% PFA for 15 min, permeabilized with 0.2% Triton X-100 for 10 min, and blocked in 3% BSA for 1 hour, all performed on ice. Cells were then incubated with primary GFP antibody for 1 hour, washed three times with 1x PBS, and incubated with secondary antibody coupled with Alexa-488 for 1 hour. Uncoupled secondary antibodies were washed out three times with 1x PBS before incubating with 50 $\mu\text{m}/\text{ml}$ PI and 100 $\mu\text{g}/\text{ml}$ RNase A in 1x PBS for 40 min. The GFP intensity and DNA content were measured for 30.000 single cells.

Obtained data was analyzed and graphs were created with FlowJo.

6.7 Statistical methods

Graphpad prism software was used to generate graphs and perform statistical tests. Mann-Whitney was used on datasets that did not follow a normal distribution. For experiments with at least three independent biological replicates, Students paired t-test was used. Data was pooled from at least two biological replicates to compare fractions, Fisher's exact test was performed. Details on each statistical test used and the significance can be found in the figure legends, along with the total number of data points (n) and biological replicates (N).

Acknowledgements

First and foremost, I would like to express my sincere gratitude to Manuel for his trust in letting me take on this project and for allowing me to explore my ideas. Thank you for all your support throughout the years, and for your immense help in improving this thesis. Your enthusiasm and knowledge have taught me a lot.

I would like to thank my Thesis Monitoring Committee and Thesis Defense Jury members Dr. Izabela Sumara, Prof. Arnaud Echard, and Prof. Juan Martin-Serrano for taking the time to critically evaluate this Ph.D. thesis, your feedback and advice have been most valuable.

I am grateful to Gilles Charvin and his lab for the great discussions and helpful advice during lab meetings. I would also like to thank the Keyes, Soutoglou, and Sumara labs, especially Matej, Ioanna, Arantxa, and Yongrong for their great experimental advice, and for sharing reagents.

All the images would not have been acquired without the expertise of the microscope facility team at IGBMC, big thanks to Bertrand, Erwan, Elvire, Marine, Marcel, and Yves. I appreciate your dedication and enthusiasm for microscopy, for always being ready to help, and for listening to my odd problems with the microscopes.

I have had many precious memories thanks to the wonderful members of the Mendoza lab, to all past and current members; Céline, Mercè, Laurine, Célia, Max, Vasia, Bogdan, Faezeh, and Sandrine, thank you all for the memorable conversations, late-work shenanigans, and cake-times. To Vasia, whom I started this Ph.D. with, thank you for the great discussions and for always being there whenever I needed help. Big thanks to Bogdan who is ready to drop whatever he is doing to help, especially that time when I called about finding a cat at IGBMC...

To my students Inès and Léna. Thank you Inès for being so patient with me when I was still trying to figure things out at the beginning of this project. Even though it was cut short due to a sudden lockdown, your commitment and hard work to see things through have inspired me to become an even better scientist. Thank you Léna for your

help on the FBH1 story, it has been incredibly rewarding to see you grow more confident in the lab in just three months!

The immense progression over the past year would not have been possible without Audrey. Thank you for all the help and dedication with this project, I am incredibly lucky to have been able to work alongside such a kind and selfless person. Thank you for helping me outside of work as well, I am forever grateful for the kindness you have shown me!

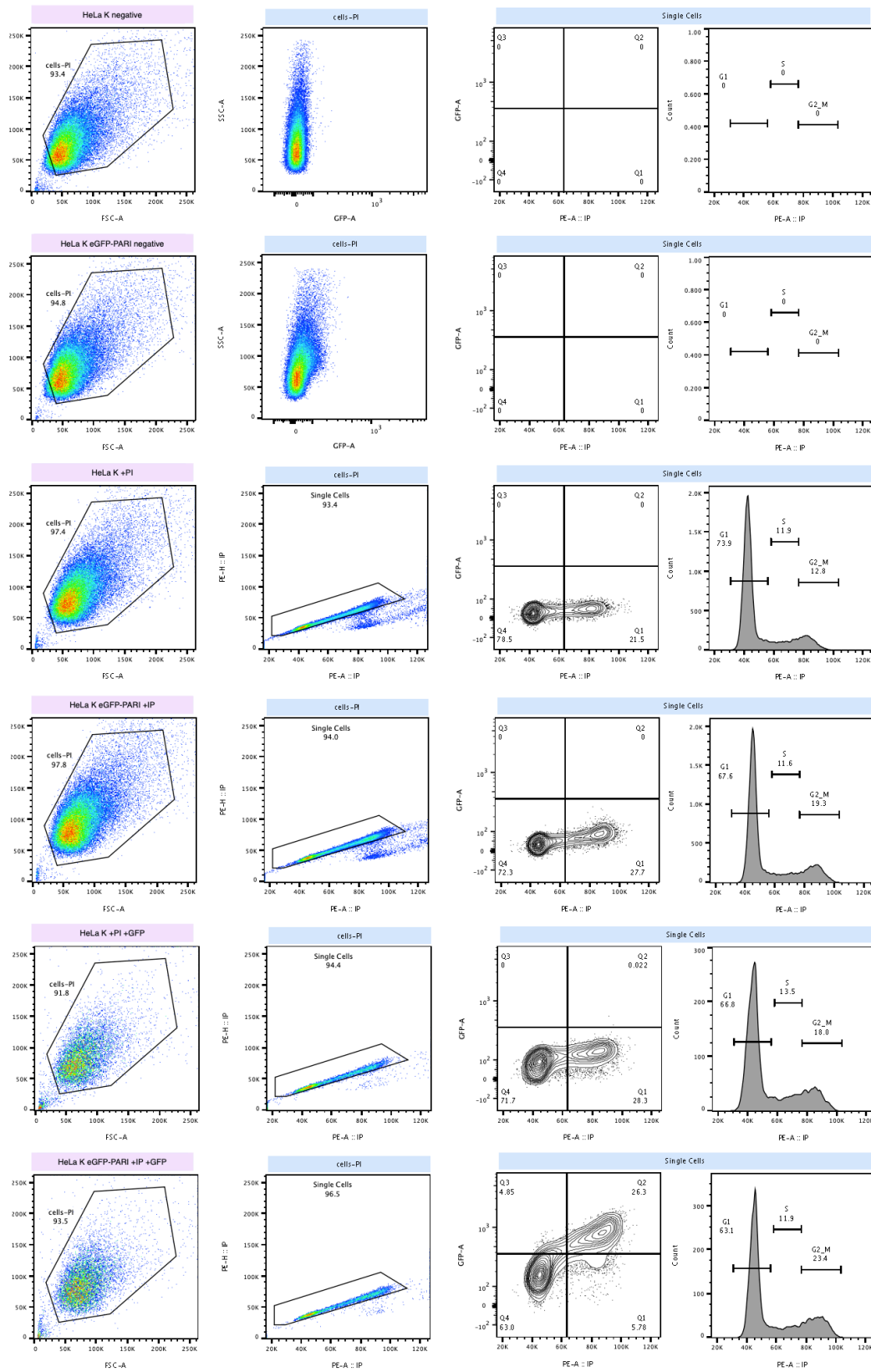
To the forever members of the Games Night team; Mónica, Dimitra, Yasenya, and Yung-Chieh. I have had so much fun organizing Games Night with you, thank you for reminding me to take a break and enjoy some board games and delicious food.

Hearty thanks to Sara, José, Salvatore, Gregoire, Vasia, and Dimitra for all the beers, tarte flambée, and endless laughter!

致我的家人，我将这篇论文献给他们。感谢你们坚定不移地支持我追寻我的激情。感谢妈妈在我回家探亲时总是做我喜欢的菜。谢谢爸爸提醒我，我总是有一个随时可以返回的家。你们的话语在困难时期给了我极大的安慰。你们教会我，努力工作和坚韧不拔的精神最终会得到回报。Tack till den snällaste Annica, 月饼 till min 秋天, min Estrella chips-langare och den bästa lillasystemen jag någonsin kan önska mig, för ditt stöd och skratt under dessa åren.

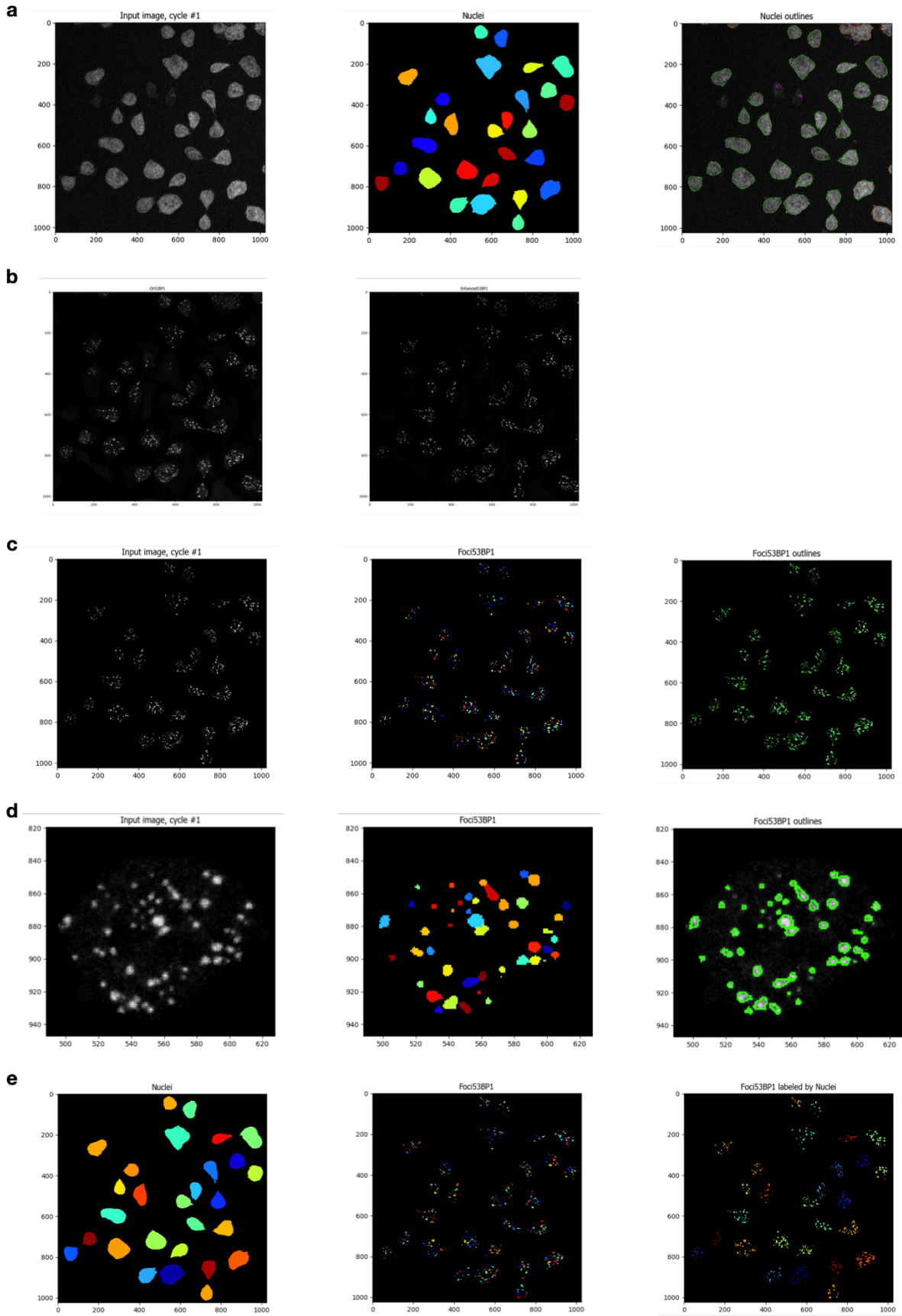
Lastly, to Stefano for being my biggest rock and the funniest person I know, you always find ways to cheer me up and make me laugh. These past years would not have been possible without your encouragement to step out of my comfort zone. I am grateful that I have you by my side and I look forward to the next adventure we embark on together.

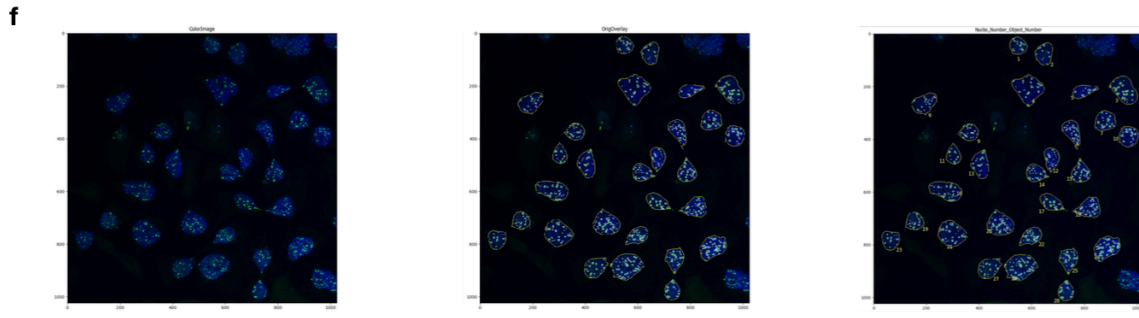
Supplementary Figures



Supplementary Figure 1. Gating strategy of eGFP-PARI

Unstained HeLa Kyoto and HeLa Kyoto stably expressing eGFP-PARI were used to first gate the cell population. Thereafter, cells stained with propidium iodide (PI) were introduced to exclude doublets from single cells, which were then gated to have the GFP levels on the y-axis (left) or the count of cells (right) relative to the DNA content on the x-axis. The graph showing GFP level relative to DNA content is divided into four squares; Q4 are GFP negative cells in G1, Q3 consist of GFP positive cells in G1, Q2 are positive GFP cells in M/G2 and lastly Q1 include negative cells in M/G2. Histogram showing the count of cells relative to the DNA content describes the fraction of single cells in G1, S and G2/M.





Supplementary Figure 2. CellProfiler pipeline to quantify the number of 53BP1 foci per nucleus

- (a) DAPI staining was used to create a mask for individual nuclei and an outline for each nucleus
- (b) The 53BP1 foci was enhanced by reducing the background signal
- (c) The image with enhanced 53BP1 foci was used to create a mask for individual foci and an outline for each focus
- (d) Zoom-in on a single nucleus from the boxed region in panel c
- (e) Nuclei mask from panel a is applied to the 53BP1 mask, generating an image with categorized 53BP1 for each respective nucleus.
- (f) Original image of DAPI and 53BP1 with the nucleus and 53BP1 focus segmented by CellProfiler. Numbering is attributed to each outlined nucleus.

References

Aboussekhra, A., R. Chanet, Z. Zgaga, C. Cassier-Chauvat, M. Heude, and F. Fabre. 1989. "RADH, a Gene of *Saccharomyces Cerevisiae* Encoding a Putative DNA Helicase Involved in DNA Repair. Characteristics of radH Mutants and Sequence of the Gene." *Nucleic Acids Research* 17 (18): 7211–19.

Addi, Cyril, Jian Bai, and Arnaud Echard. 2018. "Actin, Microtubule, Septin and ESCRT Filament Remodeling during Late Steps of Cytokinesis." *Current Opinion in Cell Biology* 50 (1): 27–34.

Addi, Cyril, Adrien Presle, Stéphane Frémont, Frédérique Cuvelier, Murielle Rocancourt, Florine Milin, Sandrine Schmutz, Julia Chamot-Rooke, Thibaut Douché, Magalie Duchateau, Quentin Gai Gianetto, Audrey Salles, Hervé Ménager, Mariette Matondo, Pascale Zimmermann, Neetu Gupta-Rossi and Arnaud Echard. 2020. "The Flemmingsome Reveals an ESCRT-to-Membrane Coupling via ALIX/syntenin/syndecan-4 Required for Completion of Cytokinesis." *Nature Communications* 11 (1): 1941.

Agromayor, Monica, Jeremy G. Carlton, John P. Phelan, Daniel R. Matthews, Leo M. Carlin, Simon Ameer-Beg, Katherine Bowers, and Juan Martin-Serrano. 2009. "Essential Role of hIST1 in Cytokinesis." *Molecular Biology of the Cell* 20 (5): 1374–87.

Agromayor, Monica, and Juan Martin-Serrano. 2013. "Knowing When to Cut and Run: Mechanisms That Control Cytokinetic Abscission." *Trends in Cell Biology* 23 (9): 433–41.

Alao, John P. 2007. "The Regulation of Cyclin D1 Degradation: Roles in Cancer Development and the Potential for Therapeutic Invention." *Molecular Cancer* 6 (1): 24.

Amaral, Nuno, Alexandre Vendrell, Charlotta Funaya, Fatima-Zahra Idrissi, Michael Maier, Arun Kumar, Gabriel Neurohr, Neus Colomina, Jordi Torres-Rosell, María-Isabel Geli and Manuel Mendoza. 2016. "The Aurora-B-Dependent NoCut Checkpoint

Prevents Damage of Anaphase Bridges after DNA Replication Stress.” *Nature Cell Biology* 18 (5): 516–26.

Antony, Edwin, Eric J. Tomko, Qi Xiao, Lumir Krejci, Timothy M. Lohman, and Tom Ellenberger. 2009. “Srs2 Disassembles Rad51 Filaments by a Protein-Protein Interaction Triggering ATP Turnover and Dissociation of Rad51 from DNA.” *Molecular Cell* 35 (1): 105–15.

Arbel, Matan, Alex Bronstein, Soumitra Sau, Batia Liefshitz, and Martin Kupiec. 2020. “Access to PCNA by Srs2 and Elg1 Controls the Choice between Alternative Repair Pathways in *Saccharomyces Cerevisiae*.” *mBio* 11 (3): e00705–20.

Arellano, Manuel, and Sergio Moreno. 1997. “Regulation of CDK/cyclin Complexes during the Cell Cycle.” *The International Journal of Biochemistry & Cell Biology* 29 (11): 559–73.

Ayyagari, Rao, Kimberly J. Impellizzeri, Bonita L. Yoder, Sonja L. Gary, and Peter M. Burgers. 1995. “A Mutational Analysis of the Yeast Proliferating Cell Nuclear Antigen Indicates Distinct Roles in DNA Replication and DNA Repair.” *Molecular and Cellular Biology* 15 (8): 4420–29.

Bai, Jian, Hugo Wioland, Tamara Advedissian, Frédérique Cuvelier, Guillaume Romet-Lemonne, and Arnaud Echard. 2020. “Actin Reduction by MsrB2 Is a Key Component of the Cytokinetic Abscission Checkpoint and Prevents Tetraploidy.” *Proceedings of the National Academy of Sciences* 117 (8): 4169–4179.

Bajorek, Monika, Heidi L. Schubert, John McCullough, Charles Langelier, Debra M. Eckert, William-May B. Stubblefield, Nathan T. Uter, David G. Myszka, Christopher P. Hill, and Wesley I. Sundquist. 2009. “Structural Basis for ESCRT-III Protein Autoinhibition.” *Nature Structural & Molecular Biology* 16 (7): 754–62.

Barber, Louise J., Jillian L. Youds, Jordan D. Ward, Michael J. McIlwraith, Nigel J. O’Neil, Mark I. R. Petalcorin, Julie S. Martin, Spencer J Collis, Sharon B Cantor, Melissa Auclair, Heidi Tissenbaum, Stephen C West, Ann M Rose, Simon J Boulton.

2008. "RTEL1 Maintains Genomic Stability by Suppressing Homologous Recombination." *Cell* 135 (2): 261–71.

Barefield, Colleen, and Jan Karlseder. 2012. "The BLM Helicase Contributes to Telomere Maintenance through Processing of Late-Replicating Intermediate Structures." *Nucleic Acids Research* 40 (15): 7358–67.

Bartek, Jiri, Claudia Lukas, and Jiri Lukas. 2004. "Checking on DNA Damage in S Phase." *Nature Reviews. Molecular Cell Biology* 5 (10): 792–804.

Basant, Angika, Sergey Lekomtsev, Yu Chung Tse, Donglei Zhang, Katrina M. Longhini, Mark Petronczki, and Michael Glotzer. 2015. "Aurora B Kinase Promotes Cytokinesis by Inducing Centralspindlin Oligomers That Associate with the Plasma Membrane." *Developmental Cell* 33 (2): 204–15.

Bassi, Zuni I., Morgane Audusseau, Maria Giovanna Riparbelli, Giuliano Callaini, and Pier Paolo D'Avino. 2013. "Citron Kinase Controls a Molecular Network Required for Midbody Formation in Cytokinesis." *Proceedings of the National Academy of Sciences of the United States of America* 110 (24): 9782–87.

Bastos, Ricardo Nunes, and Francis A. Barr. 2010. "Plk1 Negatively Regulates Cep55 Recruitment to the Midbody to Ensure Orderly Abcission." *The Journal of Cell Biology* 191 (4): 751–60.

Baumann, Christoph, Roman Körner, Kay Hofmann, and Erich A. Nigg. 2007. "PICH, a Centromere-Associated SNF2 Family ATPase, Is Regulated by Plk1 and Required for the Spindle Checkpoint." *Cell* 128 (1): 101–14.

Bembenek, Joshua N., Koen J. C. Verbrugghe, Jayshree Khanikar, Györgyi Csankovszki, and Raymond C. Chan. 2013. "Condensin and the Spindle Midzone Prevent Cytokinesis Failure Induced by Chromatin Bridges in *C. Elegans* Embryos." *Current Biology* 23 (11): 937–46.

Bhowmick, Rahul, Roshan Singh Thakur, Andrés Bueno Venegas, Ying Liu, Jakob Nilsson, Marin Barisic, and Ian D. Hickson. 2019. "The RIF1-PP1 Axis Controls Abscission Timing in Human Cells." *Current Biology* 29 (7): 1232–42.e5.

Biebricher, Andreas, Seiki Hirano, Jacqueline H. Enzlin, Nicola Wiechens, Werner W. Streicher, Diana Huttner, Lily H-C Wang, Erich A Nigg, Tom Owen-Hughes, Ying Liu, Erwin Peterman, Gijs J L Wuite, Ian D Hickson. 2013. "PICH: A DNA Translocase Specially Adapted for Processing Anaphase Bridge DNA." *Molecular Cell* 51 (5): 691–701.

Bieling, Peter, Ivo A. Telley, and Thomas Surrey. 2010. "A Minimal Midzone Protein Module Controls Formation and Length of Antiparallel Microtubule Overlaps." *Cell* 142 (3): 420–32.

Bi, Erfei, and Hay-Oak Park. 2012. "Cell Polarization and Cytokinesis in Budding Yeast." *Genetics* 191 (2): 347–87.

Boettcher, Barbara, and Yves Barral. 2013. "The Cell Biology of Open and Closed Mitosis." *Nucleus* 4 (3): 160–65.

Branzei, Dana, and Barnabas Szakal. 2016. "DNA Damage Tolerance by Recombination: Molecular Pathways and DNA Structures." *DNA Repair* 44: 68–75.

Branzei, Dana, Fabio Vanoli, and Marco Foiani. 2008. "SUMOylation Regulates Rad18-Mediated Template Switch." *Nature* 456 (7224): 915-20.

Burgess, Rebecca C., Michael Lisby, Veronika Altmannova, Lumir Krejci, Patrick Sung, and Rodney Rothstein. 2009. "Localization of Recombination Proteins and Srs2 Reveals Anti-Recombinase Function in Vivo." *The Journal of Cell Biology* 185 (6): 969–81.

Burkard, Mark E., John Maciejowski, Verónica Rodríguez-Bravo, Michael Repka, Drew M. Lowery, Karl R. Clauser, Chao Zhang, Kevan M Shokat, Steven A. Carr, Michael B. Yaffe, and Prasad V. Jallepalli. 2009. "Plk1 Self-Organization and Priming

Phosphorylation of HsCYK-4 at the Spindle Midzone Regulate the Onset of Division in Human Cells.” *PLoS Biology* 7 (5): e1000111.

Burkovics, Peter, Lili Dome, Szilvia Juhasz, Veronika Altmannova, Marek Sebesta, Martin Pacesa, Kasper Fugger, Claus Storgaard Sorensen, Marietta Y. W. T. Lee, Lajos Haracska, Lumir Krejci. 2016. “The PCNA-Associated Protein PARI Negatively Regulates Homologous Recombination via the Inhibition of DNA Repair Synthesis.” *Nucleic Acids Research* 44 (7): 3176–89.

Caballe, Anna, Dawn M. Wenzel, Monica Agromayor, Steven L. Alam, Jack J. Skalicky, Magdalena Kloc, Jeremy G. Carlton, Leticia Labrador, Wesley I. Sundquist, and Juan Martin-Serrano. 2015. “ULK3 Regulates Cytokinetic Abcission by Phosphorylating ESCRT-III Proteins.” *eLife* 4: e06547.

Caldecott, Keith W. 2022. “DNA Single-Strand Break Repair and Human Genetic Disease.” *Trends in Cell Biology* 32 (9): 733–45.

Capalbo, Luisa, Ioanna Mela, Maria Alba Abad, A. Arockia Jeyaprakash, J. Michael Edwardson, and Pier Paolo D’Avino. 2016. “Coordinated Regulation of the ESCRT-III Component CHMP4C by the Chromosomal Passenger Complex and Centralspindlin during Cytokinesis.” *Open Biology* 6 (10): 160248.

Capalbo, Luisa, Emilie Montembault, Tetsuya Takeda, Zuni I. Bassi, David M. Glover, and Pier Paolo D’Avino. 2012. “The Chromosomal Passenger Complex Controls the Function of Endosomal Sorting Complex Required for Transport-III Snf7 Proteins during Cytokinesis.” *Open Biology* 2 (5): 120070.

Carlton, Jeremy G., Anna Caballe, Monica Agromayor, Magdalena Kloc, and Juan Martin-Serrano. 2012. “ESCRT-III Governs the Aurora B-Mediated Abcission Checkpoint through CHMP4C.” *Science* 336 (6078): 220–25.

Carlton, Jeremy G., Monica Agromayor, and Juan Martin-Serrano. 2008. “Differential Requirements for Alix and ESCRT-III in Cytokinesis and HIV-1 Release.” *Proceedings of the National Academy of Sciences* 105 (30): 10541–6.

Carlton, Jeremy G., and Juan Martin-Serrano. 2007. "Parallels Between Cytokinesis and Retroviral Budding: A Role for the ESCRT Machinery." *Science* 316 (5833): 1908–12.

Carmena, Mar, Michael Wheelock, Hironori Funabiki, and William C. Earnshaw. 2012. "The Chromosomal Passenger Complex (CPC): From Easy Rider to the Godfather of Mitosis." *Nature Reviews. Molecular Cell Biology* 13 (12): 789–803.

Carminati, J. L., and T. Stearns. 1997. "Microtubules Orient the Mitotic Spindle in Yeast through Dynein-Dependent Interactions with the Cell Cortex." *The Journal of Cell Biology* 138 (3): 629–41.

Chang, Chih-Jui, Sarah Goulding, William C. Earnshaw, and Mar Carmena. 2003. "RNAi Analysis Reveals an Unexpected Role for Topoisomerase II in Chromosome Arm Congression to a Metaphase Plate." *Journal of Cell Science* 116 (23): 4715–26.

Chan, Kok-Lung, Phillip S. North, and Ian D. Hickson. 2007. "BLM Is Required for Faithful Chromosome Segregation and Its Localization Defines a Class of Ultrafine Anaphase Bridges." *The EMBO Journal* 26 (14): 3397–3409.

Chan, Kok Lung, Timea Palmai-Pallag, Songmin Ying, and Ian D. Hickson. 2009. "Replication Stress Induces Sister-Chromatid Bridging at Fragile Site Loci in Mitosis." *Nature Cell Biology* 11 (6): 753–60.

Chan, Ying Wai, Kasper Fugger, and Stephen C. West. 2018. "Unresolved Recombination Intermediates Lead to Ultra-Fine Anaphase Bridges, Chromosome Breaks and Aberrations." *Nature Cell Biology* 20 (1): 92–103.

Cheffings, Thomas H., Nigel J. Burroughs, and Mohan K. Balasubramanian. 2016. "Actomyosin Ring Formation and Tension Generation in Eukaryotic Cytokinesis." *Current Biology* 26 (15): 719-37.

Chen, Natalie Y., Paul H. Kim, Yiping Tu, Ye Yang, Patrick J. Heizer, Stephen G. Young, and Loren G. Fong. 2021. "Increased Expression of LAP2 β Eliminates Nuclear Membrane Ruptures in Nuclear Lamin-Deficient Neurons and Fibroblasts." *Proceedings of the National Academy of Sciences of the United States of America* 118 (25): e2107770118.

Chin, Cheen Fei, Alexis M. Bennett, Wai Kit Ma, Mark C. Hall, and Foong May Yeong. 2012. "Dependence of Chs2 ER Export on Dephosphorylation by Cytoplasmic Cdc14 Ensures That Septum Formation Follows Mitosis." *Molecular Biology of the Cell* 23 (1): 45–58.

Choe, Katherine N., and George-Lucian Moldovan. 2017. "Forging Ahead through Darkness: PCNA, Still the Principal Conductor at the Replication Fork." *Molecular Cell* 65 (3): 380–92.

Christ, Liliane, Eva M. Wenzel, Knut Liestøl, Camilla Raiborg, Coen Campsteijn, and Harald Stenmark. 2016. "ALIX and ESCRT-I/II Function as Parallel ESCRT-III Recruiters in Cytokinetic Abscission." *The Journal of Cell Biology* 212 (5): 499–513.

Cimini, Daniela, and Francesca Degrossi. 2005. "Aneuploidy: A Matter of Bad Connections." *Trends in Cell Biology* 15 (8): 442–51.

Connell, James W., Catherine Lindon, J. Paul Luzio, and Evan Reid. 2009. "Spastin Couples Microtubule Severing to Membrane Traffic in Completion of Cytokinesis and Secretion." *Traffic* 10 (1): 42–56.

Dambournet, Daphné, Mickael Machicoane, Laurent Chesneau, Martin Sachse, Murielle Rocancourt, Ahmed El Marjou, Etienne Formstecher, Rémi Salomon, Bruno Goud, and Arnaud Echard. 2011. "Rab35 GTPase and OCRL Phosphatase Remodel Lipids and F-Actin for Successful Cytokinesis." *Nature Cell Biology* 13 (8): 981–88.

Dandoulaki, Maria, Eleni Petsalaki, David Sumpton, Sara Zanivan, and George Zachos. 2018. "Src Activation by Chk1 Promotes Actin Patch Formation and Prevents Chromatin Bridge Breakage in Cytokinesis." *The Journal of Cell Biology* 217 (9): 3071–89.

D'Avino, Pier Paolo. 2017. "Citron Kinase - Renaissance of a Neglected Mitotic Kinase." *Journal of Cell Science* 130 (10): 1701–8.

De Boer, L., V. Oakes, H. Beamish, N. Giles, F. Stevens, M. Somodevilla-Torres, C. Desouza, and B. Gabrielli. 2008. "Cyclin A/cdk2 Coordinates Centrosomal and Nuclear Mitotic Events." *Oncogene* 27 (31): 4261–68.

De Bont, Rinne, and Nik van Larebeke. 2004. "Endogenous DNA Damage in Humans: A Review of Quantitative Data." *Mutagenesis* 19 (3): 169–85.

Deiss, Katharina, Nicola Lockwood, Michael Howell, Hendrika Alida Segeren, Rebecca E. Saunders, Probir Chakravarty, Tanya N. Soliman, Silvia Martini, Nuno Rocha, Robert Semple, Lykourgos-Panagiotis Zalmas, Peter J Parker. 2019. "A Genome-Wide RNAi Screen Identifies the SMC5/6 Complex as a Non-Redundant Regulator of a Topo2a-Dependent G2 Arrest." *Nucleic Acids Research* 47 (6): 2906–21.

Deming, P. B., C. A. Cistulli, H. Zhao, P. R. Graves, H. Piwnica-Worms, R. S. Paules, C. S. Downes, and W. K. Kaufmann. 2001. "The Human Decatenation Checkpoint." *Proceedings of the National Academy of Sciences of the United States of America* 98 (21): 12044–49.

Dhingra, Nalini, Sahiti Kuppa, Lei Wei, Nilisha Pokhrel, Silva Baburyan, Xiangzhou Meng, Edwin Antony, and Xiaolan Zhao. 2021. "The Srs2 Helicase Dampens DNA Damage Checkpoint by Recycling RPA from Chromatin." *Proceedings of the National Academy of Sciences of the United States of America* 118 (8): e2020185118.

Ditchfield, Claire, Victoria L. Johnson, Anthony Tighe, Rebecca Ellston, Carolyn Haworth, Trevor Johnson, Andrew Mortlock, Nicholas Keen, and Stephen S. Taylor. 2003. "Aurora B Couples Chromosome Alignment with Anaphase by Targeting BubR1, Mad2, and Cenp-E to Kinetochores." *The Journal of Cell Biology* 161 (2): 267–80.

Dittrich, Christina M., Katja Kratz, Ataman Sendoel, Yosef Gruenbaum, Josef Jiricny, and Michael O. Hengartner. 2012. "LEM-3 - A LEM Domain Containing Nuclease Involved in the DNA Damage Response in *C. Elegans*." *PloS One* 7 (2): e24555.

Downes, C. Stephen, Duncan J. Clarke, Ann M. Mullinger, Juan F. Giménez-Abián, Andrew M. Creighton, and Robert T. Johnson. 1994. "A Topoisomerase II-Dependent G2 Cycle Checkpoint in Mammalian Cells." *Nature* 372 (6505): 467–70.

Echard, Arnaud. 2012. "Phosphoinositides and Cytokinesis: The 'PIP' of the Iceberg." *Cytoskeleton* 69 (11): 893–912.

Elia, Natalie, Rachid Sougrat, Tighe A. Spurlin, James H. Hurley, and Jennifer Lippincott-Schwartz. 2011. "Dynamics of Endosomal Sorting Complex Required for Transport (ESCRT) Machinery during Cytokinesis and Its Role in Abscission." *Proceedings of the National Academy of Sciences of the United States of America* 108 (12): 4846–51.

Emoto, Kazuo, Hironori Inadome, Yasunori Kanaho, Shuh Narumiya, and Masato Umeda. 2005. "Local Change in Phospholipid Composition at the Cleavage Furrow Is Essential for Completion of Cytokinesis." *The Journal of Biological Chemistry* 280 (45): 37901–7.

Fang, Xiaodong, Jianying Luo, Ryuichi Nishihama, Carsten Wloka, Christopher Dravis, Mirko Travaglia, Masayuki Iwase, Elizabeth A. Vallen, and Erfei Bi. 2010. "Biphasic Targeting and Cleavage Furrow Ingression Directed by the Tail of a Myosin II." *The Journal of Cell Biology* 191 (7): 1333–50.

Fededa, Juan Pablo, and Daniel W. Gerlich. 2012. "Molecular Control of Animal Cell Cytokinesis." *Nature Cell Biology* 14 (5): 440–47.

Finardi, Alice, Lucia F. Massari, and Rosella Visintin. 2020. "Anaphase Bridges: Not All Natural Fibers Are Healthy." *Genes* 11 (8): 902.

Foe, Victoria E., and George von Dassow. 2008. "Stable and Dynamic Microtubules Coordinately Shape the Myosin Activation Zone during Cytokinetic Furrow Formation." *Journal of Cell Biology* 183 (3): 457–70.

Forsburg, Susan L., and Paul Nurse. 1991. "Cell Cycle Regulation in the Yeasts *Saccharomyces Cerevisiae* and *Schizosaccharomyces Pombe*." *Annual Review of Cell Biology* 7: 227–56.

Frémont, Stéphane, and Arnaud Echard. 2018. "Membrane Traffic in the Late Steps of Cytokinesis." *Current Biology* 28 (8): R458–70.

Frémont, Stéphane, Hussein Hammich, Jian Bai, Hugo Wioland, Kerstin Klinkert, Murielle Rocancourt, Carlos Kikuti, David Stroebel, Guillaume Romet-Lemonne, Olena Pylypenko, Anne Houdusse and Arnaud Echard. 2017. "Oxidation of F-Actin Controls the Terminal Steps of Cytokinesis." *Nature Communications* 8: 14528.

Fugger, Kasper, Martin Mistrik, Jannie Rendtlew Danielsen, Christoffel Dinant, Jacob Falck, Jiri Bartek, Jiri Lukas, and Niels Mailand. 2009. "Human Fbh1 Helicase Contributes to Genome Maintenance via pro- and Anti-Recombinase Activities." *Journal of Cell Biology* 186 (5): 655–63

Fujimitsu, Kazuyuki, Margaret Grimaldi, and Hiroyuki Yamano. 2016. "Cyclin-Dependent Kinase 1-dependent Activation of APC/C Ubiquitin Ligase." *Science* 352 (6289): 1121–4.

Gai, Marta, Paola Camera, Alessandro Dema, Federico Bianchi, Gaia Berto, Elena Scarpa, Giulia Germena, and Ferdinando Di Cunto. 2011. "Citron Kinase Controls Abscission through RhoA and Anillin." *Molecular Biology of the Cell* 22 (20): 3768–78.

Gavet, Olivier, and Jonathon Pines. 2010. "Activation of Cyclin B1-Cdk1 Synchronizes Events in the Nucleus and the Cytoplasm at Mitosis." *The Journal of Cell Biology* 189 (2): 247–59.

Germann, Susanne M., Vera Schramke, Rune Troelsgaard Pedersen, Irene Gallina, Nadine Eckert-Boulet, Vibe H. Oestergaard, and Michael Lisby. 2014. "TopBP1/Dpb11 Binds DNA Anaphase Bridges to Prevent Genome Instability." *The Journal of Cell Biology* 204 (1): 45–59.

Gisselsson, David, Louise Pettersson, Matthias Höglund, Markus Heidenblad, Ludmila Gorunova, Joop Wiegant, Frederik Mertens, Paola Dal Cin, Felix Mitelman, and Nils Mandahl. 2000. "Chromosomal Breakage-Fusion-Bridge Events Cause Genetic Intratumor Heterogeneity." *Proceedings of the National Academy of Sciences of the United States of America* 97 (10): 5357–62.

Gramont, Armand de, and Orna Cohen-Fix. 2005. "The Many Phases of Anaphase." *Trends in Biochemical Sciences* 30 (10): 559–68.

Guizetti, Julien, Lothar Schermelleh, Jana Mäntler, Sandra Maar, Ina Poser, Heinrich Leonhardt, Thomas Müller-Reichert, and Daniel W. Gerlich. 2011. "Cortical Constriction during Abscission Involves Helices of ESCRT-III-Dependent Filaments." *Science* 331 (6024): 1616–20.

Guse, Annika, Masanori Mishima, and Michael Glotzer. 2005. "Phosphorylation of ZEN-4/MKLP1 by Aurora B Regulates Completion of Cytokinesis." *Current Biology* 15 (8): 778–86.

Harrigan, Jeanine A., Rimma Belotserkovskaya, Julia Coates, Daniela S. Dimitrova, Sophie E. Polo, Charles R. Bradshaw, Peter Fraser, and Stephen P. Jackson. 2011. "Replication Stress Induces 53BP1-Containing OPT Domains in G1 Cells." *The Journal of Cell Biology* 193 (1): 97–108.

Hartwell, Leland H., and Ted A. Weinert. 1989. "Checkpoints: Controls That Ensure the Order of Cell Cycle Events." *Science* 246 (4930): 629–34.

Hengeveld, Rutger C. C., H. Rudolf de Boer, Pepijn M. Schoonen, Elisabeth G. E. de Vries, Susanne M. A. Lens, and Marcel A. T. M. van Vugt. 2015. "Rif1 Is Required for Resolution of Ultrafine DNA Bridges in Anaphase to Ensure Genomic Stability." *Developmental Cell* 34 (4): 466–74.

Heude, Martine, Roland Chanet, and Francis Fabre. 1995. "Regulation of the *Saccharomyces Cerevisiae* Srs2 Helicase during the Mitotic Cell Cycle, Meiosis and after Irradiation." *Molecular & General Genetics* 248 (1): 59–68.

Hirano, Tatsuya, and Timothy J. Mitchison. 1993. "Topoisomerase II Does Not Play a Scaffolding Role in the Organization of Mitotic Chromosomes Assembled in *Xenopus* Egg Extracts." *Journal of Cell Biology* 120 (3): 601–12.

Holm, Connie, Tadaatsu Goto, James C. Wang, and David Botstein. 1985. "DNA Topoisomerase II Is Required at the Time of Mitosis in Yeast." *Cell* 41 (2): 553–63.

Hong, Ye, Remi Sonnevile, Bin Wang, Viktor Scheidt, Bettina Meier, Alexander Woglar, Sarah Demetriou, Karim Labib, Verena Jantsch, and Anton Gartner. 2018. "LEM-3 Is a Midbody-Tethered DNA Nuclease That Resolves Chromatin Bridges during Late Mitosis." *Nature Communications* 9 (1): 728.

Hu, Chi-Kuo, Margaret Coughlin, and Timothy J. Mitchison. 2012. "Midbody Assembly and Its Regulation during Cytokinesis." *Molecular Biology of the Cell* 23 (6): 1024–34.

Hümmer, Stefan, and Thomas U. Mayer. 2009. "Cdk1 Negatively Regulates Midzone Localization of the Mitotic Kinesin Mklp2 and the Chromosomal Passenger Complex." *Current Biology: CB* 19 (7): 607–12.

Hu, Yiduo, Steven Raynard, Michael G. Sehorn, Xincheng Lu, Wendy Bussen, Lu Zheng, Jeremy M. Stark, Ellen L. Barnes, Peter Chi, Pavel Janscak, Maria Jasin, Hannes Vogel, Patrick Sung, Guangbin Luo. 2007. "RECQL5/Recql5 Helicase Regulates Homologous Recombination and Suppresses Tumor Formation via Disruption of Rad51 Presynaptic Filaments." *Genes & Development* 21 (23): 3073–84.

Ivanova, Tsvetomira, Michael Maier, Alsu Missarova, Céline Ziegler-Birling, Monica Dam, Mercè Gomar-Alba, Lucas B. Carey, and Manuel Mendoza. 2020. "Budding Yeast Complete DNA Synthesis after Chromosome Segregation Begins." *Nature Communications* 11 (1): 2267.

Janke, Carsten, Maria M. Magiera, Nicole Rathfelder, Christof Taxis, Simone Reber, Hiromi Maekawa, Alexandra Moreno-Borchart, Georg Doenges, Etienne Schwob, Elmar Schiebel, Michael Knop. 2004. "A Versatile Toolbox for PCR-Based Tagging of Yeast Genes: New Fluorescent Proteins, More Markers and Promoter Substitution Cassettes." *Yeast* 21 (11): 947–62.

Janssen, Aniek, Marja van der Burg, Karoly Szuhai, Geert J. P. L. Kops, and René H. Medema. 2011. "Chromosome Segregation Errors as a Cause of DNA Damage and Structural Chromosome Aberrations." *Science* 333 (6051): 1895–98.

Jensen, Lars H., Karin C. Nitiss, Angela Rose, Jiaowang Dong, Junfang Zhou, Tao Hu, Neil Osheroff, Peter B. Jensen, Maxwell Sehested, and John L. Nitiss. 2000. "A Novel Mechanism of Cell Killing by Anti-Topoisomerase II Bisdioxopiperazines." *Journal of Biological Chemistry* 275 (3): 2137–46.

Jentsch, Stefan, John P. McGrath, and Alexander Varshavsky. 1987. "The Yeast DNA Repair Gene RAD6 Encodes a Ubiquitin-Conjugating Enzyme." *Nature* 329 (6135): 131–34.

Johnson, Catherine, Vamsi K. Gali, Tatsuro S. Takahashi, and Takashi Kubota. 2016. "PCNA Retention on DNA into G2/M Phase Causes Genome Instability in Cells Lacking Elg1." *Cell Reports* 16 (3): 684–95.

Joukov, Vladimir, and Arcangela De Nicolo. 2018. "Aurora-PLK1 Cascades as Key Signaling Modules in the Regulation of Mitosis." *Science Signaling* 11 (543): eaar4195.

Kabeche, Lilian, Hai Dang Nguyen, Rémi Buisson, and Lee Zou. 2018. "A Mitosis-Specific and R Loop-Driven ATR Pathway Promotes Faithful Chromosome Segregation." *Science* 359 (6371): 108–14.

Kallio, Marko J., Mark L. McClelland, P. Todd Stukenberg, and Gary J. Gorbsky. 2002. "Inhibition of Aurora B Kinase Blocks Chromosome Segregation, Overrides the

Spindle Checkpoint, and Perturbs Microtubule Dynamics in Mitosis.” *Current Biology: CB* 12 (11): 900–905.

Kaulich, Manuel, Fabien Cubizolles, and Erich A. Nigg. 2012. “On the Regulation, Function, and Localization of the DNA-Dependent ATPase PICH.” *Chromosoma* 121 (4): 395–408.

Kouranti, Ilektra, Martin Sachse, Nassim Arouche, Bruno Goud, and Arnaud Echard. 2006. “Rab35 Regulates an Endocytic Recycling Pathway Essential for the Terminal Steps of Cytokinesis.” *Current Biology* 16 (17): 1719–25.

Krejci, Lumir, Stephen Van Komen, Ying Li, Jana Villemain, Mothe Sreedhar Reddy, Hannah Klein, Thomas Ellenberger, and Patrick Sung. 2003. “DNA Helicase Srs2 Disrupts the Rad51 Presynaptic Filament.” *Nature* 423 (6937): 305–9.

Kubota, Takashi, Kohei Nishimura, Masato T. Kanemaki, and Anne D. Donaldson. 2013. “The Elg1 Replication Factor C-like Complex Functions in PCNA Unloading during DNA Replication.” *Molecular Cell* 50 (2): 273–80.

Lawrence, C. W., and R. B. Christensen. 1979. “Metabolic Suppressors of Trimethoprim and Ultraviolet Light Sensitivities of *Saccharomyces Cerevisiae* rad6 Mutants.” *Journal of Bacteriology* 139 (3): 866–76.

Lenormand, Cédric, Coralie Spiegelhalter, Bertrand Cinquin, Sabine Bardin, Huguette Bausinger, Catherine Angénieux, Anita Eckly, Fabienne Proamer, David Wall, Ben Lich, Sylvie Tourne, Daniel Hanau, Yannick Schwab, Jean Salamero, Henri de la Salle. 2013. “Birbeck Granule-like ‘Organized Smooth Endoplasmic Reticulum’ Resulting from the Expression of a Cytoplasmic YFP-Tagged Langerin.” *PloS One* 8 (4): e60813.

León Ortiz, Ana María, Robert J. D. Reid, John C. Dittmar, Rodney Rothstein, and Alain Nicolas. 2011. “Srs2 Overexpression Reveals a Helicase-Independent Role at Replication Forks That Requires Diverse Cell Functions.” *DNA Repair* 10 (5): 506–17.

Lesage, Guillaume, and Howard Bussey. 2006. "Cell Wall Assembly in *Saccharomyces Cerevisiae*." *Microbiology and Molecular Biology Reviews* 70 (2): 317–43.

Liberi, Giordano, Irene Chiolo, Achille Pellicoli, Massimo Lopes, Paolo Plevani, Marco Muzi-Falconi, and Marco Foiani. 2000. "Srs2 DNA Helicase Is Involved in Checkpoint Response and Its Regulation Requires a Functional Mec1-Dependent Pathway and Cdk1 Activity." *The EMBO Journal* 19 (18): 5027–38.

Lippincott, John, Katie B. Shannon, Wenying Shou, Raymond J. Deshaies, and Rong Li. 2001. "The Tem1 Small GTPase Controls Actomyosin and Septin Dynamics during Cytokinesis." *Journal of Cell Science* 114 (7): 1379–86.

Liu, Jie, Christopher Ede, William D. Wright, Steven K. Gore, Shirin S. Jenkins, Bret D. Freudenthal, M. Todd Washington, Xavier Veaute, and Wolf-Dietrich Heyer. 2017. "Srs2 Promotes Synthesis-Dependent Strand Annealing by Disrupting DNA Polymerase δ -Extending D-Loops." *eLife* 6: e22195.

Liu, Ying, Christian F. Nielsen, Qi Yao, and Ian D. Hickson. 2014. "The Origins and Processing of Ultra Fine Anaphase DNA Bridges." *Current Opinion in Genetics & Development* 26 (June): 1–5.

Lolli, Graziano, and Louise N. Johnson. 2005. "CAK-Cyclin-Dependent Activating Kinase: A Key Kinase in Cell Cycle Control and a Target for Drugs?" *Cell Cycle* 4 (4): 572–77.

Lossaint, Gerald, Emilie Besnard, Daniel Fisher, Jacques Piette, and Vjekoslav Dulić. 2011. "Chk1 Is Dispensable for G2 Arrest in Response to Sustained DNA Damage When the ATM/p53/p21 Pathway Is Functional." *Oncogene* 30 (41): 4261–74.

Luo, Kuntian, Jian Yuan, Junjie Chen, and Zhenkun Lou. 2009. "Topoisomerase II α Controls the Decatenation Checkpoint." *Nature Cell Biology* 11 (2): 204–10.

Maciejowski, John, Yilong Li, Nazario Bosco, Peter J. Campbell, and Titia de Lange. 2015. "Chromothripsis and Kataegis Induced by Telomere Crisis." *Cell* 163 (7): 1641–54.

Mackay, Douglas R., Masaki Makise, and Katharine S. Ullman. 2010. "Defects in Nuclear Pore Assembly Lead to Activation of an Aurora B-Mediated Abscission Checkpoint." *The Journal of Cell Biology* 191 (5): 923–31.

Mackay, Douglas R., and Katharine S. Ullman. 2015. "ATR and a Chk1-Aurora B Pathway Coordinate Postmitotic Genome Surveillance with Cytokinetic Abscission." *Molecular Biology of the Cell* 26 (12): 2217–26.

Ma, Hoi Tang, and Randy Y. C. Poon. 2011. "Synchronization of HeLa Cells." *Methods in Molecular Biology* 761: 151–61.

Mankouri, Hocine W., Diana Huttner, and Ian D. Hickson. 2013. "How Unfinished Business from S-Phase Affects Mitosis and beyond." *The EMBO Journal* 32 (20): 2661–71.

Marini, Victoria, and Lumir Krejci. 2010. "Srs2: The 'Odd-Job Man' in DNA Repair." *DNA Repair* 9 (3): 268–75.

Masgrau, Aina, Andrea Battola, Trinidad Sanmartin, Leszek P. Pryszcz, Toni Gabaldón, and Manuel Mendoza. 2017. "Distinct Roles of the Polarity Factors Boi1 and Boi2 in the Control of Exocytosis and Abscission in Budding Yeast." *Molecular Biology of the Cell* 28 (22): 3082–94.

Matsumura, Fumio. 2005. "Regulation of Myosin II during Cytokinesis in Higher Eukaryotes." *Trends in Cell Biology* 15 (7): 371–77.

Matthews, Helen K., Cosetta Bertoli, and Robertus A. M. de Bruin. 2022. "Cell Cycle Control in Cancer." *Nature Reviews Molecular Cell Biology* 23 (1): 74–88.

McClintock, B. 1939. "The Behavior in Successive Nuclear Divisions of a Chromosome Broken at Meiosis." *Proceedings of the National Academy of Sciences of the United States of America* 25 (8): 405–16.

McClintock, B. 1941. "The Association of Mutants with Homozygous Deficiencies in *Zea Mays*." *Genetics* 26 (5): 542–71.

McCullough, John, Robert D. Fisher, Frank G. Whitby, Wesley I. Sundquist, and Christopher P. Hill. 2008. "ALIX-CHMP4 Interactions in the Human ESCRT Pathway." *Proceedings of the National Academy of Sciences of the United States of America* 105 (22): 7687–91.

Mendoza, Manuel, Caren Norden, Kathrin Durrer, Harald Rauter, Frank Uhlmann, and Yves Barral. 2009. "A Mechanism for Chromosome Segregation Sensing by the NoCut Checkpoint." *Nature Cell Biology* 11 (4): 477–83.

Merigliano, Chiara, Romina Burla, Mattia La Torre, Simona Del Giudice, Hsiangling Teo, Chong Wai Liew, Alexandre Chojnowski, Wah Ing Goh, Yolanda Olmos, Klizia Maccaroni, Maria Giubettini, Irene Chiolo, Jeremy G. Carlton, Domenico Raimondo, Fiammetta Verni, Colin L. Stewart, Daniela Rhodes, Graham D. Wright, Brian E. Burke and Isabella Saggio. 2021. "AKTIP Interacts with ESCRT I and Is Needed for the Recruitment of ESCRT III Subunits to the Midbody." *PLoS Genetics* 17 (8): e1009757.

Mierzwa, Beata E., Nicolas Chiaruttini, Lorena Redondo-Morata, Joachim Moser von Filseck, Julia König, Jorge Larios, Ina Poser, Thomas Müller-Reichert, Simon Scheuring, Aurélien Roux, Daniel W. Gerlich. 2017. "Dynamic Subunit Turnover in ESCRT-III Assemblies Is Regulated by Vps4 to Mediate Membrane Remodelling during Cytokinesis." *Nature Cell Biology* 19 (7): 787–98.

Mierzwa, Beata, and Daniel W. Gerlich. 2014. "Cytokinetic Abscission: Molecular Mechanisms and Temporal Control." *Developmental Cell* 31 (5): 525–38.

Mishima, Masanori, Visnja Pavicic, Ulrike Grüneberg, Erich A. Nigg, and Michael Glotzer. 2004. "Cell Cycle Regulation of Central Spindle Assembly." *Nature* 430 (7002): 908–13.

Miura, Tohru, Takehiko Shibata, and Kohji Kusano. 2013. "Putative Antirecombinase Srs2 DNA Helicase Promotes Noncrossover Homologous Recombination Avoiding Loss of Heterozygosity." *Proceedings of the National Academy of Sciences of the United States of America* 110 (40): 16067–72.

Miura, Tohru, Yoshimasa Yamana, Takehiko Usui, Hiroaki I. Ogawa, Masa-Toshi Yamamoto, and Kohji Kusano. 2012. "Homologous Recombination via Synthesis-Dependent Strand Annealing in Yeast Requires the Irc20 and Srs2 DNA Helicases." *Genetics* 191 (1): 65–78.

Mochizuki, Ayako L., Ami Katanaya, Eri Hayashi, Mihoko Hosokawa, Emiko Moribe, Akira Motegi, Masamichi Ishiai, Minoru Takata, Gen Kondoh, Hitomi Watanabe, Norio Nakatsuji, Shinichiro Chuma. 2017. "PARI Regulates Stalled Replication Fork Processing To Maintain Genome Stability upon Replication Stress in Mice." *Molecular and Cellular Biology* 37 (23): e00117-17.

Moldovan, George-Lucian, Donniphat Dejsuphong, Mark I. R. Petalcorin, Kay Hofmann, Shunichi Takeda, Simon J. Boulton, and Alan D. D'Andrea. 2012. "Inhibition of Homologous Recombination by the PCNA-Interacting Protein PARI." *Molecular Cell* 45 (1): 75–86.

Moldovan, George-Lucian, Boris Pfander, and Stefan Jentsch. 2007. "PCNA, the Maestro of the Replication Fork." *Cell* 129 (4): 665–79.

Montecucco, Alessandra, Francesca Zanetta, and Giuseppe Biamonti. 2015. "Molecular Mechanisms of Etoposide." *EXCLI Journal* 14 (January): 95–108.

Moreno, Alberto, Jamie T. Carrington, Luca Albergante, Mohammed Al Mamun, Emma J. Haagenen, Eirini-Stavroula Komseli, Vassilis G. Gorgoulis, Timothy J. Newman, and J. Julian Blow. 2016. "Unreplicated DNA Remaining from Unperturbed

S Phases Passes through Mitosis for Resolution in Daughter Cells.” Proceedings of the National Academy of Sciences of the United States of America 113 (39): e5757–64.

Morgan, David Owen. 2007. *The Cell Cycle: Principles of Control*. New Science Press.
Musacchio, Andrea, and Edward D. Salmon. 2007. “The Spindle-Assembly Checkpoint in Space and Time.” *Nature Reviews. Molecular Cell Biology* 8 (5): 379–93.

Narasimha, Anil M., Manuel Kaulich, Gary S. Shapiro, Yoon J. Choi, Piotr Sicinski, and Steven F. Dowdy. 2014. “Cyclin D Activates the Rb Tumor Suppressor by Mono-Phosphorylation.” *eLife* 3: e02872.

Neef, Rüdiger, Ulf R. Klein, Robert Kopajtich, and Francis A. Barr. 2006. “Cooperation between Mitotic Kinesins Controls the Late Stages of Cytokinesis.” *Current Biology* 16 (3): 301–7.

Nicholson, Joshua M., and Daniela Cimini. 2011. “How Mitotic Errors Contribute to Karyotypic Diversity in Cancer.” *Advances in Cancer Research* 112: 43–75.

Nicolae, Claudia M., Michael J. O’Connor, Emily M. Schleicher, Chunhua Song, Raghavendra Gowda, Gavin Robertson, Sinisa Dovat, and George-Lucian Moldovan. 2019. “PARI (PARPBP) Suppresses Replication Stress-Induced Myeloid Differentiation in Leukemia Cells.” *Oncogene* 38 (27): 5530–40.

Nielsen, Christian F., Diana Huttner, Anna H. Bizard, Seiki Hirano, Tian-Neng Li, Timea Palmai-Pallag, Victoria A. Bjerregaard, Ying Liu, Erich A. Nigg, Lily Hui-Ching Wang, Ian D. Hickson. 2015. “PICH Promotes Sister Chromatid Disjunction and Co-Operates with Topoisomerase II in Mitosis.” *Nature Communications* 6 (December): 8962.

Nielsen, Christian F., Tao Zhang, Marin Barisic, Paul Kalitsis, and Damien F. Hudson. 2020. “Topoisomerase II α Is Essential for Maintenance of Mitotic Chromosome

Structure.” Proceedings of the National Academy of Sciences of the United States of America 117 (22): 12131–42.

Nigg, Erich A. 2001. “Mitotic Kinases as Regulators of Cell Division and Its Checkpoints.” Nature Reviews. Molecular Cell Biology 2 (1): 21–32.

Nishihama, Ryuichi, Jennifer H. Schreiter, Masayuki Onishi, Elizabeth A. Vallen, Julia Hanna, Katarina Moravcevic, Margaret F. Lippincott, Haesun Han, Mark A Lemmon, John R Pringle, Erfei Bi. 2009. “Role of Inn1 and Its Interactions with Hof1 and Cyk3 in Promoting Cleavage Furrow and Septum Formation in *S. Cerevisiae*.” The Journal of Cell Biology 185 (6): 995–1012.

Nitiss, John L. 2009. “Targeting DNA Topoisomerase II in Cancer Chemotherapy.” Nature Reviews. Cancer 9 (5): 338–50.

Norden, Caren, Manuel Mendoza, Jeroen Dobbelaere, Chitra V. Kotwaliwale, Sue Biggins, and Yves Barral. 2006. “The NoCut Pathway Links Completion of Cytokinesis to Spindle Midzone Function to Prevent Chromosome Breakage.” Cell 125 (1): 85–98.

Nunes Bastos, Ricardo, Sapan R. Gandhi, Ryan D. Baron, Ulrike Gruneberg, Erich A. Nigg, and Francis A. Barr. 2013. “Aurora B Suppresses Microtubule Dynamics and Limits Central Spindle Size by Locally Activating KIF4A.” The Journal of Cell Biology 202 (4): 605–21.

O’Connor, Kevin W., Donniphat Dejsuphong, Eunmi Park, Claudia M. Nicolae, Alec C. Kimmelman, Alan D. D’Andrea, and George-Lucian Moldovan. 2013. “PARI Overexpression Promotes Genomic Instability and Pancreatic Tumorigenesis.” Cancer Research 73 (8): 2529–39.

Oliferenko, Snezhana, Ting Gang Chew, and Mohan K. Balasubramanian. 2009. “Positioning Cytokinesis.” Genes & Development 23 (6): 660–74.

Onishi, Masayuki, Nolan Ko, Ryuichi Nishihama, and John R. Pringle. 2013. "Distinct Roles of Rho1, Cdc42, and Cyk3 in Septum Formation and Abscission during Yeast Cytokinesis." *The Journal of Cell Biology* 202 (2): 311–29.

Pampalona, J., D. Soler, A. Genescà, and L. Tusell. 2010. "Telomere Dysfunction and Chromosome Structure Modulate the Contribution of Individual Chromosomes in Abnormal Nuclear Morphologies." *Mutation Research* 683 (1-2): 16–22.

Papouli, Efterpi, Shuhua Chen, Adelina A. Davies, Diana Huttner, Lumir Krejci, Patrick Sung, and Helle D. Ulrich. 2005. "Crosstalk between SUMO and Ubiquitin on PCNA Is Mediated by Recruitment of the Helicase Srs2p." *Molecular Cell* 19 (1): 123–33.

Park, Iha, and Hava Karsenty Avraham. 2006. "Cell Cycle-Dependent DNA Damage Signaling Induced by ICRF-193 Involves ATM, ATR, CHK2, and BRCA1." *Experimental Cell Research* 312 (11): 1996–2008.

Parnas, Oren, Adi Zipin-Roitman, Boris Pfander, Batia Liefshitz, Yuval Mazor, Shay Ben-Aroya, Stefan Jentsch, and Martin Kupiec. 2010. "Elg1, an Alternative Subunit of the RFC Clamp Loader, Preferentially Interacts with SUMOylated PCNA." *The EMBO Journal* 29 (15): 2611–22.

Pastor, Nuria, Inmaculada Domínguez, Santiago Mateos, and Felipe Cortés. 2002. "A Comparative Study of Genotoxic Effects of Anti-Topoisomerase II Drugs ICRF-193 and Bufalin in Chinese Hamster Ovary Cells." *Mutation Research/Genetic Toxicology and Environmental Mutagenesis* 515 (1-2): 171–80.

Peddibhotla, Sirisha, Michael H. Lam, Maria Gonzalez-Rimbau, and Jeffrey M. Rosen. 2009. "The DNA-Damage Effector Checkpoint Kinase 1 Is Essential for Chromosome Segregation and Cytokinesis." *Proceedings of the National Academy of Sciences of the United States of America* 106 (13): 5159–64.

Peters, Jan-Michael, Antonio Tedeschi, and Julia Schmitz. 2008. "The Cohesin Complex and Its Roles in Chromosome Biology." *Genes & Development* 22 (22): 3089–114.

Petronczki, Mark, Michael Glotzer, Norbert Kraut, and Jan-Michael Peters. 2007. "Polo-like Kinase 1 Triggers the Initiation of Cytokinesis in Human Cells by Promoting Recruitment of the RhoGEF Ect2 to the Central Spindle." *Developmental Cell* 12 (5): 713–25.

Petsalaki, Eleni, Tonia Akoumianaki, Elizabeth J. Black, David A. F. Gillespie, and George Zachos. 2011. "Phosphorylation at Serine 331 Is Required for Aurora B Activation." *The Journal of Cell Biology* 195 (3): 449–66.

Petsalaki, Eleni, and George Zachos. 2016. "Clks 1, 2 and 4 Prevent Chromatin Breakage by Regulating the Aurora B-Dependent Abscission Checkpoint." *Nature Communications* 7: 11451.

Petsalaki, Eleni, and George Zachos. 2021a. "An ATM-Chk2-INCENP Pathway Activates the Abscission Checkpoint." *The Journal of Cell Biology* 220 (2): e202008029.

Petsalaki, Eleni, and George Zachos. 2021b. "The Abscission Checkpoint: A Guardian of Chromosomal Stability." *Cells* 10 (12): 3350.

Pfander, Boris, George-Lucian Moldovan, Meik Sacher, Carsten Hoege, and Stefan Jentsch. 2005. "SUMO-Modified PCNA Recruits Srs2 to Prevent Recombination during S Phase." *Nature* 436 (7049): 428–33.

Piao, Lianhua, Hidewaki Nakagawa, Koji Ueda, Suyoun Chung, Kotoe Kashiwaya, Hidetoshi Eguchi, Hiroaki Ohigashi, Osamu Ishikawa, Yataro Daigo, Koichi Matsuda, Yusuke Nakamura. 2011. "C12orf48, Termed PARP-1 Binding Protein, Enhances poly(ADP-Ribose) Polymerase-1 (PARP-1) Activity and Protects Pancreatic Cancer Cells from DNA Damage." *Genes, Chromosomes & Cancer* 50 (1): 13–24.

Pigula, Adrienne, David G. Drubin, and Georjana Barnes. 2014. "Regulation of Mitotic Spindle Disassembly by an Environmental Stress-Sensing Pathway in Budding Yeast." *Genetics* 198 (3): 1043–57.

Piskadlo, Ewa, Alexandra Tavares, and Raquel A. Oliveira. 2017. "Metaphase Chromosome Structure Is Dynamically Maintained by Condensin I-Directed DNA (de)catenation." *eLife* 6 (May). <https://doi.org/10.7554/eLife.26120>.

Prakash, Rohit, Yu Zhang, Weiran Feng, and Maria Jasin. 2015. "Homologous Recombination and Human Health: The Roles of BRCA1, BRCA2, and Associated Proteins." *Cold Spring Harbor Perspectives in Biology* 7 (4): a016600.

Renvoisé, Benoît, Rell L. Parker, Dong Yang, Joanna C. Bakowska, James H. Hurley, and Craig Blackstone. 2010. "SPG20 Protein Spartin Is Recruited to Midbodies by ESCRT-III Protein Ist1 and Participates in Cytokinesis." *Molecular Biology of the Cell* 21 (19): 3293–3303.

Rong, Lei, and Hannah L. Klein. 1993. "Purification and Characterization of the SRS2 DNA Helicase of the Yeast *Saccharomyces Cerevisiae*." *The Journal of Biological Chemistry* 268 (2): 1252–59.

Sadler, Jessica B. A., Dawn M. Wenzel, Lauren K. Strohacker, Marta Guindo-Martínez, Steven L. Alam, Josep M. Mercader, David Torrents, Katharine S. Ullman, Wesley I. Sundquist, and Juan Martin-Serrano. 2018. "A Cancer-Associated Polymorphism in ESCRT-III Disrupts the Abscission Checkpoint and Promotes Genome Instability." *Proceedings of the National Academy of Sciences of the United States of America* 115 (38): e8900–8908.

Sagona, Antonia P., Ioannis P. Nezis, Nina Marie Pedersen, Knut Liestøl, John Poulton, Tor Erik Rusten, Rolf I. Skotheim, Camilla Raiborg, and Harald Stenmark. 2010. "PtdIns(3)P Controls Cytokinesis through KIF13A-Mediated Recruitment of FYVE-CENT to the Midbody." *Nature Cell Biology* 12 (4) 362–71.

Samwer, Matthias, Maximilian W. G. Schneider, Rudolf Hoefler, Philipp S. Schmalhorst, Julian G. Jude, Johannes Zuber, and Daniel W. Gerlich. 2017. "DNA Cross-Bridging Shapes a Single Nucleus from a Set of Mitotic Chromosomes." *Cell* 170 (5): 956–72.e23.

Sanchez-Diaz, Alberto, Vanessa Marchesi, Stephen Murray, Richard Jones, Gislene Pereira, Ricky Edmondson, Terry Allen, and Karim Labib. 2008. "Inn1 Couples Contraction of the Actomyosin Ring to Membrane Ingression during Cytokinesis in Budding Yeast." *Nature Cell Biology* 10 (4): 395–406.

Sanchez, Yolanda, Calvin Wong, Richard S. Thoma, Ron Richman, Zhiqi Wu, Helen Piwnicka-Worms, and Stephen J. Elledge. 1997. "Conservation of the Chk1 Checkpoint Pathway in Mammals: Linkage of DNA Damage to Cdk Regulation through Cdc25." *Science* 277 (5331): 1497–1501.

Saponaro, Marco, Devon Callahan, Xiuzhong Zheng, Lumir Krejci, James E. Haber, Hannah L. Klein, and Giordano Liberi. 2010. "Cdk1 Targets Srs2 to Complete Synthesis-Dependent Strand Annealing and to Promote Recombinational Repair." *PLoS Genetics* 6 (2): e1000858.

Sasanuma, Hiroyuki, Hana Subhan M. Sakurai, Yuko Furihata, Kiran Challa, Lira Palmer, Susan M. Gasser, Miki Shinohara, and Akira Shinohara. 2019. "Srs2 Helicase Prevents the Formation of Toxic DNA Damage during Late Prophase I of Yeast Meiosis." *Chromosoma* 128 (3): 453–71.

Saurin, Adrian T., Joanne Durgan, Angus J. Cameron, Amir Faisal, Michael S. Marber, and Peter J. Parker. 2008. "The Regulated Assembly of a PKCepsilon Complex Controls the Completion of Cytokinesis." *Nature Cell Biology* 10 (8): 891–901.

Segal, Marisa, and Kerry Bloom. 2001. "Control of Spindle Polarity and Orientation in *Saccharomyces Cerevisiae*." *Trends in Cell Biology* 11 (4): 160–66.

Shorrocks, Ann-Marie K., Samuel E. Jones, Kaima Tsukada, Carl A. Morrow, Zoulikha Belblidia, Johanna Shen, Iolanda Vendrell, Roman Fischer, Benedikt M. Kessler, and Andrew N. Blackford. 2021. "The Bloom Syndrome Complex Senses RPA-Coated Single-Stranded DNA to Restart Stalled Replication Forks." *Nature Communications* 12 (1): 585.

Singh, Amanpreet, and Yong-Jie Xu. 2016. "The Cell Killing Mechanisms of Hydroxyurea." *Genes* 7 (11): 99.

Skoufias, Dimitrios A., Françoise B. Lacroix, Paul R. Andreassen, Leslie Wilson, and Robert L. Margolis. 2004. "Inhibition of DNA Decatenation, but Not DNA Damage, Arrests Cells at Metaphase." *Molecular Cell* 15 (6): 977–90.

Slaughter, Brian D., Sarah E. Smith, and Rong Li. 2009. "Symmetry Breaking in the Life Cycle of the Budding Yeast." *Cold Spring Harbor Perspectives in Biology* 1 (3): a003384.

Song, Junfang, Alasdair D. J. Freeman, Axel Knebel, Anton Gartner, and David M. J. Lilley. 2020. "Human ANKLE1 Is a Nuclease Specific for Branched DNA." *Journal of Molecular Biology* 432 (21): 5825–34.

Spiegelhalter, Coralie, Valérie Tosch, Didier Hentsch, Marc Koch, Pascal Kessler, Yannick Schwab, and Jocelyn Laporte. 2010. "From Dynamic Live Cell Imaging to 3D Ultrastructure: Novel Integrated Methods for High Pressure Freezing and Correlative Light-Electron Microscopy." *PloS One* 5 (2): e9014.

Steigemann, Patrick, and Daniel W. Gerlich. 2009. "Cytokinetic Abscission: Cellular Dynamics at the Midbody." *Trends in Cell Biology* 19 (11): 606–16.

Steigemann, Patrick, Claudia Wurzenberger, Michael H. A. Schmitz, Michael Held, Julien Guizetti, Sandra Maar, and Daniel W. Gerlich. 2009. "Aurora B-Mediated Abscission Checkpoint Protects against Tetraploidization." *Cell* 136 (3): 473–84.

Stephens, Philip J., Chris D. Greenman, Beiyuan Fu, Fengtang Yang, Graham R. Bignell, Laura J. Mudie, Erin D. Pleasance, King Wai Lau, David Beare, Lucy A. Stebbings, Stuart McLaren, Meng-Lay Lin, David J. McBride, Ignacio Varela, Serena Nik-Zainal, Catherine Leroy, Mingming Jia, Andrew Menzies, Adam P. Butler, Jon W. Teague, Michael A. Quail, John Burton, Harold Swerdlow, Nigel P. Carter, Laura A. Morsberger, Christine Iacobuzio-Donahue, George A. Follows, Anthony R. Green, Adrienne M. Flanagan, Michael R. Stratton, P. Andrew Futreal, Peter J. Campbell.

2011. “Massive Genomic Rearrangement Acquired in a Single Catastrophic Event during Cancer Development.” *Cell* 144 (1): 27–40.

Straight, Aaron F., Wallace F. Marshall, John W. Sedat, and Andrew W. Murray. 1997. “Mitosis in Living Budding Yeast: Anaphase A but No Metaphase Plate.” *Science* 277 (5325): 574–78.

Strohacker, Lauren K., Douglas R. Mackay, Madeline A. Whitney, Genevieve C. Couldwell, Wesley I. Sundquist, and Katharine S. Ullman. 2021. “Identification of Abcission Checkpoint Bodies as Structures That Regulate ESCRT Factors to Control Abcission Timing.” *eLife* 10: e63743.

Sudakin, Verly, Gordon K. Chan, and Tim J. Yen. 2001. “Checkpoint Inhibition of the APC/C in HeLa Cells Is Mediated by a Complex of BUBR1, BUB3, CDC20, and MAD2.” *The Journal of Cell Biology* 154 (5): 925–36.

Su, Kuan-Chung, Tohru Takaki, and Mark Petronczki. 2011. “Targeting of the RhoGEF Ect2 to the Equatorial Membrane Controls Cleavage Furrow Formation during Cytokinesis.” *Developmental Cell* 21 (6): 1104–15.

Sulli, Gabriele, Raffaella Di Micco, and Fabrizio d’Adda di Fagagna. 2012. “Crosstalk between Chromatin State and DNA Damage Response in Cellular Senescence and Cancer.” *Nature Reviews. Cancer* 12 (10): 709–20.

Sumara, Izabela, Juan F. Giménez-Abián, Daniel Gerlich, Toru Hirota, Claudine Kraft, Consuelo de la Torre, Jan Ellenberg, and Jan-Michael Peters. 2004. “Roles of Polo-like Kinase 1 in the Assembly of Functional Mitotic Spindles.” *Current Biology* 14 (19): 1712–22.

Tedeschi, Antonio, Jorge Almagro, Matthew J. Renshaw, Hendrik A. Messal, Axel Behrens, and Mark Petronczki. 2020. “Cep55 Promotes Cytokinesis of Neural Progenitors but Is Dispensable for Most Mammalian Cell Divisions.” *Nature Communications* 11 (1): 1746.

Thoresen, Sigrid B., Coen Campsteijn, Marina Vietri, Kay O. Schink, Knut Liestøl, Jens S. Andersen, Camilla Raiborg, and Harald Stenmark. 2014. "ANCHR Mediates Aurora-B-Dependent Abscission Checkpoint Control through Retention of VPS4." *Nature Cell Biology* 16 (6): 550–60.

Toyoda, Yusuke, and Mitsuhiro Yanagida. 2006. "Coordinated Requirements of Human Topo II and Cohesin for Metaphase Centromere Alignment under Mad2-Dependent Spindle Checkpoint Surveillance." *Molecular Biology of the Cell* 17 (5): 2287–2302.

Tsvetkov, Lyuben, Xingzhi Xu, Jia Li, and David F. Stern. 2003. "Polo-like Kinase 1 and Chk2 Interact and Co-Localize to Centrosomes and the Midbody." *The Journal of Biological Chemistry* 278 (10): 8468–75.

Uehara, Ryota, Yuki Tsukada, Tomoko Kamasaki, Ina Poser, Kinya Yoda, Daniel W. Gerlich, and Gohta Goshima. 2013. "Aurora B and Kif2A Control Microtubule Length for Assembly of a Functional Central Spindle during Anaphase." *The Journal of Cell Biology* 202 (4): 623–36.

Umbreit, Neil T., Cheng-Zhong Zhang, Luke D. Lynch, Logan J. Blaine, Anna M. Cheng, Richard Tourdot, Lili Sun, Hannah F. Almubarak, Kim Judge, Thomas J. Mitchell, Alexander Spektor, and David Pellman. 2020. "Mechanisms Generating Cancer Genome Complexity from a Single Cell Division Error." *Science* 368 (6488): eaba0712.

Vaze, Moreshwar B., Achille Pellicioli, Sang Eun Lee, Grzegorz Ira, Giordano Liberi, Ayelet Arbel-Eden, Marco Foiani, and James E. Haber. 2002. "Recovery from Checkpoint-Mediated Arrest after Repair of a Double-Strand Break Requires Srs2 Helicase." *Molecular Cell* 10 (2): 373–85.

Veaute, Xavier, Josette Jeusset, Christine Soustelle, Stephen C. Kowalczykowski, Eric Le Cam, and Francis Fabre. 2003. "The Srs2 Helicase Prevents Recombination by Disrupting Rad51 Nucleoprotein Filaments." *Nature* 423 (6937): 309–12.

- Vos, Seychelle M., Elsa M. Tretter, Bryan H. Schmidt, and James M. Berger. 2011. "All Tangled up: How Cells Direct, Manage and Exploit Topoisomerase Function." *Nature Reviews. Molecular Cell Biology* 12 (12): 827–41.
- Walker, John R., Richard A. Corpina, and Jonathan Goldberg. 2001. "Structure of the Ku Heterodimer Bound to DNA and Its Implications for Double-Strand Break Repair." *Nature* 412 (6847): 607–14.
- Wang, Lily Hui-Ching, Bernd Mayer, Olaf Stemmann, and Erich A. Nigg. 2010. "Centromere DNA Decatenation Depends on Cohesin Removal and Is Required for Mammalian Cell Division." *Journal of Cell Science* 123 (Pt 5): 806–13.
- Watanabe, Sadanori, Tihana De Zan, Toshimasa Ishizaki, and Shuh Narumiya. 2013. "Citron Kinase Mediates Transition from Constriction to Abscission through Its Coiled-Coil Domain." *Journal of Cell Science* 126 (Pt 8): 1773–84.
- West, Stephen C., Miguel G. Blanco, Ying Wai Chan, Joao Matos, Shriparna Sarbajna, and Haley D. M. Wyatt. 2015. "Resolution of Recombination Intermediates: Mechanisms and Regulation." *Cold Spring Harbor Symposia on Quantitative Biology* 80 (September): 103–9.
- White, Erin A., and Michael Glotzer. 2012. "Central spindle: At the Heart of Cytokinesis." *Cytoskeleton* 69 (11): 882–92.
- Whitman, Charles O. 1887. "A Contribution to the History of the Germ-Layers in Clepsine." *Journal of Morphology* 1 (1): 105–82.
- Winey, Mark, and Eileen T. O'Toole. 2001. "The Spindle Cycle in Budding Yeast." *Nature Cell Biology* 3 (1): e23–7.
- Wloka, Carsten, and Erfei Bi. 2012. "Mechanisms of Cytokinesis in Budding Yeast." *Cytoskeleton* 69 (10): 710–26.

Woodruff, Jeffrey B., David G. Drubin, and Georjana Barnes. 2010. "Mitotic Spindle Disassembly Occurs via Distinct Subprocesses Driven by the Anaphase-Promoting Complex, Aurora B Kinase, and Kinesin-8." *The Journal of Cell Biology* 191 (4): 795–808.

Yang, Dong, Neggy Rismanchi, Benoît Renvoisé, Jennifer Lippincott-Schwartz, Craig Blackstone, and James H. Hurley. 2008. "Structural Basis for Midbody Targeting of Spastin by the ESCRT-III Protein CHMP1B." *Nature Structural & Molecular Biology* 15 (12): 1278–86.

Ye, Jing, Christelle Lenain, Serge Bauwens, Angela Rizzo, Adelaïde Saint-Léger, Anaïs Poulet, Delphine Benarroch, Frédérique Magdinier, Julia Morere, Simon Amiard, Els Verhoeyen, Sébastien Britton, Patrick Calsou, Bernard Salles, Anna Bizard, Marc Nadal, Erica Salvati, Laure Sabatier, Yunlin Wu, Annamaria Biroccio, Arturo Londoño-Vallejo, Marie-Josèphe Giraud-Panis, Eric Gilson. 2010. "TRF2 and Apollo Cooperate with Topoisomerase 2alpha to Protect Human Telomeres from Replicative Damage." *Cell* 142 (2): 230–42.

Yeong, Foong May. 2005. "Severing All Ties between Mother and Daughter: Cell Separation in Budding Yeast." *Molecular Microbiology* 55 (5): 1325–31.

Zeman, Michelle K., and Karlene A. Cimprich. 2014. "Causes and Consequences of Replication Stress." *Nature Cell Biology* 16 (1): 2–9.

Zerjatke, Thomas, Igor A. Gak, Dilyana Kirova, Markus Fuhrmann, Katrin Daniel, Magdalena Gonciarz, Doris Müller, Ingmar Glauche, and Jörg Mansfeld. 2017. "Quantitative Cell Cycle Analysis Based on an Endogenous All-in-One Reporter for Cell Tracking and Classification." *Cell Reports* 19 (9): 1953–1966.

Zhang, Cheng-Zhong, Alexander Spektor, Hauke Cornils, Joshua M. Francis, Emily K. Jackson, Shiwei Liu, Matthew Meyerson, and David Pellman. 2015. "Chromothripsis from DNA Damage in Micronuclei." *Nature* 522 (7555): 179–84.

Zhang, Yi, Xiaojuan Ye, Lizhi Chen, Qiong Wu, Yong Gao, and Yandong Li. 2018. "PARI Functions as a New Transcriptional Target of FOXM1 Involved in Gastric Cancer Development." *International Journal of Biological Sciences* 14 (5): 531–41.

Zhou, Bin-Bing S., and Stephen J. Elledge. 2000. "The DNA Damage Response: Putting Checkpoints in Perspective." *Nature* 408 (6811): 433–39.

Zhu, Changjun, Eric Lau, Robert Schwarzenbacher, Ella Bossy-Wetzel, and Wei Jiang. 2006. "Spatiotemporal Control of Spindle Midzone Formation by PRC1 in Human Cells." *Proceedings of the National Academy of Sciences of the United States of America* 103 (16): 6196–6201.

Zimniak, Tomasz, Katharina Stengl, Karl Mechtler, and Stefan Westermann. 2009. "Phosphoregulation of the Budding Yeast EB1 Homologue Bim1p by Aurora/Ipl1p." *The Journal of Cell Biology* 186 (3): 379–91.

The role of DNA helicase PARI in the NoCut abscission checkpoint in human cells

Résumé

L'abscission est le dernier processus de la cytokinèse au cours duquel les cellules filles sont physiquement séparées par le désassemblage du corps central et la résolution de la membrane plasmique. Les erreurs de ségrégation des chromosomes pendant l'anaphase, telles que les ponts de chromatine, peuvent entraîner des dommages à l'ADN et l'échec de la cytokinèse si elles ne sont pas résolues avant l'abscission. Dans les cellules de levure et les cellules humaines, les conséquences négatives des ponts de chromatine sont évitées par le point de contrôle de l'abscission médié par Aurora B, qui retarde l'abscission en réponse aux défauts de ségrégation des chromosomes. On pense que le retard de l'abscission laisse le temps de résoudre le pont de chromatine et de retirer la chromatine restante du plan de clivage. Cependant, la manière dont les ponts chromatiniens déclenchent la signalisation du point de contrôle de l'abscission reste inconnue. En utilisant des techniques d'imagerie en direct et la microscopie à immunofluorescence, nous avons étudié le rôle de Srs2 et de son homologue humain PARI, une ADN hélicase associée à la réplication de l'ADN et à l'appareil de réparation homologue, dans le point de contrôle de l'abscission. Nous constatons que Srs2 et PARI ont tous deux une double fonction : d'une part, ils font partie du point de contrôle médié par Aurora B et favorisent l'inhibition de l'abscission spécifiquement en présence de ponts chromatiniens caténaux induits par l'inactivation de la topoisomérase II. D'autre part, PARI agit pour promouvoir la résolution des ponts chromatiniens. Nos résultats mettent en évidence l'ADN hélicase PARI comme un composant vital dans la régulation du point de contrôle de l'abscission et éclairent la façon dont le point de contrôle est engagé pour prévenir les phénotypes cancérogènes dans le cycle cellulaire suivant.

Mots-clés : PARI, Srs2, NoCut/point de contrôle de l'abscission, stabilisation du corps central, ponts chromatiniens

Summary

Abscission is the last process of cytokinesis where the daughter cells are physically separated by midbody disassembly and plasma membrane resolution. Errors in chromosome segregation during anaphase such as chromatin bridges can lead to DNA damage and to failure of cytokinesis if not resolved before abscission. In both yeast and human cells, the negative consequences of chromatin bridge are prevented by the Aurora B-mediated abscission checkpoint, which delays abscission in response to chromosome segregation defects. The delay in abscission is thought to allow time for chromatin bridge resolution and removal of remaining chromatin from the cleavage plane. However, how chromatin bridges trigger the abscission checkpoint signaling remains unknown. Using live-imaging techniques and immunofluorescence microscopy we investigated the role of Srs2 and its human homolog PARI, a DNA helicase associated with the DNA replication and homologous repair apparatus, in the abscission checkpoint. We find that both Srs2 and PARI have a dual function, on one hand, it is part of the Aurora B-mediated checkpoint and promotes inhibition of abscission specifically in the presence of catenated chromatin bridges induced by topoisomerase II inactivation. On the other hand, PARI acts to promote the resolution of chromatin bridges. Our findings highlight the DNA helicase PARI as a vital component in abscission checkpoint regulation and shed light on how the checkpoint is engaged to prevent cancerogenic phenotypes in the next cell cycle.

Keywords: PARI, Srs2, NoCut/abscission checkpoint, midbody stabilization, chromatin bridges